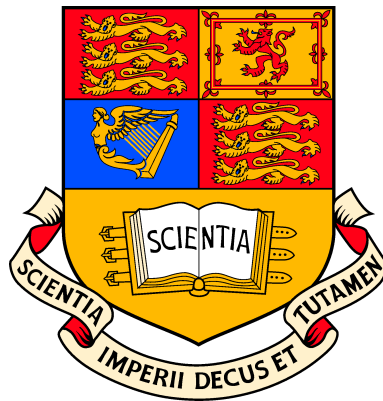# Mechanisms for flow-induced vibration of interfering bluff bodies

by

Gustavo R. S. Assi

Department of Aeronautics

Imperial College London

This thesis is submitted for the degree of

Doctor of Philosophy of the University of London

September 2009

I hereby declare that this thesis is my own work and effort and that it has not been submitted anywhere for any award. Where other sources of information have been used, they have been acknowledged.
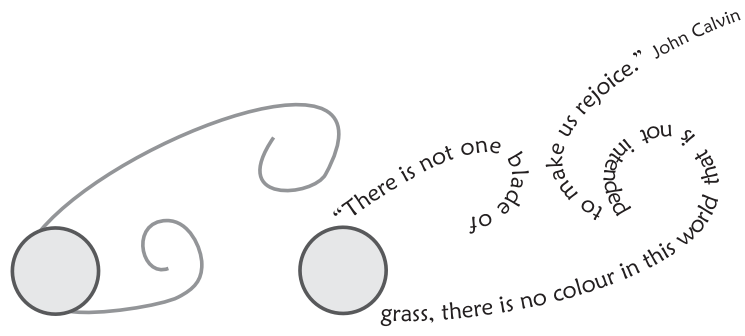
Gustavo R.S. Assi

Abstract

The mechanism of *wake-induced vibrations* (WIV) of a pair of cylinders in a tandem arrangement is investigated by experiments. A typical WIV response is characterised by a build up of amplitude persisting to high reduced velocities; this is different from a typical vortex-induced vibrations (VIV) response that occurs in a limited resonance range.

We suggest that WIV of the downstream cylinder is excited by the unsteady vortex-structure interactions between the body and the upstream wake. Coherent vortices interfering with the second cylinder induce fluctuations in the fluid force that are not synchronised with the motion. A favourable phase lag between the displacement and the fluid force guarantees that a positive energy transfer from the flow to the structure sustains the oscillations. If the unsteady vortices are removed from the wake of the upstream body then WIV will not be excited.

We introduce the concept of *wake stiffness*, a fluid dynamic effect able to sustain a body without any structural stiffness into oscillatory motion. The role played by the unsteady wake is central to this idea and contributes to the understanding of WIV as a wake-excited and wake-sustained mechanism. A simple analytical model predicts the frequency of response rather well, but fails to model the displacement because important nonlinear effects are not taken into account. We conclude that while unsteady *vortex-structure interactions* provide the energy input to sustain WIV, it is the *wake stiffness* effect that defines the character of the response.

Suppression of cross-flow and in-line VIV, with resulting drag coefficients less than that for a static plain cylinder, is achieved using two-dimensional control plates free to rotate around the body. Devices based on parallel plates show great potential to suppress VIV and WIV of offshore structures with considerable reduction in drag.

"There is not one blade of grass, there is no colour in this world that is not intended to make us rejoice." John Calvin

To Lilian, my wife,

for her love, support and inspiration beyond measure.

Acknowledgements

First of all, I would like to express my sincere gratitude to Professor Peter Bearman for supervising my research dedicating both his time and experience. It was a great pleasure and honour to work under his guidance; the fruits of which I will benefit from for the rest of my career. Both Peter and Etti, his wife, offered Lilian and myself the warmest welcome we could have ever expected. We are very thankful for their level of care and friendship.

I am also indebted to Dr Julio Meneghini, my dear friend and academic mentor. Not only did he give me advice relating to scientific matters, but he also gave me a great deal of confidence and motivation to carry out my work and studies.

My doctoral scholarship was fully sponsored by CAPES, the Brazilian Ministry of Education, for which I am very appreciative. I am also thankful to Dr. Neil Kitney, on behalf of BP Exploration Ltd, for providing the financial support for the development of suppressors.

I appreciate the valuable assistance offered by the staff members of the Department of Aeronautics, in particular the technicians from our workshops. They always displayed professional competence and a great sense of humour. It has been a great satisfaction to work alongside them.

A special thank you goes to my colleagues with whom I shared the office and many trips, books, coffees, equations, barbecues... Here I met many talented researchers, all gifted with kindness and friendship that we will never forget. It would be impossible to list each one individually, but I would like to mention two friends who, in a way, represent them all, to express my appreciation: Bruno Carmo, my friend of old from Brazil, always gentle and sensible, a dear partner for all occasions. And Ala Qubain, my new friend from Jordan, whose overflowing happiness and

excitement will be greatly missed (until we meet again and soon). I am grateful to all my dear friends who directly or indirectly contributed towards this PhD. I wish them all joy in their lives and success in their careers!

I am particularly thankful for the support of my family in Brazil. From so far away they have made themselves present in every page of this work. The values we learn at home are those that remain forever and I am sure this PhD is an achievement for them as well. I am also grateful to my brothers and sisters from London City Presbyterian Church. They have been our family in London, always taking care of the most precious things in our lives. It was a blessing to serve the Lord in their company.

Finally, I am most grateful to Lilian, my wife. Firstly, for giving up her personal ambitions when the opportunity to move to London arose; and later for so wholeheartedly supporting us throughout my studies. I know there were times when it was not easy to be the wife of a PhD student, but she was a strong encouragement to my work as well as to our marriage. In her I find love beyond measure, companionship and inspiration that is impossible to express here. It is a true blessing to have her by my side. Lilian deserves much of the credit for the completion of this thesis.

To conclude, and most importantly, this must not remain unsaid, I am grateful to God for providing me with this unique opportunity to understand the intricate wonders of creation through the eyes of science. I pray that my effort would not only benefit my own career, but I ask that the working of my mind and the meditation of my heart be pleasing in His sight. To God be all the glory!

I suspect you are finding this acknowledgement section too long already. By now, I hope you are eager to move on and treat yourself to some 'wake-induced vibrations'. But I honestly believe these are the two most important pages of my thesis. If I had to choose between them and the rest, I would throw away all my experimental data, plots and discussions, but keep the experiences I have shared with you above. They not only bring meaning to my scientific investigation, but also to my life outside the lab. If I cannot live for Christ, love, joy, family, friendship, knowledge, truth... what else shall I live for?

Contents

Publications

Author's publications related to the present thesis.

Journals

ASSI, G.R.S., BEARMAN, P.W., MENEGHINI, J.R. On the wake-induced vibration of tandem circular cylinders: the vortex interaction excitation mechanism, *Submitted for publication in the J. Fluids Mechanics*

ASSI, G.R.S., CARMO, B.S., BEARMAN, P.W., SHERWIN, S.J., WILLDEN, R.J., MENEGHINI, J.R. The role of wake-induced stiffness on the vibration of the downstream cylinder of a tandem pair, *Submitted for publication in the J. Fluids Mechanics*

ASSI, G.R.S., BEARMAN, P.W., KITNEY, N. Suppression of wake-induced vibration of tandem cylinder with free-to-rotate control plates, *Submitted for publication in the J. Fluids and Structures*

ASSI, G.R.S., BEARMAN, P.W., KITNEY, N. 2009 Low Drag Solutions for Suppressing Vortex-Induced Vibration of Circular Cylinders, *J. Fluids and Structures 25, 666-675*

ASSI, G.R.S.; MENEGHINI, J.R.; ARANHA, J.A.P.; BEARMAN, P.W.; CASAPRIMA, E. 2006 Experimental investigation of flow-induced vibration interference between two circular cylinders. *J. Fluids and Structures 22, 819-827*

In proceedings of conferences

ASSI, G.R.S., BEARMAN, P.W. 2009 VIV and WIV suppression with parallel control plates on a pair of circular cylinders in tandem, In *OMAE2009 28th Int. Conf. Ocean, Offshore and Arctic Eng., Honolulu, USA*

ASSI, G.R.S., BEARMAN, P.W. 2008 VIV suppression and drag reduction with pivoted control plates on a circular cylinder, In *OMAE2008 27th Int. Conf. Offshore Mech. and Arctic Eng., Estoril, Portugal*

ASSI, G.R.S., BEARMAN, P.W. 2008 New methods for suppressing vortex-induced vibration of circular cylinders, In *FIV-2008 9th Int. Conf. on Flow-Induced Vibrations, Prague, Czech Republic*

ASSI, G.R.S., BEARMAN, P.W., MENEGHINI, J.R. 2008 Unsteady response of a circular cylinder under wake-induced excitation from a fixed upstream cylinder. In *FIV-2008 9th Int. Conf. on Flow-Induced Vibrations, Prague, Czech Republic*

ASSI, G.R.S., BEARMAN, P.W., MENEGHINI, J.R. 2007 Unsteady force measurements on a responding circular cylinder in the wake of an upstream cylinder. In *OMAE2007 - 26th Int. Conf. Offshore Mech. and Arctic Eng., San Diego, USA*

ASSI, G.R.S., BEARMAN, P.W. 2007 Low Drag Solutions for Suppressing VIV of Circular Cylinders, In *BBVIV5 - 5th Conf. Bluff Body Wakes and Vortex-Induced Vibrations, Costa do Sauipe, Brazil*

ASSI, G.R.S., BEARMAN, P.W., MENEGHINI, J.R. 2007 Dynamic response of a circular cylinder in the wake of an upstream fixed cylinder. In *BBVIV5 - 5th Conf. Bluff Body Wakes and Vortex-Induced Vibrations, Costa do Sauipe, Brazil*

Nomenclature

Abbreviations

FIV   Flow-induced vibration

F-t-r   Free-to-rotate

PIV   Particle-image velocimetry

PSD   Power spectral density

VIV   Vortex-induced vibration

WIV   Wake-induced vibration

Non-dimensional numbers and groups

Re   Reynolds number: $\mathrm{Re} = UD/\nu$

Re_W Reynolds number based on channel width (W): $\mathrm{Re} = UW/\nu$

St   Strouhal number: $\mathrm{St} = f_s D/U$

U/Df_0 Reduced velocity

Roman symbols

A_{xy} Combined amplitude parameter [m]: $A_{xy} = \sqrt{\hat{x}^2 + \hat{y}^2}$

c Structural damping [Kg/s]

C_a Ideal flow added mass: $C_a = 1.0$

$C_x,\ \overline{C}_x,\ \hat{C}_x$ Total, steady, and fluctuating drag coefficients

$C_y,\ \overline{C}_y,\ \hat{C}_y$ Total, steady and fluctuating lift coefficients

$C_{y_P},\ C_{y_V}$ Potential and vortex components of lift coefficient

$|\ \partial\overline{C}_y\ |$ Slope of steady lift for staggered, static cylinders

D Cylinder diameter [m]

f Frequency of oscillation [1/s]

f_0	Natural frequency in air [1/s]
f_{0_x}, f_{0_y}	Natural frequency in 2-dof in air [1/s]
f_s	Frequency of vortex shedding [1/s]
f_W	Natural frequency in water [1/s]
f_w	Natural frequency associated with wake stiffness [1/s]
F_y	Cross-flow fluid force [N]
F_{y_P}, F_{y_V}	Potential and vortex components of fluid force [N]
k	Structural stiffness (spring constant) [N/m]
k_w	Wake stiffness [N/m]
L	Underwater cylinder length [m]
L_{SP}	Length of the splitter plate [m]
m	Structural mass [Kg]
m^*	Mass ratio: $m^* = 4m/\rho\pi D^2 L$
T	Period of oscillation [s]: $T = 1/f$
TI	Free stream turbulence intensity: $TI = \sqrt{\overline{u^2}}/U$
U	Free stream velocity [m/s]
u, v	Local velocity fluctuation [m/s]
x_0, y_0	Centre-to-centre separation [m]
$\hat{x}$, $\hat{y}$	Harmonic amplitude of displacement [m]: $\hat{y} = \sqrt{2}y_{\mathrm{rms}}$
y, $\dot{y}$, $\ddot{y}$	Cylinder displacement [m], velocity [m/s] and acceleration [m/s^2]

Greek symbols

α	Angle of attack [degrees]
δ	Stable angle of the splitter plate [degrees]
ϕ, ϕ_V	Phase angle between y and C_y and C_{yV} [degrees]
ν, μ	Kinematic [m^2/s] and dynamic [Kg/ms] viscosity of water
ρ	Specific mass of water [Kg/m^3]
τ_f	Torsional friction of f-t-r suppressors [Nm/m]
τ_f^*	Non-dimensionalised torsional friction: $\tau_f^* = \tau_f/\rho U^2 D^2$
ζ	Damping ratio: $\zeta = c/4\pi f_0 m$

Chapter 1

Introduction

The last two decades have seen a significant transformation in the offshore oil exploration around the world. New technologies enabled the industry to move further offshore in search for oil in water depths that were unimaginable just a few years ago. The engineering of complex floating systems made it possible to move beyond the limit of 1000m below the sea level to the so called ultra-deep waters around 3000m. As illustrated in Fig. 1.1, offshore platforms evolved from the fixed towers installed in shallow waters to the gigantic spar platforms capable of operation in great water depths.

Recently, an enormous oil reservoir has been discovered in the Campos and Santos basins, 500Km off the south-eastern coast of Brazil, with estimated 10 billion barrels of crude oil and vast quantities of gas. However, in this case, the oil is not only located at 2200m below the sea level, but also hidden between 3000 to 5000 metres below the sea bed. To make matters worse, the oil is located underneath a thick and fragile geological formation of salt-rock — thus the reservoir is known as the Pre-salt. Reaching the bottom of the sea is already a big problem in itself, drilling through a thick layer of unstable salt-rock is yet more complicated.

Technological advancements permitted the discovery of new reservoirs, but to find access to the oil is now the problem challenging offshore engineers. Because the first fixed platforms cannot operate in such depths, new floating systems appeared to dominate modern offshore exploration. Semi-submersible and FPSO (floating
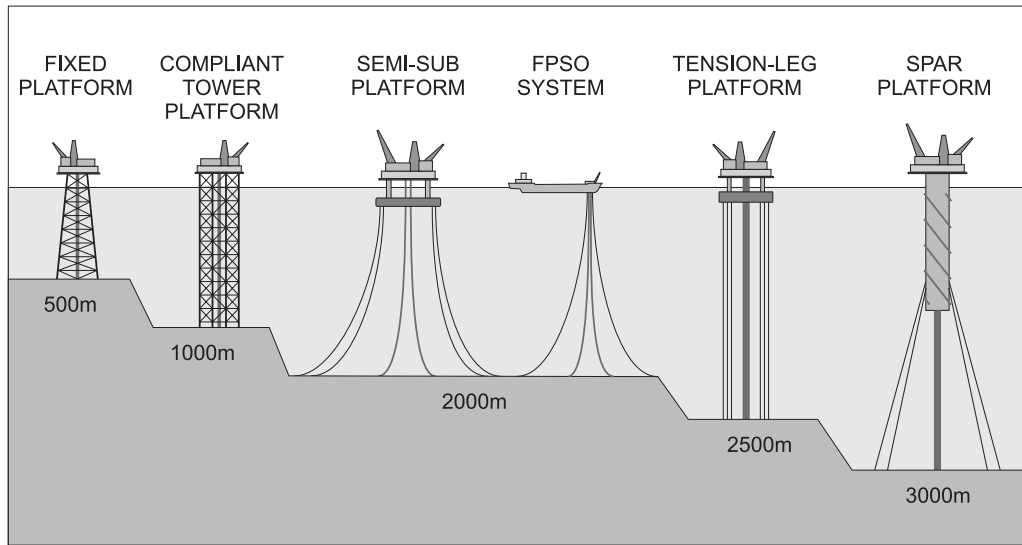
Fig. 1.1: Types of offshore platforms employed for oil exploration in different water depths (not in scale).

production, storage and offloading system) platforms for production, along with tension-leg and spar platforms for drilling, represent great leaps in the technological history line (Fig. 1.1). The complex drilling process, for example, is yet another technical breakthrough. The challenge does not stop with manufacturing the drilling apparatus, but goes far beyond to the operation of a massive dynamic system under severe conditions of wind, sea currents and waves.

Risers are long cylindrical pipes, with different functions, that connect the floating platform to the sea bed. Production risers are normally used to inject water into the well and transport oil and gas back to the rig. They can be relatively flexible structures made of layers of rubber and steel. On the other hand, rigid drilling risers, operated from the floating platform thousands of metres above, are required to perforate through rock and open the well. Some people in the industry illustrate the point by saying that drilling a well at the bottom of the ocean is like hitting the bulls-eye with a 3000m flexible stick while riding a horse.

One of the major problems during offshore drilling and production is the vibration induced on the riser by sea currents. As water flows around the riser it excites the structure into several modes of vibration that vary with many of the structural properties of the system. Because they are so long and slender, risers are better modelled by a theory of flexible strings rather than by the classical

theory of stiff beams. It is easy to imagine how the actual drilling operation can be complicated by such vibrations, but in the long term the structural integrity of the pipe can also be compromised due to structural fatigue. Therefore, it is very important for the offshore industry to find solutions that will help to suppress the flow-induced vibration of risers.

Interestingly the present work appears at a time of discussions concerning global warming caused by the excessive use of fossil fuels. At the same time that Brazil has found long-term reserves of oil the country is also investing to keep the position of leader in ethanol exportation. Even though there is a universal expectation that the use of fossil fuels will be reduced in the future, it appears that crude oil still remains a precious commodity for many decades to come.

Nevertheless *flow-induced vibration* (FIV) is not a concern for the offshore industry alone, but a problem present in many branches of engineering. Historically, the first attempts to suppress FIV are found in the civil engineering design of chimneys and suspension bridges. The vibration of transmission lines has attracted some attention from the electrical engineering community as well. The industry of heat exchangers has also invested resources to avoid the vibration of tube bundles inside pressure vessels. Later, the problem was investigated by aeronautical engineers interested in aero-elasticity and, more recently, following the exploration of oil in deep waters, it became a real concern for the offshore industry. The present study is mainly motivated by the needs of the offshore industry, but clearly has applications in many other areas of engineering.

1.1 Objectives

Modern deep-water floating systems can accumulate as many as 40 production risers and many more mooring lines in a single platform. Although Fig. 1.2 is a simple artistic representation, it illustrates rather well the point that a great number of flexible, underwater structures are susceptible to FIV and to interact with each other and the hull of the platform.

Thinking about the large drilling platforms illustrated in Fig. 1.1 (tension-leg
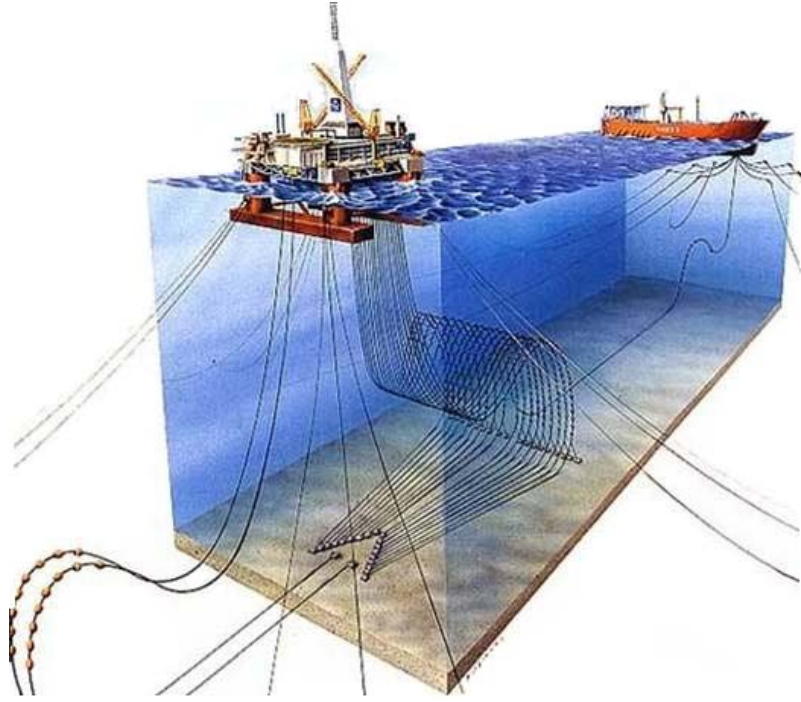
Fig. 1.2: Artistic representation of a semi-submersible platform (foreground) and a FPSO system (background) showing the large number of risers, mooring lines and other cylindrical structures susceptible to FIV. Courtesy of www.offshore-technology.com.

and spar) we can see that the drilling riser — vertically stretched from the centre of the platform down to the sea bed — is surrounded by tendons along its entire length. Flow interference from the wake generated from other structures can amplify the response of the riser, affecting its operation and increasing the risk of fatigue damage. A few solutions have been developed to suppress vibrations from isolated risers, but we believe now is time to turn our attention to the vibration problem aggravated by flow interference.

In the present study we are concerned about the fluid-elastic mechanism called *wake-induced vibrations* (WIV). Simply put it is the vibration induced on a bluff body by the interference of the wake generated from another body placed somewhere upstream. In our offshore example, one riser can fall in the wake of another depending on the direction of the current. A complex WIV excitation mechanism can be initiated and conventional suppressors may not be effective to restrain it to acceptable levels. In this context, the main objectives of the present study are:

- First, understand the physical aspects of the fluid-structure mechanism that

drives wake-induced vibrations of the downstream body. Previous works have presented the response of structures with flow interference but they failed to provide a satisfactory explanation of the mechanism therein.

- Second, propose new solutions for suppressing WIV without incurring a drag penalty to the structure. We believe that only with a solid understanding of the WIV mechanism will it be possible for successful suppression devices to be designed.

1.2 Methodology

For a long time the problem of WIV was the main concern of the heat-exchanger industry; hence most of the experiments employed heavy tubes arranged in arrays of several units in all sorts of tight configurations. A substantial amount of data has been generated and was certainly useful for that industry to improve design practices and guidelines. But following the demand of the offshore industry, experiments naturally moved from configurations of heavy, rigid tubes in close proximity to lighter, flexible pipes with larger separations.

A full-scale offshore riser cannot be reduced to laboratory scale while still keeping all of its structural properties. The complex sea current — with flow speed and direction varying along the water depth — is also impossible to be reproduced to the same scale as the structure. Even if a complete representation of the problem were possible, such a complex experiments would probably not help to fulfil the objectives set above. Experiments with many parameters and variables do not throw any light on the understanding of the fluid-elastic mechanism behind such vibrations. More careful investigators started to limit the number of tubes and degrees of freedom resulting in a few experiments that reported response curves for WIV of the downstream cylinder of a pair.

For that reason, in the present experimental investigation we will represent a section of a flexible riser by a rigid cylinder mounted on an elastic system. The structural properties of the riser will be simplified to a mass-spring-damper oscillator

free to respond to the flow excitation in one or two degrees of freedom. On the other hand, the sea current on that section of riser will be simulated in the laboratory by a uniform velocity profile generated in a recirculating water channel.

With this approach we believe it will be possible to identify significant parameters, characterise the phenomenon and eventually understand how the wake of one bluff body can interfere with the vibration of another.

1.3   Structure of the thesis

The present thesis is divided into 9 chapters, including this introduction:

- Chapter 2 presents a brief introduction to the phenomenon of vortex shedding of bluff bodies and a literature review about flow-induced vibration of a single rigid cylinder.

- Chapter 3 introduces the concept of flow interference between two bluff bodies and presents a literature review of flow-induced vibration of a pair of cylinder in tandem.

- Chapter 4 describes the experimental set-up employed in this study, comprising flow facilities, elastic rigs, cylinder models and experimental techniques.

- Chapter 5 presents preliminary results for *vortex-induced vibrations* (VIV) of a single cylinder followed by the main results of the WIV response of the downstream cylinder of a pair.

- Chapter 6 is the first discussion chapter; concerned with the flow-structure interaction responsible for the excitation of WIV. The key experiment being conducted in a steady shear flow without vortices in order to prove that the WIV mechanism is dependent on the unsteady interaction between the upstream wake and the cylinder.

- Chapter 7 is the second discussion chapter; concerned with the characteristics of the WIV response. The key experiment being conducted with a system

without springs in order to prove that there is a wake-stiffness effect, greater than the stiffness generated by the springs, dominating the response.

- Chapter 8 is an application of the theory discussed in previous chapters to the development of VIV and WIV suppressors. Devices are based on two-dimensional control plates free to rotate around the centre of the cylinder. This chapter is not essential for the understanding of the WIV mechanism, but was included as an example of how our theory can be employed in the field.

- Chapter 9 concludes the thesis summarising the main findings and contributions of the present study. It also suggests further works to advance the present investigation.

- Appendix A is a brief explanation about the method employed to generate power spectral density plots throughout the thesis.

Chapter 2

Literature review: Flow-induced vibration of a single cylinder

In fluid mechanics, a structure immersed in a fluid current is classified as a *bluff body* if it generates separated flow over a significant proportion of its surface. This definition is not strictly related to the geometry of the body itself, but with characteristics of the flow around the body, being especially associated to the existence of separated flow.

A circular cylinder is the classic example of a bluff body due to its simple axisymmetric geometry. In practical engineering applications of cylindrical structures subjected to fluid flows the fluid-elastic interaction between the flow and the structure can excite the body into *flow-induced vibrations* (FIV). The present study of FIV begins with a brief review of the phenomena of flow separation and vortex shedding of circular cylinders.

2.1   Vortex shedding from bluff bodies

Flow visualisation produced by photographing particles travelling in water current is shown in Fig. 2.1. As the free stream approaches the cylinder the flow splits around the body. Viscous boundary layers will develop from the front stagnation point while the flow remains attached to the walls. It is within the boundary layer
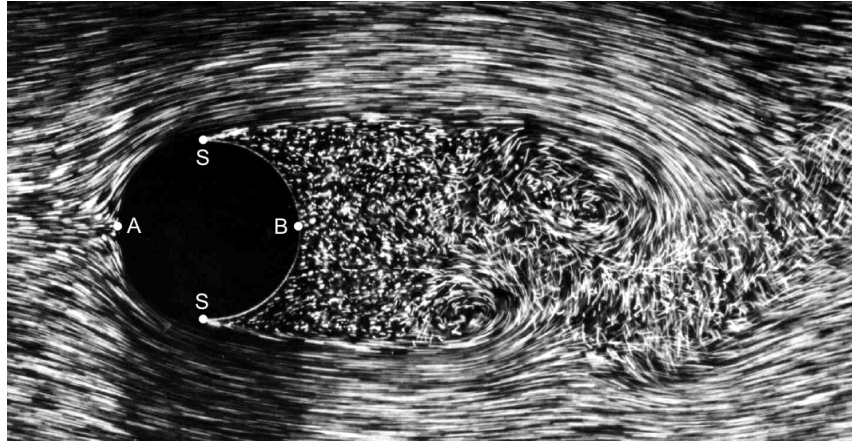
Fig. 2.1: Visualisation of the flow around a circular cylinder at Re = 2000. 'A' is the front stagnation point, 'B' is the base point and 'S' are the separation points. Adapted from van Dyke (1982).

that fluid viscous forces are playing a role. The geometry of the body generates an adverse pressure gradient that, acting on the viscous profile of the boundary layer, will cause the flow to separate from the wall at the separation points on each side. The arch at the base of the cylinder between both separation points faces a separation region of recirculating flow where the wake begins.

The pressure field around the body — that has its maximum value at the stagnation and its minimum value around the shoulder of the cylinder — is not able to recover the same stagnation value at the base point due to the separation of the flow. Therefore, a considerable portion of the cylinder is immersed in a region with roughly constant but lower pressure. The difference between the pressure integrated along the front and back half of the cylinder results in the high drag force that is characteristic of bluff bodies.

The phenomenon of flow separation is governed by the balance between inertial and viscous forces acting in the flow, more precisely within the boundary layer. The Reynolds number

$$\mathrm{Re} = \frac{\rho U D}{\mu} = \frac{U D}{\nu} \tag{2.1}$$

is a non-dimensional parameter that represents the ratio between forces with those two natures. U is the free stream velocity, D is the external diameter of the cylinder (the characteristic dimension of this geometry), ρ represents the density and μ the dynamic viscosity of the fluid (giving kinematic viscosity $\nu = \mu/\rho$).

For very low values of Re viscous forces dominate and the flow remains attached around the circumference. But as Re increases the boundary layer is not able to withstand a sufficiently high adverse pressure gradient and separation eventually occurs. Now, the boundary layer is a region of concentrated vorticity generated by the shear velocity profile close to the wall. After separation the vorticity found in the boundary layer is detached from the surface and convected into the near wake forming a free shear layer on each side of the body. The interaction of these two flow structures is the beginning of the vortex-shedding mechanism. It is the flux of vorticity at the separation points constantly supplying the circulation in the free shear layers that sustains the phenomenon.

Bearman (1984) wrote a comprehensive review on the mechanism of vortex shedding from bluff bodies. He explains that "A key factor in the formation of a vortex-street wake is the mutual interaction between the two separating shear layers. It is postulated by Gerrard (1966) that a vortex continues to grow, fed by circulation from its connected shear layer, until it is strong enough to draw the opposing shear layer across the near wake. The approach of oppositely signed vorticity, in sufficient concentration, cuts off further supply of circulation to the growing vortex, which is then shed and moves off downstream."

The vortex shedding mechanism involves the mixing of flows of oppositely signed vorticity from both sides of the cylinder. Consequently, the strength of individual vortices will be less than the total circulation fed from one side of the body during one cycle. In fact, Roshko (1954) estimated that only 43% of the circulation produced in the shear layers remain in the wake after the formation region, which is defined as the distance downstream of the cylinder where a coherent vortex is formed and released. As a result a characteristic von Kármán vortex street is formed downstream of bluff bodies and will persist even for higher Reynolds number (Fig. 2.2).

Bearman (1984) also states that "it is the presence of two shear layers, rather than the bluff body itself, that is primarily responsible for vortex shedding. The presence of the body merely modifies the process by allowing feedback between the wake and the shedding of circulation at the separation points." Therefore, the rate at which vortices are cyclically shed from the body depends essentially on the
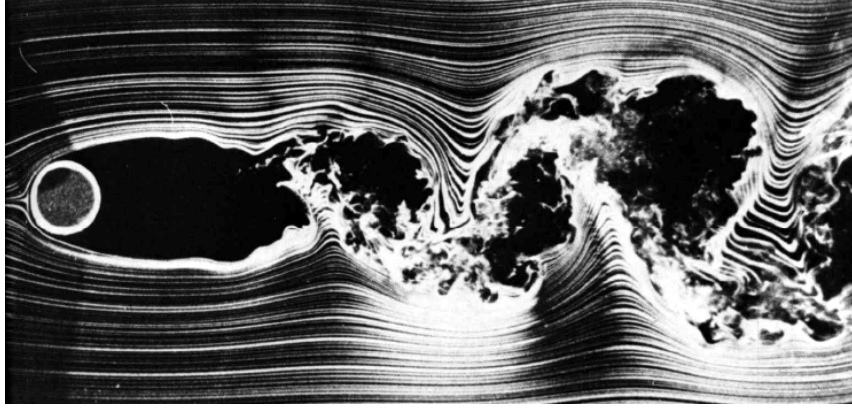
Fig. 2.2: Turbulent vortex wake of a circular cylinder at $\mathrm{Re} = 10^4$. Boundary layers are still laminar. Reproduced from van Dyke (1982).

interaction between the two shear layers as a function of the free stream velocity and the diameter of the body. The non-dimensional Strouhal number

$$\mathrm{St} = \frac{f_s D}{U} \tag{2.2}$$

relates the frequency of vortex shedding f_s with U and D. Many authors have measured St for a single static cylinder and found that it is close to 0.2 for subcritical Re. (Bearman, 1967).

As Re is further increased, a transition from a laminar to turbulent flow regime will start to happen. First the wake further downstream from the cylinder becomes turbulent, but with an additional increase in Re the start of a turbulent regime travels upstream reaching the free shear layers and eventually affecting the boundary layers. Turbulent boundary layers have more kinetic energy close to the wall and are able to resist longer the effect of an adverse pressure gradient. Hence, the separation is delayed and a narrower wake is formed, resulting in a sudden drag reduction on the body. The critical Reynolds number at which this *drag crisis* occurs for a smooth cylinder is around 2×10^5 (Zdravkovich, 1997).

Between $\mathrm{Re} = 2 \times 10^5$ and 3×10^6 the unstable turbulence transition generates a chaotic wake that lacks coherent vortices. However for postcritical Reynolds numbers above 3×10^6 a fully turbulent vortex wake reappears. In fact, well developed, organised, but fully turbulent wakes are often captured in aerial photographs taken from clouds passing around islands, representing a Reynolds number of an order higher than 10^9. As far as this study is concerned Re was kept
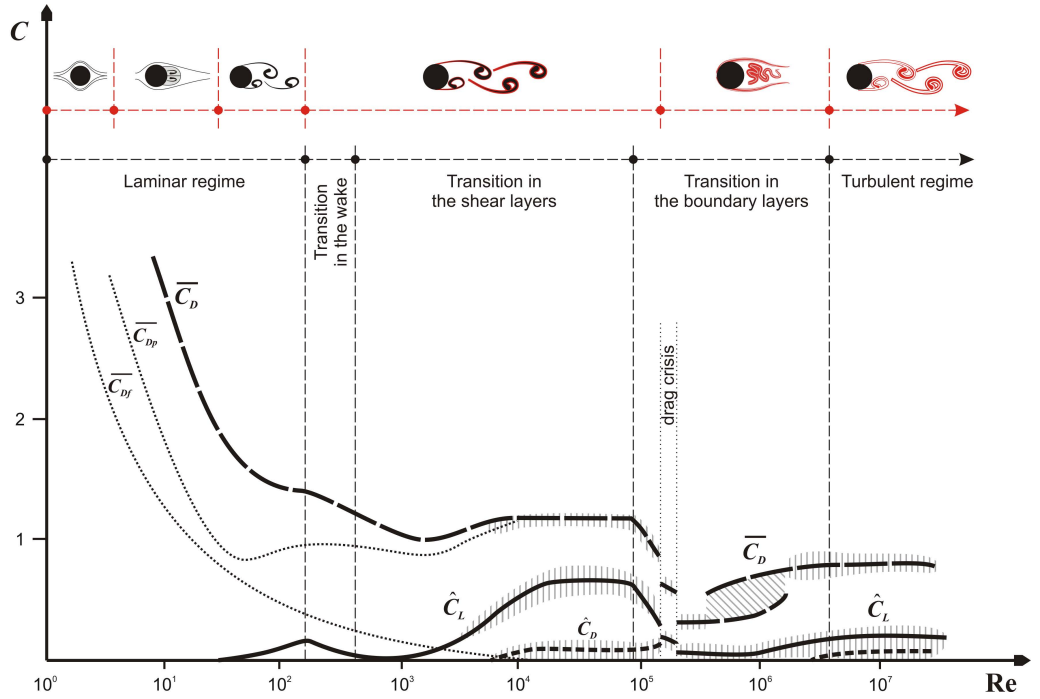
Fig. 2.3: Variation of lift and drag coefficients with Reynolds number for a circular cylinder. $\overline{C}_D$ represent mean drag; $\hat{C}_L$ and $\hat{C}_D$ represent the magnitude of fluctuating lift and drag. A small 'p' and 'f' indices represent terms due to pressure and friction drag. Dashed regions represent the scatter of experimental data. Adapted from Zdravkovich (1997).

in the subcritical region for all experiments, which means that the wake was mostly turbulent, but boundary layers were still in a laminar state at separation (as in the flow illustrated in Fig. 2.2).

Zdravkovich (1997) presents a detailed classification of the laminar-turbulent transition on a circular cylinder flow, but probably the most useful result from an engineering point of view concerns the fluid loads acting on the body (summarised in Fig. 2.3). Drag and lift coefficients are plotted against Reynolds number covering the transition from laminar to turbulent regime in the wake, shear layers and boundary layers. $\overline{C}_D$ curve represents the time-average drag coefficient acting on the cylinder, which is divided into two terms according to their nature: friction drag $\overline{C}_{Df}$ and pressure drag $\overline{C}_{Dp}$. For the range Re $= 10^3 - 10^5$, in which all experiments of this work were performed, the total drag reaches a plateau of $\overline{C}_D \approx 1$ with the friction drag component being negligible when compared to the pressure drag component.
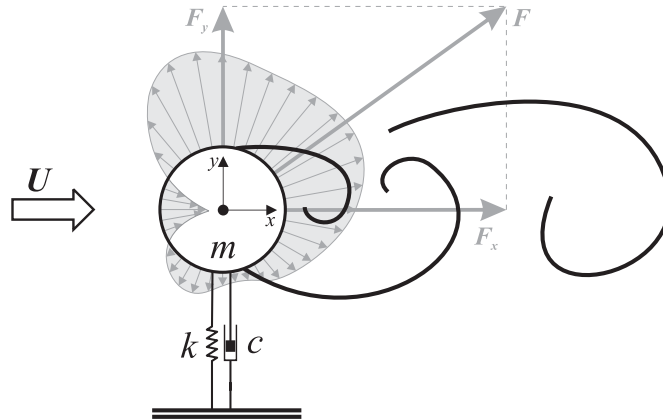
Fig. 2.4: Harmonic oscillator model representing an elastically mounted cylinder. The pressure field in the background is adapted from Drescher (1956).

2.2 Vortex-induced vibration of a single cylinder

Vortex-induced vibration is a type of FIV that has its origin in the cyclic loads generated by vortices around a bluff body. Several authors have produced comprehensive reviews about the VIV mechanism of a single cylinder (Sarpkaya, 1979; Bearman, 1984; Parkinson, 1989; Blevins, 1990; Zdravkovich, 1997). In this section we introduce the phenomenological aspects that will be useful when studying FIV mechanisms on a pair of cylinders.

In the same way that an asymmetric pressure distribution generates drag in the streamwise direction, an asymmetry of the pressure field in relation to the other orthogonal plane of the cylinder generates a fluid-dynamic lift force in the cross-flow direction. Once the symmetry in the wake is broken (very early in the Re scale) the cyclic mechanism of vortex shedding changes the pressure field around the body. Within one shedding cycle the cylinder will experience a change in the direction of lift as vortices are formed and released.

Fig. 2.4 shows a schematic representation of the pressure field around a cylinder for the instant when a vortex is being formed at the upper side of the body. Arrows pointing outwards from the cylinder wall represent relative suction. By integrating the pressure field around the circumference a resultant force F is obtained, which can be projected into a drag component F_x and a lift component F_y in relation to the x and y axes. During the cycle of vortex shedding F_y and F_x will fluctuate

according to the shedding frequency f_s. Because two vortices are shed during one cycle, one from each side of the cylinder, the frequency of fluctuation of the lift force will be f_s, while the drag component fluctuates with $2f_s$.

Turning back to Fig. 2.3 we can now examine the behaviour of the fluctuating terms of drag and lift represented by $\hat{C}_D$ and $\hat{C}_L$. When a regular wake of alternating vortices is developed around $\mathrm{Re} = 10^4 - 10^5$ we observe a fluctuation in the drag force plotted as the dashed line $\hat{C}_D$ that would have frequency $2f_s$. In the same way, fluctuations in the lift force $\hat{C}_L$ also appear with the formation of alternating vortices and follow the shedding frequency f_s. Fluctuations of lift are more intense than the drag component and a considerable reduction in both $\hat{C}_L$ and $\hat{C}_D$ is also observed after the transition to the fully turbulent regime. As mentioned before, experiments in the present work were designed to be in the range $\mathrm{Re} = 10^3 - 10^5$, where $\overline{C}_D$, $\hat{C}_D$ and $\hat{C}_L$ are stabilised around their maximum values for the developed wake regime with laminar boundary layers.

2.2.1   Elastically mounted cylinder

Now, if a cylinder is considered to be an elastic structure — which is the case for engineering applications — it will present structural properties such as mass (m), stiffness (k) and damping (c), characterizing the dynamic system represented in Fig. 2.4. Due to the cyclic nature of vortex shedding in the near wake the body experiences fluid force fluctuations that can excite the system into VIV. Allowing for displacements only in one degree of freedom (1-dof) in the y-axis, the equation of motion for the harmonic oscillator can be modelled by

$$m\ddot{y} + c\dot{y} + ky = F_y(t) \tag{2.3}$$

$$y(t) = \hat{y}\sin(2\pi ft), \tag{2.4}$$

where y, $\dot{y}$ and $\ddot{y}$ are respectively the displacement, velocity and acceleration of the body and $F_y(t)$ is the time-dependent fluid force in the cross-flow direction.

Following an analysis proposed by Bearman (1984), $y(t)$ of a cylinder under VIV may be expressed by the harmonic response of a linear oscillator. In Eq. 2.4, $\hat{y}$ and

f respectively represent the harmonic amplitude and frequency of oscillation. The fluid force and the body response oscillate at the same frequency f, which is usually close to the natural frequency of the system for large-amplitude oscillations under a steady-state regime of VIV. According to this 'harmonic forcing and harmonic motion' hypothesis the fluid force can be expressed by

$$F_y(t) = \hat{F}_y \sin(2\pi f t + \phi), \tag{2.5}$$

where ϕ is the phase angle between the displacement and the fluid force. For body excitation to occur, the phase angle between $y(t)$ and $F_y(t)$ must be between $\phi = 0°$ and $180°$. A phase angle equal either to $0°$ or $180°$ means that no energy is transferred from the fluid to the structure to excite any vibration.

A linear oscillator presents an undamped natural frequency

$$f_0 = \frac{1}{2\pi}\sqrt{\frac{k}{m}} \tag{2.6}$$

that only takes into account the structural stiffness (k) and mass of the system (m). The structural damping is generally expressed by a damping ratio

$$\zeta = \frac{c}{2\sqrt{km}}, \tag{2.7}$$

defined as a fraction of the critical damping. If the structural damping is kept sufficiently low, the damped natural frequency $f_{0_d} = f_0\sqrt{1-\zeta^2}$ can be considered approximately equal to f_0.

As one might expect F_y is non-dimensionalised into the corresponding force coefficient

$$C_y(t) = \frac{F_y(t)}{\frac{1}{2}\rho U^2 DL}, \tag{2.8}$$

which can be divided into a time-average term $\overline{C}_y$ and a transient term modelled as a sine wave with amplitude $\hat{C}_y$, hence

$$C_y(t) = \overline{C}_y + \hat{C}_y \sin(2\pi f t + \phi). \tag{2.9}$$

The drag component is similarly non-dimensionalised into a mean $\overline{C}_x$ and a fluctuating term $\hat{C}_x$; however the mean drag is different to zero most of the time. The value of $\overline{C}_x$ is of great interest for engineering applications and will be of used when we discuss techniques to suppress FIV without increasing drag.

2.2.2 Typical VIV response

Now, if the frequency of vortex shedding is close to the natural frequency of oscillation of the structure ($f_s \approx f_0$), the system will respond with a type of resonance phenomenon that amplifies the amplitude of vibration.

Experimental results showing a typical response of VIV are presented in Fig. 2.5, where non-dimensional amplitude and frequency of oscillation are plotted against reduced velocity. Williamson & Govardhan (2004) classified three different branches of response for low mass and damping cylinders: an *initial branch* in which the oscillation starts to build up; an *upper branch* of maximum amplitude around the resonance peak; and a *lower branch* that persists until the oscillations eventually die out.

It is useful to represent the flow speed non-dimensionalised by the cylinder diameter and the natural frequency of oscillation creating a parameter called reduced velocity defined as U/Df_0. The reduced velocity for maximum VIV amplitude occurs around U/Df_s (the inverse of the Strouhal number), that is around the resonance where $f_s = f_0$.

As flow speed (U) increases, vortex-shedding frequency (f_s) gets close enough to the body's natural frequency of oscillation (f_0) in a way that the unsteady pressure fluctuation in the near wake induces the body to respond in resonance. Once the cylinder starts to oscillate, high-amplitude movements will control the vortex formation and f_s will be *locked-in* by the oscillation frequency (f) near f_0. If the velocity continues to increase the typical vortex-shedding frequency will move far away from the natural frequency of the system and f_s and f will be uncoupled again

In the frequency plots of Fig. 2.5 the dashed line of St = 0.20 gives an idea of the expected vortex shedding frequency for a fixed cylinder versus reduced velocity. Where this line crosses unity the frequency of the excitation f_s is very close to the natural frequency of the system and an amplified peak of amplitude gives evidence of a resonant behaviour. The range of reduced velocity between the beginning of the initial branch and the end of the lower branch is called the synchronisation or
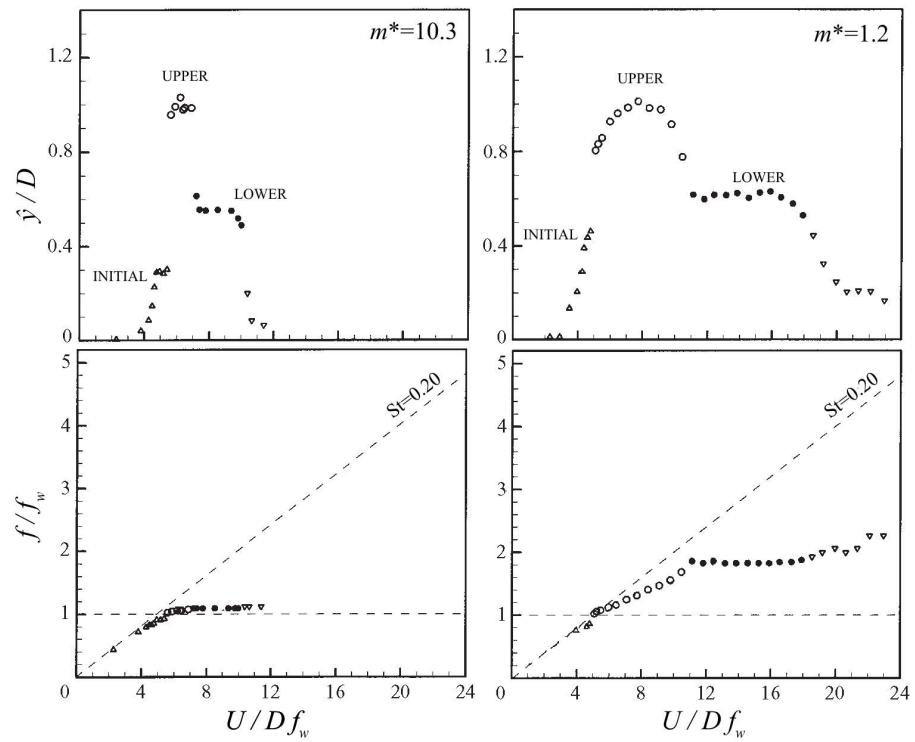
Fig. 2.5: Typical VIV response (amplitude and frequency) of a single cylinder. $m^*\zeta \approx 0.01$ for both data-sets. Note that the frequency of oscillation and the reduced velocity are non-dimensionalised using the natural frequency in still water (f_W) and not the natural frequency in air (f_0) as usual. Adapted from Govardhan & Williamson (2000).

lock-in range.

Depending on the mass of the system and the specific mass of the fluid in which the cylinder is immersed, the natural frequency of oscillation can be significantly influenced by the additional mass of fluid that is accelerated with the body. For heavy cylinders immersed in air, the added fluid mass can be neglected, but for light cylinders immersed in water the body's mass and the added fluid mass can have the same order of magnitude. For this reason, the parameter

$$m^* = \frac{m}{\rho \frac{\pi D^2}{4} L} \tag{2.10}$$

is very important for FIV analysis and represents the ratio of total oscillating structure mass (m) to the mass of displaced fluid (L being the submerged length of the cylinder). As a consequence of the added fluid mass, the body's natural frequency in air (f_0) will be different from the natural frequency in still water (f_W).

According to Bearman (1984) a simple analysis for a linear oscillator model of VIV, assuming harmonic forcing and harmonic response, shows that response is inversely proportional to the product of m^* and ζ. Differentiating $\dot{y}$ and $\ddot{y}$ from Eq. 2.4, replacing them together with Eq. 2.5 in Eq. 2.3 and equating sine and cosine terms, results in an expression for the amplitude of response non-dimensionalised by the diameter

$$\frac{\hat{y}}{D} = \frac{1}{4\pi^3} \hat{C}_y \sin \phi \left(\frac{U}{Df_0} \right)^2 \left(\frac{1}{m^*\zeta} \right) \left(\frac{f_0}{f} \right). \tag{2.11}$$

Analogously, the frequency of oscillation non-dimensionalised by f_0 can be obtained as

$$\frac{f}{f_0} = \left[1 - \frac{1}{2\pi^3} \hat{C}_y \cos \phi \left(\frac{U}{Df_0} \right)^2 \left(\frac{1}{m^*} \right) \left(\frac{D}{\hat{y}} \right) \right]^{\frac{1}{2}}. \tag{2.12}$$

Bearman (1984) comments that for large-amplitude oscillations of a bluff body in air, where the m^* parameter might be typically of order 10^3, the frequency of body oscillation should be close to its natural frequency. However, for bodies immersed in denser fluids such as water, where the m^* parameter may be of order unity, f can be significantly different from f_0. This is observed in the frequency plots of Fig. 2.5. For $m^* = 10.3$ the frequency of oscillation during the synchronisation range is very close to 1, but when m^* is reduced to 1.2 the frequency of oscillation

almost doubles. Govardhan & Williamson (2000) showed that while the maximum amplitude is related to the product $m^*\zeta$, the widening of the synchronisation range in relation to reduced velocity is associated to the m^* parameter alone. This is also shown in their results plotted in Fig. 2.5 where both data-sets have a similar value of $m^*\zeta \approx 0.01$ but with a one order of magnitude difference in m^*.

From Eqs. 2.11 and 2.12 Bearman (1984) states that "It is clear that the phase angle ϕ plays an extremely important role. The amplitude response does not depend on $\hat{C}_y$ alone but on that part of $\hat{C}_y$ in phase with the body velocity. Hence, measurements of the sectional fluctuating lift coefficient on a range of stationary bluff-body shapes will give little indication of the likely amplitudes of motion of similar bodies flexibly mounted". Combining Eqs. 2.11 and 2.12 it is possible to calculate

$$\phi = \arctan \frac{2\zeta(f/f_0)}{1 - (f/f_0)^2} \tag{2.13}$$

by knowing ζ and f_0 and measuring f.

Khalak & Williamson (1999) also performed experiments with low mass-damping systems in order to investigate the behaviour of ϕ in relation to the response branches. Fig. 2.6 presents their results showing a clear identification of the initial, upper and lower branches of response mentioned above. The bottom graph reveals a phase shift of almost 180° in ϕ when the response changes from the upper to the lower branch. This phase shift is associated with different modes of vortex shedding in the wake as will be explained below.

2.2.3   Decomposition of fluid forces

As discussed by Williamson & Govardhan (2004), the total fluid force acting on the cylinder can be divided into two components: a *potential-force* component F_{y_P}, given by the ideal flow inertia force; and a *vortex-force* component F_{y_V}, due only to the dynamics of the vorticity field around the body:

$$F_y = F_{y_P} + F_{y_V}. \tag{2.14}$$

By definition, F_{y_P} is always opposing the body's acceleration and its magnitude is proportional to the product of the displaced fluid mass and the acceleration of the

body. On the other hand, F_{y_V} essentially depends on the dynamic of vortices in the wake and may be expressed in terms of another phase angle ϕ_V in relation to the displacement of the cylinder $y(t)$, resulting in

$$\hat{C}_y \sin(2\pi ft + \phi) = \hat{C}_{y_P} \sin(2\pi ft + 180°) + \hat{C}_{y_V} \sin(2\pi ft + \phi_V), \qquad (2.15)$$

expressed in terms of force coefficients. Later in the present work this decomposition will be applied to analyse fluid forces acting on the downstream cylinder of a tandem pair.

The transition between branches is accompanied with an almost 180° phase shift first in ϕ_V and then in ϕ. The phase shift in ϕ_V is associated with a transition between two different modes of vortex shedding and occurs as the oscillation frequency (f) passes through the body's natural frequency in water (f_W). For cylinders oscillating in the initial branch (as well as static bodies) we observe *two single* vortices being shed per cycle, therefore the name '2S mode' as illustrated by PIV measurements in Fig. 2.6. But for oscillations occurring in the upper and lower branches, *two pairs* of vortices are shed during each cycle, suggesting the nomenclature '2P mode'. The phase shift in ϕ occurs when f passes through f_0 and marks the beginning of the lower branch.

Khalak & Williamson (1999) talk about interesting phenomena of hysteresis and intermittence associated with the first and second transitions between branches. It is important to note that in such a self sustained regime of oscillation a change in the response is clearly related to a change in the vortex shedding mode in the wake. That is to say that the response of the structure is strongly dependent on the vortex shedding mechanism, and vice versa, within the synchronization range. This emphasises the importance of the phase angle between F_y and y in inputting energy into the system to sustain different regimes of VIV.

Equating sine and cosine terms in Eq 2.15, it is possible to determine

$$\phi_V = \arctan \frac{\hat{C}_y \sin \phi}{\hat{C}_y \cos \phi - 2\pi^3 \frac{\hat{y}}{D} \left(\frac{f}{f_0}\right)^2 \left(\frac{U}{Df_0}\right)^{-2}}, \qquad (2.16)$$

given that the amplitude and frequency of vibration and fluid forces are known. Since F_{y_P} is by definition in antiphase with the acceleration and proportional to the
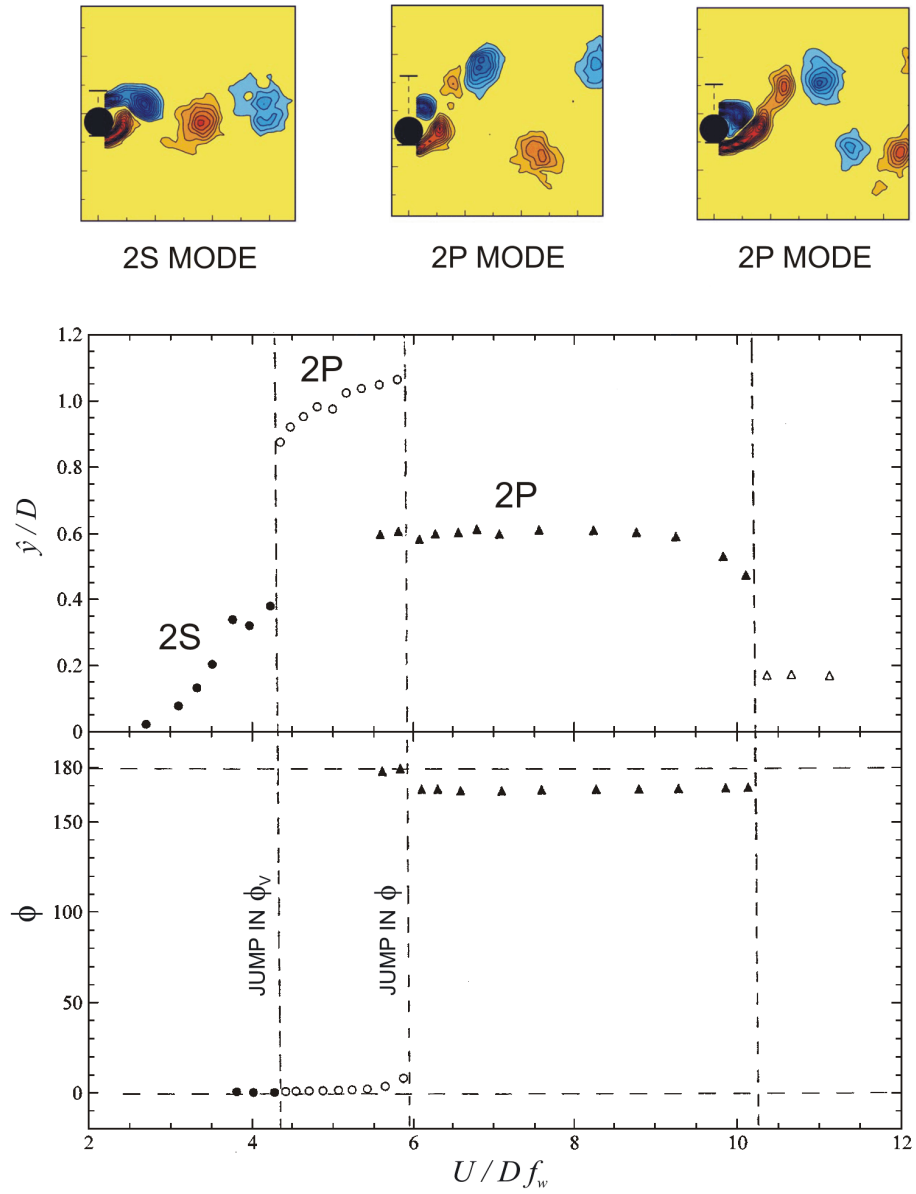
2S MODE   2P MODE   2P MODE

Fig. 2.6: Amplitude response and phase angle ϕ versus reduced velocity (non-dimensionalised using the natural frequency in still water f_W). Data points are for $m^* = 3.3$, reproduced from Khalak & Williamson (1999); modes of vortex shedding obtained with PIV are adapted from Govardhan & Williamson (2000).

mass of displaced fluid, $\hat{C}_{y_P}$ can be expressed by

$$\hat{C}_{y_P} = 2\pi^3 \frac{\hat{y}}{D} \left(\frac{f}{f_0}\right)^2 \left(\frac{U}{Df_0}\right)^{-1} \tag{2.17}$$

and the remaining vortex-force term $\hat{C}_{y_V}$ by

$$\hat{C}_{y_V} = \left(\hat{C}_y^2 + \hat{C}_{y_P}^2 - 2\hat{C}_y\hat{C}_{y_P}\cos\phi\right)^{1/2}. \tag{2.18}$$

2.3   Other types of FIV

VIV appears to be the FIV mechanism with greater relevance to the present work. However, there are other fluid-elastic mechanisms that occur for a single cylinder that may shed some light on the understanding of WIV of interfering structures. Before we move on to a pair of interfering cylinders, let us discuss briefly some of these other mechanisms.

While VIV has its origin in the vortex shedding mechanism, other types of FIV may as well come from different sources of excitation in the flow. Assuming that an elastic structure can be usually represented by the second order system presented on the left-hand side of Eq. 2.3 the fluid force $F_y(t)$ may be modelled in different ways other than Eq. 2.5 in order to describe distinct flow phenomena. Surface waves in water, for example, can also generate harmonic fluctuations in the pressure field around the body causing vibrations that are amplified around the resonance. But the characteristic frequency of this excitation is not related to the bluff body shedding frequency nor is synchronised by the oscillation of the body.

Non-harmonic excitations from the fluid may also generate vibrations. Random fluctuations in the free stream such as turbulence may induce a type of vibration called *buffeting*. Turbulent flows present unsteady components with many different scales and frequencies spread across a wide spectrum. Depending on turbulence intensity and structural properties the body may respond with vibrations around the natural frequency, as if it were excited by a random 'white noise'. Acoustic fluctuations and other sources of random pressure fluctuation may also have a similar effect.

An elastic structure placed in front of a steady jet may be excited into vibrations as the jet switches from one side of the body to the other, inputting energy into the system in a mechanism called *jet-switching*. The presence of the structure interacts with the jet causing a change in momentum that generates fluid forces acting on the body. A low-momentum shielded flow (the opposite of a high-momentum jet) may excite structures in a similar fashion.

2.3.1   Classical galloping of noncircular bodies

A second FIV mechanism that is most relevant to the present study is *classical galloping*. In principle, the terminology 'galloping' can be associated to any fluid-elastic instability that occurs in one degree of freedom. In this sense, the typical VIV of a cylinder oscillating only in the transverse direction is a type of galloping. However, 'galloping' has been generally employed to describe a specific type of FIV mechanism that occurs for bluff bodies with non-circular cross sections. In the present work we shall refer to it as 'classical galloping' to avoid confusion. Comprehensive reviews of the classical galloping theory were written by Parkinson (1971, 1989) and Blevins (1990). Yet a brief description of the mechanism presented here will help the understanding of other FIV mechanisms to be discussed later in this text.

Classical galloping of non-circular cylinders is caused by a fluid-dynamic instability of the cross section of the body such that the motion of the structure generates forces which increase the amplitude of vibration (Bearman *et al.*, 1987). Consider the bluff body presented in Fig. 2.7. A square section with sides D is mounted on an elastic system (m, c, k) allowing displacements in the y-axis only. It is exposed to a steady flow with velocity U normal to one of its sides. If a small perturbation happens to displace the body from rest the relative velocity of the flow will be a vectorial sum of U and the body's velocity $\dot{y}$, defined by an angle of attack α in relation to the free stream.

Differently from a circular cylinder, a square body presents sharp edges causing shear layers from both sides to separate at fixed separation points located at the
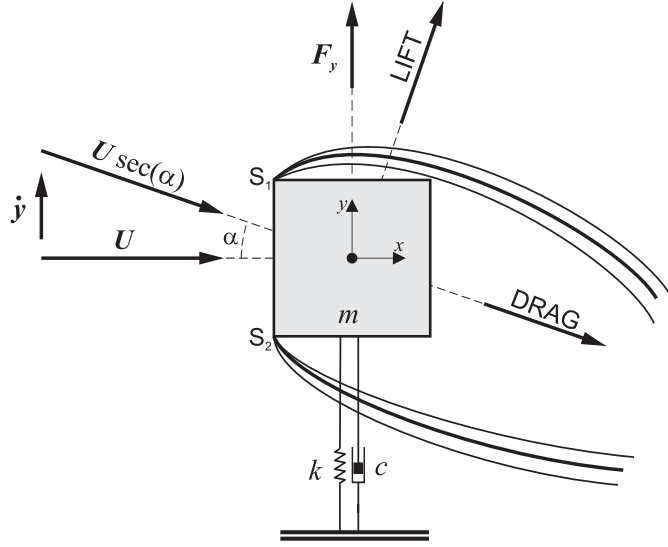
Fig. 2.7: One-degree-of-freedom model for classical galloping of a square section bluff body. Adapted from Blevins (1990).

front corners. Now, if the body presents relative cross-flow motion $\dot{y}$ the shear layers separating from each side will generate an asymmetric flow field with consequent asymmetric pressure distribution, resulting (in this case) in a fluid force F_y in the same direction as the motion that contributes to increase the displacement.

Evidently the stiffness of the spring will act to restore the body back to $y = 0$, but when it reaches a maximum displacement and $\dot{y}$ changes direction the process is inverted, though with F_y still acting in the same direction as $\dot{y}$. Therefore, in the classical galloping mechanism the cross-flow fluid force is in phase with the body's velocity acting as a negative damping term in the equation of motion (Eq. 2.19). Hence, classical galloping is classified as a damping-controlled fluid-elastic mechanism. The magnitude of F_y increases with α, which itself increases with $\dot{y}$, resulting in a continuous increase in the body's steady state amplitude of vibration with increasing flow speed. "For while VIV is typically limited to amplitudes less than $1D$, galloping amplitudes can be many times D" (Parkinson, 1971).

As discussed, classical galloping is not associated with the vortex shedding mechanism of bluff bodies. Of course a vortex wake will develop further downstream of a square section as in any other bluff body, but this instability is not a resonant mechanism that depends on matching values of f_0 and f_s. For this reason classical galloping allows for modelling with a quasi-steady approach considering that the
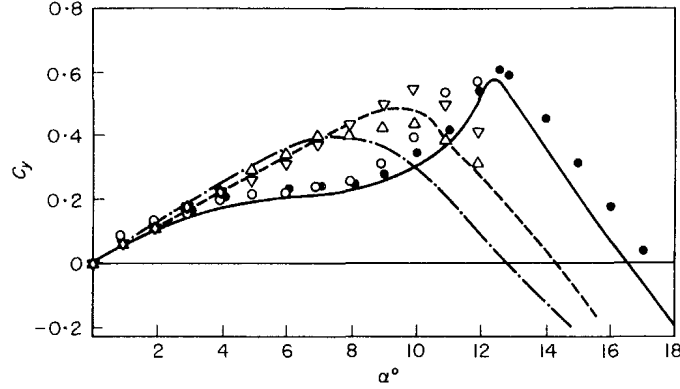
Fig. 2.8: Transverse force coefficient C_y as a function of angle of attack α for square section. $Re = 12 \times 10^3 - 32 \times 10^3$, $TI = 0\% - 12\%$. Reproduced from Bearman *et al.* (1987).

fluid force on the structure is assumed to be determined solely by the instantaneous relative velocity. "The quasi-steady assumption is valid only if the frequency of periodic components of fluid force, associated with vortex shedding or time-lag effects, is well above the vibration frequency of the structure ($f_s \gg f_0$)" (Blevins, 1990). This is generally the case for high values of reduced velocity.

Of course a square section bluff body is also susceptible to typical VIV for low reduced velocities, however this may be combined with a galloping excitation that will persist even after the resonant VIV range has finished. "While vortex-induced oscillations occur only in discrete ranges of [flow] speed, galloping will occur at all flow speeds above a critical value determined by the structural damping" (Parkinson, 1971).

Parkinson (1971), referring to den Hartog (1956), presents a simplified quasi-steady analysis that is very useful in predicting the stability of a 1-dof system to classical galloping. Consider that the lift force acting on the body is a function of angle of attack and can be measured experimentally by rotating a static body in a steady flow. This result is presented in Fig. 2.8 revealing a similar behaviour for C_y versus α for different Reynolds numbers and turbulence intensity. In a first order approximation for small oscillations F_y can be expanded in power series neglecting terms of order higher than α^2, as shown in the right-hand side of

$$m\ddot{y} + c\dot{y} + ky = \frac{1}{2}\rho U^2 D \left[C_y|_{\alpha=0^\circ} + \left.\frac{\partial C_y}{\partial \alpha}\right|_{\alpha=0^\circ} \alpha + O(\alpha^2) \right]. \qquad (2.19)$$

As a result, the dynamic stability of the body will depend only in the slope of C_y

38

at attitude $\alpha = 0°$, with the condition for galloping to develop being

$$\left. \frac{\partial C_y}{\partial \alpha} \right|_{\alpha=0°} > 0. \tag{2.20}$$

According to Fig. 2.8 it is evident that this condition is satisfied for a square section.

Classical galloping oscillations will develop if F_y (which is in phase with $\dot{y}$ and takes the form of a negative damping) is large enough to overcome the positive damping of the structure. Therefore, both flow speed for the onset of galloping and amplitude of oscillation will depend on the structural damping of the system. By balancing the negative damping generated by F_y and the structural damping term of the equation of motion $(c\dot{y})$ it is possible to determine the critical reduced velocity for classical galloping to occur, given by

$$\left[\frac{U}{Df_0} \right]_{\text{crit}} = 2\pi^2 m^* \zeta \left[\left. \frac{\partial C_y}{\partial \alpha} \right|_{\alpha=0°} \right]^{-1}. \tag{2.21}$$

Parkinson (1971) performed experiments with different values of structural damping verifying that the critical flow speed for the onset of the classical galloping instability indeed depends on the mass-damping parameter of the system as well as $\partial C_y / \partial \alpha$ at $\alpha = 0°$, which defined by the geometry of the body. Depending on structural parameters m^* and ζ galloping instability can appear for relatively low reduced velocities, overlapping with the VIV range.

Such a linear approach is useful for predicting the onset velocity for galloping, but as the oscillations grow in amplitude this first order simplification is not valid any longer. An improved model must take into account the nonlinear variation of C_y versus α. A first order theory predicts that if C_y increases indefinitely with α the amplitude will also increase with flow speed ad infinitum. It is evident from Fig. 2.8 that this is not the case, but the slope of the curve changes with the angle of attack ($\alpha = 14°$ means that that $\dot{y}$ is almost 25% of U). In fact, the amplitude of oscillation is limited by non-linear effects between C_y and α that are not incorporated in this first approximation.

Blevins (1990) writes that "the major limitation of the [classical] galloping theory is that the aerodynamic coefficients are assumed to vary only with angle of attack, but experience shows that the coefficients are affected by turbulence and vortex

shedding." He states that the quasi-steady assumption employed in this analysis requires that the vortex shedding frequency be well above the natural frequency so that "the fluid responds quickly to any structural motion.". Based on experimental works found in the literature he concluded that "the reduced velocity must exceed 20 [] and the amplitude of vibration cannot exceed 0.1 to $0.2D$ for application of the quasi-steady theory." Such considerations bring tight restrictions to quasi-steady assumptions and question the application of this approach to flow-induced vibrations of circular cylinders with interference (as will be described later in this text).

Following the same principle presented above, the terminology *flutter* can be associated with fluid-elastic mechanisms occurring in two degrees of freedom. As will be described later, 2-dof oscillations of a cylinder in the xy-plane can be classified as a type of flutter. However, the common use of the term is historically attached to the problem of wing instability caused by a combined effect of vertical and torsional displacements. Blevins (1990) extends an analogous quasi-steady analysis for a 2-dof system and describes the classical example of flutter of an aerofoil.

More than one single FIV mechanism may be acting on a structure at the same time. For example, an offshore riser may be subject to turbulence buffeting, classical galloping, vortex-induced vibrations and wave excitation all at once. Sometimes different FIV mechanisms will be coupled, making it an impossible task to identify and model them independently. But careful experiments are designed to limit the number of parameters and variables in the system in order to separate only those relevant to a specific fluid-elastic mechanism.

Chapter 3

Literature review: Flow-induced vibration of the downstream cylinder

With a better understanding of the fluid-elastic mechanism occurring for a single cylinder we are ready to add another identical body in the system and expand our investigation into FIV of a pair of cylinders. This chapter introduces a few characteristics of the flow around a pair of cylinders and discusses some of the mechanisms that have been suggested in the literature as the origin of vibrations of bluff bodies with flow interference.

As we saw in Chapter 2, the alternate shedding of vortices from a bluff body is the origin of its vortex-induced vibrations, but other types of excitation from the flow may also result in different types of flow-induced vibrations.

3.1   Flow interference around a pair of cylinders

In the present work we are particularly concerned with the flow interference between a pair of cylinders in tandem (both cylinders aligned with the free stream, $y_0 = 0$ in Fig. 3.1). The streamwise separation x_0 is defined from the centre of one cylinder to the centre of the other. It is not difficult to imagine that coherent flow structures
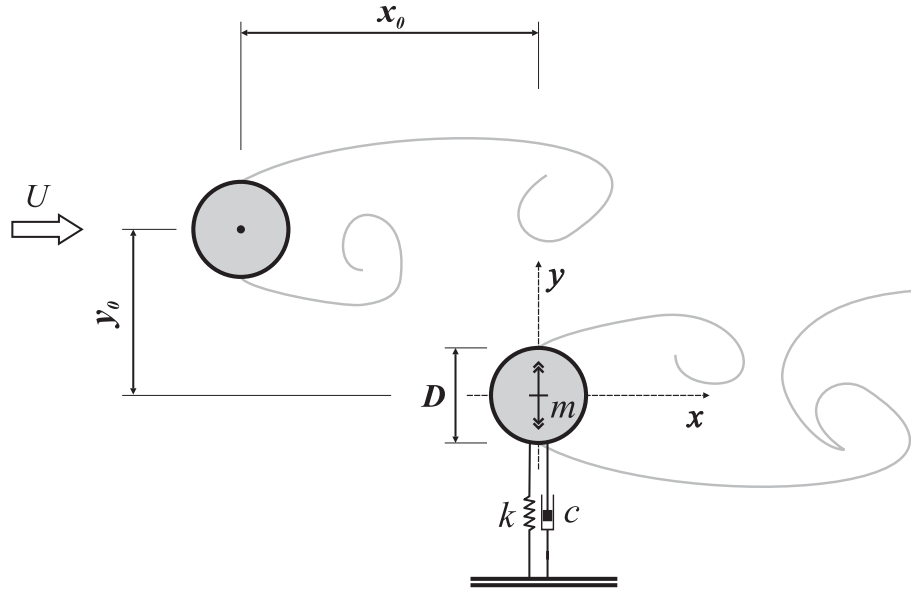
Fig. 3.1: Tandem arrangement of a pair of circular cylinders. x_0 is measured from centre to centre.

from a source located upstream will interfere with the fluid-elastic dynamic of a second body placed downstream. The cylinder placed upstream is exposed to a clear free stream with velocity U, but the downstream body is immersed in a disturbed flow region created by the wake of the first cylinder. (Reynolds number is based on the velocity for the upstream body.)

Vortices shed from the first body will not only pass by or impinge on the second cylinder, but also interfere with its own vortex shedding process forming the downstream wake. Now, if the second cylinder is mounted on an elastic base, as the one described in Chapter 2, the response of the body will not be a simple VIV, but a type of vibration that is influenced by the wake coming from the upstream body. But before we analyse in detail the dynamic response of this body, we should consider some fundamental aspects of the flow interference around two static cylinders.

3.1.1 Interference regimes in the wake of a pair of static cylinders

Early experiments with tandem static cylinders identified two different interference regimes associated with the formation of a developed vortex street in the gap between the bodies. The gap flow is characterised by the presence of two unstable shear
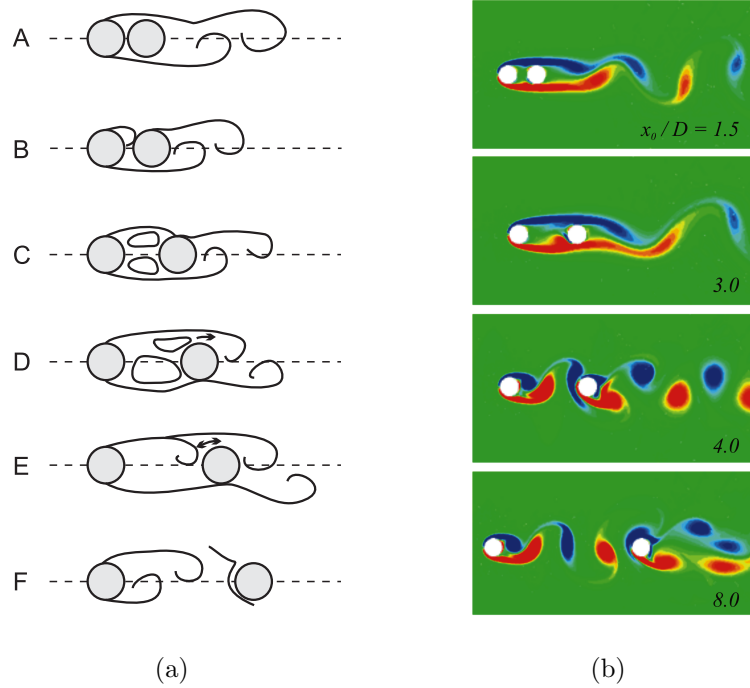
Fig. 3.2: Regimes of flow interference for tandem cylinders for different separations. (a) Classification of tandem interference regimes proposed by Igarashi (1981). (b) Numerical simulations from Carmo (2005), Re = 300.

layers that, depending on x_0 and Re, may reattach to the second cylinder, form regions of recirculation or even a fully developed vortex street in the gap. Igarashi (1981) presented a detailed classification dividing this behaviour into six categories, as illustrated from 'A' to 'F' in Fig. 3.2(a). More recently, Sumner *et al.* (2000) produced a detailed classification of interference regimes for various configurations of staggered cylinders.

When both cylinders are close to each other the shear layers released from the upstream cylinder do not interact in the gap flow but create a streamlining effect around both bodies. They reattach to the downstream cylinder such that no vortex shedding is produced in the gap flow and only one wake is observed for both bodies ('A' and 'B'). Increasing the separation, two recirculation zones appear in the gap ('C' and 'D'). First, they are symmetric, but later they alternate as the reattachment of the shear layer is also alternating. Hori (1959) observed that the side of the downstream cylinder "facing the gap between the cylinders had a very low pressure, which was almost the same as the corresponding value of the base pressure of the

upstream cylinder. This fact is an indication that the flow in the gap is almost stagnant." This was verified by measuring the velocity profile with a hot-wire probe in the gap between the cylinders (Zdravkovich & Stanhope, 1972). Hori (1959) also found that, for certain separations, the negative gap pressure coefficient was lower than that on the base side of the downstream cylinder. "Hence the downstream cylinder experienced a negative drag."

Measuring the pressure distribution around the downstream cylinder, Zdravkovich & Stanhope (1972) found two symmetrically positioned maxima that were believed to correspond to the reattachment of the flow separating from the upstream cylinder. These two peaks rotate closer together to the front of the downstream cylinder as the separation x_0 increases. Consequently, they inferred the existence of two major flow patterns: (i) the first happening for separations below a critical value, with the downstream cylinder presenting two maxima in the pressure distribution; (ii) and the second for separations greater than a critical value, with the downstream cylinder only presenting one maximum in the pressure distribution (corresponding to the frontal stagnation point). Zdravkovich (1977) suggests that during the first regime an "elastic upstream cylinder should be less prone to vibrations due to vortex shedding" since no developed wake is formed in its vicinity.

The beginning of the second regime is associated with the transition from flow pattern 'E' to 'F' in Fig. 3.2(a). For a sufficiently large separation beyond a critical x_0 the shear layers start to roll up in the gap (pattern 'E') and finally reach a regime in which a fully developed vortex street is formed behind the upstream cylinder (pattern 'F'). Entrained flow is observed in the gap and the stagnant velocity profile immediately changes into a typical wake profile. Both regimes are illustrated in the numerical simulations performed by Carmo (2005) and presented in Fig. 3.2(b), where the critical separation is located somewhere between $x_0/D = 3.0$ and 4.0. Zdravkovich (1977) comments that "the commencement of vortex shedding behind the upstream cylinder strongly affects and synchronises the vortex shedding behind the downstream one. Hence, both cylinders should be equally prone to flow-induced vibrations due to vortex shedding".

Nevertheless, the critical x_0 appears to have some dependency on Reynolds

number with most of the literature agreeing in a value between $x_0/D = 3.0$ and 4.0 for subcritical Re (Ljungkrona *et al.*, 1991). It is known that the vortex formation length of a single cylinder varies with Re. Lin *et al.* (1995) and Norberg (1998) show that it decreases with increases in Re in the range Re $= 10^3 - 10^5$, resulting in vortices forming closer to the base of the cylinder. Lin *et al.* (2002) and Assi (2005) also show similar results for a pair of tandem cylinders. Turbulence intensity in the free stream also affects the angle of separation on the upstream cylinder. Therefore, contrary to what has been done in the past, we believe it is not prudent to denote a universal value for a critical separation as we now know it depends on other parameters as well. While Zdravkovich & Stanhope (1972) found a critical $x_0/D = 3.6$ for Re $= 8.8 \times 10^3$, Zdravkovich (1972) did not observe a developed wake in the gap for $x_0/D < 4.0$ for low Reynolds numbers between 40 and 250. Based on a compilation of results from Zdravkovich (1977) we infer that the critical separation varies between $x_0/D = 3.1$ and 3.8 within the range Re $= 5 \times 10^3 - 2 \times 10^5$.

3.1.2   Interference regime in the wake of oscillating cylinders

The classification of flow interference regimes presented so far is attributed to a pair of tandem cylinders that are stationary. "When either or both of the cylinders are elastic or vibrate, the flow field becomes significantly more complicated because of the interaction of the fluid flow and the cylinder motion" (Chen, 1986).

Assi *et al.* (2006) showed that when the downstream cylinder is allowed to oscillate the interference between both bodies will be drastically changed depending on the amplitude of oscillation and Reynolds number. Fig. 3.3 presents two different regimes for the same centre-to-centre separation of $x_0/D = 3.0$ but at different Re and amplitude $\hat{y}$. When the maximum amplitude of oscillation is about 0.2 diameters both shear layers were found to reattach to the second cylinder (Fig. 3.3(a)). But, when the amplitude builds up to about 1 diameter, the large displacements of the downstream cylinder breaks the reattachment of the shear layers and a vortex street is formed in the gap flow close to the upstream cylinder (Fig. 3.3(b)).
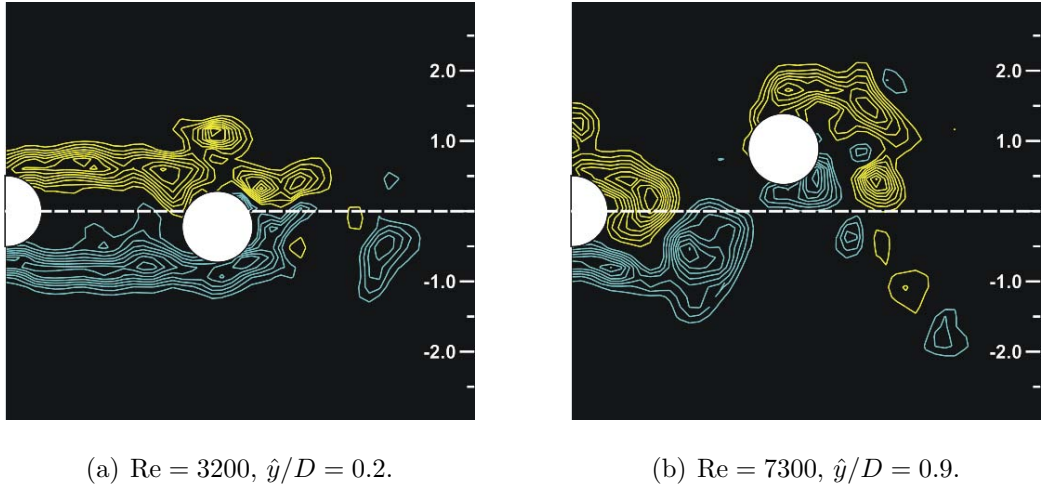
(a) Re = 3200, $\hat{y}/D = 0.2$.   (b) Re = 7300, $\hat{y}/D = 0.9$.

Fig. 3.3: Different regimes of flow interference for the same separation $x_0/D = 3.0$ at different Re and $\hat{y}$. Downstream cylinders are shown at maximum displacement. Vorticity contours obtained with PIV. Reproduced from Assi *et al.* (2006).

3.2 FIV of cylinders with flow interference

Resuming the topic discussed in Chapter 2, we can now bring together concepts developed in the previous section to study the flow-induced vibration of a pair of cylinders with flow interference. The complexity of such a study is significantly increased simply by having two bodies placed together in one fluid-dynamic system; the number of variables and parameters more than double. For example, now we not only consider structural properties (m, c, k) of both cylinders, but also new degrees of freedom and geometric variables such as the initial position (x_0, y_0) of the cylinders in relation to themselves and the free stream.

Zdravkovich (1988) stated that "the different number of degrees of freedom of cylinders employed in various experiments showed such a wide variety of responses in wind and water tunnels that the governing mechanisms appeared obscure and incomprehensible". Following the same philosophy of work, we will restrain the problem to as few variables as possible in order to identify important parameters and understand the fluid-structure mechanism behind the vibrations. Therefore, our first simplifying assumption will consider that the upstream cylinder is stationary and only the downstream cylinder is free to respond in one degree of freedom (1-dof) in the cross-flow direction (y-axis).
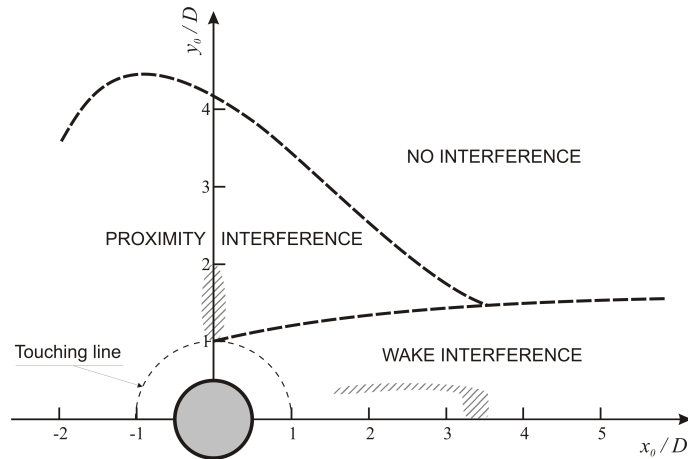
Fig. 3.4: Sketch of interference regions. Hatched areas mean bistable flow regions. The upstream cylinder is stationary. Adapted from Zdravkovich (1988).

As mentioned above, the main purpose of the present work is to investigate FIV of cylinders that are initially arranged in tandem. But during the oscillations the downstream cylinder will naturally be displaced sideways from the centreline of the upstream cylinder. For that reason, we believe it is helpful to make some considerations about FIV of a pair of cylinders in staggered arrangements ($x_0/D > 1$, $y_0 \neq 0$, in Fig. 3.1).

3.2.1 Fluid-elastic interference regions

Following a collection of several works, Zdravkovich (1988) compiled a map of interference regions that affect FIV of a pair of cylinders in different staggered arrangements (Fig. 3.4). He identified three regions according to the nature of the excitation. If the second cylinder is too far apart from the static cylinder it will not suffer any interference from its presence and should respond as an isolated cylinder. This is identified as the 'no interference' region outside the dashed lines in Fig. 3.4.

'Proximity interference' is the region where the second cylinder is close enough to suffer interference from the flow deflected by the static cylinder, but is not immersed in its wake. In this region the unsteady phenomenon of vortex shedding from the static cylinder has a minor effect on the second body and is generally neglected. The most investigated of these configurations is the side-by-side arrangement. Finally, when the second cylinder is immersed or under the influence of the wake of the

stationary cylinder it is said to experience 'wake interference'. This third region is where we will concentrate our attention from now on.

3.2.2 Steady fluid forces

Before considering the fluid-dynamic mechanism of a cylinder oscillating in the wake of another, it is appropriate to analyse the fluid forces that appear if the second cylinder is also stationary. This analysis is the foundation for quasi-static and quasi-steady assumptions that have been widely employed in the literature and will be referred to later in this text.

We saw in Chapter 2 that a single cylinder with VIV will experience a harmonic lift force with mean equal to zero ($\overline{C}_y = 0$ in Eq. 2.9). Now, if the flow is biased towards one side of the cylinder — say by tripping one of the boundary layers so that the separation along that side is delayed — the unsteady lift force will have a time-average component that is different to zero.

Consider then a pair of stationary cylinders that can be arranged in several staggered arrangements (including the special tandem arrangement with $y_0 = 0$). The downstream cylinder, which is displaced from the centreline of the wake, will predominantly suffer interference from the upstream wake on the internal side (the side facing the centreline) rather than on the external side. Therefore, it is straightforward to expect that the lift force that will be generated on this cylinder will also have a time-average component that is not zero.

It was shown that the wake is a region of recirculating flow that presents a deficit of streamwise velocity when compared to the free stream. That is similar to considering that the wake is a 'shielded' region with a retarded velocity profile caused by the presence of the upstream cylinder. Savkar (1970) employed a potential flow theory representing the wake of the upstream cylinder only by its shear layers and showed that the internal side of the cylinder facing the centreline of the wake would experience lower velocities than the external side due to the retarded mean velocity profile of the wake. His conclusion was that the lift force acting on the downstream cylinder should point outwards, i.e. away from the centreline of the
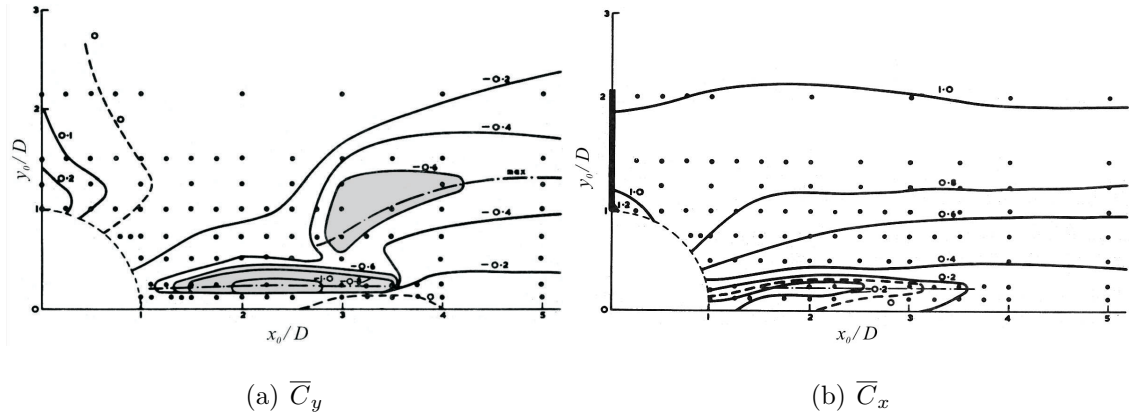
(a) $\overline{C}_y$ (b) $\overline{C}_x$

Fig. 3.5: Contours of (a) mean lift and (b) mean drag for the downstream cylinder of a static pair in staggered arrangements. $\text{Re} = 6.1 \times 10^4$. Adapted from Zdravkovich (1977).

wake. However, the wake of a cylinder, with strong coherent vortices, is far from being considered a potential flow field and this force prediction is not observed in experimental investigations.

Fig. 3.5(a) presents a map of the lift force acting on the second cylinder of a pair for different staggered arrangements at $\text{Re} = 6 \times 10^4$. Zdravkovich (1977) obtained this measurement by holding the upstream cylinder fixed and traversing the downstream one across different stations (each marked by a small dot) in the wake interference region. A negative value of $\overline{C}_y$ indicates lift force acting towards the centreline.

The first evident observation is that the steady lift force points in the direction of the centreline for all investigated configurations when the downstream cylinder is at $x_0/D > 1$. It is possible to identify two main regions of $\overline{C}_y$ lower than -0.6. The first one, occurring for separations around $x_0/D = 1.2 - 3.5$ and $y_0/D = 0.25$ (dash-dotted line in the figure), is associated with the interference regime in which the shear layers from the upstream cylinder are able to reattach to the downstream body. A small $y_0/D > 0$ offset within this regime will result in a sudden force of $\overline{C}_y < -0.6$ towards the centreline while the internal shear layer still remains attached. Once the lateral separation gets too large for viscous effects to keep the internal shear layer deflected the reattachment will no longer hold and a free shear layer will appear on that side, increasing $\overline{C}_y$. This might be associated with a similar flow pattern to regimes 'C' and 'D' for tandem cylinders presented in Fig. 3.2(a).
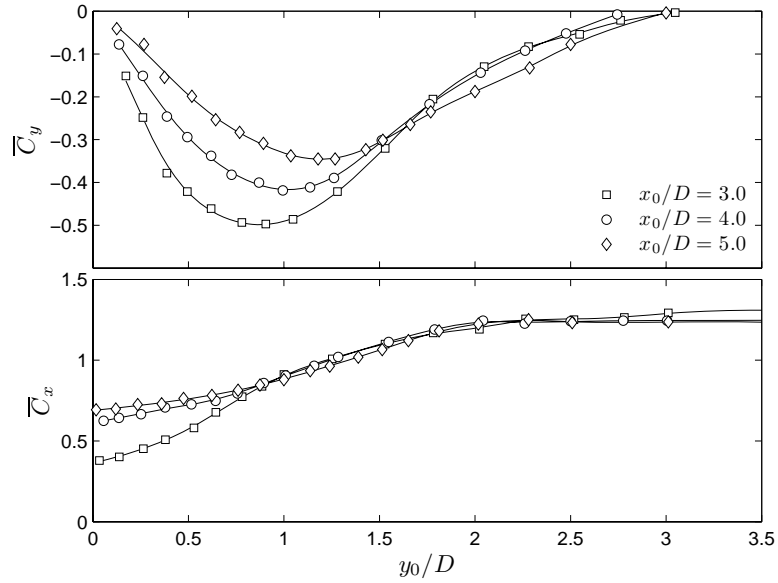
49

Fig. 3.6: Steady lift and drag on a static cylinder in various staggered positions at Re = 5900. Reproduced from Bokaian & Geoola (1984).

The second region with $\overline{C}_y < -0.6$ occurs for larger lateral separations around $y_0/D = 0.8 - 1.4$. It begins at around $x_0/D = 3.0$ and develops a trend of minimum $\overline{C}_y$ that will decrease in intensity as x_0 is increased (indicated by another dash-dotted line in Fig. 3.5(a)). This second region is associated with the second interference regime in which the upstream shear layers are not able to reattach but roll up to form a developed vortex wake in the gap. Bokaian & Geoola (1984) presented more detailed measurements across the wake for three separations, as shown in Fig. 3.6. Their measurements make it clear that the maximum lift towards the centreline is decreasing as the second cylinder moves farther downstream. This is where we will concentrate our attention and, as will be argued in the following chapters, we believe the steady lift towards the centreline generated in this second regime is induced by vortices coming from the upstream wake and interfering with the downstream cylinder.

It is important to emphasise that within the whole range of longitudinal and lateral separations investigated the steady lift force is always acting towards the centreline of the wake. This is enough to disprove the potential flow assumption developed by Savkar (1970). Both regions present an overlap around $x_0/D = 2.7 - 3.5$ showing a bistable nature of the reattachment of the shear layers

50

at this location at specific Re. The present work is only concerned with the flow mechanism that excites vibrations in the second regime, where a fully developed wake is present in the gap flow, thus our experiments will concentrate on $x_0/D > 4.0$.

In a similar way, a map of steady drag $\overline{C}_x$ is presented in Fig. 3.5(b). Positive values of $\overline{C}_x$ indicate drag acting in the direction of the free stream. A dotted line indicates a contour of zero drag below which $\overline{C}_x$ is negative and the downstream cylinder is drawn towards the upstream body. As explained before, this happens due to the low pressure that appears in the gap region when both shear layers reattach to the second cylinder. Beyond $x_0/D = 3.0$ the downstream cylinder only experiences positive drag indicating that a developed wake can now be formed in the gap. This critical separation coincides with the overlap of the two trends of maximum $\overline{C}_y$ presented in Fig. 3.5(a). While the downstream cylinder is immersed in the wake of the upstream cylinder the steady drag will be lower than that expected for a single cylinder exposed to a free stream. Only for lateral separations greater than $y_0/D = 2.0$ will $\overline{C}_x$ reach values around 1.0.

This brings us back to the definition of interference regions proposed in Fig. 3.4. Zdravkovich (1977) says that "the wake boundary is a line along which the [mean] velocity becomes the same as the free stream one. The [wake] interference boundary is the line along which lift force becomes zero or negligible". These two lines do not necessarily coincide, but the wake interference boundary is always outside the wake boundary.

3.3 Wake-induced vibration of the downstream cylinder

After a few considerations about static cylinders we enter the main topic of the present work concerning the response of a downstream cylinder that is free to oscillate in the wake of a static upstream cylinder. Following Fig. 3.4 above we will investigate vibrations in the 'wake interference' region, therefore called *wake-induced vibrations*, or simply WIV for short.

This phenomenon was also referred to by different names in the literature, such as: 'interference galloping' (Ruscheweyh, 1983), 'wake-induced galloping' (Bokaian & Geoola, 1984) and 'wake-displacement excitation' (Zdravkovich, 1988).

3.3.1 Response

Reflecting the need from the heat exchangers and transmission lines industry, the earliest experiments were performed with flexible tubes in order to supply WIV response data to the engineering design desk. A more complete understanding of the fluid-mechanics of the phenomenon was gradually developed when researchers started to limit the number of variables performing tests with rigid cylinders in 2-dof. A further step was to simplify even more and allow a rigid cylinder only to vibrate either in the in-line or in the cross-flow direction.

Flexible cylinders

King & Johns (1976) performed experiments in water (Re $= 10^3 - 2 \times 10^4$) with two flexible cylinders for separations in the range $x_0/D = 0.25 - 6.0$. They observed that for $x_0/D = 5.5$ the upstream cylinder responded with a typical VIV curve reaching amplitudes around $\hat{y}/D = 0.45$ in the resonance peak, comparable to their tests with a single cylinder at same Re. On the other hand the downstream cylinder also started to build up oscillations together with the upstream one, but instead of the oscillations disappearing after the synchronisation range they remained at roughly the same level for reduced velocities up to the highest tested. They identified the response of the second cylinder as a type of buffeting, since it originated from the wake interference coming from the upstream cylinder.

Brika & Laneville (1999) performed tests with a pair of long cylinders in a wind tunnel in the range Re $= 5000 - 27000$ with a flexible cylinder positioned from 7 to 25 diameters downstream of a rigid cylinder. The cross-flow response of the second cylinder is compared with the VIV curve of a single flexible cylinder in Fig. 3.7. A series of curves for different separations reveal that as x_0 increases the interference effect from the upstream wake is reduced until the response resembles that of a single
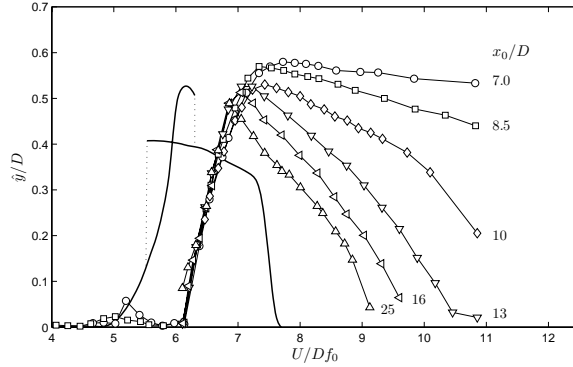
Fig. 3.7: WIV response of a flexible cylinder in the cross-flow direction for various separations. —,
single cylinder. $m^* = 821$, $\zeta = 0.83 \times 10^{-4}$, Re $= 5000 - 27000$. Adapted from Laneville
& Brika (1999).

cylinder without any (or with very little) interference. It is interesting to note that
even between separations 16 and 25 they were still able to identify some change in the
interference effect with the second cylinder positioned so far downstream. Because
their experiments were performed in air the mass ratio $(m^* = 821)$ is two orders of
magnitude higher that other experiments in water. Yet their damping parameter is
extremely low, resulting in a combined mass-damping of only $m^*\zeta = 0.068$.

Rigid cylinders with 2-dof

Moving from flexible to rigid cylinders we recall experiments performed by
Zdravkovich (1985) with two rigid cylinders free to respond in 2-dof mounted
in a wind tunnel (Re $= 1.5 \times 10^4 - 9.5 \times 10^4$, $m^* = 725$ and $\zeta = 0.07$). Due to
a very high combined parameter of $m^*\zeta = 50$, Zdravkovich was only able to
observe a build up of oscillations at $x_0/D = 4.0$ for reduced velocities beyond
$U/Df_0 = 50$, asymptotically reaching a maximum of $\hat{y}/D = 1.7$ for the last point of
his experiments at around reduced velocity 80. Nevertheless, he has also recorded a
monotonically increasing branch of response that was qualitatively very similar to
those results discussed above.

In a further study of the effect of mass and damping in this type of FIV,
Zdravkovich & Medeiros (1991) performed similar 2-dof tests in a wind tunnel
varying $m^*\zeta$ between 6 and 200 (Re $= 5 \times 10^3 - 1.4 \times 10^5$). Once more, cross-
flow vibrations presented the same monotonic-asymptotic behaviour with amplitude

increasing with reduced velocity. Their results revealed a strong dependency of the response on $m^*\zeta$, but more importantly showed that very high values of mass-damping are required to inhibit WIV on the second cylinder. Maximum amplitude was obtained at a maximum reduced velocity of 120, but in order to reduce the $\hat{y}/D$ by half (from 2.2 to 1.1) it was required to increase $m^*\zeta$ ten times (from 6.4 to 64).

## Rigid cylinders with 1-dof, cross-flow oscillations

Going one step further in the idealisation of the problem we find a few results for rigid cylinders responding only in 1-dof. Bokaian & Geoola (1984) performed experiments with two rigid cylinders in tandem in a water channel (Re = 700 − 2000). The upstream cylinder was fixed while the downstream cylinder was elastically mounted on air bearings and free to respond only in the cross-flow direction.

They varied centre-to-centre separation in the range $x_0/D = 1.09 - 5.0$ covering both interference regimes (with and without a developed wake in the gap). Results for amplitude of response versus reduced velocity (with f_W being the natural frequency in still water) are presented in Fig. 3.8(a) for three values of x_0. A vigorous build-up of oscillations with increasing flow speed was observed for all flow speeds greater than a critical threshold velocity. Such a severe 1-dof vibration was observed to resemble the response of classical galloping of non-circular bodies; therefore it was referred to as 'wake-induced galloping'. They noted that "*galloping* carries the strong connotation of a negatively damped single degree of freedom oscillation, and its use to describe the problem under study is only because of the many similarities between the two kinds of instability". However, somewhere else in their work, Bokaian & Geoola (1984) stated that "whilst some characteristics of wake-excited galloping were found to be similar to those of galloping of sharp-edged bodies, others were observed to be fundamentally different".

The authors concluded that depending on x_0, m^* and ζ the downstream cylinder "exhibited (i) a vortex-resonance, (ii) or a galloping, (iii) or a combined vortex-resonance and galloping, (iv) or a separated vortex-resonance and galloping" response. In Fig. 3.8(a) two examples of these different responses are found with $x_0/D = 1.5$ presenting a vortex-resonance that is followed by (or combined with) a
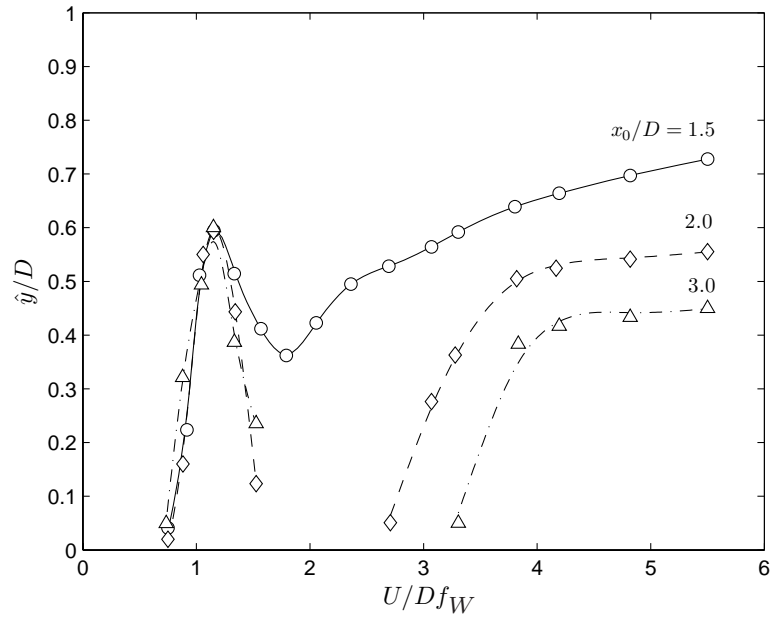
(a)
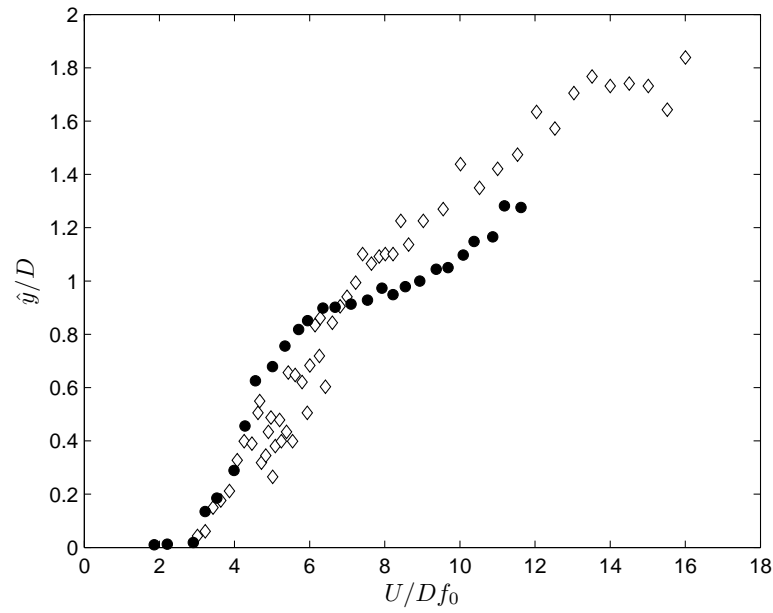
(b)

Fig. 3.8: Response in the cross-flow direction of the downstream cylinder under WIV. (a) Varying x_0, $m^* = 8.4$, $\zeta = 0.013$, $\mathrm{Re} = 700 - 2000$ (Bokaian & Geoola, 1984). (b) $\diamond$, $x_0/D = 4.75$, $m^* = 3.0$, $\zeta = 0.04$, $\mathrm{Re} = 3 \times 10^4$ (Hover & Triantafyllou, 2001); $\bullet$, $x_0/D = 4.0$, $m^* = 1.9$, $\zeta = 0.007$, $\mathrm{Re} = 3000 - 13000$ (Assi *et al.*, 2006).

'galloping response' at about reduced velocity 2; and $x_0/D = 2.0$ and 3.0 presenting separated vortex-resonance and 'galloping' regimes. A pure vortex-resonance is not shown in Fig. 3.8(a) but it would be similar to the typical VIV response discussed above.

Hover & Triantafyllou (2001) measured displacements and forces of rigid cylinders under WIV in a water towing tank at a constant Reynolds number ($\mathrm{Re} = 3 \times 10^4$). They made use of a closed-loop control system that forces the oscillation of the cylinder in response to a measured and integrated fluid force. This way they were able to tune the m-c-k parameters in the equation of motion in order to generate any artificial combination of f_0, m^* and ζ. As a result, their curve presented in Fig. 3.8(b) was obtained for a constant $\mathrm{Re} = 3 \times 10^4$ adjusting f_0 in order to vary reduced velocity. The resulting parameter $m^*\zeta = 0.12$ is very close to $m^*\zeta = 0.11$ obtained by Bokaian & Geoola (1984) in Fig. 3.8(a), however the difference in the level of amplitude might be related to a difference of one order of magnitude in Re, as will be discussed later.

For a separation of $x_0/D = 4.75$ Hover & Triantafyllou (2001) observed one single branch of response that builds up monotonically reaching amplitudes of $[\hat{y}/D]_{\max} = 1.9$ for reduced velocities around 17 (their curve represents an average of the 10% highest peaks of displacement). Although they referred to the branch of high amplitude as an "upward extension of the frequency lock-in branch" that occurs for the VIV response of a single cylinder, there is no evidence that the vortex shedding frequency of either cylinders is synchronised with the frequency of oscillation, on the contrary, their results reveal that vibrations occur "without any clear signature of vortex resonance".

More recently, Assi *et al.* (2006) performed 1-dof experiments with two rigid cylinders in a recirculating water channel ($\mathrm{Re} = 3 \times 10^3 - 1.3 \times 10^4$). Their results, also presented in Fig. 3.8(b), are comparable to Hover & Triantafyllou (2001) since they are closer in the Re range, however Assi *et al.* (2006) employed a very low damping elastic system resulting in $m^*\zeta = 0.013$ one order of magnitude lower. Both curves are in good agreement showing an expected branch of high amplitude oscillation building up as reduced velocity is increased. But the data points from Assi

et al. (2006) also reveal a smooth hump corresponding to a local vortex-resonance response around $U/Df_0 = 6.0$.

3.3.2 Mechanisms attempting to explain WIV

After exploring typical responses of the downstream cylinder (flexible, 2-dof rigid, 1-dof rigid) we now turn our attention to attempts offered in the literature to explain and model the WIV mechanism described above.

From an analytical point of view Parkinson (1989) presents a good outline about modelling theories for FIV of bluff bodies, while Price (1995) reviews several theoretical models for fluid-elastic instability of cylinder arrays. Chen (1987) proposed a generalised theory to model fluid-elastic instabilities of any nature in arrays of cylinders (as inspired by the heat exchanger industry, with a pair of cylinders in tandem being a simplification). The latter explains that analytical models based on motion-dependent fluid forces are divided into three categories: *quasi-static*, *quasi-steady* and *unsteady* flow theories. While some phenomena can be modelled successfully by quasi-steady approaches (like classical galloping described in Chapter 2), others will have to be free from simplifying assumptions and may require a complete unsteady approach. According to Chen (1987) the fundamental difference between each approach is summarised below:

- *Quasi-static flow theory.* The fluid-dynamic characteristics of cylinders oscillating in a flow are equal at any instant to the characteristics of the same stationary cylinders in identical configuration. That is to say that the fluid forces depend only on the position of the bodies. This theory can account only for fluid-stiffness-controlled instability.

- *Quasi-steady flow theory.* The fluid-dynamic characteristics of cylinders moving in a flow are equal at any instant to the characteristics of the same cylinder moving with constant velocities equal to the actual instantaneous values. The fluid forces depend on the cylinder configuration and are proportional to cylinder motion, reflected by changes of amplitude and phase

of the fluid force with respect to cylinder motion. This theory can account for fluid-stiffness-controlled or fluid-damping-controlled instabilities.

- *Unsteady flow theory.* In general, the fluid-force components are nonlinear functions of the cylinder position, velocity and acceleration. This theory can account for fluid-stiffness-controlled or fluid-damping-controlled instabilities, but requires a complete modelling of all unsteady flow phenomena.

As will be seen below, previous works have attempted to apply quasi-steady models to WIV. To some extent they were successful in applying semi-empirical methods to predict the critical flow speed for the onset of instabilities — since at the onset the motion of the cylinder is rather small and simplifying assumptions still have some value — but once the cylinder builds up considerable oscillations the theory does not hold true.

Although we could classify all types of instabilities occurring in a wake as WIV we are seeking to explain the excitation that drives 1-dof oscillations of a cylinder at large separations, i.e. x_0 large enough for a developed wake to form in the gap. In order to clarify the scope of our work, we find it useful to briefly explain other mechanisms that are not to be mistaken for the subject of the present study: *gap-flow-switching*, for cylinders in close proximity and *wake-flutter*, for cylinders far apart but with two degrees of freedom.

Gap-flow-switching

Gap-flow-switching sustains vibrations of cylinders in close proximity. It occurs for the first regime of flow interference when the upstream shear layers reattach to the second body and no vortex wake is developed in the gap flow. Therefore, the steady flow in the gap can switch from one side to the other of the downstream cylinder as it oscillates across the wake.

Similarly to the jet-switching phenomenon observed for side-by-side cylinders, the gap-flow-switching mechanism also has a bistable nature (Fig. 3.9). Initially, when the cylinders are in perfect tandem alignment, there is no mean lift force acting on the downstream body since both upstream shear layers reattach symmetrically
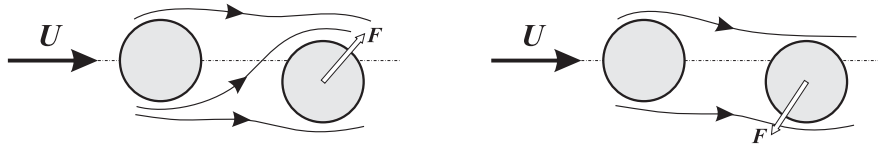
Fig. 3.9: Bistable flow pattern due to gap flow switch. Adapted from Zdravkovich (1988).

around the second cylinder. However, if the downstream cylinder is displaced beyond a critical y_0 the shear layers will not be able to remain attached to both sides of the downstream body and a gap flow will originate. This severe change in the flow pattern generates an abrupt and strong lift force pointing inwards — the first region of $C_y < -0.6$ in Fig. 3.5(a) — forcing the cylinder back to the centreline (Zdravkovich, 1974).

Theoretically, this restoring force tends to suppress any perturbation. But the fluid-structure mechanism presents a hysteresis in relation to the movement of the second body. Zdravkovich (1974) observed that the "gap flow persisted longer than for stationary cylinders" when the downstream cylinder was displaced towards the centreline from a staggered initial condition. On the other hand, the gap flow would start later "as the cylinder passed the critical lateral spacing moving in the opposite direction". When the gap flow is intense, a high-lift pressure distribution appears; when the gap flow is stagnant the magnitude of the lift coefficient is significantly reduced. So, the feeding force which maintained the large-amplitude mode was found to be due to a hysteresis effect acting on the timing as the gap flow switches from one regime to the other (Fig. 3.9), interchanging with irregular intervals. Thus, the fluid-dynamic forces "are in phase with the elastic forces for a longer time feeding the large amplitude vibration". Zdravkovich (1974) offers a convincing explanation for the excitation of tandem cylinders with close proximity, but he leaves an open question for the mechanism when cylinders are farther apart.

Gap-flow-switching entirely disrupts the vortex shedding and distorts the near wake of the upstream cylinder (Zdravkovich, 1988) inhibiting the formation of any coherent vortex structure in the gap. It also resembles the classical galloping instability because it requires displacement of the body and happens for 1-dof

systems. However the fluid force is not in perfect phase with the body's velocity, but a hysteresis is present relative to the cylinder position across the centreline of the wake and depending on the direction of the cylinder motion. For this reason, the same quasi-steady approach applied for classical galloping mechanism is not valid in this case.

Ruscheweyh (1983) did not observe self-excited oscillation induced by gap-flow-switching for a tandem arrangement in his experiments performed in air. However, the author states that low mass and damping cylinders, as for example in water, can be excited into large vibrations by the gap-flow-switch mechanism even in tandem arrangements. Overall, this mechanism only explains how vibrations are sustained for cylinders with close proximity where a developed wake is not formed. It falls short of explaining how vibrations can be sustained for larger separations.

Wake-flutter

Wake-flutter is another mechanism that can excite the downstream cylinder into 2-dof vibrations, typically in an elliptical orbit. Consider that the downstream cylinder is placed further downstream in the wake in an initial staggered condition. A fully developed wake is now able to originate in the large gap between the bodies, but wake-flutter can be excited in spite of the unsteadiness of the flow, being sustained only by the steady fluid forces present in the wake. Fig. 3.10 illustrates the mechanism.

Force maps presented in Fig. 3.5 (page 49) show that the downstream cylinder will be subjected to changes in the steady fluid force for considerably large separations. A reduced drag force has minimum values on the centreline of the wake; and a steady lift force develops maximum values close to the wake interference boundary. If the downstream cylinder is able to respond in two degrees of freedom following the elliptical orbit described in Fig. 3.10 it will move across different gradients of steady lift and drag. A counter-clockwise orbit on that side of the wake extracts energy from the flow to sustain the oscillations. Areas W_y and W_x greater than zero in the force-displacement diagrams mean positive work of the lift and drag forces in one cycle.
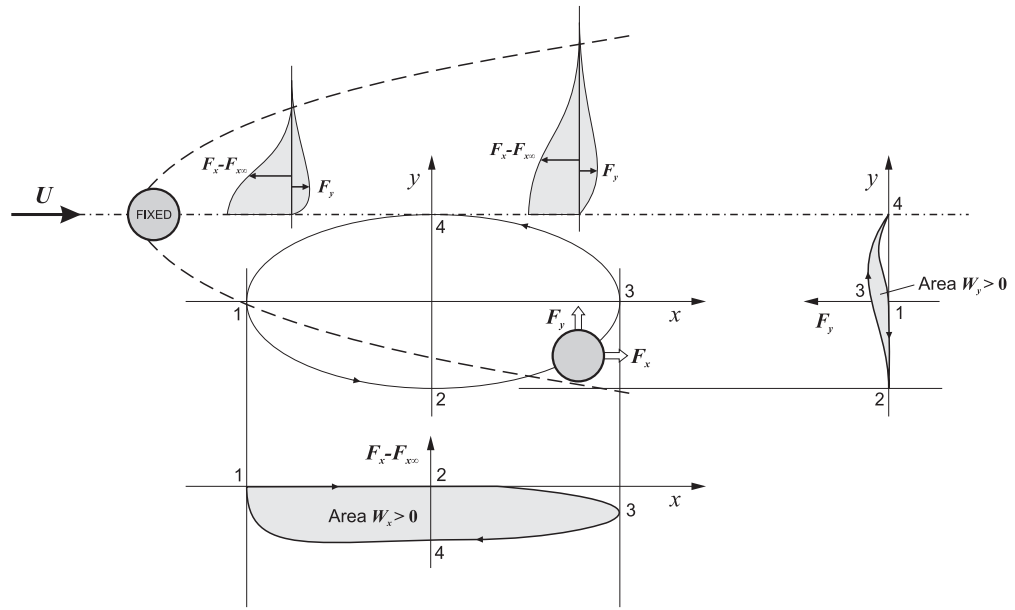
Fig. 3.10: Wake flutter of a cylinder with x and y degrees of freedom in the wake of another. Adapted from Naudascher & Rockwell (1994).

This quasi-steady approach does not take into account the vortex wake from upstream, but only the steady effect of lift and drag. Also, this mechanism would not excite systems with 1-dof, since it requires an orbit in x and y for a positive input of energy. Naudascher & Rockwell (1994) comments that wake-flutter, like other coupled instabilities, occurs only if the natural frequencies in the x and y directions are reasonably close. This mechanism was called 'wake galloping' by Zdravkovich (1997) and Blevins (1990), but we prefer to stick to the terminology 'wake-flutter' since it requires response in 2-dof to be sustained.

Elliptical vibrations can happen in different regions of the wake wherever the steady velocity profile is favourable. The amplitude of the oscillation is directly related to the intensity of the lift and drag gradient in the wake. Therefore oscillations are reduced for larger separations as the steady force profiles get attenuated.

Bokaian & Geoola (1984) noted that the fluid-elastic instability reported in their work (Fig. 3.8(a)) must not be mistaken by the wake flutter mechanism described above, since their experiment presented only a single degree of freedom. This is also the case for the present work. As a conclusion, this mechanism does not explain

why a cylinder with 1-dof responds with severe vibration when it is immersed in the wake of another bluff body.

3.3.3 Mechanisms for 1-dof and large separations

Several works proposed possible explanations for the origin of WIV but a complete and convincing theory is yet to be produced. Following the line of thought developed by Zdravkovich (1988) we will introduce his own understanding of the problem followed by a few others. Most of them are presented in review papers in the literature (Price, 1976; Zdravkovich, 1977; Chen, 1986; Zdravkovich, 1988; Paidoussis & Price, 1988; Moretti, 1993; Price, 1995), but it is necessary to analyse a few main points here if we want to develop a comprehensive explanation later.

Wake-displacement

In between the gap-flow-switching (for close proximity) and wake-flutter (for 2-dof systems) Zdravkovich (1977) pushed further the quasi-steady models in order to explain 1-dof vibrations in the wake interference region proposing the *wake-displacement* mechanism. It follows the same idea as the gap-flow-switching mechanism, but differs from it in the sense that it does not disrupt the vortex shedding of the upstream cylinder. He suggested that both mechanisms are analogous in the fact that they displace the wake coming from upstream. "The downstream cylinder is not *immersed* in the upstream cylinder wake but *displaces* it instead" (Zdravkovich, 2003, his emphasis), deflecting more flow towards the wake centreline and inducing a lift force towards the centreline around the wake boundary.

The displacement of the wake would be the cause of the steady lift force for larger separations shown in Fig. 3.5(a). But in order for vibrations to be sustained in this steady force field a hysteresis effect would have to be present as the cylinder moves across the wake "switching or dislocating the developed wake". (Zdravkovich, 1988). This effect would generate a phase lag between the fluid force and the displacement of the cylinder as it crosses the centreline. Bokaian & Geoola (1985) also held to this mechanism to explain their results.

The concept of wake-displacement may be correct but it needs to be supported by evidence on how the downstream cylinder actually displaces the wake. It may be reasonable to think that the movement of the downstream cylinder is able to deflect the steady flow in a small gap (as in gap-flow-switching). However, for larger separations where a fully developed wake is present, the displacement of the downstream cylinder may not have such a strong effect on the flow in the gap. Of course it will interfere and interact with vortices as they approach the second body, but the shedding mechanism — the actual flow regime — is not altered by the presence or movement of the downstream cylinder at large x_0.

Wake-buoyancy

Maekawa (1964) attributed the excitation mechanism to a buoyancy effect. The static pressure is a minimum at the centreline of the wake; hence the pressure gradient across the wake generates a buoyancy force towards the centreline. However, later works (Best & Cook, 1967; Wardlaw & Watts, 1974) integrated the pressure field around the second cylinder to show that only 30-50% of the total lift could be attributed to a buoyancy effect. In addition, this explanation does not deal with the need for a hysteresis effect (or phase lag) to exist in order to sustain vibrations in a symmetrical pressure field.

Turbulent transition in one of the shear layer

Maekawa (1964) also suggests that turbulence generated by the wake may affect the separation on the internal side of the cylinder, changing the symmetry of the pressure field around the second body. However this phenomenon was not confirmed by experiments that measured turbulence intensity and transition in the shear layers (Zdravkovich, 2003). Price (1976) notes that although the variation of turbulence intensity across the wake is large with maximum intensity on the centreline the scale of turbulence in a wake is dominated by large vortices being shed on the upstream cylinder. "Whether turbulence at this scale can affect transition [in the boundary layer] is a matter for doubt."

Resolved drag

Mair & Maull (1971) proposed that the side force was caused by a type of wake entrainment mechanism that generates an inclined free stream velocity approaching the second body. The lift force towards the centreline would be due to resolved drag as the second body faces entrained flow from outside towards the centreline of the wake.

Price (1976) measured the pressure distribution around the downstream cylinder in different positions across the wake. As expected, the pressure distribution is symmetric when the cylinder is placed on the centreline (as it is symmetric for a cylinder in a free stream), but as the cylinder moves across the wake the position of the frontal stagnation point rotates around the cylinder. Also, the points of maximum negative pressure (just before separation) rotates further away from the stagnation point (i.e. separation is delayed) as the cylinder moves across the wake approaching the centreline (hence resulting in less drag as well). In general, the suction of the inner wall was greater than that on the outer wall as would be expected to produce a lift force towards the centreline.

Analysing pressure distribution plots, "it seems that the lift force is mainly due to the asymmetry of the base pressure region, with the reduction in drag appearing to be mainly due to the reduction of the front positive pressure region" (Price, 1976). Assuming that the rotation angle indicates the incidence velocity direction, and calculating the drag from the integration of the pressure distribution around the cylinder, Price estimated that the lift force due to resolved drag is only 25% of the total lift force measure on the cylinder. When he repeated the experiment with a perforated cylinder downstream (so that no component due to circulation or buoyancy would affect the body) the resolved drag contributed only 10% of the total measured lift. His conclusion was that the total lift force could not be attributed only to resolved drag.

Circulation

Rawlins (after Price, 1976) employed an improved inviscid flow theory and ascribed the lift force to circulation around the cylinder. He stated that because of variations of velocity and turbulence across the wake each boundary layer of the downstream cylinder feeds different amounts of vorticity into their associated shear layers. Applying Kelvin's circulation theorem he concluded that a circulation is built up around the cylinder until rates at which vorticity is discharged from the two boundary layers are equal. This circulation would generate lift towards the centreline.

Rawlins' lift curves have the same general shape as the lift profile measured experimentally (Fig. 3.5(a) for example), but do not obtain the required magnitude generating only 75% of the lift measured at the maximum position. Hence it seems that Rawlins' expression cannot satisfactorily explain the origin of the inward lift force. Price (1976) comments that "for a mechanism that is so obviously dependent on the viscous nature of the flow, a potential-flow solution, however ingenious, is unlikely to succeed".

Conclusion

Several attempts to explain the fluid-mechanics of the WIV excitation were discussed. Probably the wake-displacement mechanism proposed by Zdravkovich (1977) is the most convincing phenomenological explanation so far (assuming that a phase lag between displacement and lift exists). But it still lacks experimental verification and analytical modelling. In the present work we aim to provide new insights about the origin of the inward, steady lift force acting on the downstream cylinder attempting to explain WIV.

3.3.4 Improved quasi-steady models

Quasi-steady theories have been applied in the study of fluid-elasticity and fluid-induced vibration for some time (Parkinson, 1971; Blevins, 1990). As explained by Chen (1987) this theory allows the motion-induced fluid forces on an oscillating body

to be estimated by using static fluid force coefficients determined on a stationary body. "It is well accepted, and physically reasonable, that this assumption is valid for high values of reduced flow velocity" (Granger & Paidoussis, 1996).

However, it is also known that a strict quasi-steady theory is not able to predict the fluid-elastic instability of the downstream cylinder if it is only free to oscillate in 1-dof. Price (1984) improved the quasi-steady model by inserting a time delay between the cylinder displacement and the fluid force. This phase lag was intended to account for a possible flow retardation generated in the gap flow between the pair of cylinders, however the physical origin of this effect still remains unclear. Granger & Paidoussis (1996) proposed yet another improvement of the quasi-steady theory employed by Price (1984) with the aim to model the most relevant unsteady effects neglected by the quasi-steady approach. In essence their model, referred to as *quasi-unsteady*, incorporates a memory effect into the same time delay idea, "the physical origin of which arises from the diffusion-convection process of the vorticity induced by successive changes in the velocity of the body".

Paidoussis *et al.* (1984) employed potential-flow theory to investigate fluid-elastic instability of an array of cylinders. Although they were not calculating any viscous forces in their model itself, they had to include a phase lag effect in the fluid force in order to generate any oscillatory instability. Probably the most intuitive explanation for the existence of a phase lag on the fluid force was offered by Paidoussis & Price (1988) who attributed this effect to a time delay associated with the reorganisation of the viscous wake flow as the cylinder is displaced. Paidoussis *et al.* (1984) concluded that "if viscous effects are neglected altogether, then the only form of instability possible is divergence, which is a static, non-oscillatory instability."

Conclusion

Each of the improved quasi-steady models gave better comparisons to experimental data than their precursors. They all agree that a phase lag between the cylinder displacement and the fluid force must be implemented into quasi-steady models in order to account for a physical time delay in the flow-structure interaction. Yet a precise explanation about the origin and effects of this time delay has not been

produced. In the present work we aim to bring new light over that matter as well.

We sum up this section quoting Price's (1976) conclusion that "none of the [suggested mechanisms] gives a satisfactory explanation for the origin of the lift force. However, several interesting points were noted; for instance the dependence of the lift profiles for the [downstream] cylinder on its own characteristics in the wake and not particularly on the wake characteristics." Consequently, a complete unsteady theory may be required to correctly model this type of fluid-elastic phenomenon.

Chapter 4

Experimental set-up

Experiments in the present study were performed through 15 sessions in the Hydrodynamics Laboratory of the Department of Aeronautics at Imperial College London between 2006 and 2009. This chapter presents a description of the apparatus employed in the experiments.

4.1 Flow facility

Tests were carried out in a recirculating water channel with a test section 0.6m wide, 0.7m deep and 8.4m long, as seen in Fig. 4.1. Sidewalls and bottom of the section were made of glass mounted on a steel frame, allowing access through the free surface and a complete view of the models for flow visualisation purposes. A carriage, installed at the top of the structure, covered the whole length of the test section and could be used as a positioning system or to tow models up to speeds of 1m/s. This is particularly useful for test conditions with very low Reynolds number or more complex oscillatory flows.

The water flow was driven by a single propeller through a pipe system before reaching the settling chamber. A wire screen and a honeycomb were employed to stabilise the flow before a three-dimensional contraction with ratio of 4.5:1. The accelerated flow then enters a long parallel test section which ends in a sink directing the flow to the propeller, closing the circuit. The flow speed was continuously variable by controlling the rotation of the propeller. An electromagnetic flow meter

Fig. 4.1: Recirculating water channel at Imperial College London.

installed just before the settling chamber provided a reading of the instantaneous flow rate, which was divided by the area of the test section yielding the value of U.

4.1.1 Flow quality

All experiments presented in this work were conducted at the first third of the test section, within the first 2m downstream of the end of the contraction. At this location the boundary layers developed on the sidewalls and bottom of the section were estimated to be approximately 20mm thick for the maximum flow speed of 0.6m/s (according to formulation of Schlichting, 2000).

The velocity profile across the working section was mapped using a hot-film probe. Local velocity fluctuation u was acquired at 42 stations across the area of the section for four values of U within the range of study. In Fig. 4.2(a) we see the map obtained for the most irregular profile measured for $Re_W = 2.3 \times 10^5$ (Reynolds number based on the width of the test section). Velocity contours at this cross section show a smooth gradient with lower velocities from the middle-height towards the free surface. This feature is well known to happen in water channels
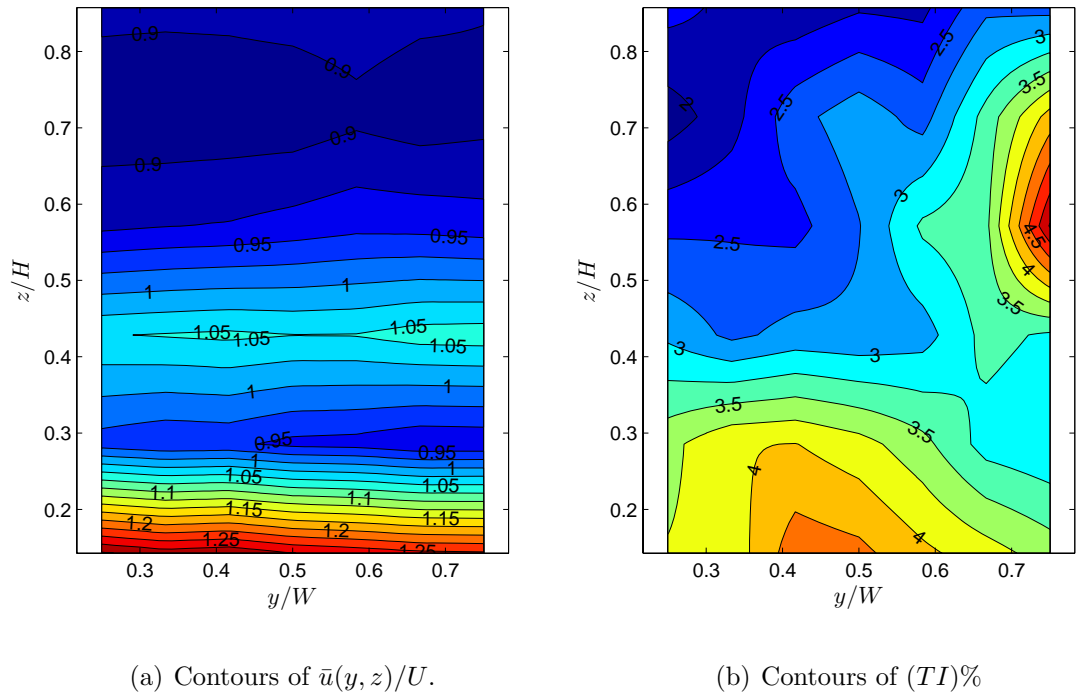
(a) Contours of $\bar{u}(y,z)/U$.

(b) Contours of $(TI)\%$

Fig. 4.2: Contours of the free stream velocity profile (a) and turbulence intensity (b) at the working cross section for $\mathrm{Re}_W = 2.3 \times 10^5$. H and W are the height and width of the test section respectively.
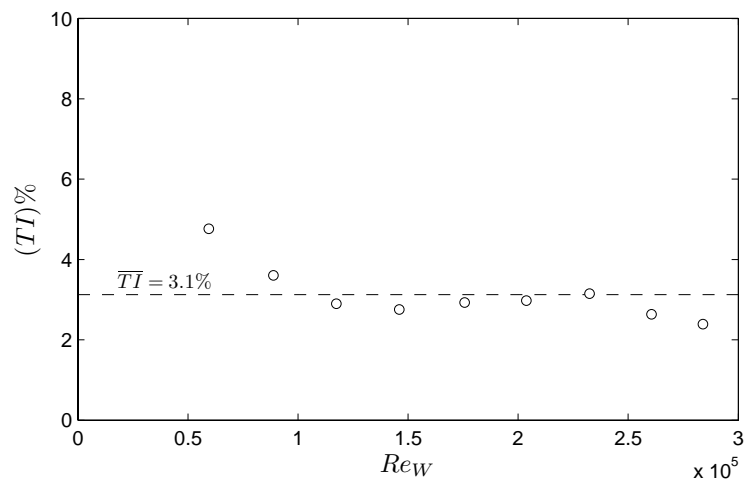

Fig. 4.3: Free stream turbulence intensity versus Re_W measured at the centre of the working section. $\overline{TI} = 3.1\%$.

with free surface and there are a few techniques known to artificially accelerate the surface flow (SNAJ, 1986), although none was employed in this study. On the other hand, there was a region of accelerate flow close to the bottom of the section showing a velocity increase of up to 25% of U. The effect of boundary layers was not captured by this mapping since the probe was always positioned 150mm away from the walls.

Free stream turbulence intensity calculated as

$$TI = \frac{\sqrt{\overline{u^2}}}{U}, \tag{4.1}$$

where u is the streamwise fluctuating velocity, was also mapped across the section for the same four values of U and one of the results is shown in Fig. 4.2(b). A spatial average of the 42 stations results in $\overline{TI} = 3.1\%$ for the plotted cross section. There were two main regions of higher free stream turbulence located at the bottom and on the right-hand side of the test section. Both reached levels of 4.5% but still the deviation from $\overline{TI}$ remains within 20% for the whole of the cross section.

In order to have an idea of the variation of TI throughout the whole range of flow speed one measurement was performed with the hot-film probe positioned at the centre of the test section varying U up to 0.6m/s. The result presented in Fig. 4.3 shows that the free stream in the section begins with a level of about $TI \approx 5\%$ for lower flow speeds, but the turbulence intensity quickly falls to levels around 3% for most of the range of U required for the experiments. In fact, the average value of turbulence intensity for $\text{Re}_W = 0.5 \times 10^5 - 3.0 \times 10^5$ at the centre of the section was $\overline{TI} = (3.1 \pm 0.7)\%$. We suggest that the flow quality in the channel could be substantially enhanced by installing a set of screens downstream of the honeycomb, reducing free stream turbulence, as well as improving the velocity profile.

Although the uncertainty of the flow meter was very low (around 1%), the variance in the velocity profile, as exemplified in Fig. 4.2(a), raises the uncertainty level of U to about 13% for the most irregular profile, varying with Re. Nevertheless, the actual flow quality described above was proved to be adequate to perform our FIV tests. This was validated with a good agreement between our preliminary VIV results and other experiments presented in the literature (please refer to Chapter 5).

Bokaian & Geoola (1984) performed experiments with a pair of cylinders in a water channel and found no significant difference in their results for two levels of free stream turbulence intensity of 6.5% and 11.9%. Also, their velocity profile showed a 7% variation around the mean free stream velocity.

4.2 Circular cylinder models

Several circular cylinder models were constructed for the experiments. The pair mainly employed throughout the present work was made from a 50mm diameter acrylic tube, giving a maximum Reynolds number of approximately 30000, based on cylinder diameter D, at $U = 0.6$m/s. With a wet-length of $L = 650$mm (total length below water level H) the resulting aspect ratio of the model was $L/D = 13$. Cylinders were hollow and filled with air in order to keep the mass as low as possible.

It was judged preferable not to install end plates on the cylinder in order not to increase the fluid damping in the system. Instead it was chosen to have the models terminating as close as possible to the glass floor of the test section. In a similar way the disturbances due to surface waves were considered to be negligible and the models were not fitted with end plates at the top either.

One single cylinder occupies 8.3% of the total area of the test section. If one cylinder is oscillating behind the other, the maximum projected area of both cylinders would result in a blockage ratio of 16.6% if it is displaced by more than $1D$. Brankovic (2004) performed VIV tests on a single cylinder in the same water channel with three ratios of blockage: 11.3%, 13.6% and 17%. She concluded that although the maximum amplitude of oscillation decreased slightly for higher blockage ratios the results remained qualitatively the same, meaning that the hydrodynamic mechanism did not change for the three cases studied.

4.3 One-degree-of-freedom rig

The upstream cylinder was rigidly attached to the structure of the channel preventing displacements in any direction, while the downstream cylinder was fixed
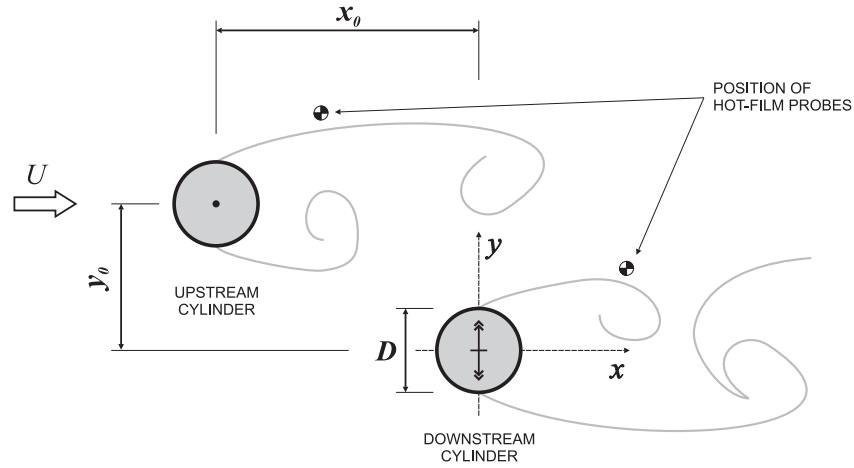
Fig. 4.4: Arrangement of a pair of cylinders. The static upstream cylinder may be removed during experiments with a single cylinder.

from its upper end to a one-degree-of-freedom elastic mounting (named the 1-dof rig). The initial streamwise and cross-flow separations between cylinders (x_0 and y_0 in Fig. 4.4) could be varied by changing the position of the upstream model, so that the downstream cylinder always oscillated around the centreline of the test section. For most of the experiments performed in the present work, both cylinders were initially aligned with the free stream direction ($y_0 = 0$), arranged in what is called the tandem configuration.

Fig. 4.5 shows a schematic representation of the 1-dof rig on which the downstream cylinder was mounted and helps in describing the operation of the system. Both models were aligned in the vertical direction passing through the free water surface down to almost the full depth of the section. The downstream cylinder was mounted such that there was a 2mm gap between the lower end of the cylinder and the glass floor of the test section. The support system was firmly installed on the channel structure and the sliding cylindrical guides were free to move in the transverse direction defined by the y-axis. A pair of tension springs connecting the moving base to the fixed supports provided the restoration force of the system.

A pair of sliding guides was made out of a carbon fibre tube with a smooth finish and ran through a pair of air bearings spanning the width of the section. They were connected at mid-length by a light, stiff table machined out of a block of aluminium, from which the cylinder was firmly attached. A rigid load cell (described
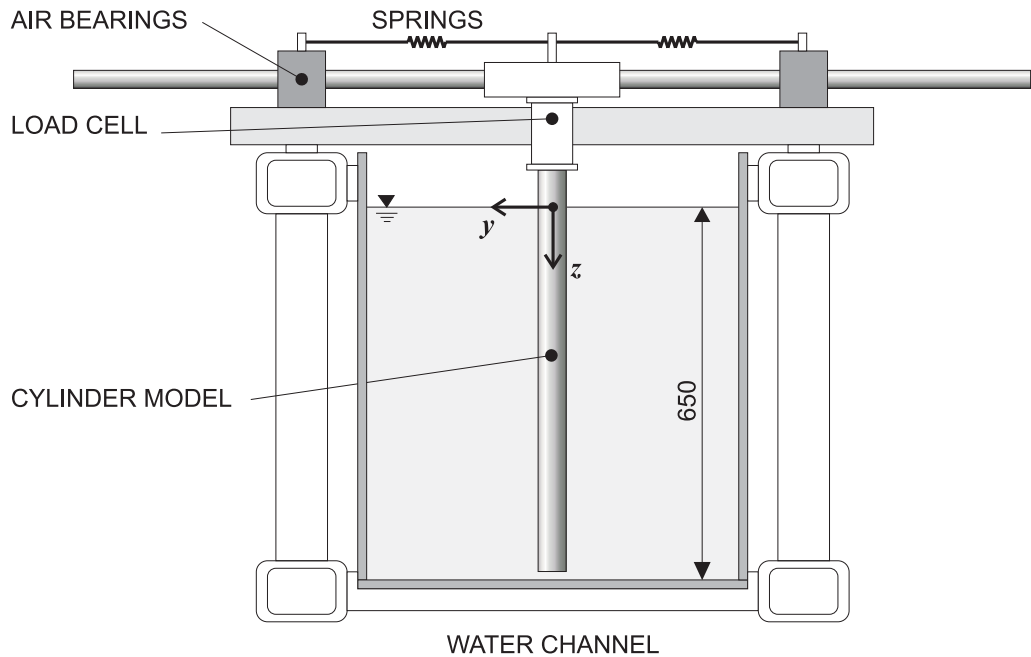
Fig. 4.5: Schematic representation of the 1-dof rig holding the downstream cylinder. The free stream flows out of the page in the x-axis direction.

later) connected the moving table to the top end of the cylinder and was adjusted to measure instantaneous fluid forces acting on the cylinder in the cross-flow and streamwise directions (lift and drag, respectively). An optical positioning sensor was installed to measure the y-displacement of the cylinder without introducing extra friction to damp the oscillations.

This configuration proved to combine high stiffness with low mass and damping, solving the structural problem observed by Assi *et al.* (2006) — who employed a flexing-blade rig — and pushing the reduced velocity range to higher limits. The whole of the experimental apparatus was manufactured in the workshop of the Department of Aeronautics and a photograph of the rig installed on the water channel is shown in Fig. 4.6.

Completing the instrumentation, a pair of hot-film probes was employed to measure velocity fluctuations in the gap between the cylinders and in the developed wake downstream of the second cylinder (see Fig. 4.4). A Dantec particle-image velocimetry (PIV) system was employed to map velocity fields. A laser sheet entered the section through one of the sidewalls illuminating the flow at the mid-height of the section. A digital camera was positioned underneath the channel and the
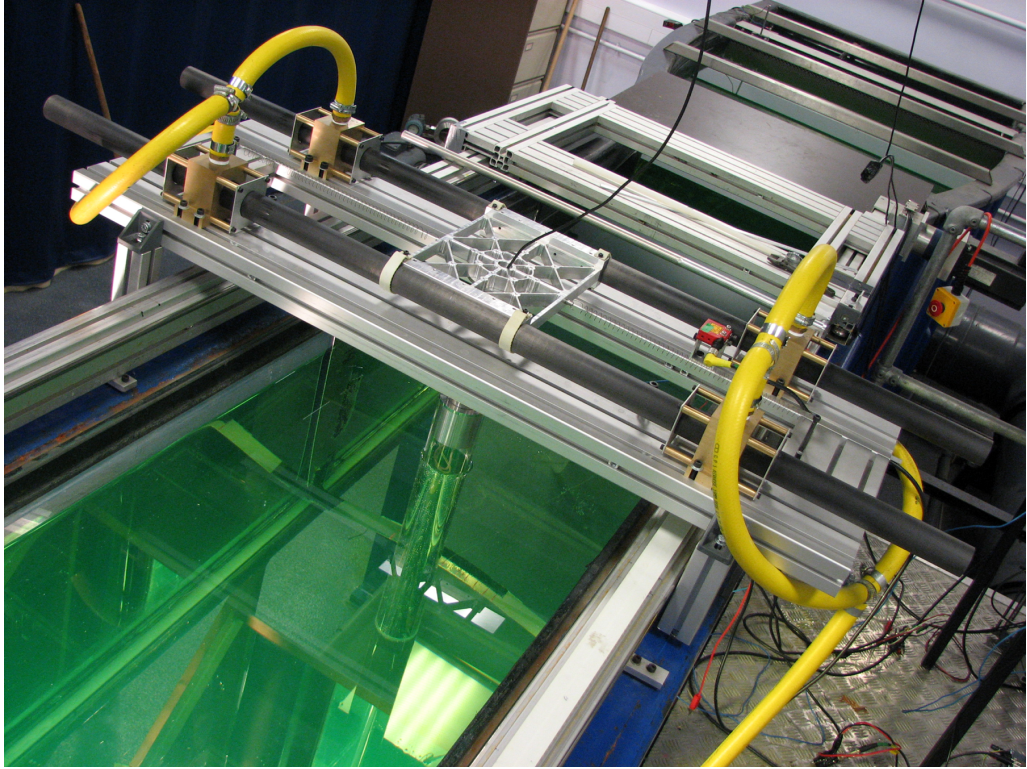
Fig. 4.6: Photograph of the 1-dof rig mounted on top of the water channel. The cylinder is seen submerged in water.

illuminated plane was visualised through the glass floor avoiding any interference caused by the free surface. Flow visualisation was also carried out using the same laser to illuminate fluorescent dye or hydrogen bubbles.

4.3.1 Structural mass, natural frequency and damping

As discussed in Chapter 2, the dynamic response of an FIV oscillator is extremely sensitive to the structural characteristics of the system; therefore extra care was taken to determine the precise value of natural frequency, mass and damping of the structure.

A pair of steel coil springs was installed between the moving table and the rigid supports in order to provide the structural restoration force of the oscillator. The spring stiffness (k) combined with the mass of all oscillating parts (m) results in the undamped natural frequency of oscillation f_0, already defined in Eq. 2.6. More than one set of springs could be employed resulting in an array of possible natural frequencies. However, most of the experiments were performed with one main pair

of springs, which provided the system with a natural frequency of oscillation of $f_0 = 0.30$Hz, determined by performing a series of free decay tests in air without any extra mass added to the rig. The other sets of springs gave values of f_0 between 0.1 and 0.5Hz for the same conditions. With the main set of springs it was possible to vary reduced velocity to a maximum of $U/Df_0 = 40$ when U was increased up to 0.6m/s. The minimum flow speed that the channel could run at was $U = 0.03$m/s, resulting in the lower limit of $U/Df_0 = 2.0$.

All moving parts of the elastic base contributed to the effective mass oscillating along with the cylinder. Therefore, m could be altered by adding extra mass on top of the rig, but not to the cylinder itself. This way the actual mass of the cylinder was always kept constant while the mass ratio of the system (m^*) could be varied as required (see Eq. 2.10). For most of the experiments, when the lightest configuration was used, the mass ratio was found to be $m^* = 2.6$ for a 50mm-diameter cylinder.

The structural damping of the system was mainly caused by friction between the sliding guides and the air bearings. As explained before, the main principle was to keep the damping as low as possible and increase it in controlled steps if necessary. The air bearings proved to be an efficient way to reduce damping without compromising the stiffness of the structure, especially in resisting drag loads for higher flow speeds. By carrying out free decay tests in air it was possible to estimate the structural damping of the system for each configuration of mass and springs. Most of the experiments were conducted with $m^* = 2.6$ and $f_0 = 0.30$Hz and the structural damping measured for this configuration was $\zeta = 0.7\%$, calculated as a percentage of the critical damping as defined in Eq. 2.7. Therefore, the product $m^*\zeta = 0.018$ for the majority of the experiments.

However, at times it was required to vary the parameter $m^*\zeta$ or one of its terms independently. As mentioned before, extra mass could be added to the rig in order to increase m^*, but the damping factor ζ could also be varied by adding artificial damping to the system. A small reservoir filled with thick machine oil was installed along the rig and a small arm holding a steel screen was immersed in the oil. The amount of damping was varied by changing the height of the screen submerged in oil. The new value for ζ was then measured with free decay tests in air. This

method proved to give good control of the damping level enabling small variations of ζ between 0.7% and 20% of the critical damping.

4.3.2 Load cell

A load cell was attached between the model and the table to measure instantaneous and time-averaged hydrodynamic forces acting on the cylinder. It consisted of two independent load cells machined out of one block of a hard aluminium alloy. Each cell was perpendicular to each other in order to measure components of the hydrodynamic force in the streamwise and cross-flow directions.

Fig. 4.7 illustrates the concept of the load cell. Two small webs of about 0.5mm in thickness were machined and instrumented with four strain gauges each. Each set of four strain gauges was wired to form a complete Wheatstone bridge, which was connected to a power supply and signal amplifier. This configuration permitted each individual cell to be insensitive to moments but responsive only to the force component acting in its direction. The load cell was also insensitive to force variations in the vertical axis, such as the weight or buoyancy of the model. Each cell was calibrated individually and there was observed to be no significant cross-talk between them. The load cell was designed to measure a load of up to 50N with an uncertainty of 1% in each direction.

Fig. 4.8 presents the result of a computational study developed during the design process. Colour contours show a concentration of strain on one of the webs when a nominal load was applied in the corresponding direction. The bright red area indicates where the strain gauges should be placed. This was used to estimate not only the necessary thickness of the webs to give enough resolution to the measurements, but also to evaluate the critical load above which the webs would fracture.

The fluid force projected in the streamwise direction (drag) could be measured straight away from the load cell, since the cylinder was not allowed to move in the x-axis. However, the cross-flow component needed to be corrected in order to remove the inertia force of the cylinder also captured by the cell. The inertia term is given

Fig. 4.7: Photograph of the load cell showing a pair of strain gauges installed on one of the webs.
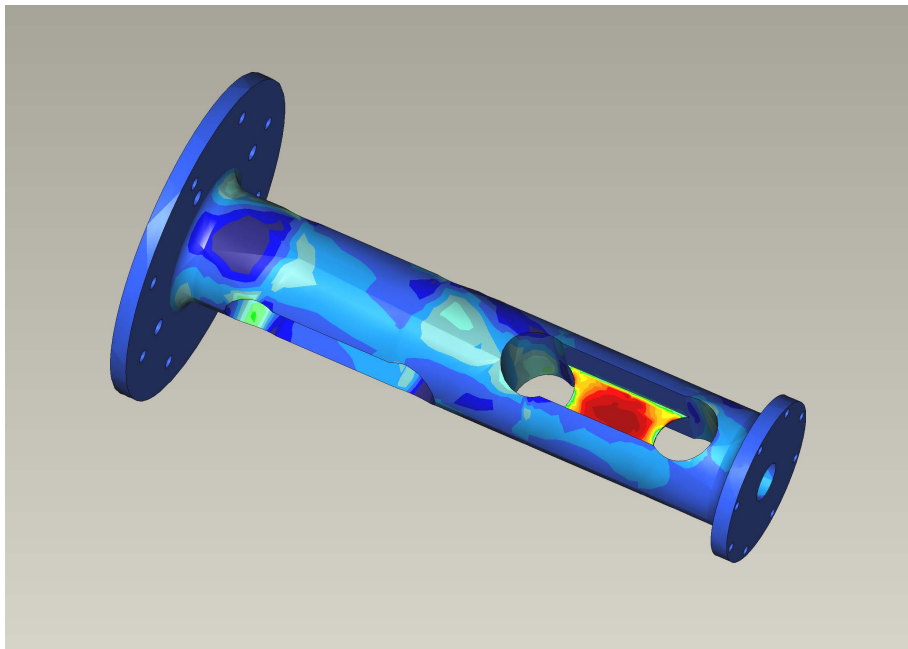

Fig. 4.8: Finite element structural analysis. Colour contours represent strain magnitude and show strain concentration (in red) on the bottom web.

by the acceleration of the cylinder times the mass of the structure hanging below the load cell. Since extra weight was added on top of the table and never below the load cell, the mass hanging on the load cell was practically that of the cylinder and its structural components (m_{cyl}). Hence, the fluid force acting on the cylinder can be calculated by subtracting the inertia term from the actual force signal measured by the load cell (F_{cell}). Yet, the load cell measures the reaction force and the direction of the fluid force has to be inverted, resulting in

$$F_y = \ddot{y}m_{cyl} - F_{cell}. \tag{4.2}$$

The upstream cylinder was also instrumented with a similar load cell allowing for measurements of instantaneous lift. In that case no force correction was necessary since the body was held static at all times.

4.4   Two-degree-of-freedom rig

In addition to the 1-dof rig presented above, a second rig with 2 degrees of freedom (2-dof rig) was also built during the present study and was employed to investigate the effectiveness of devices to suppress FIV. Results obtained with the 2-dof rig are only presented in Chapter 8.

The 2-dof rig, allowed the cylinder to freely respond in both transverse and in-line directions. A schematic representation is shown in Fig. 4.9 while a photograph of the 2-dof rig during experiments of VIV of a single cylinder is presented in Fig. 4.10. The cylinder model was mounted at the lower end of a long carbon fibre tube which formed the arm of a rigid pendulum. The top end of the arm was connected to a universal joint fixed at the ceiling of the laboratory so that the cylinder model was free to oscillate in any direction in a pendulum motion. The distance between the bottom of the cylinder and the pivoting point of the universal joint was 2800mm. Two independent optical sensors were employed to measure displacements in the x and y-directions. It should be noted that for a displacement equal to 1 diameter the inclination angle of the cylinder was only just over 1° from the vertical. All displacement amplitudes presented for 2-dof measurements are for a location at the
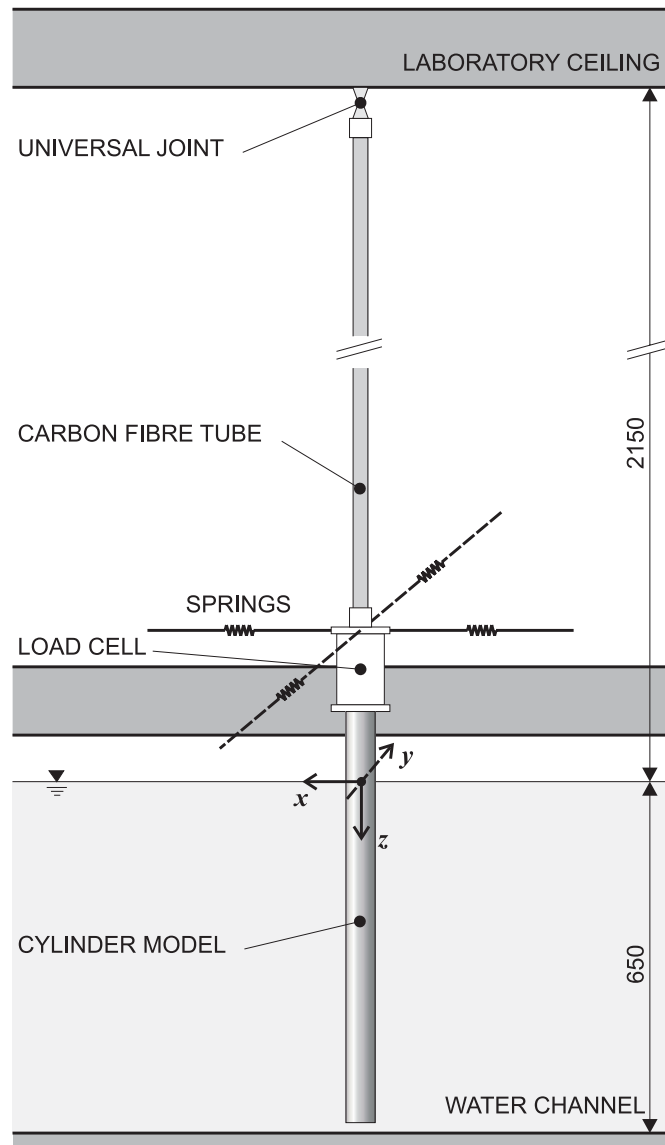
79

Fig. 4.9: Schematic representation of the 2-dof rig holding the downstream cylinder. The free stream flows in the x-axis direction.
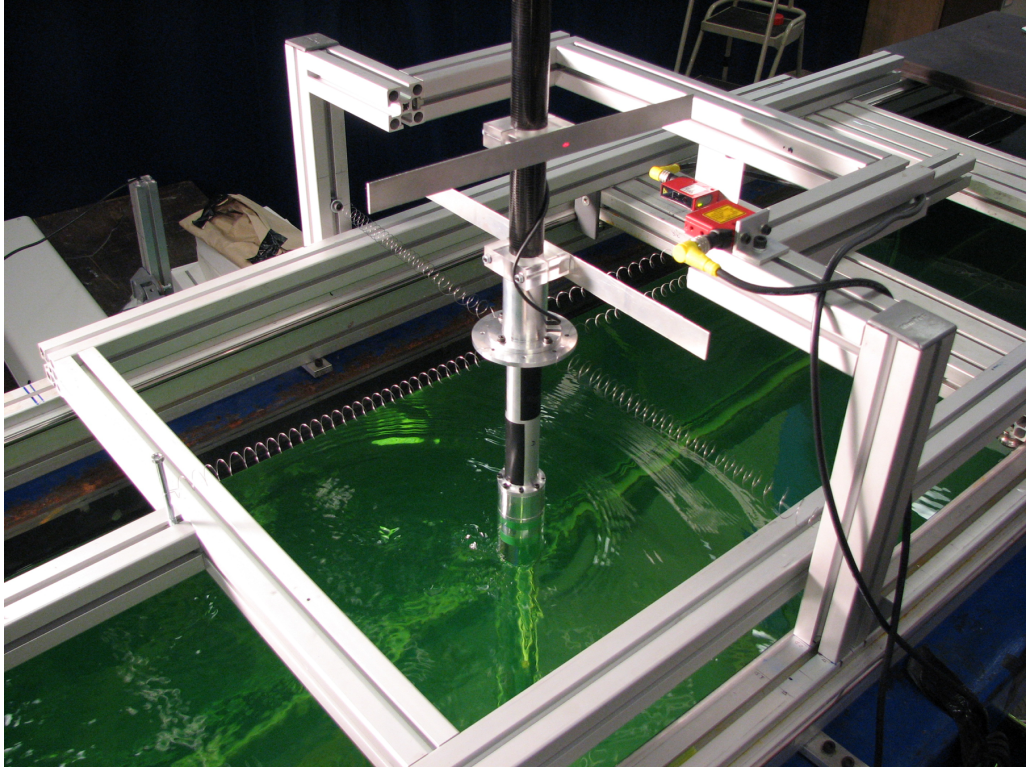
Fig. 4.10: Photograph of the 2-dof rig. The cylinder is seen submerged in water. This photograph does not show the final configuration of the 2-dof rig; the in-line springs are not mounted on long wires yet.

mid-length of the model.

Two pairs of coil springs were installed in the x and y-axes allowing the setting of different natural frequencies in each direction. Therefore, we define two natural frequencies f_{0_y} and f_{0_x} corresponding to the cross-flow and streamwise direction for 2-dof experiments. Although the cylinder was initially aligned in the vertical position, in flowing water the mean drag displaced the cylinder from its original location. To counteract this effect, the in-line pair of springs was attached to a frame that could be moved back and forth in the direction of the flow. For each flow speed there was a position of the frame that maintained the mean position of the cylinder in the vertical direction, balancing the drag force with a displacement of the springs.

Using two pairs of springs perpendicular to each other resulted in nonlinear spring constants in the transverse and in-line directions. Movement in the transverse direction will cause a lateral spring deflection in the in-line direction and vice versa.

This nonlinearity was minimised by making the springs as long as possible, hence the in-line springs were installed at the end of 4m-long wires fixed at the extremities of the frame.

It is known that during the cycle of vortex shedding from bluff bodies the fluctuation of drag has double the frequency of the fluctuation of lift. Hence a particularly severe vibration might be expected to occur if the hydrodynamic forces in both directions could be in resonance with both in-line and transverse natural frequencies at the same time. For this reason, we set the in-line natural frequency f_{0_x} to be close to twice the transverse f_{0_y} by adjusting the stiffness of both pairs of springs.

Because the carbon fibre pendulum was lighter than the oscillating parts of the 1-dof rig, the mass parameter obtained for the 2-dof rig could reach a value below $m^* = 2.6$. The structural damping of the 2-dof rig was $\zeta = 0.3\%$, approximately the same for both principal directions of motion and lower than the one measured for the 1-dof rig. Again, values for f_{0_x}, f_{0_y} and ζ were determined by measuring free oscillations in air in both directions.

The same load cell described above could be installed in the 2-dof rig in order to measure instantaneous lift and drag acting on the cylinder. However, since the model presented displacements in both directions, the inertia correction presented for the lift force in Eq. 4.2 had to be employed also for the unsteady drag force considering the acceleration of the body in the in-line direction.

Chapter 5

WIV response of the downstream cylinder

This chapter presents the main experimental results obtained in the present work. It starts with a brief validation of the experimental methodology by comparing the VIV response of a single cylinder with other results found in the literature. Afterwards the WIV response of the downstream cylinder is characterised in terms of displacement amplitude and frequency of oscillation. Instantaneous fluid force measurements and decomposition are also discussed.

5.1   VIV response of a single cylinder

A preliminary experiment was performed with a single cylinder free to oscillate in 1-dof in a uniform flow to serve as reference for comparison and validation of the experimental methodology. The same elastically mounted cylinder was employed in experiments with a single or a pair of cylinders; therefore the experimental parameters are exactly the same for both cases allowing direct comparison between the results.

5.1.1 Displacement and frequency of oscillation

Throughout the study, cylinder displacement amplitude ($\hat{y}$) was found by measuring the root mean square value of response and multiplying by $\sqrt{2}$. Such a harmonic amplitude assumption is likely to give an underestimation of maximum response but was judged to be perfectly acceptable for assessing the average amplitude of response for many cycles of steady state oscillations. An alternative method was to measure the amplitude of individual peaks of displacement in order to estimate an average value, but this was found to give very similar results as the harmonic amplitude mentioned above, thus proving that a sinusoidal approximation for the response is indeed very reasonable. The same procedure was employed to determine the magnitude of all other fluctuating variables, such as $\hat{C}_y$ and $\hat{C}_x$.

Fig. 5.1 presents experimental results for the dynamic response of a cylinder under VIV in terms of displacement amplitude, frequency of oscillation and phase angle ϕ. Since U is increased in order to vary the reduced velocity, Re also varies along the reduced velocity axis and is plotted as a reference in a parallel axis. In the middle graph of f/f_0 a variation from blue to red represents higher peaks in the normalised power spectral density (PSD) of the frequency of oscillation (please refer to Appendix A for an explanation about how PSD plots were compiled).

In the $\hat{y}$ curve (top graph) it is possible to identify the typical three branches of response discussed by Williamson & Govardhan (2004). An initial branch showing a build up of response at lower reduced velocities is clearly detached from the upper branch, the latter being characterised by a peak of $\hat{y}/D = 0.8$ just before a reduced velocity of 4. At this point the frequency of oscillation crosses the natural frequency of oscillation in water, which is identified by the dashed line f_W/f_0 in the middle graph. At this same point, the vortex-force phase angle (ϕ_V) goes through an almost 180° shift associated with the transition in the vortex shedding mode, as shown in the bottom graph.

A lower branch with predominant amplitude of about $\hat{y}/D = 0.5$ smoothly follows the upper branch after a reduced velocity of 5, when the frequency of oscillation rises above the natural frequency in air ($f/f_0 = 1.0$). At this reduced
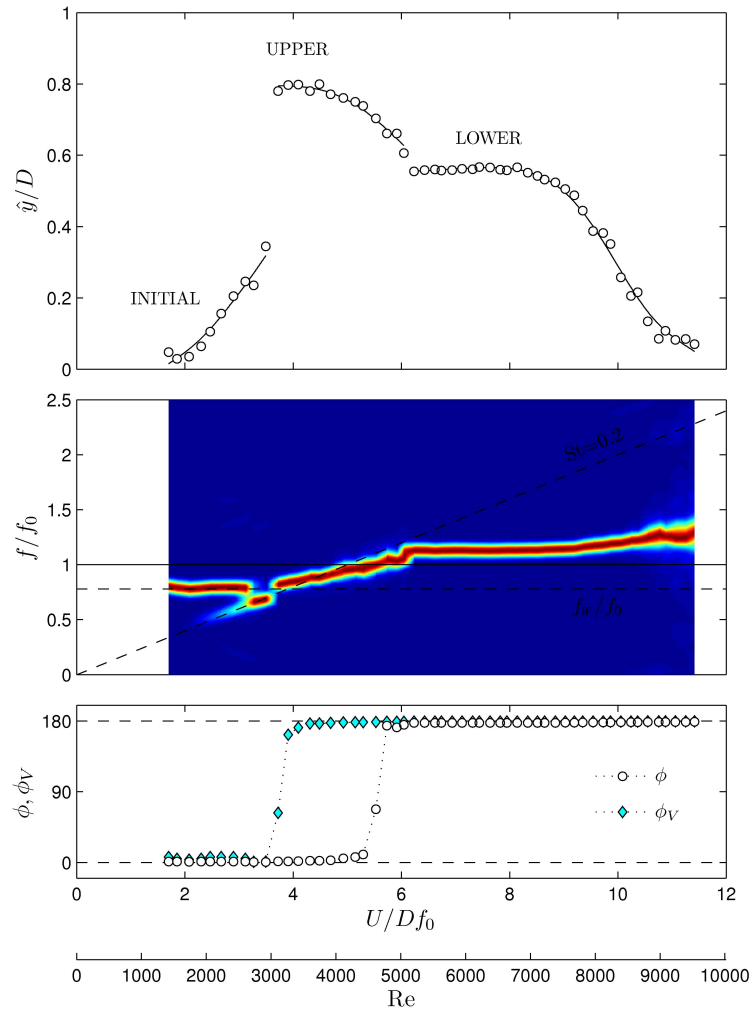
Fig. 5.1: VIV response of a single cylinder free to oscillate in the cross-flow direction. Top: displacement; middle: normalised PSD of frequency of oscillation; bottom: phase angles ϕ and ϕ_V. Please refer to Appendix A.
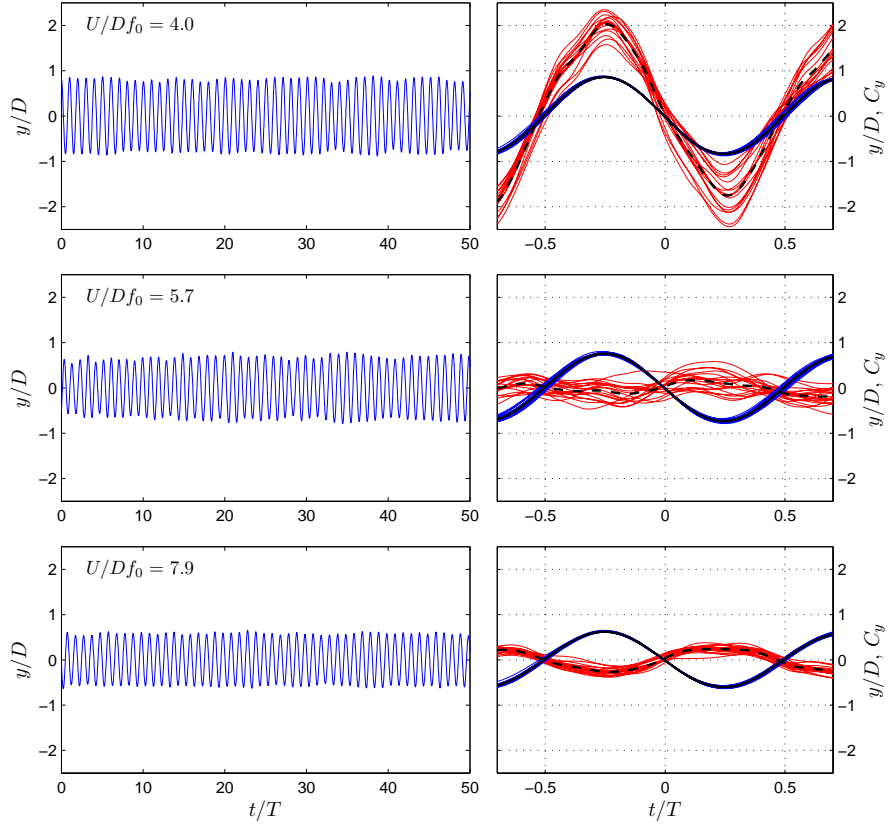
Fig. 5.2: Three examples of VIV time series. Left column: displacement signal for around 50 cycles of oscillation. Right column: superimposed plots of similar cycles. $\hat{y}$ in blue and C_y in red with average cycle in black. Top: upper branch; middle: transition between branches; bottom: lower branch.

velocity the phase angle of the total lift force (ϕ) experiences a shift of almost 180°. The frequency of oscillation remains at a roughly constant level until the end of this synchronisation range, up to a reduced velocity of 10, when the amplitude of oscillation drops to levels below $\hat{y}/D = 0.1$. These first results are in very good agreement with those presented by Govardhan & Williamson (2000) and discussed in Chapter 2.

5.1.2 Branches and mode transitions

Time series of $\hat{y}$ for about 50 cycles of oscillation are plotted for different reduced velocities in the left-hand side graphs of Fig. 5.2 (T being the period of an average cycle). The first data-set ($U/Df_0 = 4.0$) is collected from a point in the upper branch

of VIV; the second ($U/Df_0 = 5.7$) is in the transition between the upper to the lower branch; and the third ($U/Df_0 = 7.9$) is in the lower branch. In the first and third series it is possible to note that the envelope of $\hat{y}$ is very well behaved, i.e. the peak amplitude has small variations in time. But for the series in the transition between branches the peak amplitude shows more variations from one cycle to another and the envelope of amplitude is more irregular than the other two.

The plots on the right compare several cycles of $\hat{y}$ and C_y superimposed in one figure, each representing around 20% of the total number of acquired cycles with displacement around the average $\hat{y}/D$. Again it is evident that the deviation of $\hat{y}$ from the mean curve (continuous line in black) is accentuated during the transition between branches. Looking at C_y curves of Fig. 5.2 we observe that although the magnitude of lift shows considerable variations the phase angle between cycles is reasonably constant in the upper and lower branches. C_y is clearly almost in phase with $\hat{y}$ in the upper branch and in antiphase in the lower. However, the behaviour of C_y for only a few cycles of oscillation is enough to show that a constant phase angle ϕ is not observed during the transition between the upper to the lower branch. A disarray of red lines in the plot on the right reveals that both magnitude and phase of lift are changing during the transition between modes.

Fig. 5.3 reveals more details of the phase transition associated with the modes of vortex shedding for the same data-sets illustrated in Fig. 5.2. The instantaneous behaviour of ϕ at different reduced velocities was analysed by employing a Hilbert analytical transform to the signal, as described in Hahn (1996) and Khalak & Williamson (1999). The value of ϕ in the initial and upper branches remains very close to $0°$ (top left graph, $U/Df_0 = 4.0$). The graph on the right illustrates the same behaviour by plotting C_y versus $\hat{y}$. A Lissajous figure that resembles a straight line inclined towards the first and third quadrants reveals that both signals have the same dominant frequency and are almost in phase.

The opposite is observed for $U/Df_0 = 7.9$. ϕ remains very close to $180°$ for the whole time series and the Lissajous figure with opposite inclination indicates an almost anti-phase relationship between lift and displacement. However, the transition from the upper to the lower branch does not occur all of a sudden, but
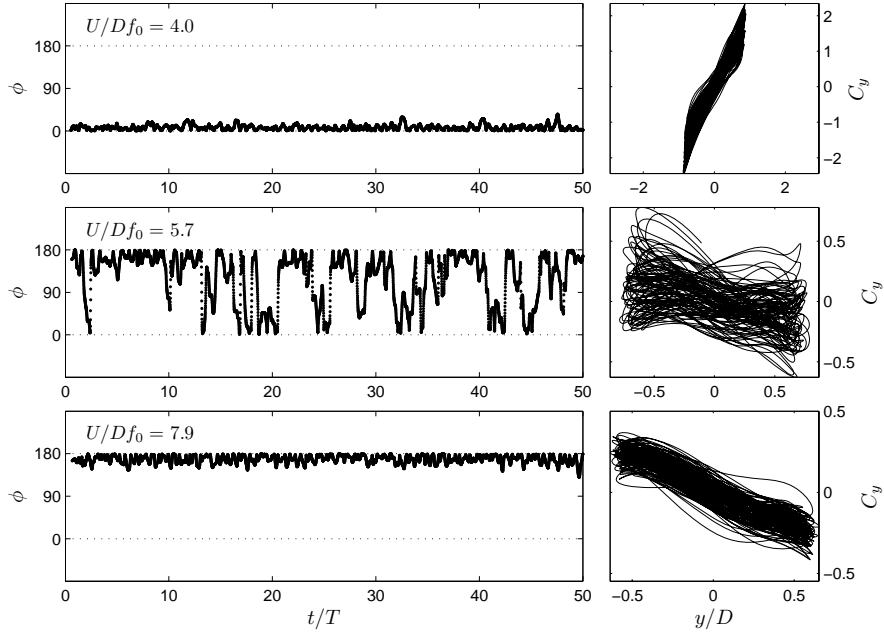
Fig. 5.3: Three examples of VIV phase angles. Left column: instantaneous phase angle ϕ for around 50 cycles of oscillation. Right column: Lissajous figures of C_y versus $\hat{y}$. Top: upper branch; middle: transition between branches; bottom: lower branch.

shows an intermittent and gradual behaviour. ϕ alternates between $0°$ and $180°$ as the flow switches between the first and the second sub-regimes of the 2P mode of vortex shedding (Williamson & Govardhan, 2004).

The transition occurs as the number of cycles with $\phi = 180°$ is gradually increased as VIV moves from the upper to the lower branch. If the time series is long enough to minimise statistical errors it will produce a smooth transition between the upper and lower branches as shown in the displacement plot of Fig. 5.1. But this does not mean that a real intermediate phase angle is present. The instantaneous value of ϕ and the Lissajous figure for the example given in Fig. 5.3 (middle) reveals that an average value for ϕ cannot be accurately attributed to represent the whole series. Therefore the point around $\phi = 80°$ in Fig. 5.1 must be understood as an average of the phase angle that is intermittently switching between $0°$ and $180°$.
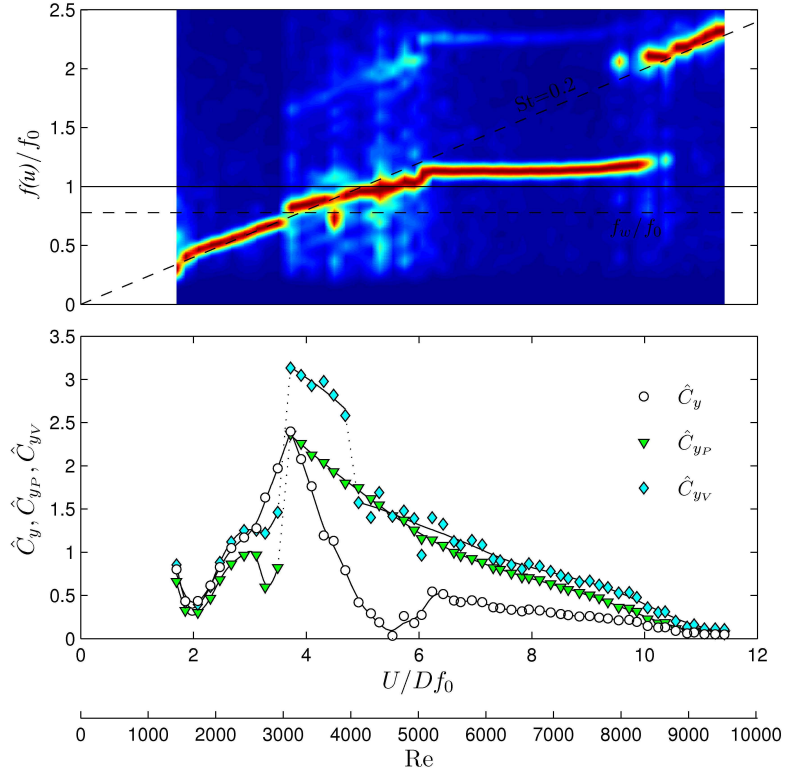
Fig. 5.4: Top: normalised PSD of velocity fluctuation (u) in the wake of a single cylinder. Please refer to Appendix A. Bottom: Decomposition of lift coefficient into potential and vortex components.

5.1.3 Fluid force decomposition

The top graph in Fig. 5.4 presents the frequency spectrum of velocity fluctuation (u) measured with a hot-film probe at a station in the near wake of the cylinder. This represents the shedding frequency f_s plotted against reduced velocity in a similar way to the frequency graph of Fig. 5.1. As the flow speed is increased from rest the cylinder, which is still stationary, sheds vortices following the Strouhal law. The inclined dashed line corresponds to a Strouhal number of 0.2 for a static cylinder, which is closely followed by f_s before and after the synchronisation range.

In the lock-in range the vortex shedding mechanism shows a distinct behaviour. As the cylinder builds up amplitude in the initial branch the displacement of the body interferes with its own process of vortex formation, f_s departs from the Strouhal line and is locked by f within $3 < U/Df_0 < 10$. But as reduced velocity is further increased both frequencies become too far apart for this fluid-structure

mechanism to be sustained, f_s and f decouple and an almost stationary cylinder allows f_s to return to the line of St $= 0.2$ marking the end of the synchronisation range.

The bottom graph in Fig. 5.4 shows the behaviour of fluid force versus reduced velocity. $\hat{C}_y$ was directly measured with the load cell and $\hat{C}_{y_P}$ and $\hat{C}_{y_V}$ were calculated from Eqs. 2.17 and 2.18 (page 35). $\hat{C}_y$ shows a characteristic curve that reaches its maximum value at the resonance but abruptly falls to its minimum at the end of the upper branch. $\hat{C}_{y_V}$, which quantifies the actual force from the vortices in the flow, is the component associated with the excitation and shows a distinct jump in the upper branch when f is between f_W and f_0. This corresponds to the transition from the 2S to 2P mode and shows that a change in the wake mode has a significant effect in sustaining high amplitudes of vibration. $\hat{C}_{y_P}$ only quantifies the inertia force associated with the product of the mass of displaced water and the acceleration of the body.

Force measurements and decomposition are in good agreement with results presented by Khalak & Williamson (1999). In addition, PIV measurements (not presented in this text for brevity) also found good agreement with their work in identifying the correct vortex shedding modes in the wake.

5.2 Overview of the WIV response

Since WIV has its origin in the wake developed in the gap between the cylinders, it is expected that the centre-to-centre separation between a tandem pair has some effect on the response of the downstream body. This is clearly confirmed in Fig. 5.5 showing that the response curve has indeed a strong dependency on x_0. In this plot there are only curves for WIV in the second regime of wake interference, i.e. when a fully developed vortex wake is able to form in the gap between the bodies, including the smallest separation of $x_0/D = 4.0$. Results are in good qualitative agreement with Laneville & Brika (1999) presented in Fig. 3.7 (page 53), even though they have performed test with flexible cylinders.

The characteristic build-up of response reported in previous works is clearly

observed in Fig. 5.5 and contrasts with the typical VIV response obtained for a single cylinder in Fig. 5.1. A discrete hump is found to occur for all separations at around $U/Df_0 = 5.0$ and corresponds to the local peak of VIV resonance; although this happens slightly later in the reduced velocity scale due to the shielding effect of the wake that reaches the second cylinder. Beyond that a branch of monotonically increasing amplitude starts to build-up with increasing reduced velocity. As expected, it reveals that displacement amplitude is inversely proportional to separation x_0. As the downstream cylinder is moved farther away, the effect of WIV is reduced until the response curve eventually resembles that of VIV of an isolated cylinder. While at $x_0/D = 4.0$ the cylinder reaches displacement amplitudes around $\hat{y}/D = 1.6$ and increasing, a cylinder at $x_0/D = 20$ shows only the VIV peak with levels $\hat{y}/D$ around 0.2 for the rest of the regime.

The curve for $x_0/D = 8.0$ is a particularly interesting one because the intensity of the WIV effect is just enough to sustain the same level of response observed for VIV through the whole range of reduced velocities. Nevertheless all presented cases show some type of combined VIV and WIV responses, with the maximum amplitude of VIV $U/Df_0 = 5.0$ showing a minor dependency on x_0.

The bottom graph of Fig. 5.5 shows the dominant frequency of oscillation for each case plotted above. At a first view it is remarkable that all data points collapse over a very well behaved frequency response independently of x_0. During the beginning of the VIV regime the frequency curve follows closely the St $= 0.2$ line until $f = f_0$, but later departs from it to follow the lock-in behaviour observed for a single cylinder within the synchronisation regime. But where the typical VIV regime would have finished for a single cylinder, say for $U/Df_0 > 15$, the f curve remains on the same trend as before, which is distinctively lower than St $= 0.2$. Even for large separations of $x_0/D = 20$, in which the response resembles that of simple VIV, the dominant frequency is observed not to return to St $= 0.2$ after the end of the supposed synchronisation, but remains at a much lower level for the rest of the reduced velocity range with $\hat{y}/D$ around 0.2.

This is the first evidence that there must be a fluid force with a lower frequency that dominates the excitation — lower than the vortex shedding frequency of both
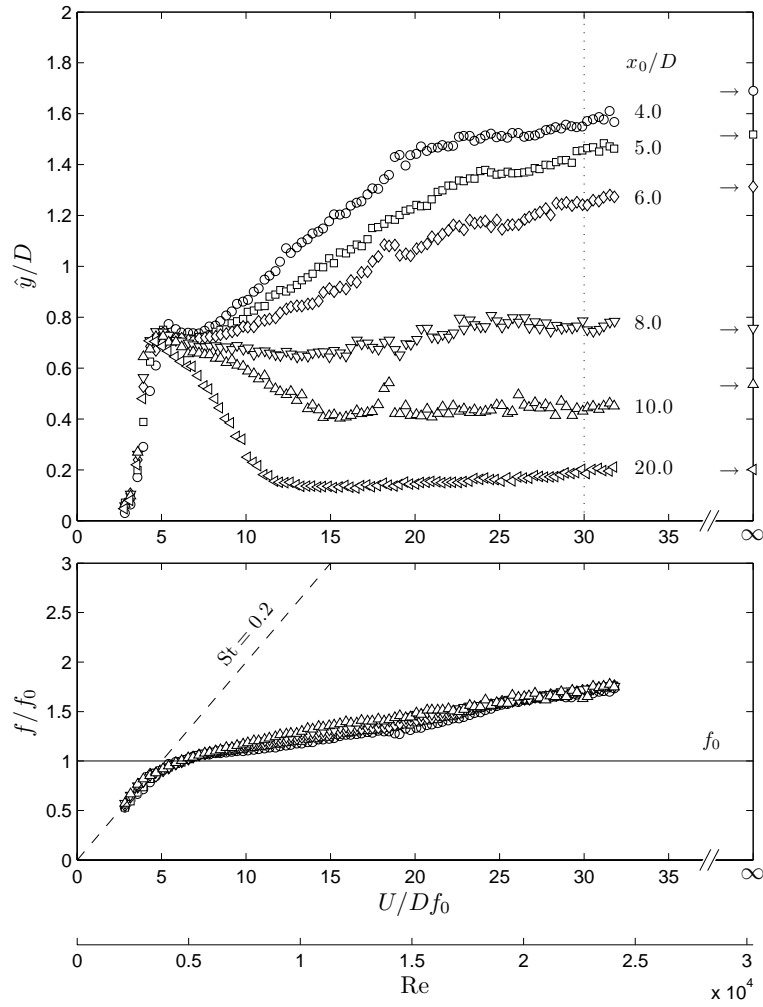
Fig. 5.5: WIV response of the downstream cylinder for various x_0 separations. Top: displacement; bottom: dominant frequency of oscillation.
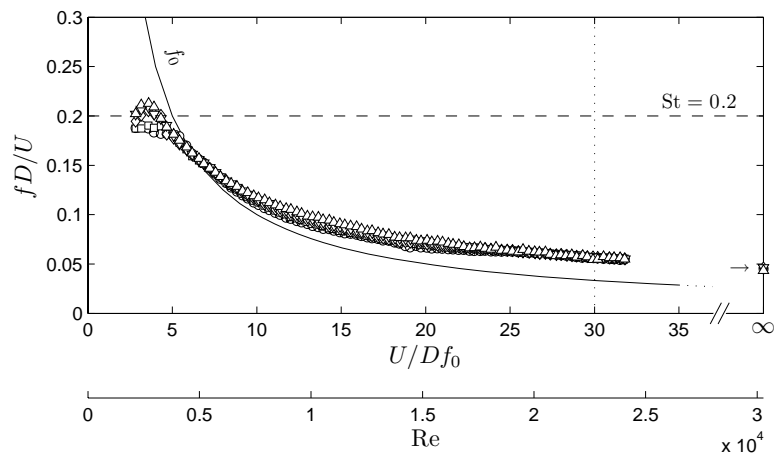

Fig. 5.6: Non-dimensionalised dominant frequency of oscillation of the downstream cylinder for various x_0 separations. Symbols from Fig. 5.5.

cylinders. The frequency of the force appears not to vary with x_0 and shows only a small dependency on reduced velocity or Reynolds number when compared to the St $= 0.2$ line, for example.

In order to remove the structural natural frequency (f_0) from the problem, a new non-dimensional frequency fD/U (a type of Strouhal number) is plotted against reduced velocity and Re in Fig. 5.6. The St $= 0.2$ line now becomes a constant and f_0 is expressed as a curved line for reference. It shows that fD/U is asymptotically converging to a value that is greater than f_0 but still much lower than St $= 0.2$. Although we will only deal with this plot later in this text it is convenient to place it here along with Fig. 5.5, where the data came from. Data points at U/Df_0 tending to infinity will also be discussed later.

5.3 WIV of the downstream cylinder at $x_0/D = 4.0$

With an understanding of the interference regimes from Chapter 3 and an overview of the characteristic 1-dof response of WIV presented in Fig. 5.5 we will now focus on one x_0 separation in order to remove another variable from the system. A separation of $x_0/D = 4.0$ was chosen for various reasons: (i) it was beyond the critical separation where a bistable reattachment of the shear layers may occur and a developed wake was observed to be present in the gap for all flow speeds; (ii) it gave a WIV response that is qualitatively consistent with other larger separations; (iii) the displacement and magnitude of fluid forces were rather large and provided accurate measurements with the load cell; (iv) and the separation was small enough to fit in the PIV field of view.

Following the same discussion for a single cylinder, Fig. 5.7 presents the WIV response of the downstream cylinder of a pair, initially in tandem, with $x_0/D = 4.0$. The same pair of springs was employed during the whole experiment and the velocity of the flow in the test section was varied in order to cover a large range of reduced velocity, therefore yielding Re $= 2000 - 25000$. Again, the upstream cylinder was kept static at all times.

The first graph in Fig. 5.7 plots the displacement versus reduced velocity. $\hat{y}$

is the harmonic amplitude of displacement discussed above and gives a good idea of the average amplitude of vibration for many cycles of oscillation. However $\hat{y}$ does not give a good estimation of the maximum amplitude the cylinder might reach if displacement is varying from cycle to cycle. By actually counting individual peaks of oscillation it was possible to estimate a maximum and a minimum peak amplitude taking an average of the 10%-highest and 10%-lowest peaks of the whole series, yielding $[\hat{y}/D]_{\max}$ and $[\hat{y}/D]_{\min}$ respectively. Therefore we can say that for a certain reduced velocity the cylinder oscillates on average with $\hat{y}/D$ but reaches the maximum and minimum limits given by the other curves. This brings considerable new information about the response since it shows that $\hat{y}$ is not only building-up with reduced velocity, but also the deviation from the average amplitude is also increasing; i.e. the variation of the envelope is also increasing.

The second graph in Fig. 5.7 shows the frequency of oscillation versus reduced velocity, the same data presented for $x_0/D = 4.0$ in Fig. 5.5 but now plotted as normalised PSD. It shows that the frequency of oscillation indeed follows a branch greater than f_0 but still not related to $\mathrm{St} = 0.2$. But the PSD contours also reveal that any other secondary frequency or harmonic present in the spectrum of oscillation is much smaller than the single dominant branch that is evident across the reduced velocity range. That is to say that there is no significant trace of a frequency branch associated with $\mathrm{St} = 0.2$ beyond reduced velocity 10, with only a hint appearing between 5 and 10.

As we saw before in Fig. 5.2, the envelope of the single cylinder VIV response is fairly regular except during the transition between branches. This is not the case for the WIV response illustrated in Fig. 5.8. For three data-sets at different reduced velocities we note that the envelope of response is already very irregular for only 50 cycles at $U/Df_0 = 4.6$. It only gets more irregular for higher reduced velocities of 5.8 and 30.6. This is also revealed in the graphs on the right column, which compile cycles of the 20%-highest peaks.

By comparing how C_y and $\hat{y}$ vary during one cycle it is possible to estimate the phase difference between them and also the frequency content of the signals. For $U/Df_0 = 4.6$, very close to the VIV resonance hump, we note that lift and
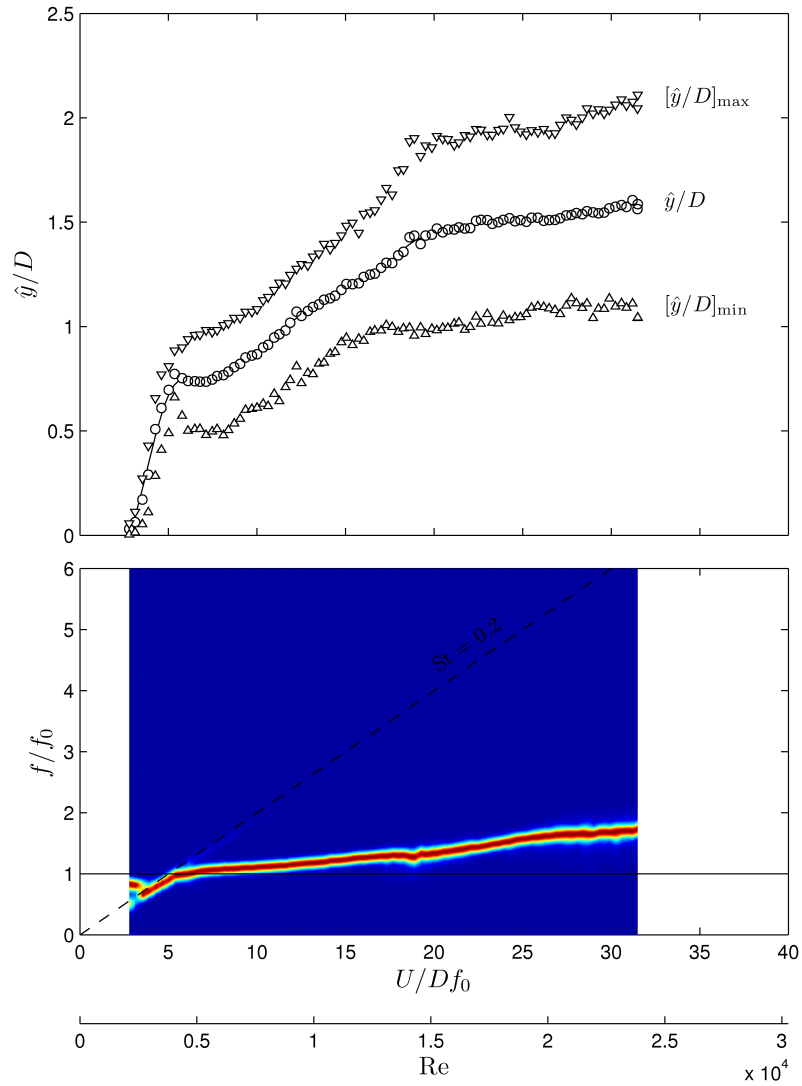
Fig. 5.7: WIV response of the downstream cylinder at $x_0/D = 4.0$. Top: average displacement and average of maximum and minimum peaks. Bottom: normalised PSD of frequency of oscillation. Please refer to Appendix A.
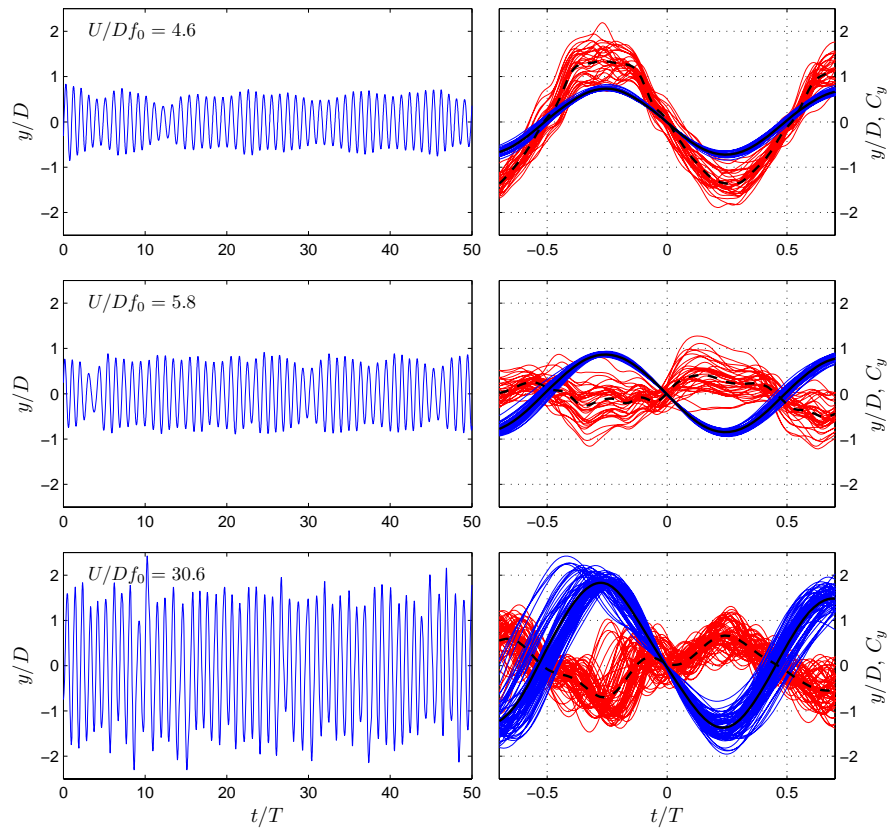
Fig. 5.8: Three examples of WIV time series. Left column: displacement signal for around 50 cycles of oscillation. Right column: superimposed plots of similar cycles. $\hat{y}$ in blue and C_y in red with average cycle in black.

displacement are almost in phase and there seems to be a single dominant frequency present in C_y. But moving to a slightly higher reduced velocity of 5.8 the behaviour of lift changes considerably. Not only a second frequency appears in the signal, but also the magnitude and phase of C_y are rather inconstant. Moving away from the VIV influence towards the end of the reduced velocity range we note that a higher frequency has definitely established in C_y, though it is not noticeable in the displacement curves.

Even though the upstream cylinder was kept static at all times in these experiments, it was also mounted on a load cell allowing instantaneous lift measurements. Analysing the normalised PSD of the lift force on both cylinders it is possible to identify and correlate other branches of frequency in C_y. Fig. 5.9 plots the normalised PSD of lift measured on both cylinders. From the top graph it is evident that the lift force acting on the upstream cylinder originates in the vortex shedding mechanism of that static body. There is only one distinct frequency branch that follows very closely the St = 0.2 line. It can also be concluded that the force on the upstream cylinder sees no effect of the oscillation of the downstream one, since no significant trace of that lower frequency branch is identified.

On the other hand, the bottom graph shows that the lift force on the downstream cylinder has two clear branches bifurcating from the VIV resonance point. The lowest branch corresponds to the frequency of oscillation in Fig. 5.7, but the highest branch is clearly associated with a vortex shedding frequency that follows the St = 0.2 line. This frequency may originate in the vortex shedding mechanism occurring on the upstream cylinder, or on the downstream cylinder, or on both. (The normalisation applied to all PSD graphs does not allow comparison of energy magnitudes across the reduced velocity axis, but only over vertical slices for a fixed reduced velocity. Please refer to Appendix A for more information.)

Now, this vortex-shedding branch is predominant at lower reduced velocities, probably related to the typical synchronisation range of VIV, but diminishes beyond reduced velocity 15. The lowest branch appears around reduced velocity 5 but only becomes dominant beyond reduced velocity 10. Within the range $U/Df_0 = 10 - 20$ both branches appear with equivalent energy content determining the region where
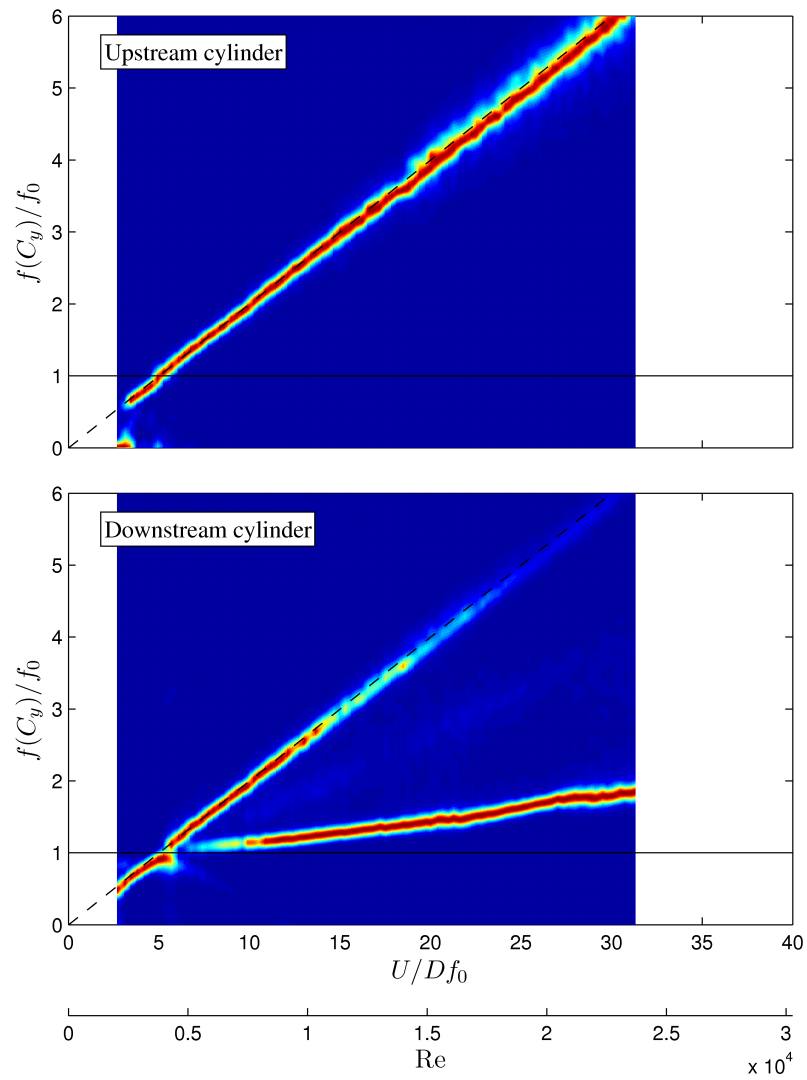
Fig. 5.9: Normalised PSD of lift force acting on the upstream static cylinder (top) and downstream oscillating cylinder (bottom). Please refer to Appendix A.

both VIV and WIV are occurring together.

In fact, looking again at the response curve in Fig. 5.7 it is quite apparent that three different regimes can be identified by different inclinations of the displacement curve: (i) a VIV resonance hump (upper branch) around $U/Df_0 = 5$; (ii) a combined VIV (lower branch) and WIV regimes roughly in the range $U/Df_0 = 5 - 17$; and (iii) a WIV regime for $U/Df_0 > 17$.

It is consistent to think that the VIV regime should involve synchronisation between vortex shedding from both cylinders, since their f_s frequencies must be rather similar. In order to investigate this we measured velocity fluctuations with hot-film probes at two stations downstream of both cylinders (please refer to Fig. 4.4, page 73). Fig. 5.10 presents the results confirming that the upstream cylinder is undoubtedly shedding vortices as a static, isolated cylinder with no interference from the oscillation of the downstream body.

On the other hand no clear identification of vortex shedding close to St $= 0.2$ was observed for the downstream cylinder that is oscillating. Of course once the cylinder is vigorously moving upstream of a fixed probe it is very difficult to measure any fluctuating component in the flow velocity other than that associated with the movement of the body. Even when the low frequency branch was filtered out no clear trace of vortex shedding was identified. This does not mean that the downstream cylinder is not shedding vortices — on the contrary, fully developed vortices were observed in PIV measurements as will be demonstrated later — it only means that the hot-film probe was not appropriate to capture this phenomenon.

Finally, in Fig. 5.11 we analyse the fluid force components acting on the downstream cylinder as expressed from Eq. 2.13 to 2.18 (page 32). Although one may argue that the 'harmonic forcing and harmonic motion' assumption employed in that analysis is not valid for the multi-frequency response of WIV, it might still bring some light into the phenomenon since for higher reduced velocities the same low frequency of oscillation is found in the lift content.

The top graph plots ϕ and ϕ_V versus reduced velocity showing that the phase shift from almost $0°$ to almost $180°$ occurs at around the same reduced velocity as for typical VIV. It shows that beyond the resonance peak ϕ and ϕ_V both remain close

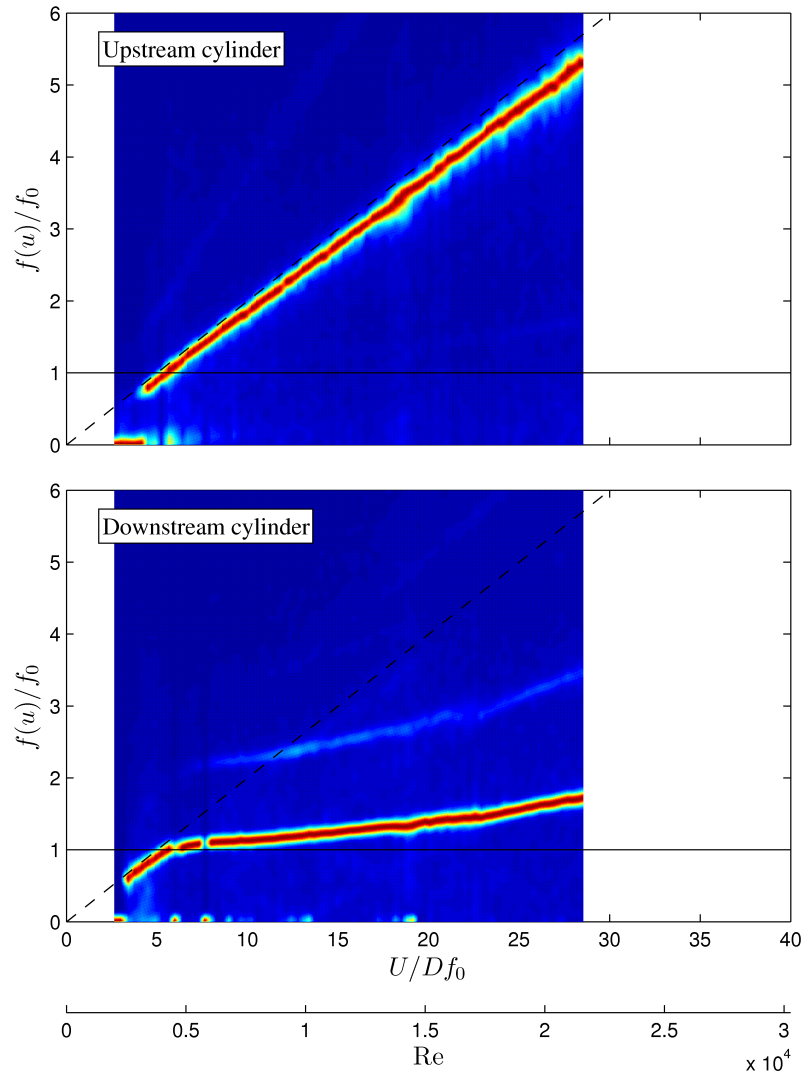Fig. 5.10: Normalised PSD of velocity fluctuation in the wake of the upstream static cylinder (top) and downstream oscillating cylinder (bottom). Please refer to Appendix A.
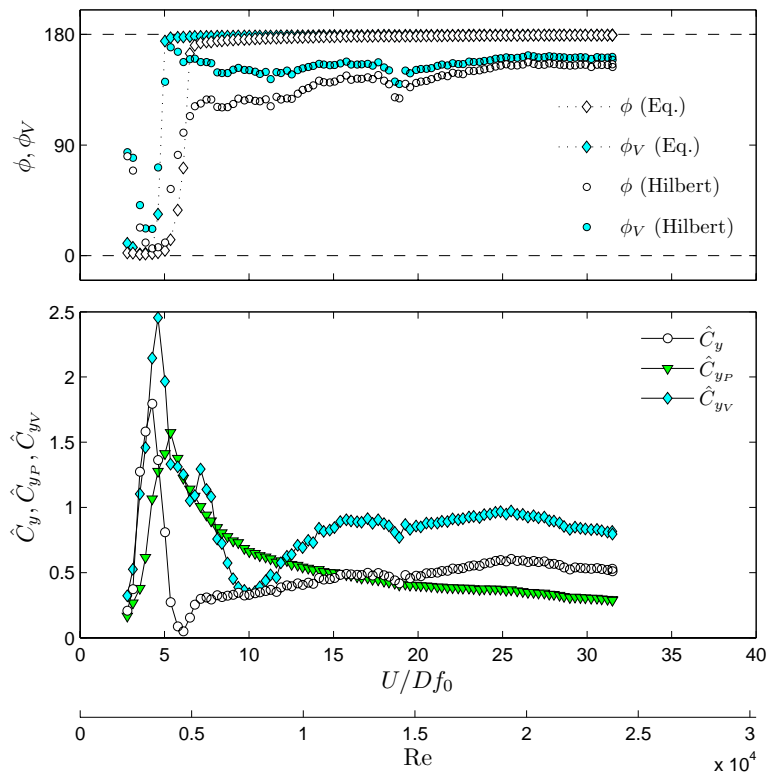
Fig. 5.11: Top: WIV phase angles calculated from Eqs. 2.13 and 2.16 and the Hilbert transform of the signals; bottom: decomposition of lift coefficient into potential and vortex components calculated from Eqs. 2.13, 2.17 and 2.18.

to 180° until the end of the reduced velocity range. This plot also compares ϕ and ϕ_V calculated by two different methods: the first solves Eqs. 2.13 and 2.16, which assumes harmonic response and lift with one dominant frequency; and the second averages the phase angles from the instantaneous Hilbert transform for the whole series. If the force and the response indeed present a single harmonic frequency — as they do for single cylinder VIV — both approaches are equivalent and the curves collapse. But Fig. 5.11(top) shows that the harmonic hypothesis must be an oversimplification of the WIV phenomenon. The actual phase angles calculated with the Hilbert transform of the displacement and lift signals do not follow the results from the idealised equations, but remain in a lower level for the whole range of the WIV excitation. This result reveals that the average phase lag between displacement and lift would actually be larger than the one predicted by a harmonic assumption.

The bottom graph shows the decomposed lift coefficient. For lower reduced velocities up to the VIV resonance hump the curves show very similar behaviour to that found for a single cylinder VIV (see Fig. 5.4). But instead of C_y and C_{y_V} reducing and tending to zero by the end of the synchronisation range, both rise up from around reduced velocity 7 up to 17, marking the second regime of combined VIV (a possible lower branch) and WIV. A clear WIV regime is identified in C_y and C_{y_V} curves for $U/Df_0 > 17$, as mentioned above, and their values remain roughly at the same level as reduced velocity is increased.

Fig. 5.12 presents a detailed analysis of the instantaneous variation of ϕ during 50 cycles of oscillation. ϕ remains very close to 0° for the whole time series at $U/Df_0 = 4.6$, resulting in a clean Lissajous figure in the right column. During the transition at $U/Df_0 = 5.8$ it appears that an intermittent phase shift is also present, corroborating with the observation in Fig. 5.8 (middle). Once the regime reaches a higher reduced velocity of $U/Df_0 = 30.6$ the phase is predominantly close to $\phi = 180°$ but it is not as well behaved as that for the pure VIV for a single cylinder. The corresponding Lissajous figure may suggest that a second dominant frequency may also be playing a role, in agreement with Fig. 5.8 (bottom).
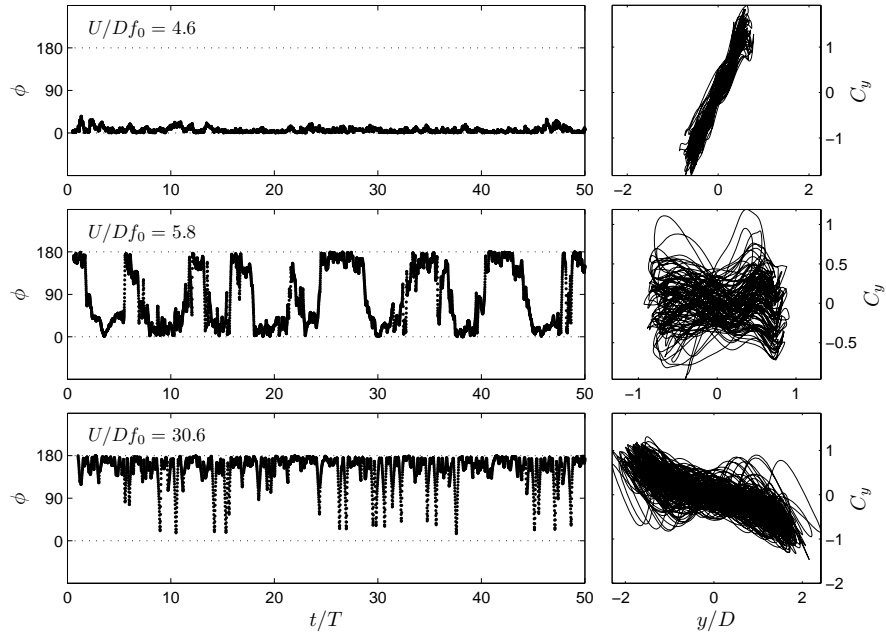
Fig. 5.12: Three examples of WIV phase angles. Left column: instantaneous phase angle ϕ for around 50 cycles of oscillation. Right column: Lissajous figures of C_y versus $\hat{y}$.

5.4   Conclusion

The WIV response of the downstream cylinder of a pair is distinctively different from the VIV response of a single cylinder. Although some aspects are common to both types of FIV, especially those related to the overlap of VIV regime in the WIV response, others are very different. The intermittent transition that occurs around the VIV regime was observed for both mechanisms and is thought to be purely related with this type of excitation. On the other hand, the low frequency of response observed for high reduced velocities is not associated with the vortex shedding mechanism of either cylinder.

In the next chapter we will turn from the response to investigating the origin of the lift force that is driving WIV on the second cylinder.

Chapter 6

The WIV excitation mechanism

This chapter discusses primarily the origin of the lift force acting on the downstream cylinder. It starts by presenting results for steady forces on a pair of static cylinders in staggered arrangements, detailing the force field for separation $x_0/D = 4.0$. Then it investigates unsteady forces acting on staggered, static cylinders before tackling the full problem in which the second cylinder is free to respond to the fluid excitation. The discussion is closely supported by PIV measurements of the instantaneous flow fields.

In an attempt to clarify the origin of the phase lag between displacement and fluid force, we present results from an idealised experiment with an artificial steady wake generated by a set of screens.

6.1   Steady fluid forces on static cylinders

We have performed experiments with a pair of static cylinders in order to evaluate the behaviour of fluid forces acting on the downstream body in various staggered arrangements. Measurements were obtained by holding the upstream cylinder fixed and traversing the downstream cylinder across 160 stations (each marked by a small cross in the next plots) in and out of the wake interference region at Re = 19200. Results are presented in a series of maps that are symmetrical in relation to the centreline of the wake.

Fig. 6.1 presents the steady lift and drag acting on the downstream cylinder for different regions of wake interference. A negative value of $\overline{C}_y$ indicates lift force acting towards the centreline. As expected, the first evident observation is that there is a steady lift force pointing in the direction of the centreline for all investigated configurations. For $x_0/D > 3.0$, it is observed that the magnitude of the $\overline{C}_y$ continually decreases on increasing the separation, but the transverse extent of the force field increases farther downstream as the wake widens. This is also evident from Bokaian & Geoola (1984) and Zdravkovich (1977).

The map reveals two regions of intense steady lift as high as $\overline{C}_y = -0.8$. As discussed in Chapter 3, the first region between $x_0/D = 1.5 - 2.5$ is associated with the gap-flow-switching mechanism occurring in the first wake-interference regime, i.e. when fully developed vortices do not form in the gap. The second region with $\overline{C}_y < -0.8$ occurs for larger lateral separations around $y_0/D = 0.8$. It begins around $x_0/D = 2.5 - 3.0$ and develops a trend of maximum $\overline{C}_y$ (indicated by the dash-dotted line) that will decrease in intensity as the second cylinder moves farther downstream. This second region is associated with the second interference regime in which the upstream shear layers are not able to reattach but roll up to form a developed vortex wake in the gap.

In the steady drag map presented in Fig. 6.1(b) positive contours of $\overline{C}_x$ denote drag in the streamwise direction. Dotted lines represent contours of zero or negative drag that occur when the cylinders are close enough for the gap flow to be enclosed by the reattaching shear layers. For $x_0/D > 2.5$ the tandem downstream cylinder only experiences positive drag indicating that a developed wake can now be formed in the gap. This critical separation coincides with the overlap of the two trends of maximum $\overline{C}_y$ presented in Fig. 6.1(a). While the downstream cylinder is immersed in the wake of the upstream cylinder the steady drag will be lower than that expected for a single cylinder exposed to a free stream. Only for lateral separations greater than $y_0/D = 1.5$ does this shielding effect disappear and $\overline{C}_x$ reaches values above 1.0.

So far we have only looked at the steady component of the fluid forces. If a quasi-steady assumption is to be used to understand WIV these steady maps should

(a) Mean lift $(\overline{C}_y)$

(b) Mean drag $(\overline{C}_x)$
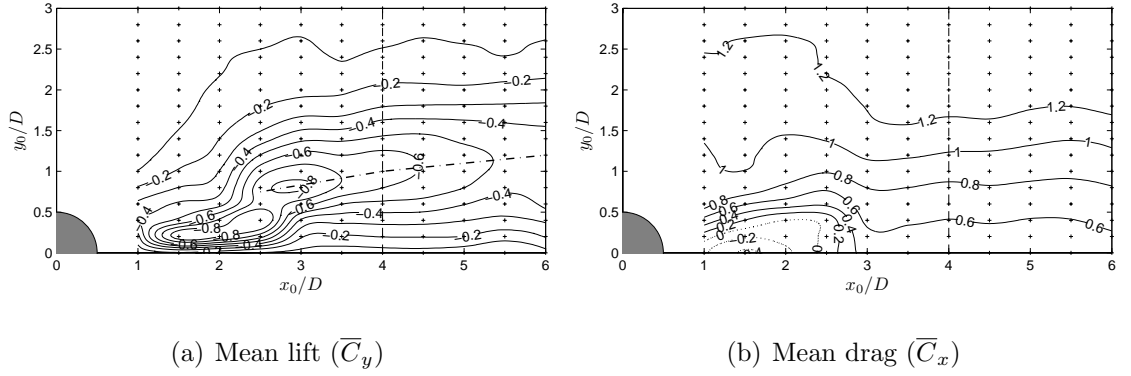
Fig. 6.1: Contours of steady fluid forces on the downstream cylinder of a static pair. Re = 19200.
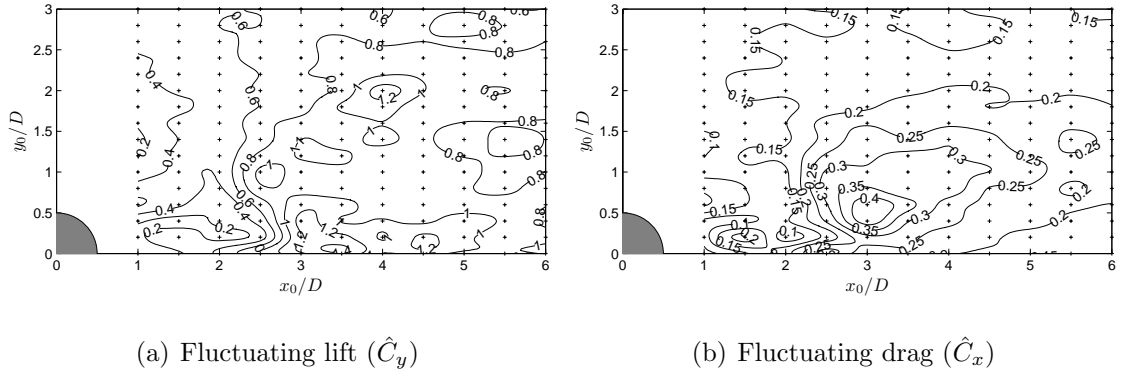

(a) Fluctuating lift $(\hat{C}_y)$

(b) Fluctuating drag $(\hat{C}_x)$

Fig. 6.2: Contours of fluctuating fluid forces on the downstream cylinder of a static pair. Re = 19200.

(a) Frequency of lift $(f(C_y)/f_s)$

(b) Frequency of drag $(f(C_x)/f_s)$

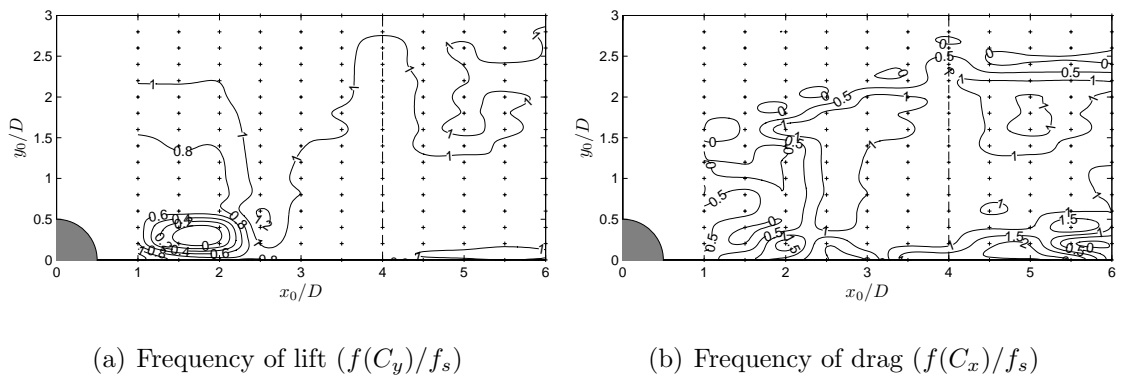Fig. 6.3: Contours of normalised frequency of fluctuating fluid forces on the downstream cylinder of a static pair. Re = 19200.

be adequate to provide the necessary gradients of C_y and C_x to satisfy a classical-galloping-like model. However, by also analysing the fluctuating components of the fluid force it is possible to identify if and where the unsteadiness of the flow is playing a significant role.

Figures 6.2(a) and 6.2(b) show similar maps to those presented in Figures 6.1(a) and 6.1(b) but plot contours of the fluctuating terms $\hat{C}_y$ and $\hat{C}_x$ (see Eq. 2.3). Both graphs show regions of increased fluctuating lift and drag that only occur for $x_0/D > 2.5$ when a developed wake is more likely to appear in the gap. A contour of $\hat{C}_y > 1.0$ appears for tandem arrangements but it is quite evident that relatively high values of $\hat{C}_y > 0.8$ will also appear for other staggered locations around the wake interference region. For separations below the critical value when vortices are not formed in the gap the fluctuating lift is reduced to levels below $\hat{C}_y = 0.4$.

Interestingly, the region of maximum $\hat{C}_x$ does not occur for tandem arrangements but when the downstream cylinder has an offset of about $y_0/D = 0.5$. $\hat{C}_x = 0.4$ is observed for the second interference regime at $x_0/D = 3.0$ and a trend of higher fluctuating drag is developed from this point decreasing in intensity as x_0 is increased.

The distribution of $\hat{C}_y$ and $\hat{C}_x$ across the wake gives support to the idea that coherent vortices from the upstream cylinder contribute to the fluctuating component of the fluid forces. Fluctuations due to the bistable nature of the separating flow are expected to occur for a close proximity between the bodies. But in this case we show considerable levels of steady and fluctuating fluid forces acting on the downstream cylinder when it is positioned much farther downstream, from separations of $x_0/D = 3.0$.

The magnitude of $\hat{C}_y$ is also another important factor. Taking the example for $x_0/D = 4.0$ and $y_0/D = 1.0$ we observe that the magnitude of the fluctuating lift is greater than the steady lift; i.e. the actual lift on the cylinder is $C_y = -0.6 \pm 0.8$, probably even reaching an instantaneous positive (outwards) value once in a few cycles. Even though one may attribute this enormous fluctuation to the vortex shedding mechanism of the second cylinder, a fluctuation of $\hat{C}_y = 0.8$ is comparatively higher than the value of $\hat{C}_y = 0.35$ measured in the present

experiments for an isolated cylinder at an equivalent Re. In Fig. 2.3 (page 25) Zdravkovich (1997) shows that values of $\hat{C}_y$ for a static single cylinder show significant scatter, varying between 0.3 and 0.7 for this Re range. We believe this to be strong evidence that the steady lift force acting towards the centreline, as well as the fluctuating component, originate from an amplification of the unsteady interference of the vortex wake coming from upstream with the wake being formed from the second cylinder.

If this is true we expect to find that the frequency of fluctuation of C_y and C_x is somehow related to the frequency of vortex shedding from upstream. Now, we know that the upstream cylinder is shedding vortices as an isolated body, with f_s following close to the line of St = 0.2 (Fig. 5.10). Fig. 6.3 presents a map of the frequency of C_y and C_x normalised by the equivalent shedding frequency f_s for the same U and St = 0.2. We observe that the relative frequency of the dominant component of the fluctuating forces is not much different from 1 once the second regime of interference is established. In fact, it is rather clear that for close separations in the first regime the frequency of C_y is distinctively lower than f_s, revealing that a developed wake is indeed not present in the gap. This result is in agreement with Alam *et al.* (2003) who measured lift coefficients for both cylinders in tandem arrangements.

Our experimental results for the steady components are in very good agreement with other works found in the literature, including the maps of steady lift and drag produced by Zdravkovich (1977) and presented in Fig. 3.5(a) (page 49). We believe this is the first time the magnitude and frequency of the fluctuating component of the fluid force are mapped for staggered arrangements of cylinders.

6.1.1 Detailed map for $x_0/D = 4.0$

Since we are concentrating our attention on $x_0/D = 4.0$ we present a more detailed investigation of the steady fluid forces acting on the downstream cylinder for this separation. These results will be the basis for our discussion in the next chapter, when we will propose an explanation for the frequency of response in the WIV mechanism.
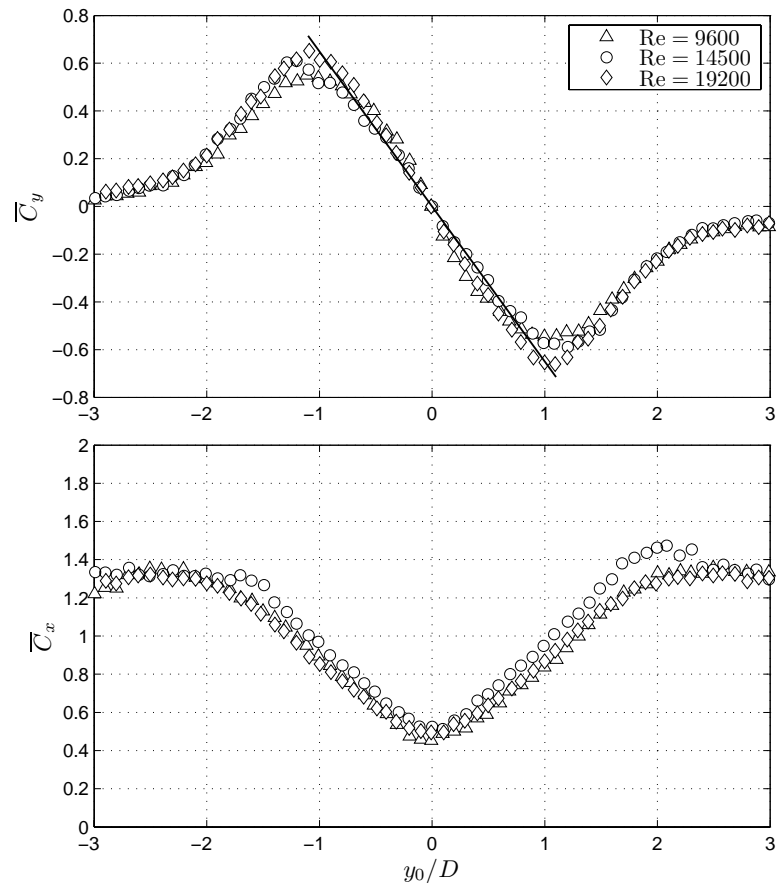
Fig. 6.4: Steady fluid forces on a static downstream cylinder at $x_0/D = 4.0$ and various staggered positions.

Starting from the $\overline{C}_y$ and $\overline{C}_x$ maps above, we can keep the downstream cylinder at $x_0/D = 4.0$ and traverse it in finer steps across the wake along the vertical dashed line plotted in Fig. 6.1. If we now vary Re for each one of these stations we have the detailed curve presented in Fig. 6.4. Once more it shows that the steady lift acting on the downstream cylinder points towards the centreline of the wake for all y_0 separations. An almost linear behaviour is observed for $-1.0 < y_0/D < 1.0$ with a maximum of absolute $\overline{C}_y = 0.65$ found just past $y_0/D = 1.0$. Beyond that separation the steady lift gradually reduces until it is out of the influence of the wake and reaches zero around $y_0/D = 3.0$.

In the second plot the steady drag curve reveals the shielding effect of the wake by showing an almost 60% reduction in drag at the centreline of the wake, however the mean drag never gets to negative values (drag inversion) for this separation. Bokaian & Geoola (1984) observed that the distribution of the drag coefficient is insensitive to a limited increase of Reynolds number from Re = 2600 to 5900. Price (1975) also observed the same independency from Re for a range one order of magnitude higher.

We also conclude that the steady fluid forces, lift and drag, do not vary with Reynolds number for the range of the experiments Re = 2000 − 25000. In fact, several values of Re within this range were analyzed but only three are plotted in Fig. 6.4 for clarity. This explains why our maps from Fig. 6.1 for Re = 1.9×10^4 are in good agreement with Zdravkovich's (1977) for Re = 6×10^4 in Fig. 3.5(a).

6.1.2 Analysis of steady lift on static cylinders

Fig. 6.5 goes into the detail of characterising the actual steady flow field around the static cylinders associated with those steady fluid forces. Contours of normalised velocity magnitude ($\sqrt{\overline{u}^2 + \overline{v}^2}/U$) obtained with PIV are presented for four staggered separations across the wake, including the tandem arrangement. At $y_0/D = 0$ we can see that there is no evident asymmetry in both wakes but it seems that the wake coming from the upstream cylinder is split around the downstream body keeping a fairly symmetric flow field around the second body. But as the cylinder moves outwards from the centreline an asymmetric steady flow is produced around the

(a) $y_0/D = 0$ (b) $y_0/D = 1.0$

(c) $y_0/D = 2.0$ (d) $y_0/D = 3.0$
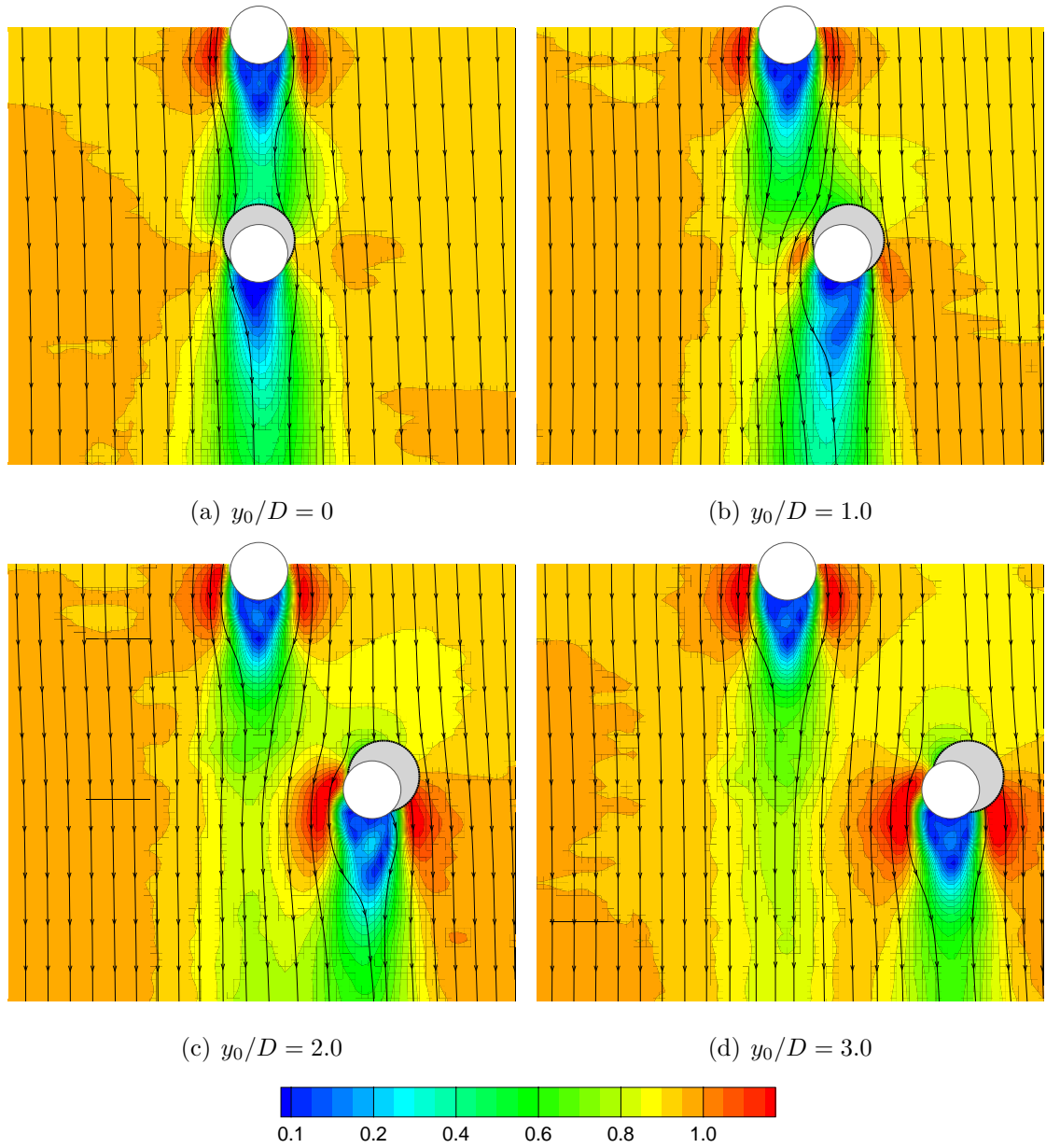
0.1   0.2   0.4   0.6   0.8   1.0

Fig. 6.5: Steady flow velocity field around a pair of static cylinders in four staggered arrangements. $x_0/D = 4.0$, Re = 19200. Contours of velocity magnitude normalised by free stream velocity ($\sqrt{\overline{u}^2 + \overline{v}^2}/U$). The grey circle behind the downstream cylinder represents the shadow region where PIV data is not available.

downstream body. Streamlines show that the steady wake of the upstream cylinder is displaced by the presence of the second body. A slight rotation of the mean wake of the downstream cylinder can be noted for $y_0/D = 1.0$, which is precisely the separation where the downstream cylinder experiences the highest $\overline{C}_y$. This effect seems to be reduced as the cylinder moves further out from the centreline in agreement with force measurements in Fig. 6.4.

We believe these maps represent the phenomenon described by Zdravkovich (2003) as *wake-displacement* when he writes that "the downstream cylinder is not *immersed* in the upstream cylinder wake but *displaces* it instead". It is evident at $y_0/D = 1.0$ that the wake of the upstream cylinder is deflected, probably rotating the front stagnation point of the second cylinder. Following the streamlines around the downstream cylinder in Fig. 6.5(b) it does look like the second body experiences an incident flow that is inclined inwards in relation to the free stream. However the streamlines downstream of the flow seem to be parallel to the free stream, indicating a change in steady flow momentum, thus generating lift towards the centreline. We are not certain if this is the mechanism observed by Zdravkovich, but it certainly offers a possible explanation for the origin of the steady lift based on the steady flow field around the cylinders.

Now, a quasi-static analysis of WIV requires the downstream cylinder to extract energy from the flow as it moves across the steady force fields discussed above. In other words, the excitation force acting on the body should not depend on its movement or any unsteady interaction with the upstream wake, but only in the relative position of the cylinder across the wake. This might be true for bodies with very small transverse velocities $\dot{y}$, but certainly this is not the case observed in the WIV response presented above.

Even a quasi-steady hypothesis may be too much of an oversimplification in this case. Based on data from Fig. 5.7 we can estimate the maximum transverse speed the cylinder reaches as it crosses the centreline of the wake for the maximum reduced velocity point. On average, $\dot{y}$ is around 55% of the free stream velocity U, but it can reach values up to 67% for the most severe cycles. With such vigorous cross-flow movement it is difficult to accept that the downstream cylinder is not affecting or

interacting with the wake coming from the upstream one, making it implausible to hold on to any quasi-static or quasi-steady assumptions. Therefore we believe a completely unsteady investigation of the force-displacement interaction is required to understand how the WIV mechanism works.

But before we jump into the investigation of the instantaneous force acting on a moving cylinder we shall consider the unsteady flow field that is generating the steady and fluctuating forces on a pair of static cylinders.

6.2   Analysis of unsteady lift on static cylinders

We turn now to the unsteady analysis of the instantaneous flow field that generates lift on the downstream cylinder of a staggered pair. Fig. 6.6 presents a short time series of C_y measured on a static downstream cylinder at $x_0/D = 4.0$ and $y_0/D = 1.0$. The dot-dashed line represent a steady lift of $\overline{C}_y = -0.65$ estimated from Fig. 6.4. The variation of C_y from one cycle to another exemplifies the irregularity of the lift force, and the average fluctuation of $\hat{C}_y = 0.6$ can also be noted in this plot.

There are two data points marked with circles that represent the maximum and minimum C_y in this short time series for which we will investigate the corresponding flow fields. Fig. 6.7 shows instantaneous vorticity contours and the corresponding velocity field from instant 'a' in the trough, i.e. when $C_y = -1.4$ is strongest towards the centreline; and for instant 'b' on the crest, which presents a small $C_y = 0.32$ pointing outwards. Vortices identified with A and B were respectively shed from the upstream and downstream cylinders; odd indices mean that vortices have positive vorticity and were shed from the right-hand side of the bodies, even indices mean the opposite. Vortices are identified in both instants so we can follow the development of the wake from 'a' to 'b'.

As the flow passes around the upstream cylinder a fully developed wake is formed in the gap. In Fig. 6.7 we see the instant when vortex A4 is being formed very close to the cylinder, inducing a high speed flow that is shown with red vectors in the velocity field. A fully developed vortex A3, which was formed half a cycle before, is convected
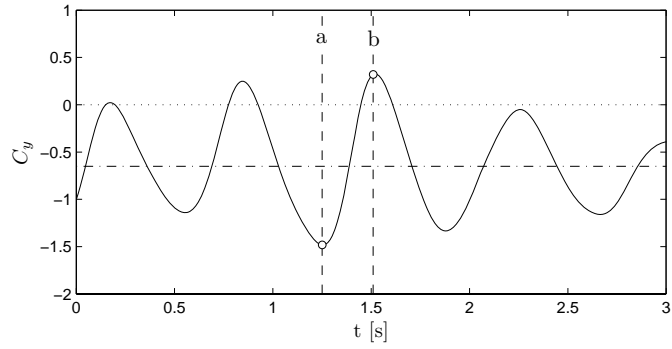
Fig. 6.6: Time series of lift on the downstream cylinder of a static pair in staggered arrangement $x_0/D = 4.0$ and $y_0/D = 1.0$. The dot-dashed line represents $\overline{C}_y = -0.65$. Re = 19200.
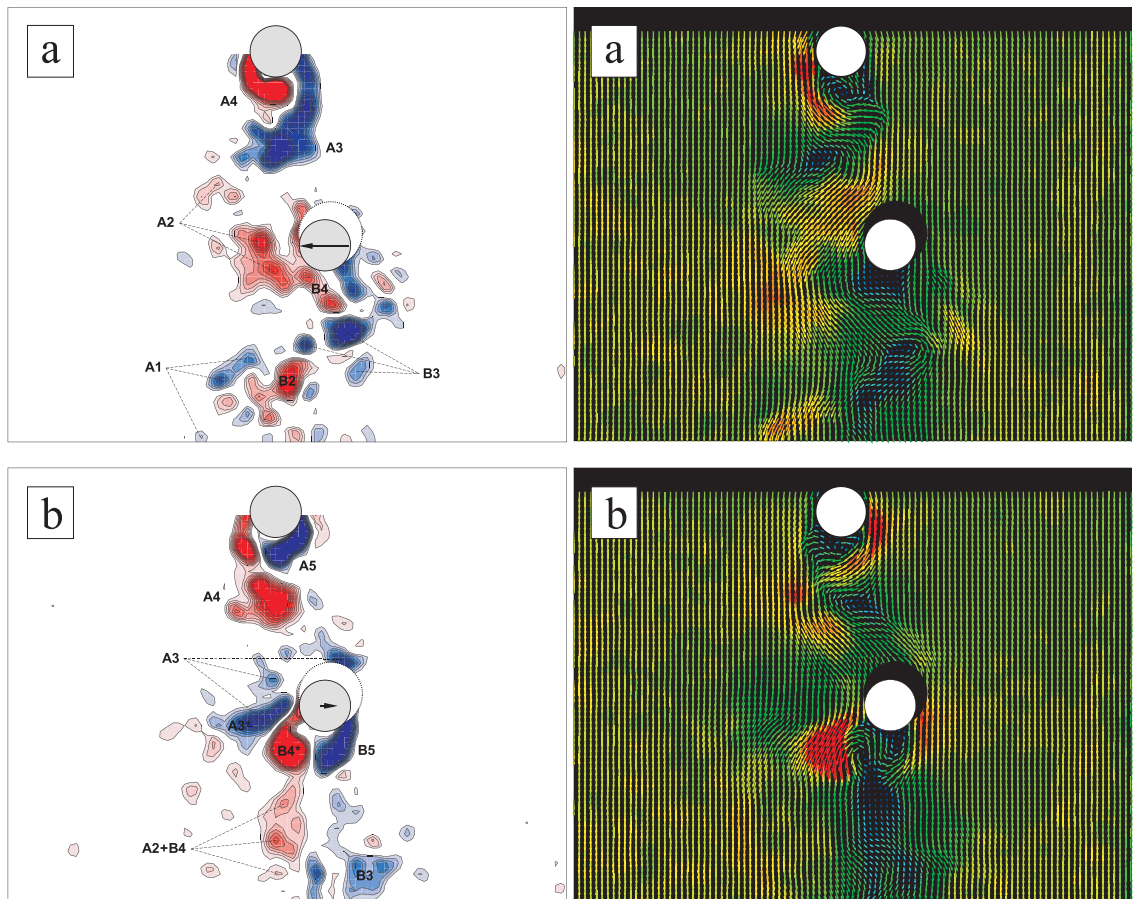

Fig. 6.7: Instantaneous vorticity contours and velocity field (coloured by velocity magnitude) obtained with PIV around a pair of static cylinder in staggered arrangement. $x_0/D = 4.0$, $y_0/D = 1.0$, Re = 19200. Please refer to Fig. 6.6.
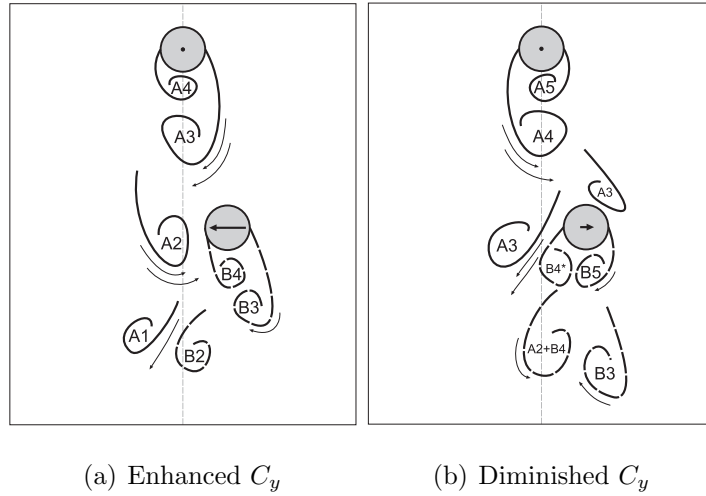
(a) Enhanced C_y (b) Diminished C_y

Fig. 6.8: Sketch of vortex-structure interaction that generates minimum and maximum C_y on the downstream cylinder at $x_0/D = 4.0$ and $y_0/D = 1.0$. Please refer to Figs. 6.6 and 6.7.

downstream and induces high speed flow on the inner side of the downstream cylinder. This high speed jet accelerates the boundary layer flow running on that side contributing to add more circulation into the shear layer. Consequently, vortex B4 forming on the second cylinder must have a higher circulation than a typical vortex on a single cylinder would. However, fully developed vortex A2, shed in the previous cycle, passes around the downstream cylinder and induces a flow field that will push B4 closer to the downstream cylinder.

We believe that this combination of high speed flow induced in the inner side added to the a strong vortex being formed and held closer to the second cylinder is generating the high lift of $C_y = -1.4$ found in Fig. 6.6. Of course the interaction between vortices from previous cycles is occurring in the wake downstream of the second body — with vortices from both cylinders merging together and moving in pairs — but what is happening around the second cylinder has significantly more influence on the force being generated than the wake far apart.

Now, moving to instant 'b' in Fig. 6.7 we observe that vortices have been convected further downstream and a new vortex A5 is being formed on the upstream cylinder. Downstream of the second cylinder we observe that A2 has merged with B4, forcing B3 to be released and giving way to a new B4* that starts to roll up. A fully developed A3 impinges and splits around the second cylinder with a portion A3* moving through the inner side and the rest following an outer path. As A3*

115

and the new B4* interact they induce a very high speed flow across the wake that forces the formation of B4* further inwards. On the other side, B5 is also forced and rolls up closer to the downstream cylinder contributing to generating a small lift $C_y = 0.32$ acting outwards.

Fig. 6.8 summarises the explanation presented above highlighting the main vortex-structure interactions occurring in the wake. The effect of upstream vortices on the downstream cylinder is seen to be paramount in both cases: (a) when A3 induces high speed flow on the inner side and A2 displaces the downstream wake outwards; and (b) when A3 splits around the body and interacts with B4 to generate high speed flow inwards. Both configurations are associated with a change in momentum induced by the vortices interacting with the cylinder wall.

Price (1976) performed experiments with sensitive paint on the surface of the cylinder to determine the location of stagnation and separation points for several staggered arrangements. He noted that although the position of the front stagnation point on the second cylinder could be resolved, "the position of the separation points could not be found with any accuracy." He was referring to the fluctuation that occurs on the inner wall of the downstream cylinder, proving that the unsteadiness of the wake is strong and may be dynamically acting to change the separation point from one cycle to another.

We know that identical wake patterns are not repeatable as vortices from both cylinders may be forming at different rates and strengths. Nevertheless we believe this flow field investigation offers a good illustration of the complex vortex dynamics occurring in the wake associated with severe lift fluctuation on the downstream cylinder. We should expect to find even more complex dynamics when the downstream cylinder is oscillating with high transverse velocities.

When cylinders are in close proximity (like tight tubes in heat exchangers) — and no vortices are formed in the gap — the flow may resemble some sort of potential flow. That is why Paidoussis *et al.* (1984) decided to employ a potential-flow theory to model the problem for an array of cylinders, even though he had to account for some viscous effect by introducing a time delay in the fluid force. But when the separation is large, like the one presented above, the wake in the gap is far from a

steady flow and does not resemble irrotational flow whatsoever; on the contrary, it is full of vortices that cannot be neglected. A time delay (or phase lag) must always be accounted for when modelling this problem, otherwise no oscillatory instability would be sustained. But to think of an explanation for the time delay that ignores the vortex-structure interaction is an oversimplification of the problem, at least for the second regime with large separations and a developed wake in the gap.

6.2.1 Conclusion

Zdravkovich (1977), Bokaian & Geoola (1985) and others attributed the phase lag in the force to the switching of a low-speed steady wake from one side to the other as the second cylinder crosses the centreline. This was Zdravkovich's natural conclusion since a similar hysteretic phenomenon had been found to exist for the gap-flow-switching mechanism in close proximity. We believe his wake-displacement model works by extrapolating a concept based on the quasi-steady gap-flow-switching idea rather than offering proper evidence for a new WIV mechanism.

We saw that a strong and complex vortex-structure interaction is present and hence must be involved in the excitation mechanism. We cannot guarantee a priori that a quasi-steady assumption of the fluid forces (even if it accounts for hysteretic effects) will represent the phenomenon with all its unsteadiness. Instead we suggest that a phase lag is generated as the unsteady wake is modified by the movement of the second cylinder. In other words, a simple steady wake without the unsteadiness of the vortices is not able to generate the necessary phase lag to excite WIV.

In order to evaluate this hypothesis we will proceed in two steps. First we present an idealised experiment designed to reproduce a wake with its steady shear flow profile but without the unsteadiness of the vortices. Then later we will investigate lift force measurements paired with instantaneous flow fields to assess if there is a phase lag related to the vortex-structure interaction as the second cylinder oscillates.

6.3 Shear flow experiment

The main assumption of a quasi-steady approach for WIV is that the fluid forces on the downstream cylinder do not depend on the unsteadiness of the wake but only on the steady flow velocity profile and the relative position of the cylinder. Therefore if we could generate a wake with a similar steady profile but without the unsteadiness of the vortices and immerse an elastically mounted cylinder in this velocity field, we should expect to see a response similar (at least qualitatively) to the WIV of two cylinders. A cylinder immersed in a similar steady velocity profile would be able to experience the predicted phase lag and therefore be excited into WIV. In principle any shielded profile that has the same steady characteristics of the wake would work, produced or not by an upstream bluff body.

According to this hypothesis, the phase lag between lift and displacement would still be present in such a flow as the wake switches from one side to the other as the body crosses the centreline. A qualitatively similar WIV response would be good evidence that unsteady vortices are not necessary to generate the phase lag and sustain vibrations. Note that this hypothesis only requires that the steady velocity profile be similar to a shielded flow but it does not carry the necessity that this wake be full of unsteady vortices. In other words, if this is correct, only a steady wake without unsteady vortices should be enough to generate the excitation due to the phase lag in the wake-displacement mechanism.

6.3.1 Experimental set-up

For this experiment a set of screens made of thin stainless steel wires was cut in stripes of different widths. Then a set of superimposed screens was positioned vertically in the centre of test section in order to alter the mean velocity profile from the free surface to the floor. The set of screens was fixed on an aluminium honeycomb with the purpose of removing major cross flow components. The set-up is illustrated in Fig. 6.9, where $\overline{u}$ represents the resultant shear flow profile.

Such a technique is employed by naval engineers studying hydrodynamics of propellers. The velocity profile downstream of a ship hull is measured on a scaled
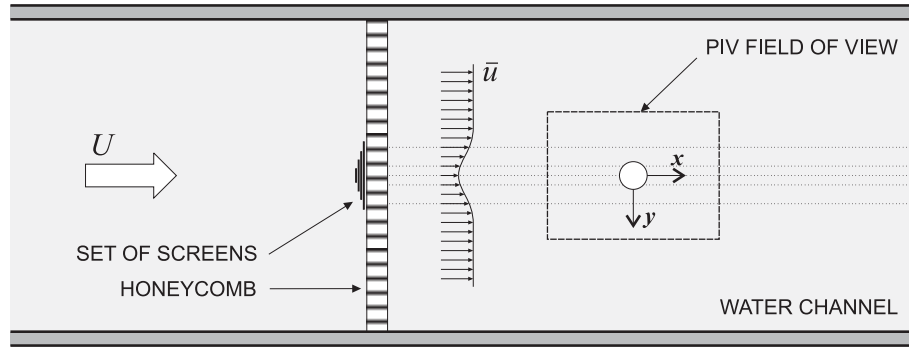
Fig. 6.9: Set-up of set of screen and honeycomb for the shear flow experiment.

model towed in still water. Usually the size of the model is too small to allow study of the propeller in the same scale, especially if cavitation is to be considered. By sewing together sets of screens to form a wire panel, the velocity profile of the hull can be artificially scaled up to match the dimensions of the propeller and the interaction between wake and propeller can now be studied in a cavitation tunnel.

The flow field around a pair of cylinders under WIV was measured with PIV to serve as reference. The steady velocity profile of the fully developed wake was averaged from a number of snapshots (corresponding to more than 100 cycles of oscillation and many more cycles of vortex shedding), resulting in the flow fields presented in Fig. 6.10. The process was repeated for four Re within the range of the experiments, although only two are plotted here for brevity. Two dashed circles mark the average amplitude of oscillation the downstream reached during the measurements.

When considering fluid forces acting on the second cylinder Price (1976) had already noticed that the lift profile on the body depends "on its own characteristics in the wake and not particularly on the wake characteristics". He concluded that "the use of wake parameters, measured without the presence of the [second] body when attempting to assess the forces thereon, is an oversimplification of the situation as far as lift is concerned, while appearing to work quite well for drag". For this reason, flow field measurements were performed with the downstream cylinder in place and oscillating in order to account for the interaction between the body and the upstream wake.
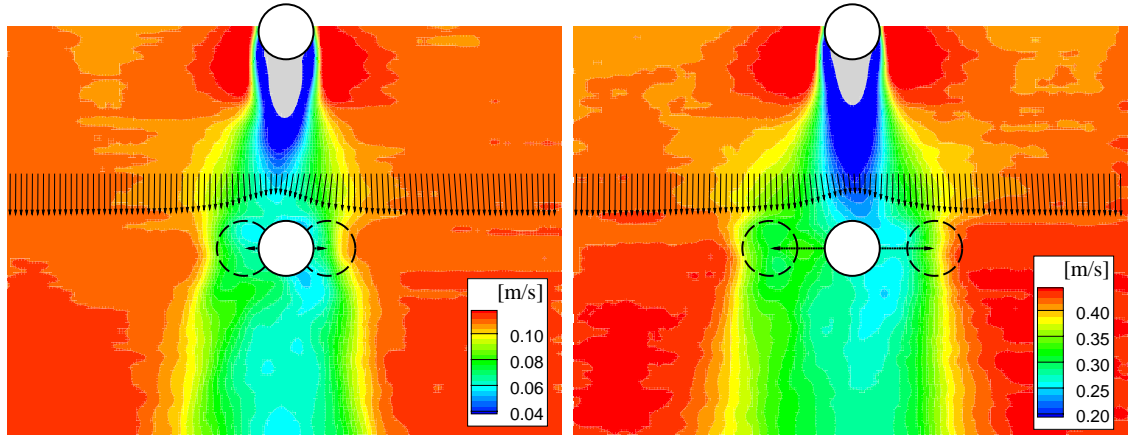
(a) Re = 4800

(b) Re = 19200

Fig. 6.10: Steady flow velocity field around a pair of cylinders while the downstream cylinder is oscillating under WIV. Contours of $\overline{u}$ coloured by velocity magnitude.
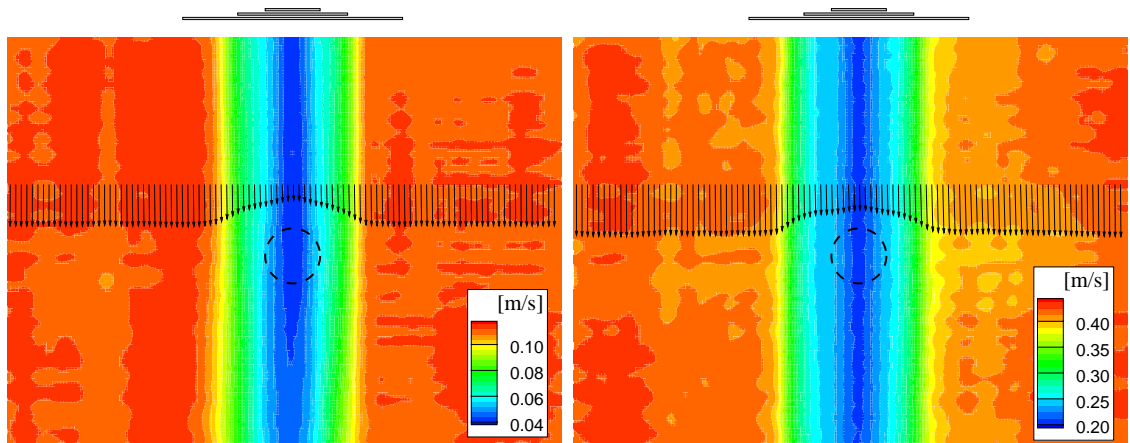
(a) Re = 4800

(b) Re = 19200

Fig. 6.11: Steady flow velocity field generated by a set of screens. Contours of $\overline{u}$ coloured by velocity magnitude.

Fig. 6.12: Comparison between steady velocity profiles for various flow speeds measured across the wake at $x_0/D = 3.0$: —— set of screens; $- \cdot -$ pair of cylinders.

With the profiles around a pair of cylinder in hand, we removed the upstream cylinder and adjusted the set of screens in order to generate the b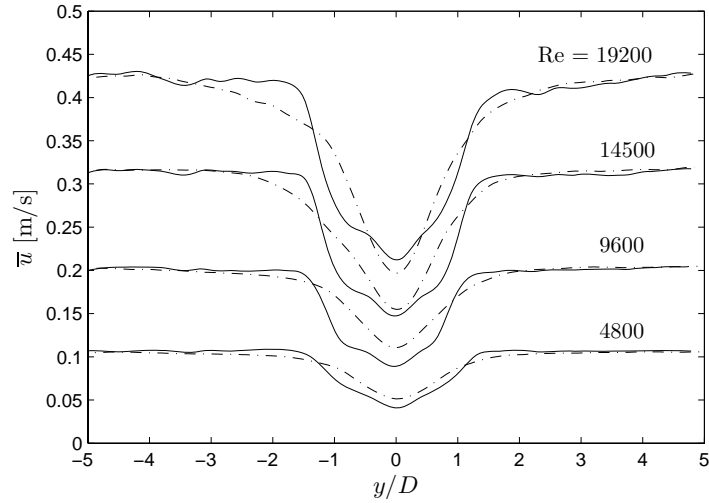est possible profiles to match the reference cases. Several screens of different mesh densities were combined in order to obtain equivalent velocity profiles for the range of Re of the experiments. Fig. 6.11 presents the steady profiles obtained downstream of the screens for two of the Reynolds numbers investigate (Re based on the cylinder diameter). The dashed circle represents the position where the cylinder would be placed, although it was not immersed in the wake during these measurements.

The streamwise velocity profile across the wake at $x_0/D = 3.0$ was extracted from the PIV flow fields and used to validate the comparison. The result is plotted in Fig. 6.12 for the four Re investigated. The same profile can also be seen in Figs. 6.10 and 6.11 represented by an array of vectors plotted across the wake in the gap between the cylinders and at the equivalent distance downstream of the screens. The two most important wake parameters tuned in the calibration of the screens were the average breadth of the wake and the minimum flow speed on the centreline. Fig. 6.12 reveals a reasonably good agreement between reference and generated profiles in spite of the complexity of the set-up designed to achieve these results.

In order to verify the effect mentioned by Price (1976) and discussed above,
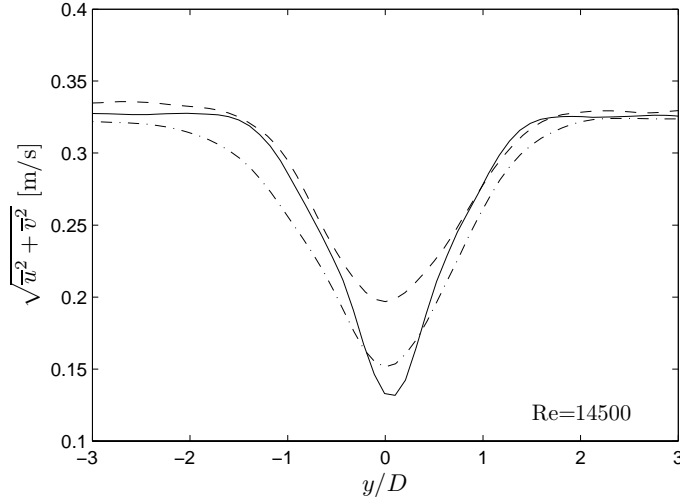
121

Fig. 6.13: Comparison between steady velocity profiles measured across the wake at $x_0/D = 3.0$: —— set of screens; $- - -$ single cylinder; $- \cdot -$ pair of cylinders. Re = 14500.

Fig. 6.13 compares the velocity profile generated by screens with other two profiles measured with and without the second cylinder in place. We notice that when the downstream cylinder is present and oscillating it not only has an effect of extending the breadth of the wake, but also reducing the flow speed on the centreline. This plot shows that although the profile generated by the screens was calibrated to reach a streamwise velocity deficit similar to the case with two cylinders it still lies in between the other two curves as far as the breadth of the wake is concerned.

An instantaneous snapshot of the vorticity field plotted in Fig. 6.14(b) reveals that the shear profile generated by the screens does not have coherent vortices related to bluff body vortex shedding. This is even clearer when the instantaneous wake is contrasted with the wake of a static cylinder shedding vortices in the 2S mode (Fig. 6.14(a)). Both vorticity fields in Fig. 6.14 have the same contour-colour scale, allowing direct comparison between fully developed wakes. (The magnitude of vorticity is not relevant for this analysis.)

The position of the screens in Figs. 6.11 and 6.14(b) is merely illustrative. In reality the set of screen was positioned at around $10D$ upstream of the cylinder, as shown in Fig. 6.9.

Finally, we were able to conclude that an artificial velocity profile equivalent to the steady velocity profile in the gap between a pair of cylinders was generated

(a)   (b)
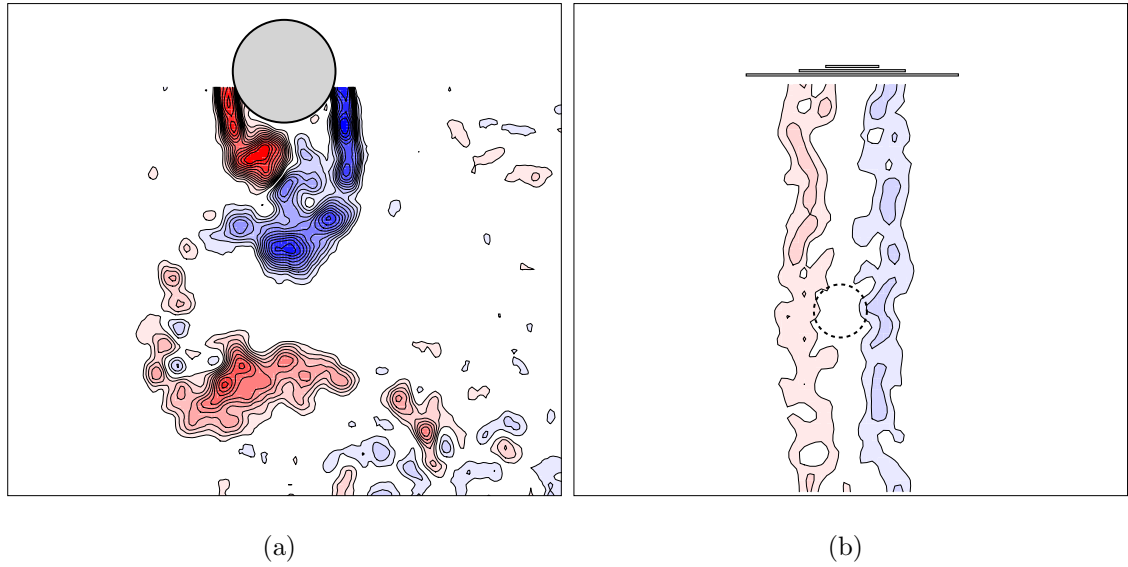
Fig. 6.14: Instantaneous vorticity contours of the wake downstream of (a) a single cylinder and (b) a set of screens. Both images have the same contour-colour scale to allow direct comparison. Re = 9600 based on cylinder diameter.

without the unsteadiness of the vortices. Now we are ready to investigate the effect this artificial shear flow would have on an elastically mounted cylinder.

6.3.2 Steady forces on a static cylinder

We begin by investigating the steady fluid forces acting on a static cylinder as it is traversed across the wake for various Reynolds number. Fig. 6.15 presents maps of lift and drag that can be compared to the steady force map of a pair of cylinders in Fig. 6.4 (page 109). Similarly to the case of a pair of cylinders, we note that the behaviour of the fluid forces does not vary with Re. However, we immediately see a considerable difference in the lift curve when both cases are compared. While for a pair of cylinders the minimum lift towards the centreline reached $\overline{C}_y = -0.65$ at around $y_0/D = 1.0$, the cylinder immersed in a shear flow only reaches a minimum of $\overline{C}_y = -0.2$ for the same position. This represents a 69% reduction in steady lift if vortices are removed from the wake.

Nevertheless, the similarity in steady drag between the two cases is remarkable. Both reach a minimum around $\overline{C}_x = 0.5$ on the centreline of the wake with a very similar behaviour as the cylinder is displaced outwards, recovering around $\overline{C}_x = 1.3$
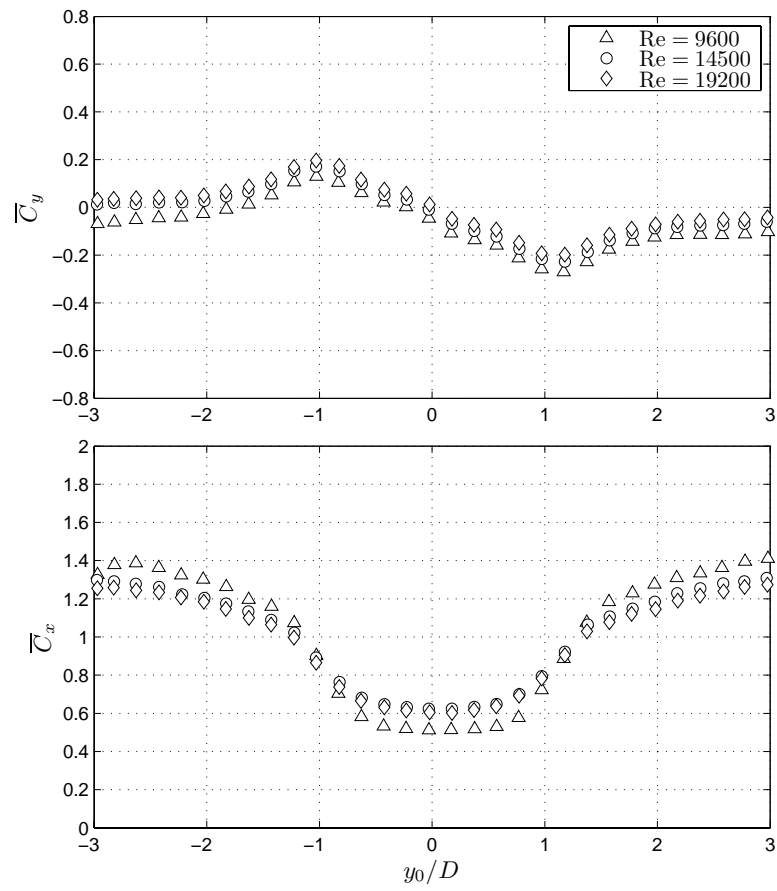
Fig. 6.15: Steady fluid forces on a static cylinder in shear flow for various positions across the wake.
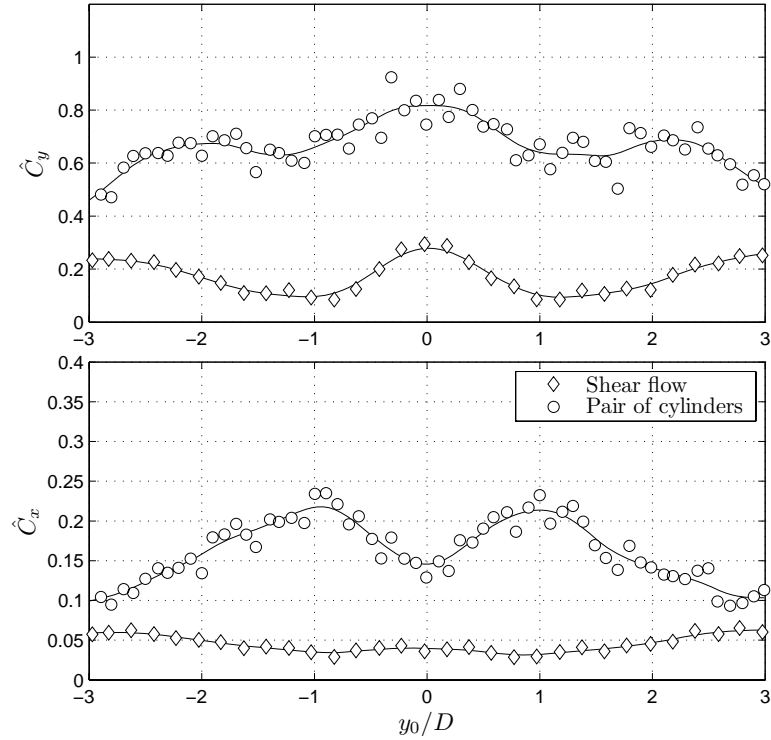
Fig. 6.16: Fluctuating fluid forces on a static cylinder in shear flow and on the downstream cylinder of a pair with $x_0/D = 4.0$. Re $= 19200$.

out of the wake interference region. This correspondence must be related to the fact that the streamwise component in both cases is very similar, therefore the shielding effect observed in the steady flow field is well reproduced by the screens.

In addition to that we can also note a remarkable reduction in the fluctuating fluid forces if vortices are not present in the upstream wake. Fig. 6.16 compares $\hat{C}_y$ and $\hat{C}_x$ on static cylinders for both experiments. While the fluctuating lift coefficient reaches values around $\hat{C}_y = 0.8$ for the downstream cylinder of a tandem pair, the maximum fluctuation of lift in the shear flow is only around $\hat{C}_y = 0.3$, which is very close to the magnitude of $\hat{C}_y = 0.35$ due to vortex shedding measured for a single static cylinder. The fluctuation in drag is also affected, with an amplification from $\hat{C}_x = 0.035$ to 0.23 at $y_0/D = 1.0$ if vortices are present in the upstream wake. Note that for larger separations out of the wake interference region the curves for both cases seem to be converging to the value of an isolated cylinder.

This is strong evidence supporting that vortex interactions from the upstream

125

wake are responsible for the high steady and fluctuating lift on static cylinders in staggered arrangements. Remove the unsteadiness from the wake and the steady lift towards the centreline is considerably reduced, almost disappearing, with the fluctuating term tending towards values measured for a single cylinder.

Previous works tried to attribute the existence of a steady force towards the centreline to mechanisms such as: wake-buoyancy, turbulent transition in one shear layer, resolved drag and circulation around the cylinder (to cite the most relevant described in Chapter 3). However, as noted by Price (1976), none of these mechanisms accounted for the total magnitude of $\overline{C}_y$ on the second cylinder. In Fig. 6.15 we showed that only a residual $\overline{C}_y = -0.2$ at $y_0/D = 1.0$ still remains even when vortices are removed from the upstream wake.

Apparently this residual lift in a steady shear flow is equivalent to the maximum $\overline{C}_y$ predicted by the wake-buoyancy and resolved drag hypothesis discussed before. Both mechanisms are based on a steady flow field — exactly what was reproduced by the screens — and they may well be responsible for the residual lift we observed in the shear flow experiment. But of course not all the unsteady vorticity in the wake could be removed, as seen in the instantaneous flow contours of Fig. 6.14, and the residual $\overline{C}_y$ towards the centreline may as well be an effect of this weak unsteady vorticity field that still remains. Nonetheless, we were able to show that the presence of vortices is indeed responsible for the high $\overline{C}_y$ measured for staggered cylinders and accounts for raising the residual steady lift generated by a steady shear flow up to $\overline{C}_y = -0.65$ measured when a fully developed wake is present in the gap.

In summary, considering that $\overline{C}_y = 0$ for a single cylinder in uniform flow, the presence of a steady shear flow contributes to a minimum $\overline{C}_y = -0.2$, but only with the presence of unsteady vortices will the total $\overline{C}_y = -0.65$ be reached. Not to mention the effect of unsteady vortices in enhancing the fluctuating term of the fluid force presented in Fig. 6.16. This result combined with the unsteady analysis presented in Fig. 6.7 (page 114) offers a good explanation for the role of vortical structures in enhancing lift on the downstream body.
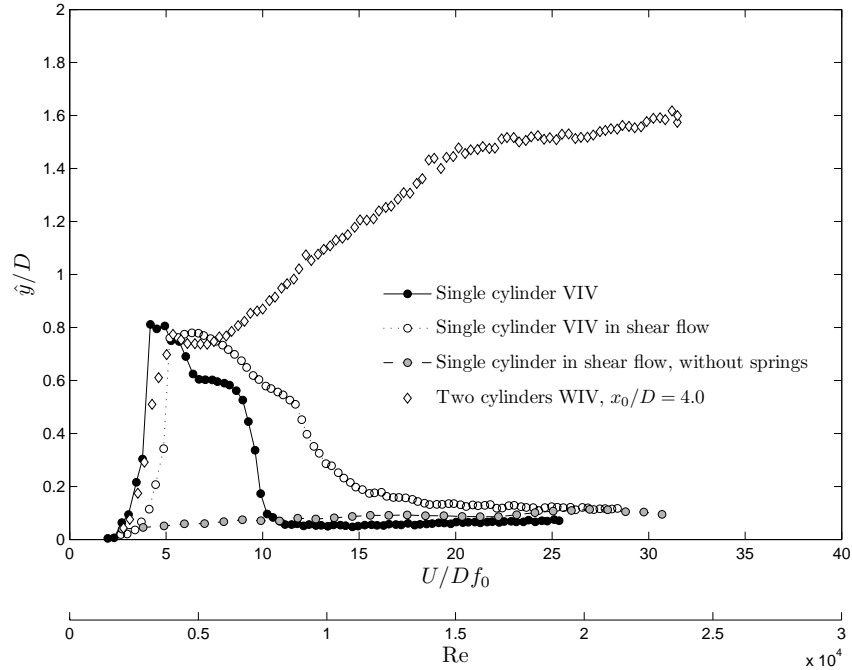
Fig. 6.17: Response of the downstream cylinder in shear flow compared with other typical VIV and WIV responses.

6.3.3 Response of a cylinder in shear flow

We then placed an elastically mounted cylinder immersed in the shear flow described above in order to investigate the FIV response. Were WIV to be excited by the steady flow we would be able to see a build up of amplitude similar to the response obtained for a pair of cylinders. However, the response was completely different from previous WIV results. Fig. 6.17 brings the comparison.

Instead of developing a high-amplitude branch that increases with reduced velocity, the response resembled that of a single cylinder under VIV. A clear resonant peak is observed around $U/Df_0 = 7$, but the amplitude suddenly dies out towards a residual level below $\hat{y}/D = 0.2$ for reduced velocities higher than 15. Even though upper and lower branches are not as clearly distinguishable as for a single cylinder VIV, an evident synchronisation range is still noticeable. Of course the response is slightly different from the typical VIV curve, but it is strikingly similar to that rather than to the measured WIV curve also plotted in Fig. 6.17. In fact, the similarity is so strong that we cannot avoid concluding that the cylinder in shear flow is only responding with a type of modified VIV altered by the steady shear flow.

127

The fact that the peak of resonance is slightly offset towards higher reduced velocities is in agreement with the shielding effect of the steady wake. From the velocity profiles presented before (Fig. 6.12) we note that the deficit in streamwise velocity in the wake is on average around 45% of the free stream velocity, resulting in precisely the observed offset from the VIV peak for a single cylinder. (The data-set tagged 'without springs' will be discussed in the next chapter.)

We conclude that the response of the cylinder is evidence that coherent vortices in the wake are necessary to sustain WIV. Removing the vortices we only observed a distorted type of VIV, but not a build-up of response typical of WIV. Although we are convinced that vortex-structure interaction is important and necessary for the mechanism to be sustained, so far it is still not clear how vortices from the upstream wake interact with the downstream cylinder in oscillation. In other words, we still need to investigate why vortices enhance the steady and fluctuating lift terms on the downstream cylinder and also how the phase lag is generated. For this reason we now turn our attention to the unsteady forces and flow fields around a pair of cylinders in WIV.

6.4 Analysis of unsteady lift on an oscillating cylinder

As discussed before, the WIV response is characterised by considerable variations between cycles as far as displacement is concerned. We have also noticed that an irregular envelope of displacement is more evident in WIV than in a typical VIV response for one cylinder. Therefore it is straightforward to presume that a somewhat irregular response must be excited by an irregular fluid force.

Fig. 6.18 brings an example of the time series of displacement and lift for around 250 cycles of oscillation for the case analysed in this section; located at high reduced velocity, far enough from the influence of the VIV regime. The dashed lines in Fig. 6.18 represent the average amplitudes $\hat{y}/D = 1.5$ and $\hat{C}_y = 0.7$ obtained from Figs. 5.7 and 5.11. The irregularity of both envelopes — with a number of peaks
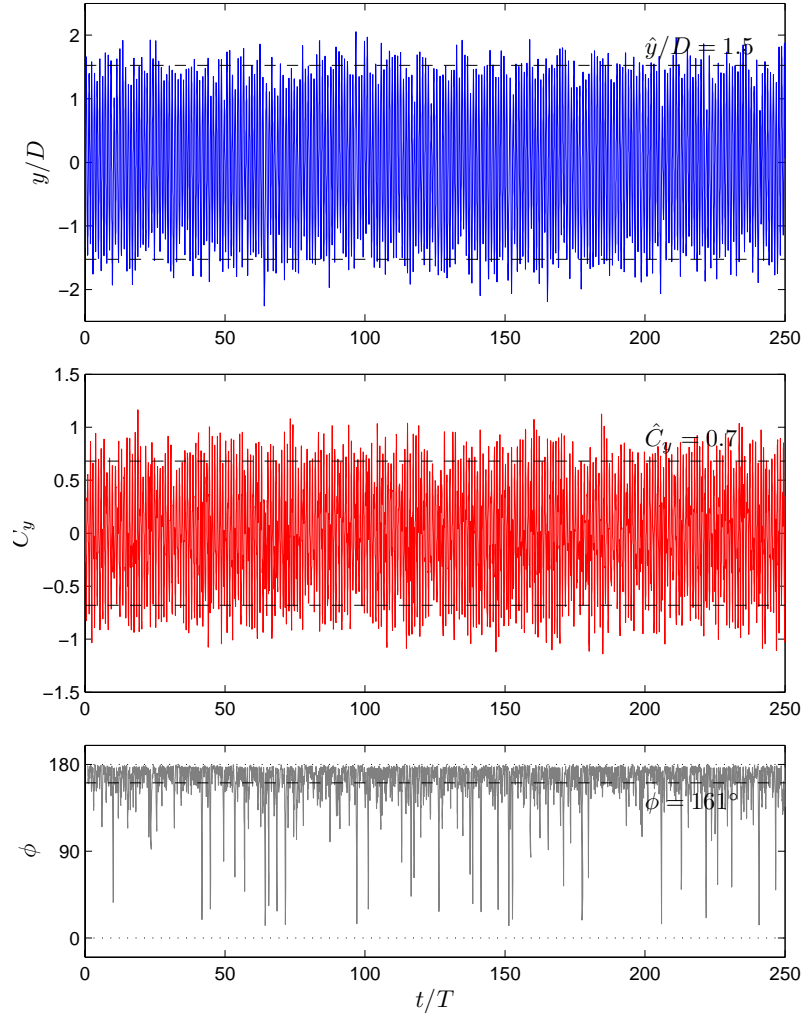
Fig. 6.18: Time series of displacement (top), lift coefficient (middle) and instantaneous phase angle (bottom) for around 250 cycles of WIV. $x_0/D = 4.0$, $U/Df_0 = 25$, Re = 19200.

appearing above and below the dashed lines — clearly shows that the response and the excitation force indeed present considerable variation. The bottom graph shows the instantaneous phase angle ϕ calculated by the Hilbert transform directly from the y and C_y signals. The dashed line indicates the value of $\phi = 161°$ averaged for the whole time series in Fig. 5.11.

One would imagine that for such a high reduced velocity the frequency of vortex shedding would be so much higher than the frequency of oscillation that the unsteadiness of the wake could be ignored. In that case we would be entering the territory where quasi-steady theory is applicable. At that point, with the wake resembling a steady flow, the expected steady-state response should also present
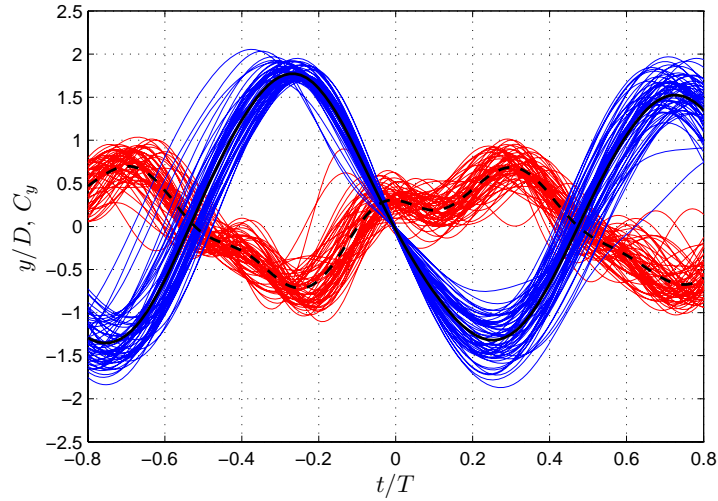
Fig. 6.19: Superimposed plots of WIV cycles with similar amplitude. y in blue and C_y in red with average cycle in black. $x_0/D = 4.0$, $U/Df_0 = 25$, Re = 19200.

a well behaved envelope. However this does not agree with the evidence. Instead we observe growing irregularity from cycle to cycle with the difference between the maximum and minimum peaks ever increasing with reduced velocity.

In order to investigate in more detail the relation between displacement and fluid force we shall plot a collection of several cycles with similar displacement amplitude superimposed in one graph. Fig. 6.19 shows the displacement and lift for 20% of the total number of cycles around the average amplitude of $\hat{y}/D = 1.5$. Once more the variation in both y and C_y is evident. It is also clear that the fluid force signal shows a component of higher frequency apart from the lower frequency that matches the oscillation.

Taken as a whole it appears that the fluid force is indeed in antiphase with the displacement, but if we look carefully at the multitude of red lines crossing $C_y = 0$ we will note that the lift force anticipates the displacement practically in all cycles. In fact, if we consider the average cycle given by the black lines we conclude that the displacement lags the lift by around $\phi = 180°$ minus one-tenth of a period. Here is the phase lag we were looking for. An average delay of $0.1t/T$ is equivalent to $\phi = 162°$, which is remarkably close to the average value of $\phi = 161°$ presented in Fig. 6.18 (obtained from Fig. 5.11, page 101).

In fact, if we start from Eq. 2.11 (based on the harmonic assumption discussed in

Chapter 2) and take all other variables from the results presented before we conclude that for such very low values of mass and damping ($m^*\zeta = 0.018$) a minute phase lag of $\phi = 179.4$ would be enough to excite the system with $\hat{y}/D = 1.5$ at $U/Df_0 = 25$. This is the curve 'ϕ (Eq.)' in Fig. 5.11. However, if we employ the same harmonic hypothesis for the actual $\phi = 161°$ averaged from the Hilbert transform we conclude that the amplitude of oscillation would reach the unrealistic value of $\hat{y}/D = 45$. Hence we conclude that a simple 'harmonic forcing and harmonic motion' hypothesis does not apply directly to the WIV mechanism. Rather a more complex modelling that considers multiple frequencies present in the wake should be developed.

Turning again to Fig. 6.19, it appears that the phase lag is actually a consequence of the higher frequency existent in the lift signal. Since f_s from the upstream cylinder is increasing with flow speed and the oscillation frequency of the downstream cylinder is increasing at a different rate, the relationship between both frequencies is also changing. Essentially, this higher frequency must be associated with the vortex shedding frequency of the upstream wake — at least this is observed for static cylinders — but one cannot tell how repeatable this forcing is as the downstream cylinder oscillates and interacts with upstream vortices.

The only conclusion we can make is that with such an irregular forcing it is most likely that the fluid force will not be perfectly in phase (or in antiphase) with the displacement, especially as the cylinder crosses the centreline of the wake where strong vortices are present. Therefore the phase lag must be coming from the unsteadiness of the wake, i.e. from the vortex-structure interaction as we have been arguing so far.

Similarly to the investigation presented for a static cylinder at the staggered arrangement of $y_0/D = 1.0$ (Fig. 6.7, page 114), we can analyse the wake configuration that generates the corresponding lift trace. Fig. 6.20 presents a short sample from the time series presented above for which the flow field was captured with PIV. The lift coefficient curve represents the vortex-component of the fluid force discussed in Chapter 2, Eq. 2.18; it only accounts for the force generated by the vorticity in the wake and not the inertia reaction due to the ideal flow added mass.
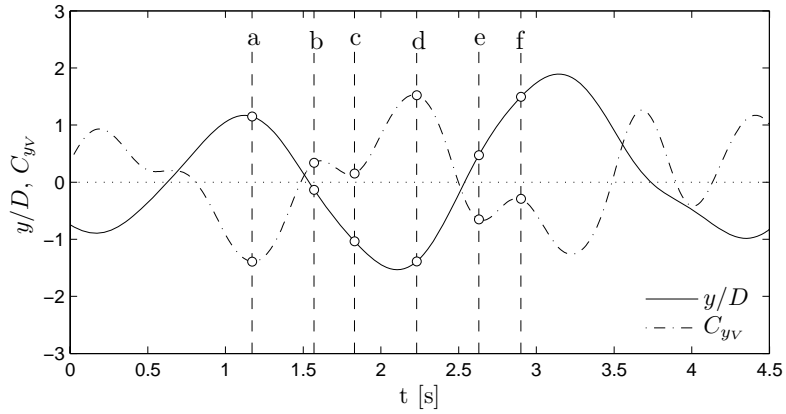
Fig. 6.20: Time series of displacement and vortex-force component of lift on the downstream cylinder under WIV. $x_0/D = 4.0$, $U/Df_0 = 25$, Re = 19200.

Vorticity contours and velocity fields for six instants marked from 'a' to 'f' are shown in Fig. 6.21. Following the same notation employed before, vortices tagged with 'A' were shed from the upstream cylinder, while vortices 'B', from the downstream one. Also, odd indices designate vortices shed from the right-hand side (positive vorticity in blue), while even indices, from the left-hand side (negative vorticity in red). The same vortices are identified from frames 'a' to 'f' to reveal the development of the sequence.

Frame 'a' was taken with the cylinder very close to maximum displacement when lift was the strongest towards the centreline. Like the wake configuration observed for static cylinders, we find vortex A2 inducing high speed flow close to the inner side of the cylinder while A1 induces vortex B3 to form closer to the wall. However, as the cylinder accelerates towards the centreline B3 is suddenly released and a new vortex B5 forms in its place. In Fig. 6.20 we see that the lift force changes its direction slightly before the cylinder crosses the centreline.

In frame 'b' we see that vortex A2 impinges on the second cylinder, splitting in two parts around the body as it crosses the centreline; a part will merge with B4 and a part will join B5 in the downstream wake. At the same time we see that A3 coming from the upstream cylinder induces a high speed flow that is contrary to the second cylinder motion. This strong interaction is responsible for the local peak in the lift curve in Fig. 6.20. A moment later in frame 'c' vortex A3 is splitting around the second cylinder and inducing A2+B4 away from the body, while a strong B5

132

Fig. 6.21: Instantaneous vorticity contours and velocity field (coloured by velocity magnitude) obtained with PIV around a pair of cylinder under WIV. $x_0/D = 4.0$, $U/Df_0 = 25$, Re = 19200. Horizontal arrows represent the lift acting on the cylinder; please refer to Fig. 6.20. *Continued on next page.*
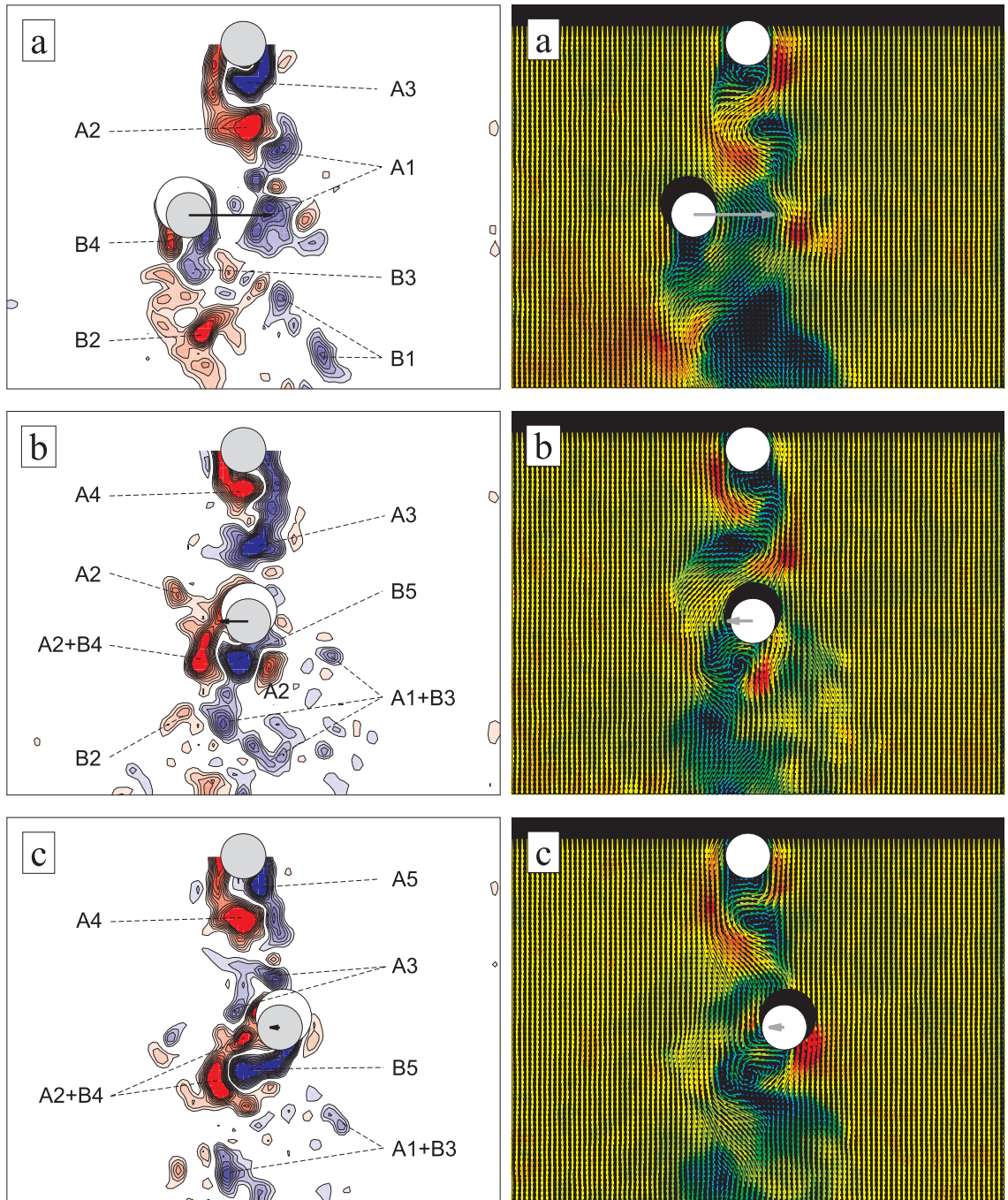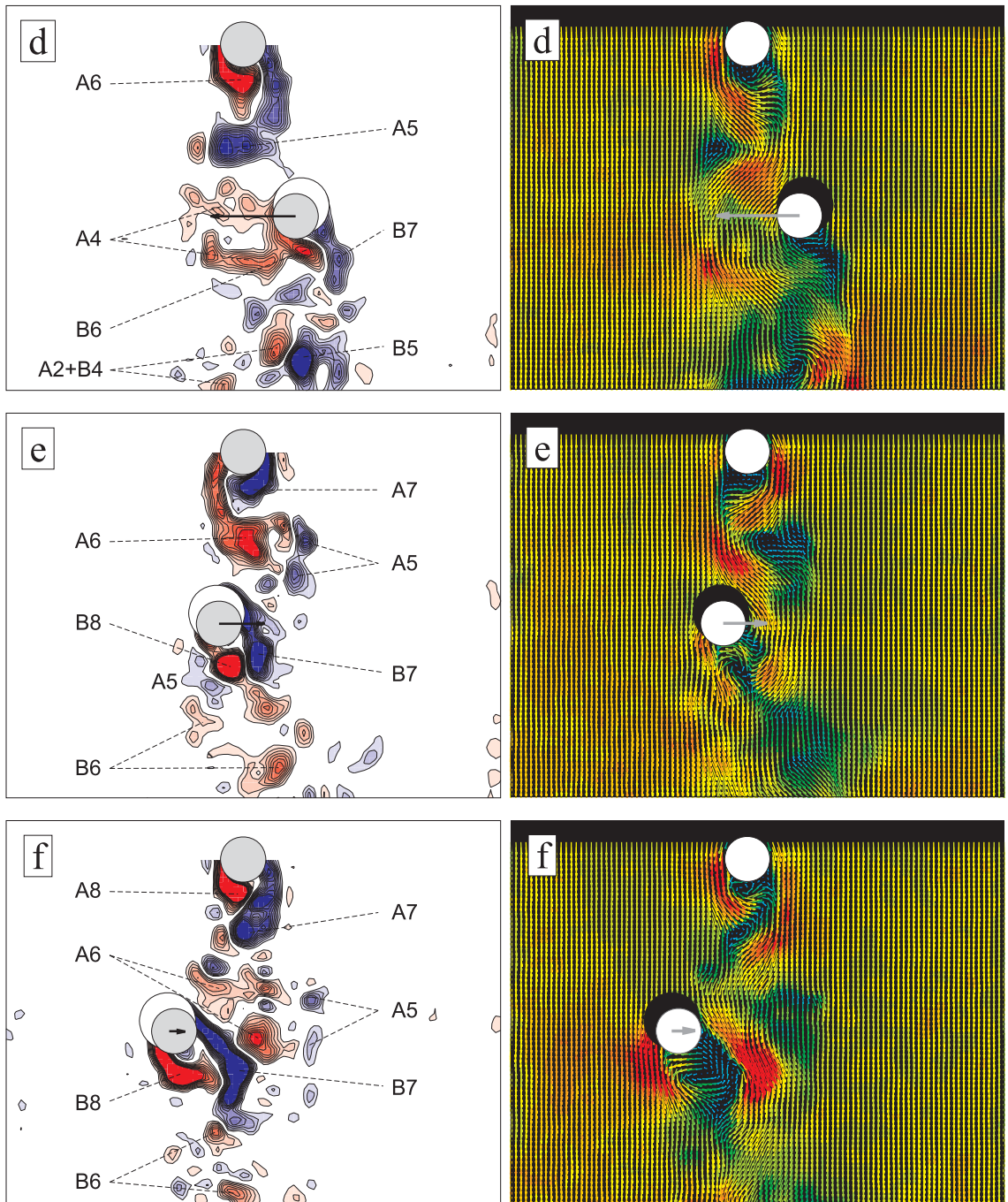
Fig. 6.21: *Continued from previous page.* Instantaneous vorticity contours and velocity field (coloured by velocity magnitude) obtained with PIV around a pair of cylinder under WIV. $x_0/D = 4.0$, $U/Df_0 = 25$, Re = 19200. Horizontal arrows represent the lift acting on the cylinder; please refer to Fig. 6.20.

rolls up on the other side resulting in an almost zero lift as the cylinder decelerates towards the minimum peak of response.

The process is repeated for the other half of the cycle as the cylinder crosses the wake in the opposite direction. Frame 'd' shows that maximum lift towards the centreline occurs when vortex A5 induces high speed flow on the inner side of the body, while A4 induces B6 to form closer to the cylinder. Note that maximum lift was not registered for the lowermost displacement, but when the cylinder encountered that particular wake configuration on its way towards the centreline. Again, the lift inversion happened slightly before the cylinder crossed the centreline. Similarly, another local peak of lift shown in frame 'e' is caused by the impingement of vortex A5; it splits around the cylinder merging with B7 on the inner side and with B8 on the outer side. An almost zero lift is obtained in frame 'f' when the cylinder experiences the same wake interaction as in 'c', though in the opposite direction.

We chose to analyse this example of the time series because the lift force in the first half of the cycle is mirrored by the second half, therefore giving more insight into the wake-structure interaction taking place. However we note that the peak of amplitude in frame 'a' is different from the peak the cylinder will reach just after frame 'f'. Once more this reveals that the response of the body is very dependent on the configuration of the wake it encounters for each cycle. With the crossing velocity $\dot{y}$ changing for each cycle, the vortex-structure interaction will also be different, resulting in different responses. In fact, if we look again to the short time series presented in Fig. 6.20 we will note that the trace of lift for the previous cycle between $t = 0$s and 1.0s is different from the cycle we investigated between $t = 1.1$s and 3.1s and also different from the following cycle after $t = 3.1$s.

Consequently, the phase lag varies from cycle to cycle. In Fig. 6.20 the phase lag at $t = 3.5$s is larger than in the previous cycle. At $t = 0.7$s the opposite is also observed and now it is the displacement that anticipates the fluid force. All this variation between successive cycles confers to the system the irregularity in response that was observed in the displacement and lift envelopes. But the fact that the phase lag will rarely be equal to zero also guarantees that energy will be transferred from

the fluid to the structure sustaining WIV, albeit in irregular amounts from cycle to cycle.

6.4.1 Three-dimensionality of the wake

At this point one might ask if the lift force measured with the load cell for the cylinder as a whole can be directly associated with the instantaneous flow fields presented in Fig. 6.21. Of course three-dimensional vortical structures are present in the wake for this Re range — especially streamwise vortices related to three-dimensional modes described by Carmo *et al.* (2008) — but coherent vortex tubes parallel to the cylinder axis still dominate the dynamics of the flow.

Although not presented here for brevity, we have obtained visualisations and PIV measurements of the flow illuminating a vertical plane parallel to the cylinders axes. Oblique shedding was sometimes observed to occur, especially from the bottom half near the floor, however once the downstream cylinder was allowed to oscillate its movement tended to correlate not only its own shedding but also the shedding of the upstream body. This effect was reduced as x_0 was increased, but still vertical vortex tubes shed from the cylinder were roughly parallel to the cylinders axes, at least in the gap of $x_0/D = 4.0$.

The wake downstream of the second cylinder was verified to be more complex than the wake in the gap due to strong interactions between vortices and the movement of the second cylinder. As a result, significant three-dimensional flow structures were observed to occur primarily downstream of the second cylinder rather than in the gap.

The transverse velocity of the cylinder across the wake may as well be generating perturbations that propagate upstream and interfere with the three-dimensional wake of the first body. For separations less than $x_0/D = 3.0$ we observed that this effect enforced the correlation on the upstream shedding, sometime even synchronising the wake with the movement of the downstream cylinder.

6.5 Conclusion

As we have discussed in Chapter 3, the wake-displacement mechanism proposed by Zdravkovich (1977) seemed to be the most plausible explanation for the WIV phenomenon, even though he could not conclude how the wake was being displaced to generate the necessary phase lag to sustain the vibrations.

Based on the results presented in this chapter we can now conclude that it is the unsteadiness of the wake that is playing a role in the WIV process and not simply the displacement of a steady flow field. We could say that Zdravkovich's 'wake-displacement' theory needs to be understood more as a 'vortex-displacement' mechanism that inputs energy into the system by means of unsteady vortex-structure interaction as the cylinder oscillates. We may refer to this concept as a 'vortex-impulse' mechanism. To sum up, we list the main findings that support our theory.

6.5.1 Fluid force

Energy input from the fluid to the structure will only occur when there is a phase lag between fluid force and displacement.

- When the downstream cylinder oscillates across the wake it finds strong vortices from the upstream body that can induce considerable change in the lift force. We have shown characteristic flow fields with the most severe vortex-structure interactions that enhance or diminish lift.

- A phase lag between lift and displacement is most likely to occur in a disturbed wake that is constantly changing and interacting with the body. Coherent vortices impinging on the second cylinder and merging with its own vortices induce fluctuations in lift that are not synchronised with the motion.

- The shear flow experiment proved that a steady shear flow without vortices cannot excite a cylinder into WIV. Remove the unsteady vortices from the wake and the response will resemble a typical VIV, only distorted by the shear flow field.

6.5.2 Cylinder response

The characteristic response of the second cylinder agrees with the hypothesis for the fluid force summarised above.

- Irregular envelopes of displacement and lift indicate that the second cylinder encounters different wake configurations for each cycle. This is not possible in a steady flow, but is in agreement with an irregular vortex-structure interaction.

- The response of the cylinder decreases as x_0 is increased. As the second cylinder is moved farther downstream, vortices coming from the upstream wake have more time to diffuse and the induced vortex-structure interaction is weakened. This is in agreement with the fact that the lift and drag maps (both steady and fluctuating terms) also diminish with x_0.

- Increased three-dimensionality may also contribute to reduce the response. When the cylinder is positioned farther downstream it weakens the effect of correlating the upstream wake and oblique or irregular shedding may return. Less correlation of the wake may be related to less resultant lift acting on the second body, thus giving a reduced response.

6.5.3 Concluding remarks

We observe that WIV is not a resonant phenomenon. While VIV finds its maximum amplitude of vibration when f_s is very close to f_0, WIV keeps increasing $\hat{y}/D$ even when f_s is much higher than f_0. At a first look, f_s and f_0 are the only two frequencies present in the system, yet the response of the cylinder is found to be in another frequency branch; much lower than f_s but still higher than f_0. Another interesting fact is that the oscillation frequency is increasing with reduced velocity at a rate that is not at all correlated with f_s.

In the shear flow experiment we removed the upstream shedding frequency of the system, leaving only f_s that is generated in the second cylinder. As a result, the oscillations returned to a typical VIV response meaning that the upstream

frequency — or the upstream vortex shedding — was somehow important to sustain the excitation.

Now, if WIV does not depend in the resonance between f_0 and f_s, what would happen if we remove the natural frequency of the system? That is to investigate what would happen if we remove the springs of the downstream cylinder, making $k = 0$ and $f_0 = 0$. This is the topic of the next chapter.

Chapter 7

Characteristics of the WIV

response

Based on the investigation presented in Chapter 6 we are convinced that the interaction between the oscillating cylinder and the unsteady wake from upstream is crucial to sustain the WIV mechanism. The necessary phase lag that drives and maintains the excitation was shown to originate in this complex vortex-structure interaction. But one question was still left unanswered: Why is the cylinder oscillating at a frequency that is distinctively different from both the upstream vortex shedding frequency (f_s) and the natural frequency of the system (f_0)?

7.1 Experiment without springs: $f_0 = 0$

WIV turned out to be understood as a non-resonant mechanism with the amplitude of response increasing far beyond any synchronization range. The fact that the excitation mechanism is not dependent on the forcing frequency matching f_0 gave us the idea of removing yet another fundamental frequency of the system. In the previous experiment we made $f_s = 0$ by generating a steady shear profile without vortices; now we make $f_0 = 0$ by removing the springs of the oscillator.
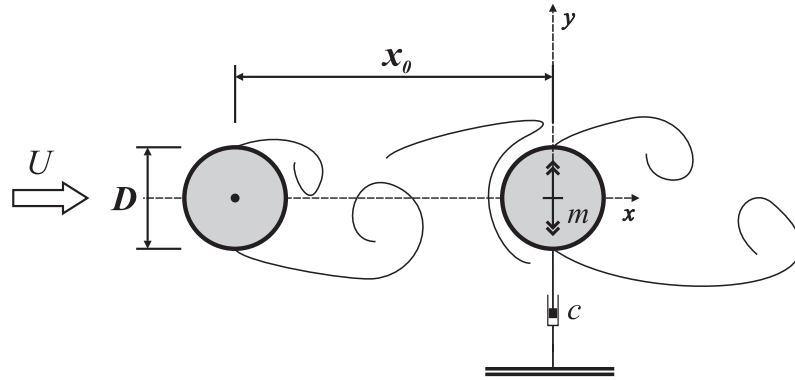
Fig. 7.1: Arrangement of a pair of cylinders in tandem. The downstream cylinder, mounted without springs, is free to oscillate in the cross-flow direction.

7.1.1 Experimental set-up

The same experimental set-up was kept from previous experiments but, while m and c remained unchanged, the pair of springs was removed from the system making $k = 0$ and $f_0 = 0$, as presented in Fig. 7.1. Therefore, for a downstream cylinder immersed in still water there was no structural stabilising force whatsoever to keep it in position. Cylinders were initially aligned in tandem, but the downstream body would drift away from the centreline responding to any perturbation coming from the flow or from the rig.

No other works were found on WIV of cylinders where all stiffness had been removed. Zdravkovich (1974) performed experiments with a downstream cylinder mounted on a horizontal swinging arm without springs, but he was still left with a restoration force generated by the steady flow. The drag acting on the cylinder generated a stabilising force component towards the centreline — in the same way the weight stabilises a vertical pendulum in free oscillation — resulting in an equivalent stiffness generated by the flow. Most of his experiments were concerned with the gap-flow-switching mechanism, hence were concentrated in the proximity interference region. For $x_0/D < 3.5$ he observed severe vibrations with a clear dominant frequency; yet the response was abruptly reduced for separations between $x_0/D = 3.5 - 7.0$ with no clear dominant frequency being identified.

Beyond that critical separation the downstream cylinder was not prone to gap-flow-switching any longer but entering the WIV region, still the expected build

up of response was not observed. Zdravkovich's experiment was performed in air and his elastic rig presented a very high damping factor of $\zeta = 0.24$. Probably, we believe, a high value of combined $m^*\zeta$ was enough to suppress WIV but not gap-flow-switching, only suggesting that the content of energy in the first mechanism is lower than in the latter. Apart from this experiment we have not seen any other WIV investigation on cylinders mounted without springs — and even in this case there was still a remaining stabilising force left due to resolved drag.

7.1.2 WIV response without springs

In the WIV response with springs we found that a VIV resonance peak always occurred around $U/Df_0 = 5.0$, before a pure WIV mechanism could prevail. A hypothesis is that the cylinder was being excited by VIV up to a condition of motion (coupled displacement and frequency) from which WIV could eventually take over. But now, once the springs are removed, we do not expect to see the local peak of VIV appearing, consequently the cylinder may not be excited into the critical motion for WIV to start. Would it still be possible to obtain a WIV response without first passing through a VIV resonance peak?

We already know (Fig. 6.4, page 109) that a static downstream cylinder in staggered arrangements experiences a steady lift force towards the centreline. Keeping this stabilising effect in mind, we expect that a free downstream cylinder mounted without springs would respond in three possible ways:

- *Drift sideways.* The impulse generated by the vortex-structure interaction would be strong enough to overcome $\overline{C}_y$ towards the centreline; the cylinder would drift away beyond the wake-interference region (static divergence) and no oscillatory motion would be sustained.

- *Remain stable on the centreline.* The impulse generated by the vortex-structure interaction when the cylinder is on the centreline would be too weak to displace the cylinder and initiate any WIV; the cylinder would find a stable position on the centreline due to a strong $\overline{C}_y$ field and no oscillatory motion would be sustained.

- *Develop oscillatory motion.* The impulse generated by the vortex-structure interaction would be strong enough to displace the cylinder, but the stabilising $\overline{C}_y$ would restore the cylinder towards the centreline. A phase lag between force and displacement would appear to build up the WIV mechanism and sustain oscillatory motion even without springs.

In principle it appears that the existence of oscillatory motion depends on the balance between the impulse force from the vortex-structure interaction and the stabilising lift towards the centreline, at least in a system without springs. But since both force components depend on the unsteady wake configuration and motion of the body we cannot predict a priori if the system will respond with sustainable oscillatory motion — and even if some oscillation is developed there is no indication that it would resemble the WIV response obtained when springs were present.

Displacement and frequency

Let us now move to the WIV response itself. Fig. 7.2 presents the WIV response for the downstream cylinder mounted without springs compared with the curve (already presented) for a cylinder with springs. Both curves were obtained for the same variation of the flow speed; therefore both data sets share the same Reynolds number scale. But because the system without springs has no inherent f_0 it does not make sense to plot this curve with a reduced velocity axis. In fact, by making $f_0 = 0$ we are effectively making $U/Df_0 = \infty$ for all points of the response without springs; the variation of flow speed can only be represented by Re in this case.

From among the three hypotheses presented above, the response certainly agrees with the third one concerned with sustainable oscillatory motion. Not only the cylinder was able to sustain oscillations, but most surprisingly the amplitude of response was remarkably similar to the case with springs. As far as the amplitude of response is concerned, it appears that the absence of springs is insignificant for the WIV mechanism. As expected, the local peak of VIV around $U/Df_0 = 5.0$ disappeared once the resonance $f_s = f_0$ was eliminated by removing the springs. But the overall response for both cases, with and without springs, is notably similar.
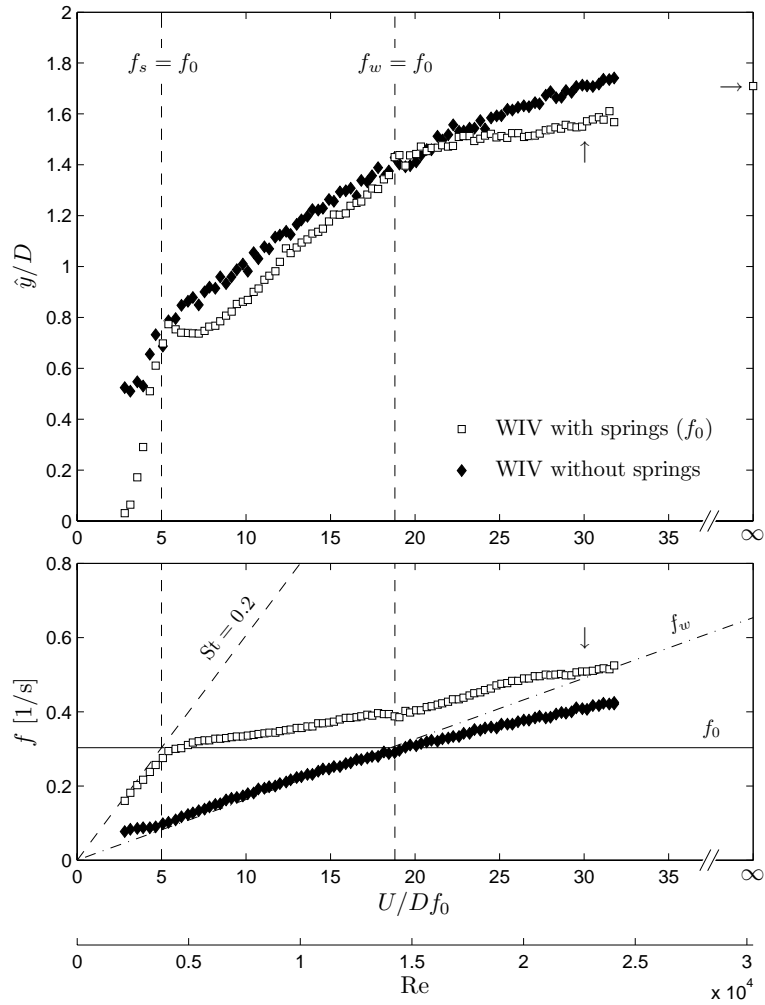
Fig. 7.2: WIV response of a downstream cylinder mounted with and without springs at $x_0/D = 4.0$. Top: displacement; bottom: dominant frequency of oscillation.
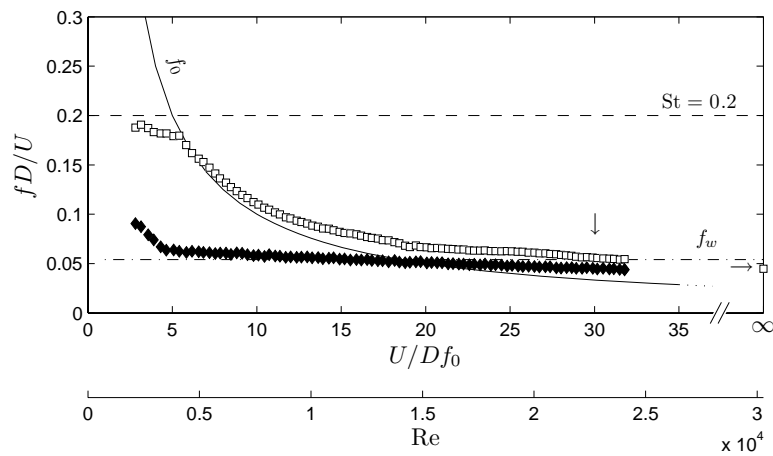

Fig. 7.3: Non-dimensionalised dominant frequency of oscillation of a downstream cylinder mounted with and without springs. Please refer to Fig. 7.2.

The fact that $\hat{y}/D$ increases with flow speed is not an effect of reduced velocity. In other words, the increase in WIV response observed for a cylinder without springs cannot be related to any structural stiffness. Instead, it seems that the response reveals some dependency simply on Reynolds number. Since both curves are essentially very similar, we suggest that an independence of response from reduced velocity and a dependency on Re might as well be occurring for the cylinder mounted with springs. We shall return to this subject later on this chapter.

Let us turn now to the frequency of response presented in the bottom graph of Fig. 7.2. Since f_0 is not defined for the case without springs, we can only compare both curves if they are plotted in dimensional form (1/s). The response with springs was analysed in Chapter 5, but it is convenient to summarise it here once more: f follows the St $= 0.2$ line up to the VIV resonance; follows close to f_0 through a distorted synchronisation range, but eventually continues on a distinct branch dominated by pure WIV. On the other hand, the frequency of response without springs shows no effect of VIV synchronisation — that is obvious since there is no f_0 for it to be synchronised with — but follows an almost straight line as the flow speed is increased. In fact, we note that it follows very closely a dash-dotted line marked as f_w, which we shall explain later.

Another way to analyse this result is to create a non-dimensional parameter fD/U, a type of Strouhal number, plotted in Fig. 7.3. This way, the St $= 0.2$ line presented in Fig. 7.2 becomes a constant in Fig. 7.3 and all the data is distorted to incorporate the effect of U varying in both axes. We shall return to this graph after some analytical modelling that will follow in the next sections. Before that we shall look at the time series of displacement and lift.

Displacement and fluid force

Fig. 7.4 shows three examples of times series for the WIV response without springs. The flow speed in each case, represented by Re, would correspond to a reduced velocity of $U/Df_0 = 10$, 20 and 30 for the cylinder mounted with springs. As mentioned before, the displacement plots on the first column show that the system is indeed responding with oscillatory motion. Although the frequency of response
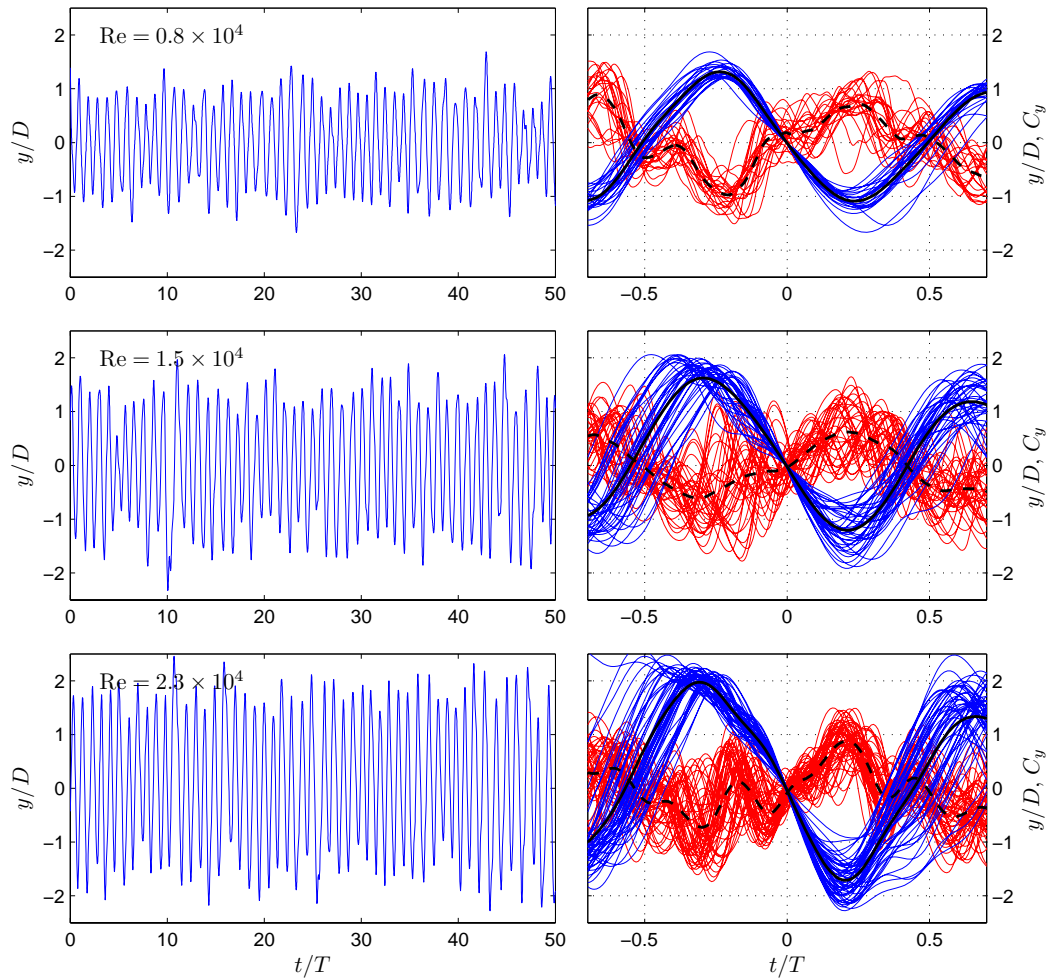
Fig. 7.4: Three examples of time series for WIV without springs. Left column: displacement signal for around 50 cycles of oscillation. Right column: superimposed plots of similar cycles. y/D in blue and C_y in red with average cycle in black.

seems to be rather regular, it is evident that the envelope of amplitude varies from cycle to cycle throughout the series. The second column presents superimposed plots of displacement and lift for similar cycles around the average value of $\hat{y}/D$ given in Fig. 7.2.

A considerable variation in displacement is evident from the deviation of blue lines from the average cycle represented in black. But besides that, it is the irregularity of the lift force that really catches the attention. A clutter of red lines reveals that almost no cycle is identical to any other and a wealth of higher frequencies induce C_y to present significant fluctuations within a single cycle of displacement.

Once more we can note that intense fluctuations in lift help to generate the phase lag between y and C_y that is necessary to input energy from the flow to the structure. However, by looking at the average cycle of lift, given by a dashed-black line, we can still note a lower frequency component almost in antiphase with the displacement. This term must have some inertia component reacting against the acceleration of the body — what was called C_{y_P} in Eq. 2.15 (page 33) — but part of it must also be related to the steady $\overline{C}_y$ field acting towards the centreline.

Analysing the PSD of C_y in Fig. 7.5 we note that the upstream cylinder is shedding vortices as an isolated body, with no interference from the motion of the second cylinder propagating upstream. This was also observed for the case with springs and there is no reason to expect that it would be different for the same separation. On the other hand, the PSD of lift on the downstream cylinder shows two distinct branches of frequency: the higher $f(C_y)$ branch is clearly an effect of vortex shedding from the upstream cylinder; whereas the lower $f(C_y)$ branch is promptly identified with the frequency of response in Fig. 7.2.

It is important to note that in this case there is no f_0 defined by springs (that is why $f(C_y)$ has a dimension of 1/s), hence the fact that $f(C_y)$ presents a lower branch is not associated with any structural stiffness. It is only at the very beginning of the scale, for Re $< 0.3 \times 10^4$, that we see the vortex shedding branch having more energy than the lower one; otherwise for the rest of the response the lower frequency branch clearly dominates the character of C_y. Now, with such a clear preponderance of the
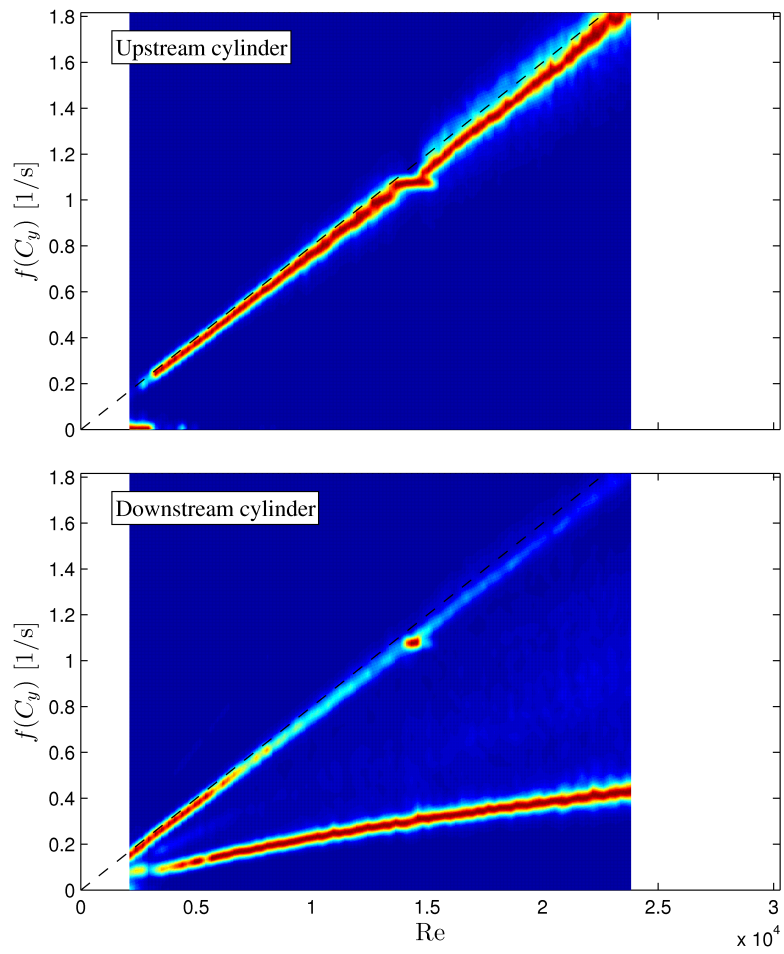
Fig. 7.5: Normalised PSD of lift force acting on the upstream static cylinder (top) and downstream cylinder without springs (bottom). Please refer to Appendix A.

lower $f(C_y)$ branch it is not surprising that the dominant frequency of response matches this major excitation.

The body is able to sustain oscillatory motion even without any springs to create structural stiffness. But we are still left with the question about the origin of a lower frequency force that is not related to either f_s or f_0. The only possibility left is that there must be another force acting to restore the body to equilibrium. Since the body is essentially absent of any structural stiffness, such a stabilising force has to be coming from the flow itself. That is to say that there must be a fluid force playing the role of the stiffness in the oscillator, otherwise no oscillatory motion would be observed.

7.2   The wake stiffness concept

Now that we have observed that the WIV response without springs indeed presented oscillatory motion — with amplitude increasing with Reynolds number and a frequency distinct from f_s or f_0 — we should spend some time to model the problem of a cylinder with no structural stiffness.

The equation of motion (Eq. 2.3, page 27) has the stiffness term removed if we make $k = 0$ for a downstream cylinder without springs, resulting in

$$m\ddot{y} + c\dot{y} = C_y \frac{1}{2} \rho U^2 D, \tag{7.1}$$

where all forces are per unit length of cylinder. Applying the same 'harmonic forcing and harmonic motion' assumption employed to the analyses of VIV for a single cylinder, where $y = \hat{y}\sin(2\pi ft)$ and $C_y = \hat{C}_y \sin(2\pi ft + \phi)$, results in

$$\frac{\hat{y}}{D} = \frac{1}{4\pi} \hat{C}_y \sin\phi \frac{\rho U^2}{cf}. \tag{7.2}$$

Notice that neither the mass nor any stiffness comes into the equation, but the excitation is simply balancing the structural damping of the system given by c (friction damping per unit length of cylinder). Rearranging Eq. 7.2 into non-dimensional groups yields

$$\frac{\hat{y}}{D} = \frac{1}{4\pi} \hat{C}_y \sin\phi \left(\frac{U}{Df}\right) \left(\frac{\rho U D}{\mu}\right) \left(\frac{\mu}{c}\right). \tag{7.3}$$

Knowing that μ is a physical property of the fluid and assuming that viscous damping c is only based on the friction of the air bearings, we conclude that μ/c does not vary with Reynolds number. We are left with three non-dimensional groups that might have some dependence on flow speed: $C_y \sin \phi$ is associated with the excitation force and we shall consider it later; U/Df represents the inverse of a non-dimensional frequency of oscillation; $\rho U D/\mu$ is the Reynolds number itself.

7.2.1 Frequency of oscillation and natural frequency of wake stiffness

Now let us first investigate the behaviour of the non-dimensional oscillation frequency (fD/U). If we consider the map of steady lift across the wake for $x_0/D = 4.0$ presented in Fig. 6.4 (page 109) we note that $\overline{C}_y$ acting towards the centreline has a rather good linear behaviour between $-1.0 < y_0/D < 1.0$ and does not vary with Reynolds number. Of course nonlinearities appear for larger separations, but we can estimate the slope

$$|\partial \overline{C}_y| \equiv \left| \frac{\partial \overline{C}_y}{\partial (y_0/D)} \right| = 0.65 \tag{7.4}$$

(represented by a straight line in Fig. 6.4, page 109) within 95% confidence inside the wake interference region. For convenience, we shall refer to this slope simply as $|\partial \overline{C}_y|$ from now on.

We know that this steady lift works as a restoring force towards the centreline. Similarly to the stiffness generated by a spring, the magnitude of $\overline{C}_y$ increases linearly with transverse displacement of the cylinder, at least within the wake interference region. For that reason, the $\overline{C}_y$ field can be understood as a fluid-dynamic stiffness generated by the flow; such an effect will be referred to as *wake stiffness* from now on. The equivalent spring constant (k_w) that would generate such a flow effect is given by

$$k_w = |\partial \overline{C}_y| \frac{1}{2} \rho U^2; \tag{7.5}$$

thus an equivalent natural frequency f_w could also be associated with wake stiffness,

as expressed by

$$f_w = \frac{1}{2\pi}\sqrt{\frac{k_w}{(m^* + C_a)\rho\frac{\pi D^2}{4}}}, \tag{7.6}$$

where C_a denotes the potential added mass coefficient.

Since wake stiffness is a fluid-dynamic force, its effect would be equivalent to a spring with a constant k_w that increases with U^2 (Eq. 7.5), hence the associated natural frequency f_w increases linearly with Re. Replacing Eq. 7.5 in Eq. 7.6 and multiplying it by D/U results in the Strouhal-type non-dimensional parameter

$$\frac{f_w D}{U} = \frac{1}{2\pi}\sqrt{\frac{2}{\pi}\frac{|\partial\overline{C}_y|}{(m^* + C_a)}}. \tag{7.7}$$

We already know that $|\partial\overline{C}_y|$ is invariant with Re. Regarding that C_a cannot vary with Re either, we conclude that $f_w D/U$ is also a constant irrespective of Re.

Turning back to Fig. 7.2 we will note that f for a cylinder without springs presents a remarkable linear behaviour that grows with Re, which is represented by an almost constant curve far from St $= 0.2$ in Fig. 7.3. This suggests that there must be a fluid force with a characteristic frequency lower than f_s dominating the excitation. Note that this force cannot be related to f_0 because the system has no springs. Therefore we are left with the possibility that this restoration is indeed coming from the $\overline{C}_y$ field and must be related to $|\partial\overline{C}_y|$.

Now if we substitute $|\partial\overline{C}_y| = 0.65$, $m^* = 2.6$ and $C_a = 1.0$ in Eq. 7.7 we find that $f_w D/U = 0.054$ and can be represented by the f_w dot-dashed line in Figs. 7.2 and 7.3. The agreement between f_w and the WIV response without springs is remarkable. This is evidence that a cylinder without springs may as well be responding to the wake stiffness with $f = f_w$ for the whole range of Re. That is to say that the excitation frequency identified in the lower branch of $f(C_y)$ in Fig. 7.5 — that matches the response frequency f in Fig. 7.2 — is actually governed by the wake stiffness effect described in Eqs. 7.5 to 7.7.

If it is true that $f = f_w$, Eq. 7.7 tells us that fD/U is also a constant and the cylinder indeed oscillates with f that increases linearly with Re. In Fig. 7.2 we note that f closely follows f_w up to around Re $= 1.5 \times 10^4$ when the response amplitude reaches about $\hat{y}/D = 1.4$. Beyond this point the amplitude grows towards values

around $\hat{y}/D = 1.8$ meaning that the cylinder is oscillating further out of the wake interference region. From the $\overline{C}_y$ map for $x_0/D = 4.0$ (Fig. 6.4) we know that the steady lift grows linearly with lateral separation up to around $y_0/D = 1.0$. Farther than that nonlinear effects start to appear and the wake stiffness is not able to be represented simply by the slope $|\partial \overline{C}_y| = 0.65$ but would gradually be reduced. This is exactly what is observed as the frequency curve begins to depart from the f_w line as $\hat{y}/D$ increases. Of course some effect in reducing f must be coming from the fact that secondary effects in the effective added mass of fluid may appear as the cylinder moves in and out of the wake interference region. But even considering that the effective added mass is constant at $C_a = 1.0$ throughout Re the agreement is still very good.

Although it might be helpful to think the wake stiffness effect is acting as a linear spring, a quasi-static lift map still is an oversimplification of the problem. If the restoring fluid force towards the centreline is induced by complex vortex-structure interactions — as we have proposed in Chapter 6 — it should also present unsteady variations as the cylinder moves across the wake. However we can still imagine that if the cylinder is displaced farther away from the wake interference region ($y/D \gg 1.0$) the induced force on that instant must be reduced. On the other hand, if in another instant the cylinder is located closer to the wake boundary the vortex-induced force must be amplified.

For that reason we could understand that the total excitation force as being composed of two fluctuating terms with distinct frequencies. One term is associated with the wake stiffness, which obviously depends on the position of the body across the wake and is related to f. The other is associated with the impulse vortex-force induced on the cylinder, which also depends on the lateral position of the cylinder and is thus related to f_s. We believe that while a series of vortices streaming along the wake induces a steady force towards the centreline, each individual vortex also induces an instantaneous force fluctuation (an impulse) on the cylinder. The magnitude of both *wake-stiffness* and *vortex-impulse* terms will depend on the relative position of the body and a particular interaction with the wake.

7.2.2   VIV and WIV resonances: $f_s = f_0$ and $f_w = f_0$

If the wake-stiffness is dominant over the vortex-impulse term it is straightforward to predict that the cylinder should respond with $f = f_w$ and not $f = f_s$. As we have seen so far $f_w D/U$ does not vary with flow speed, thus f_w increases linearly with Re. Since f_0 is a constant defined by the springs, there must be a critical point where the wake stiffness has the same intensity as the spring stiffness, i.e. $k_w = k$ and $f_w = f_0$. This occurs in Figs. 7.2 and 7.3 where f_w crosses the f_0 line at Re $= 1.2 \times 10^4$ (equivalent to $U/D f_0 = 18.8$ for the case with springs). We know that the present set of coil springs provides the system with a stiffness of $k = 11.8$N/m. But considering the steady lift map with $|\partial \overline{C}_y| = 0.65$ in Eq. 7.5 we see that the wake stiffness can reach values as high as $k_w = 34$N/m at the end of the Re range of the experiments.

For the case with springs we find f following closer to the f_0 line during the range where VIV is relevant, with the lock-in peak occurring around the intersection of f with both f_0 and St $= 0.2$ lines. This first VIV resonance is marked by the vertical line $f_s = f_0$ in Figs. 7.2 and 7.3. At this point $k_w = 1.8$N/m is only 15% of k provided by the springs. As the flow speed is increased the VIV synchronisation tends to disappear as St $= 0.2$ moves away from f_0. At the same time the wake stiffness is also getting stronger until both k_w and k have the same value. As we saw, this occurs for $U/D f_0 = 18.8$ and is marked by the second WIV resonance line $f_w = f_0$, beyond which k_w is greater than k.

The two resonance lines divide the response for a cylinder with springs in three regimes that are best identified in Fig. 7.2. (i) Before $f_s = f_0$, when St $= 0.2$ is approaching f_0, the displacement resemble an initial branch of VIV and f follows the Strouhal line up to the resonance peak. (ii) The second regime, between $f_s = f_0$ and $f_w = f_0$, is marked by a steep slope in the displacement curve; f remains rather close to f_0 as the VIV synchronisation range gradually gives way to a wake stiffness that is growing stronger with Re. (iii) The third regime, beyond the second resonance $f_w = f_0$ is characterised by a change of slope in both the displacement and frequency curves. With $k_w > k$ the WIV response is established and dominates alone for the

rest of the Re range.

It works as if the set of springs is important only in the first regimes before the $f_w = f_0$ resonance, but the system completely overlooks its small structural stiffness given by f_0 as k_w gets relatively stronger. It appears that out of the resonances $f_s = f_0$ and $f_w = f_0$ the spring acts against the WIV excitation with the effect of reducing the amplitude of vibration. This idea is in agreement with the classical theory of linear oscillators; if the excitation force is out of the resonance of the system the response will not be as high as the resonance peak.

Various experiments have investigated the flux of energy in the system for a cylinder oscillating in forced vibrations in a flow. Recently, Morse & Williamson (2009) have presented a detailed energy map for VIV of a single cylinder. If we take values of displacement and frequency from our own WIV curves and plot them in their VIV energy map we will see that the structure is actually losing energy to the flow. If we think that the major forcing term is coming from the WIV mechanism governed by wake stiffness, the VIV part governed by spring stiffness is contributing to dissipate energy and reduce the vibration. That is why the response curve with springs shows reduced amplitude out of the two resonance lines when compared with the case without springs. Because our excitation force is believed to have a wake-stiffness and a vortex-impulse component, each related to one characteristic frequency, the response will be slightly accentuated when $f_s = f_0$ (VIV resonance) and $f_w = f_0$ (WIV resonance).

Possibility of a third resonance $f_s = f_w$

One could ask if it would be possible to have a third resonance $f_s = f_w$, potentially occurring also for a cylinder without springs. Since both f_s corresponding to St = 0.2 and f_w are linearly dependent on Reynolds number, they would have to be equal throughout the whole Re range. Starting from Eq. 7.7 and considering that the Strouhal number of a cylinder is roughly constant with Re, there are only two ways to bring both St = 0.2 and f_w lines together.

Firstly, fixing the mass of the system we would have to generate a steady lift field with $|\partial \overline{C}_y| = 8.9$ which is one order of magnitude higher than the maximum value

measured for staggered cylinders. Now, if the steady lift towards the centreline has its origin in the unsteady vortex-structure interaction (as proposed in Chapter 6) both f_s and f_w originate in the same phenomenon and have to coexist within physical boundaries. By this we mean that the wake structure required to generate such an intense steady field would have to be very different from the vortex shedding mechanism that we know. Therefore we do not expect $f_s = f_w$ due to an intense $\overline{C}_y$ field.

Secondly, knowing that $|\partial \overline{C}_y|$ is invariant with Re, we can change the mass of the system in order to change the natural frequency f_w. Keeping $|\partial \overline{C}_y| = 0.65$ and $C_a = 1.0$ constants in Eq. 7.7 and equating the right-hand side to St $= 0.2$ results in $m^* = -0.74$. Since this result is impossible in a physical system we can affirm that St $= 0.2$ and f_w will never overlap.

In fact, since we know the cylinder is responding to WIV with $f = f_w$, to have $f_w = f_s$ means that the cylinder would be oscillating in the frequency of vortex shedding for the whole Re range. This is the WIV equivalent of the phenomenon described by Govardhan & Williamson (2002) for VIV of a single cylinder. They verified that for m^* below a critical value around 0.54 the VIV response would persist for an infinite regime as if the lower branch were extended indefinitely. It was observed that the frequency of oscillation f would follow the vortex shedding frequency f_s, linearly increasing with reduced velocity, sustaining a regime they called 'resonance forever'. Although this appears to be physically impossible to occur in our case, we cogitate that if we could artificially bring both St $= 0.2$ and f_w lines together — in a force feedback system this would be possible — the cylinder would vibrate indefinitely with both VIV and WIV perfectly combined.

7.2.3 Response without springs in a shear flow

In Chapter 6 we have seen that the unsteadiness of the wake was necessary to excite WIV. A cylinder immersed in an artificial wake without vortices did not respond with WIV but only a distorted type of VIV. In the present chapter we investigated the importance of the wake-stiffness effect in sustaining the vibration of a cylinder

mounted without springs. Finally, we can combine both concepts of wake-stiffness and vortex-impulse in the response of a cylinder immersed in a shear flow (without unsteady vortices) but also without springs (without structural stiffness).

To allow for comparison with other response curves, the result is presented in Fig. 6.17 (page 127). Although some small wake-stiffness effect was left in the shear flow after vortices were removed — a $|\partial \overline{C}_y| \approx 0.2$ can be estimated from Fig. 6.15 (page 124) — it was not strong enough to sustain oscillatory motion and the cylinder did not respond with vibrations. If our theory is correct, we need to bring the excitation term from the vortex-structure interaction acting together with the wake-stiffness effect in order to produce a WIV response.

A clear response was observed for the reference cases with and without springs because the system had unsteady vortices to provide both vortex-structure interaction and wake stiffness. By removing the unsteadiness of the upstream wake we are essentially left without the WIV excitation term, therefore the response will be that of VIV. But by removing both the unsteadiness of the wake and the springs at the same time we are left with no response at all.

7.3 Dependency on Reynolds number

Back to Eq. 7.3, we can now analyse the behaviour of the non-dimensional parameter $\hat{C}_y \sin \phi$ in respect of Reynolds number. We already know that the cylinder is responding with $f = f_w$, a dominant frequency produced by the wake stiffness effect. In the harmonic assumption applied in Eq. 7.1 we only consider that the fluid force is represented by a single dominant frequency and phase angle. But in Figs. 7.4 and 7.5 we clearly saw that C_y in fact presents two significant frequencies: a lower branch associated with wake stiffness and a higher branch associate with vortex-impulse.

But still holding a bit longer to the harmonic hypothesis we could split the actual effect of C_y into two parts. Because f_w is clearly dominant over f_s let us consider that the magnitude of $\hat{C}_y$ is only produced by the wake stiffness effect and has very little influence from vortex-impulse fluctuations. Consequently, the fluid force would have a dominant component $f = f_w$, with magnitude depending only in $|\partial \overline{C}_y|$
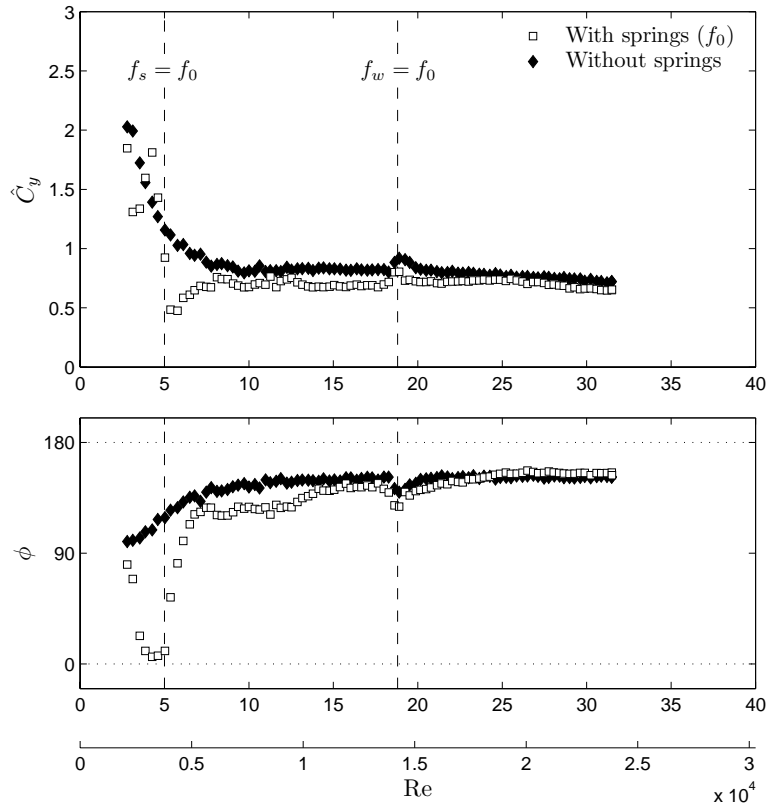
Fig. 7.6: Comparison between lift coefficient (top) and phase angle (bottom) for the WIV response of a cylinder with and without springs at $x_0/D = 4.0$.

and acting in antiphase with the displacement. (Again we are entering quasi-static territory, but at least now we are supported by having $U/Df_0 = \infty$.)

On the other side, we need to account for the phase lag necessary to sustain the vibration. We have already proposed that it is generated by the complex vortex-structure interaction as the body crosses the wake, therefore we could attribute the existence of $\phi \neq 0°$ and $180°$ to vortex-impulse fluctuations operating at f_s.

We have shown in the previous section that $|\partial \overline{C}_y|$ does not vary with Re, therefore $\hat{C}_y$ should also be invariant. But we have also demonstrated that, due to fluctuations caused by vortex-impulse, the phase angle varies from cycle to cycle as the cylinder interacts with different wake configurations. Albeit not being very strong, this supposition finds some support in the time series presented in Fig. 7.4. Therefore, let us now investigate $\hat{C}_y$ and ϕ independently.

Fig. 7.6 compares the total lift coefficient for both WIV responses with and without springs. An abrupt reduction in $\hat{C}_y$ for the case with springs is characteristic

of the VIV phase shift and occurs at the $f_s = f_0$ resonance. We can still note some differences between both cases while VIV is losing strength between the resonances, but yet it is beyond the resonance $f_w = f_0$ that WIV clearly dominates and both curves follow closely together for the rest of the Re range. Apart from a small range of $\mathrm{Re} < 0.5 \times 10^4$, $\hat{C}_y$ without springs shows a fairly constant behaviour with a small negative slope.

The bottom graph of Fig. 7.6 compares average values of ϕ for WIV responses with and without springs. Each data point was obtained by employing the Hilbert transform to calculate instantaneous values of phase angles (as presented in Fig. 6.18) and then averaging ϕ for more than 500 cycles of oscillation. The curve shows that ϕ without springs presents a relatively constant value around 153° for $\mathrm{Re} > 0.5 \times 10^4$.

Although both $\hat{C}_y$ and ϕ appear to be fairly invariant with Re, we cannot forget that values plotted in Fig. 7.6 are averaged for as many as 500 cycles of oscillations. We have already seen in Fig. 7.4 how irregular C_y can be from cycle to cycle. Variations within the present Re range are also expected to occur due to the complex characteristic of the wake. For example, it is known that the vortex formation length presents a strong variation with Re; and the three-dimensionality of the wake may as well present some Re dependency. Nevertheless, although $\hat{C}_y$ and ϕ cannot be confirmed as strictly constants we are able to conclude that, to a first approximation, the non-dimensional term $\hat{C}_y \sin \phi$ should be roughly invariant with Re, at least within the subcritical Re range of the experiments.

Turning back to Eq. 7.3 we can now verify that μ/c, U/Df and $\hat{C}_y \sin \phi$ are approximately invariant with Re, leaving only the Reynolds number term itself on the right-hand side of the equation. As a result it is evident from this analysis that $\hat{y}$ is linearly dependent on Re and the WIV response should increase with flow speed up to a critical amplitude. Once the cylinder starts to be displaced out of the wake interference region nonlinear effects become important limiting the response to an asymptotic value. Secondary effects may be acting on U/Df and $\hat{C}_y \sin \phi$ conferring on the response the curved shape presented in Fig. 7.2.

The analysis developed above is in good agreement with displacement curves

presented for both cases with and without springs. Therefore we conclude the mechanism that is building up the amplitude of vibration in WIV is definitely not a consequence of reduced velocity but a direct effect of Reynolds number.

Picking a displacement point from the curve without springs at an arbitrary value of $\mathrm{Re} = 2.3 \times 10^4$ (represented by a vertical arrow in Fig. 7.2) we are able to estimate the limiting value the response is asymptotically approaching to as $U/Df_0 \to \infty$ for that specific Re. Of course this is the data point from the curve without springs immediately above the vertical arrow, but it can also be represented on the right-hand side axis for $U/Df_0 = \infty$ (this will be useful later when comparing different x_0 separations).

Such a strong Re dependency turned out to be a rather unexpected result. It took us some time to comprehend how a fluid-elastic system could show considerably high variations in such a short Re range. But if we consider that our system actually possess a fluid-dynamic spring that increases stiffness with U^2 (Eq. 7.5) we are left with the only conclusion that $\hat{y}/D$ must indeed vary with flow speed.

7.3.1 Experiments with constant Re

At this point one may recall the results from Hover & Triantafyllou (2001), presented in Fig. 3.8(b) (page 55), who measured the WIV response of a cylinder at $x_0/D = 4.75$ and constant $\mathrm{Re} = 3 \times 10^4$. They achieved that by varying the spring stiffness of a force-feedback system. In spite of operating at a fixed Reynolds number, they were able to measure a build up of response that increased with reduced velocity. In principle, this seems to contradict our theory that the WIV response is not affected by reduced velocity.

Considering that their separation of $x_0/D = 4.75$ must provide a wake stiffness effect in the order of $|\partial \overline{C}_y| = 0.55$, we can estimate that the critical reduced velocity at which the wake stiffness equals the spring stiffness ($k_w = k$) is as high as $U/Df_0 = 21$ (based in our $\overline{C}_y$ map of Fig. 6.1, $C_a = 1.0$ and their value of $m^* = 3.0$). However, the maximum reduced velocity achieved in their experiment is only around 17. Hence the regime Hover & Triantafyllou (2001) observed was still between the
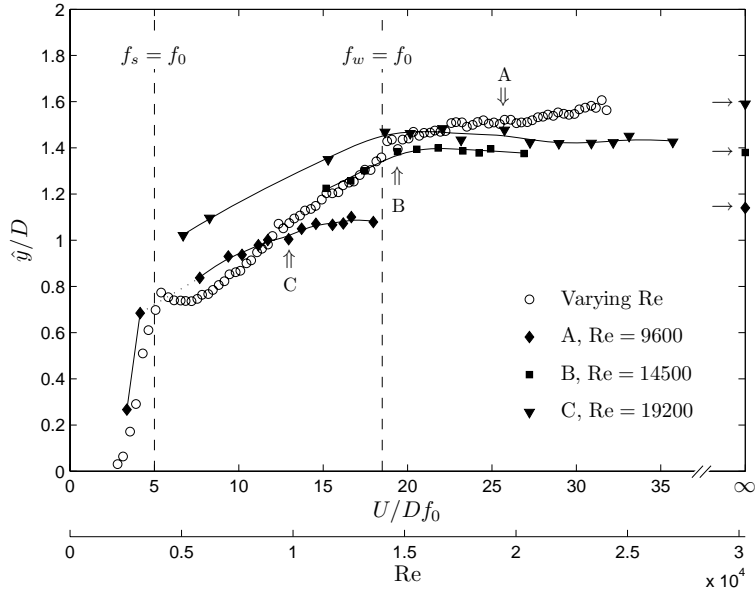
Fig. 7.7: WIV response at constant Re for $x_0/D = 4.0$. Reduced velocity varied by changing the springs.

resonances $f_s = f_0$ and $f_w = f_0$, a region where VIV still has some significance.

According to our theory, we would expect their results to reach an asymptotic value around $\hat{y}/D = 1.5$ for Re $= 3 \times 10^4$, which is in good agreement with their curve reproduced in the present work. Note, however, that Hover & Triantafyllou (2001) do not plot $\hat{y}/D$ but an average of the 10% highest peaks of displacement. As we have seen in Fig. 5.7 (page 95) the maximum displacement of the cylinder can be considerably greater than the averaged $\hat{y}/D$ that we usually employ.

The same observation is also true for the results obtained by Assi *et al.* (2006) also presented in Fig. 3.8(b). Even though k was constant, they could not reach the regime above the WIV resonance $f_w = f_0$ due to a limitation in the maximum flow speed.

In order to verify this phenomenon, we have prepared a series of experiments for three constant Reynolds numbers at $x_0/D = 4.0$. The flow speed was fixed and reduced velocity was varied by changing the set of springs and, consequently, changing f_0. Fig. 7.7 presents the results compared to our reference WIV response of a cylinder with fixed springs and varying U/Df_0 by varying flow speed (the secondary axis of Re refers to this curve only).

Three vertical arrows, one for each Re curve, mark the condition where the

stiffness of the varying spring matches the fixed spring k. Hence all data points to the right of these arrows have a spring that is softer than our reference curve (and stiffer to the left). None of the curves was able to span the three regimes defined by the resonance lines $f_s = f_0$ and $f_w = f_0$, but considering the results of all three curves as a whole we are able to understand the general behaviour of the response at a constant Re.

The curve for Re = 9600 does not have enough data points to reveal a local peak of VIV at $f_s = f_0$, but the majority of the points fall within the first regime between the resonances, where VIV is gradually losing its influence to WIV. In our experiment with varying Re we have noticed that the amplitude of response generally presents a positive slope in this first regime; this is verified now for a constant Re as well. As we have discussed above, Hover & Triantafyllou (2001) found increasing response also for a constant Re in this regime. Our data agrees with theirs in showing a build up of response between $f_s = f_0$ and $f_w = f_0$. Such an effect is also observed for our curve at Re = 19200.

Let us move on to the other curves at Re = 14500 and 19200 that are able to cross $f_w = f_0$ and enter the second regime where WIV dominates. Now that the wake stiffness is greater than the spring stiffness we see that the response is not influenced by reduced velocity anymore, but presents a rather constant level of amplitude for each fixed value of Re. Even if the reduced velocity is increased from 20 to 35 the amplitude of response seems not to be much affected and the data points appear to follow the same trend as long as Re is kept constant. Going back to the curve without springs in Fig. 7.2 we are able to find a displacement amplitude for each of our Re curves at $U/Df_0 = \infty$ towards which the data points should be converging. We note that they are slightly higher than the level of amplitude the curves are reaching beyond $f_w = f_0$, but we have to remember that we are still operating with springs, although soft ones, that might be contributing to reduce the response away from the resonance lines.

While on one hand the VIV peak at $f_s = f_0$ seems to always reach $\hat{y}/D$ around 1.0 (for this value of $m^*\zeta$), the amplitude at the end of the first regime, at $f_w = f_0$, varies with the intensity of the wake stiffness effect. Because k_w increases with Re

the amplitude at $f_w = f_0$ must also increase with Re. This level of amplitude is already very close to the asymptotic value predicted by the experiments without springs; hence, as the spring stiffness gets softer beyond $f_w = f_0$, we expect the curves to be converging towards the values plotted at $U/Df_0 = \infty$.

This series of experiments at constant Re proved that while the response below $f_w = f_0$ is dependent on both Re and reduced velocity, the response for $f_w > f_0$ is clearly governed by Re only. In other words, we conclude that in the first regime where VIV and WIV are competing (or cooperating) the response increases due to a combination of spring and wake-stiffness effects. Even with constant Re we note a build up of response while the ratio between k and k_w makes reduced velocity an important parameter. But once the wake stiffness becomes dominant over the springs the response takes no note of the structural stiffness and is only governed by wake stiffness. Now this second regime is clearly dominated by a Reynolds number effect.

7.3.2 Equivalent damping

Another way to comprehend the behaviour of the amplitude of response is to think in terms of an equivalent damping ratio. As we saw in Eq. 2.7 (page 28) we can define ζ by the ratio between c and a critical damping, rewritten as

$$\zeta = \frac{c}{4\pi f_0 m}. \tag{7.8}$$

Note that the natural frequency and the mass of the system are present in the denominator.

Apart from removing the pair of springs we kept exactly the same set-up from previous experiments, therefore we assume all other parameters were kept constant including the structural damping c. In other words, we presuppose the friction in the air bearings was kept the same; hence the system would dissipate the same amount of energy for a similar velocity of the cylinder. However, now that the springs were removed we do not have f_0 that can be used to non-dimensionalise ζ as expressed in Eq. 7.8.

Govardhan & Williamson (2002) also encountered problems to define a suitable damping ratio when performing experiments with a cylinder mounted on air bearings without springs. They also wanted to investigate the VIV response for $U/Df_0 \to \infty$ and achieved that by removing the springs from the elastic system, making $k = 0$ and $f_0 = 0$. Since there were no springs, but f followed the shedding frequency throughout the oscillatory regime, they employed an equivalent damping ratio non-dimensionalised by f_s instead of f_0.

But in the present WIV investigation the frequency of oscillation was observed not to follow the vortex shedding frequency; instead f increases linearly with flow speed following f_w — the natural frequency given by wake stiffness — as demonstrated above. Therefore, unlike in Govardhan & Williamson (2002), it does not make sense to define an equivalent damping ratio based on the shedding frequency f_s, but based on the oscillation frequency $f = f_w$ instead, hence

$$\zeta_w = \frac{c}{4\pi f_w m}. \tag{7.9}$$

According to this definition of ζ_w the damping ratio varies with flow speed since f_w is also varying with U (Eq. 7.6). The same occurred for Govardhan & Williamson (2002), where their damping ratio was based on f_s which also varies with U according to the Strouhal law. (This was not the case with the traditional ζ as defined in Eq. 2.7, which is invariant with U given a constant natural frequency f_0 defined by structural stiffness.)

Now, replacing c from Eq. 7.9 into Eq. 7.3 results in a combined $m^*\zeta_w$ parameter appearing in the denominator

$$\frac{\hat{y}}{D} = \frac{1}{4\pi}\hat{C}_y \sin\phi \left(\frac{U}{Df}\right)^2 \left(\frac{1}{m^*\zeta_w}\right). \tag{7.10}$$

Similarly to the analysis presented for VIV of a single cylinder in Chapter 2 we can observe that the amplitude of response should be inversely proportional to this new $m^*\zeta_w$. However this time the combined mass-damping parameter is not constant but incorporates a variation with flow speed. Because f_w increases with Re, ζ_w decreases with flow speed and, thinking about an equivalent damping term, we reach the same conclusion that the response should in fact increase with Re.

7.4 Wake stiffness for other separations

Now that we have analysed the WIV response for a pair of cylinders at $x_0/D = 4.0$ we shall bring the wake stiffness concept back to our starting point and investigate the effect it has on other separations. We already know that moving the second cylinder farther downstream does not affect the wake formed in the gap, i.e. the upstream vortex shedding process is not affected if the separation changes from $x_0/D = 4.0$ up to 20.0, the last case investigated in the present work.

The development of a von Kármán wake from a static cylinder has been diligently studied in the literature. Schaefer & Eskinazi (1958) performed experiments in a wind tunnel in order to model the effect of fluid viscosity in diffusing a vortex from the instant it is shed from the cylinder. The core of concentrated circulation expands with time as vortices travel downstream towards the second body, so if the cylinder is farther away we expect weaker vortices (at least with less concentrated circulation) to reach that specific position of the wake. Weaker vortices induce weaker fluid forces, therefore we would expect both wake-stiffness and vortex-impulse terms to decrease with increasing x_0.

Looking back at the steady lift map presented in Fig. 6.1 (page 106) we see that the maximum $\overline{C}_y$ is indeed decreasing for larger separations, consequently $|\partial \overline{C}_y|$ is also reduced with increases in x_0. To a certain extent it is straightforward to think that the wake stiffness effect is inversely proportional to x_0 and results in lower values of $f_w D/U$ for larger separations. As a consequence, the frequency of oscillation should also be reduced. However, Eq. 7.3 tells us that the amplitude must increase if fD/U is reduced and all other terms are kept constant. This is clearly not observed in the response with springs presented in Fig. 5.5 (page 92). Instead $\hat{y}$ for the WIV regime is seen to be reduced with increasing x_0, up to a separation where no effect from the upstream wake can be sensed by the downstream cylinder and it returns to a simple VIV regime. Therefore, some other non-dimensional terms in Eq. 7.3 must be dominating over the effect of fD/U to reduced the response as x_0 is increased.

Fig. 7.8 presents the effect of x_0 on the response of a cylinder mounted without
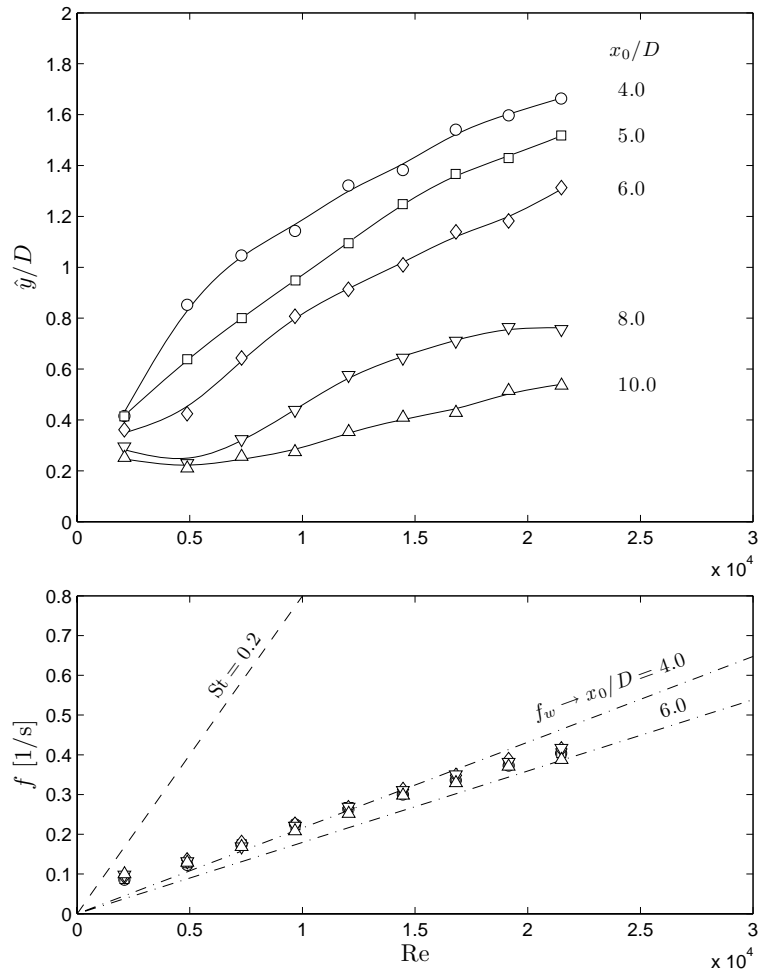
Fig. 7.8: WIV response of a downstream cylinder mounted without springs at various x_0 separations. Top: displacement; bottom: dominant frequency of oscillation.
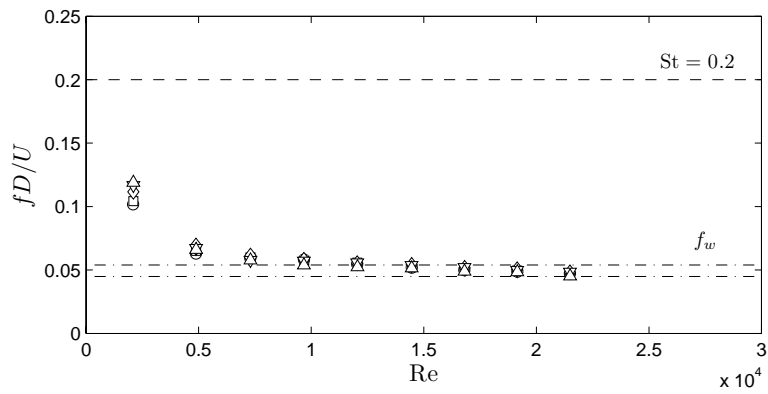

Fig. 7.9: Non-dimensionalised dominant frequency of oscillation of a downstream cylinder mounted without springs at various x_0 separations. Please refer to Fig. 7.8.

springs. In accordance to Eq. 7.3, the amplitude of displacement should increase with Reynolds number for a fixed separation, while $\hat{y}$ should be reduced for larger separations if Re is kept constant. Although this plot is not as densely populated with data points as Fig. 5.5 it can still reveal the overall behaviour of the response in relation to Re and x_0. The main difference now being that no VIV resonance peak is identified because the system lacks any f_0 conferred by springs, but still the WIV response seems to diminish as the second cylinder is moved farther downstream.

Remember that every point in Fig. 7.8 represents an infinite reduced velocity. Therefore variations observed in the curves are an effect of Re and x_0 only. Repeating the same process employed above, we can pick one data point from each x_0/D curve at Re $= 2.3 \times 10^4$ and plot them back in Fig. 5.5 (page 92) at $U/Df_0 = \infty$. Every point plotted there on the right-hand side axis represents the asymptotic value the response would reach if Re were kept constant beyond the vertical dashed line of 2.3×10^4. This agreement confirms that beyond the flow speed range in which VIV is important reduced velocity has no effect on the WIV response and the cylinder is expected to sustain a constant level of vibration for the rest of the Re range. It is also verified that the asymptotic value that limits $\hat{y}$ is indeed a function of Re and x_0 alone and must be related to the actual configuration of the wake at those conditions.

As we saw in Fig. 7.2 for $x_0/D = 4.0$ the frequency of oscillation shows a fairly linear behaviour with Re, which is represented by a constant line when plotted non-dimensionally as fD/U in Fig. 7.3. Interestingly, we know that as far as separation is concerned $|\partial \overline{C}_y|$ decreases with x_0. But when this effect is reflected into f_w it seems to cause only a small variation in the frequency of response, making all f curves for different x_0 collapse over each other. A similar result was observed in Fig. 5.5 for the response with springs, where, differently from the displacement, f does not show much variation with x_0.

Considering our smallest separation of $x_0/D = 4.0$ we saw that the steady lift field generates, to a first approximation, a wake stiffness effect proportional to $|\partial \overline{C}_y| = 0.65$ (Fig. 6.4). Again we can plot f_w (Eq. 7.6) associated with this steady field as a dot-dashed line in Fig. 7.8. However, moving the second cylinder farther
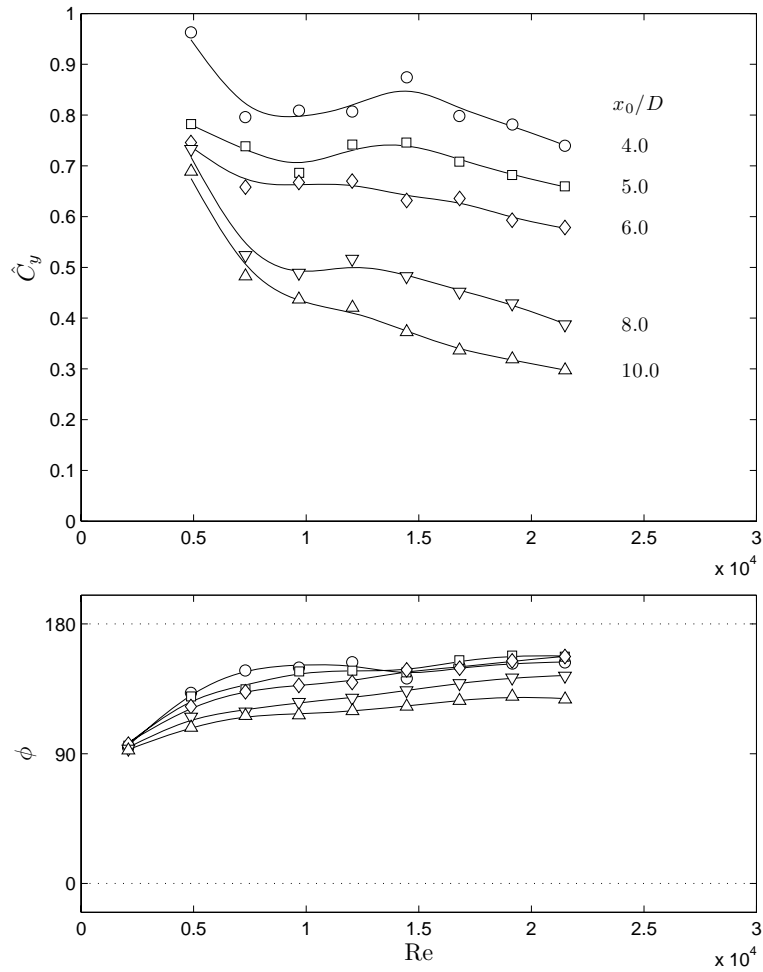
166

Fig. 7.10: Fluctuating lift coefficient (top) and phase angle (bottom) for WIV responses without springs at various x_0 separations.

downstream in the wake we saw that $|\partial\overline{C}_y|$ is reduced. Considering the maximum separation measured in the $\overline{C}_y$ map of Fig. 6.1 (page 106) we can estimate a wake stiffness effect proportional to $|\partial\overline{C}_y| = 0.45$ for $x_0/D = 6.0$. If we then plot f_w associated with this weaker wake stiffness in Fig. 7.8 we are able to verify that the expected variation for f between both separations is actually rather small. This is made even clearer when the data is plotted in the non-dimensional form of fD/U in Fig. 7.9

Turning back to our analysis of Eq. 7.3 versus separation, we conclude that the variation of fD/U versus x_0 may be rather small and unlikely to dominate over other non-dimensional groups. Leaving us with $\hat{C}_y \sin\phi$ that might present some significant variation with x_0.

As suggested above, the diffusion of vortices in the wake may be responsible for the reduction of the wake stiffness effect observed in Fig. 6.1. But since we argue that both wake-stiffness and vortex-impulse terms originate in the same phenomenon, we believe that vortex diffusion may also be responsible for changes in $\hat{C}_y \sin\phi$ versus x_0.

Fig. 7.10 presents the variation of $\hat{C}_y$ and ϕ with both Re and x_0. We have shown in Fig. 7.6 that $\hat{C}_y$ has a small dependency on Re, resulting in a mild decreasing slope for $x_0/D = 4.0$. However, as separation is increased in Fig. 7.10 we observe that not only the overall level of $\hat{C}_y$ is reduced, but also the negative slope with Re is accentuated. On the other hand, the bottom graph shows that although ϕ is roughly constant with Re it is also reduced for larger x_0. Now, depending on the combination of both terms $\hat{C}_y \sin\phi$ can show significant variation with x_0, as much as to dominate over fD/U and govern the behaviour of the response versus separation.

7.5 Conclusion

In Chapter 6 we have concluded that the WIV excitation mechanism has its origin in the unsteady vortex-structure interaction encountered by the cylinder as it oscillates across the wake. It was possible to verify that a phase lag between y

and C_y could drive and sustain the mechanism, but we were not able to understand how that excitation could result in the displacement and frequency signature that characterised the WIV response.

In the present chapter we have introduced the concept of *wake stiffness*, a fluid dynamic effect that can be associate, in a first approximation, with a linear spring with stiffness proportional to $|\partial \overline{C}_y|$ and Re. By a series of experiments with a cylinder mounted without springs we verified that such wake stiffness was not only strong enough to sustain oscillatory motion, but could also dominate over the structural stiffness of the system.

The main findings of this chapter are summarised in the section that follows.

7.5.1 Characteristics of the WIV response

Response without springs

A cylinder mounted without springs is able to develop oscillatory motion and the response showed a strong dependency on Reynolds number.

- The restoration force provided by wake stiffness is strong enough to balance the flow excitation and produce oscillatory motion. The cylinder was not observed to drift away from the centreline, but presented WIV throughout the Re range of the experiments.

- The analytical modelling for a system without springs revealed that the amplitude of response should increase with Reynolds number. This was verified by experimental data. However, a simple model that did not account for nonlinear effects in the fluid force was not able to predict the correct level of amplitude.

- We found that the WIV response should converge to an asymptotic value that depends only on Re. As $\hat{y}/D$ is increased beyond a certain limit the cylinder starts to reach amplitudes out of the wake interference region. The wake stiffness effect cannot be represented by a linear spring anymore, but the

overall stiffness tends to be reduced. This effect was in agreement with cases with and without springs and also with various x_0 separations.

- A simple linear model was able to predict the frequency of response rather well. It was confirmed that the cylinder without springs does not respond following the vortex shedding frequency f_s. Instead the response matches the frequency branch f_w associated with wake stiffness, which was well predicted by the model. A cylinder with springs responds with a frequency that combines some effect from f_w and f_0, yet different from both.

WIV regimes for a cylinder with springs

In our experiments we observed a gradual transition from an initial VIV regime to a dominating WIV regime as flow speed was increased. The boundaries between them were found to be related to two resonances: $f_s = f_0$ and $f_w = f_0$.

- The first regime has a clear VIV character, with a local peak of displacement occurring at $f_s = f_0$. The wake stiffness is still smaller than the spring stiffness, making U/Df_0 a significant parameter. The amplitude of the VIV peak is in agreement with the response curve for a single cylinder and does not depend on Re.

- The second regime is characterised by an established WIV response that suffers no influence of VIV. Beyond $f_w = f_0$ the wake stiffness effect is dominant over the spring stiffness and reduced velocity becomes irrelevant. The amplitude of response is governed by Re and tends towards an asymptotic value estimated by experiments at $U/Df_0 = \infty$.

- During the transition between both regimes we find an intermediate condition in which VIV is losing strength and WIV is taking control. Between the resonances $f_s = f_0$ and $f_w = f_0$ the response takes off from the VIV peak until it reaches a characteristic value at $f_w = f_0$ that is dependent on Re. During the transition, reduced velocity gradually loses its influence until the WIV response is only dominated by Re as it enters the second regime.

- The total stiffness of the system is not only caused by either the wake stiffness (k_w) or the spring stiffness (k) alone, but it is a combinations of both. k is very relevant in the first regime, but k_w becomes dominant in the second. Nevertheless, both k and k_w contribute in parts to the characteristic displacement and frequency responses.

Effect of centre-to-centre separation

As expected, the x_0 separation between both cylinders was confirmed to have a significant effect over the response. We suggest this effect is related to an increase in vortex diffusion and flow three-dimensionality as the gap is enlarged.

- The WIV response changed as the second cylinder was moved farther downstream. The first VIV regime suffered no influence of x_0 and the local resonance peak kept the same level of displacement for all separations between 4.0 and 20.0. On the other hand, the second WIV regime showed a strong influence of the separation. The characteristic WIV branch of response gradually disappeared with increasing x_0 until the response resembled only that of a typical VIV phenomenon.

- In contrast with the displacement, the frequency of oscillation showed only a small variation with x_0, with curves for all separations collapsing over the value predicted by the wake stiffness effect, especially for the case without springs.

- Such a strong x_0 dependency was associated with the fact that vortices from the upstream cylinder have more time to diffuse as they travel to reach a cylinder located farther downstream. Together with that is the fact that increase three-dimensionality of the flow also weakens the coherent wake. Weaker vortices induced weaker forces. Both the wake-stiffness effect (proportional to $|\partial \overline{C}_y|$) and the vortex-impulse term (related to $\hat{C}_y \sin \phi$) are affected.

7.5.2 Concluding remarks

The experiment without springs was crucial in the understanding of the phenomenon. It not only revealed the existence of a dominant wake stiffness effect that can sustain vibrations even if springs are removed, but also helped to explain different regimes of the response when springs are present. We proved that $\overline{C}_y$ towards the centreline not only provides some restoration for a quasi-static system but is in fact responsible for the characteristic WIV response of a cylinder that is free to vibrate.

The wake stiffness concept does not explain the excitation mechanism but it predicts rather well the characteristic signature of the WIV response both in terms of displacement and frequency. We can say that while unsteady vortex-structure interactions provide the energy input to sustain the vibrations, it is the wake stiffness phenomenon that defines the character of the WIV response.

Need for an improved, nonlinear model

By modelling a linear oscillator without springs but incorporating the stiffness as a consequence of the fluid force (wake stiffness) we were able to predict the frequency behaviour rather well. But no matter how good this approach was in regards to the frequency response, the displacement response is somewhat more complex and is not fully captured by this first approximation. We believe this is due to the simplicity in modelling the term $\hat{C}_y \sin \phi$. Although in some analysis we have considered $\hat{C}_y$ and ϕ to be independently related to the wake-stiffness and vortex-impulse terms, we are fully aware that this decomposition is not ideal and must overlook significant secondary effects.

A simple harmonic model as the one we have employed cannot account for nonlinear effects that might be important to the system. It will not be able, for example, to predict the asymptotic effect that is limiting the displacement. The complex interaction between body and wake causes $|\partial \overline{C}_y|$ and $\hat{C}_y \sin \phi$ to be coupled in such a way that we cannot simply analyse them independently. Since we believe both wake-stiffness and vortex-impulse terms originate in the same fluid

mechanic phenomenon, we are not able to uncouple and isolate their effects into linear concepts.

We argue that an improved, nonlinear model is necessary to account for more complex fluid-dynamic phenomena that we have identified to exist but were not considered in our model.

WIV and classical galloping

In previous chapters we have discussed the idea that WIV could be understood by the classical galloping theory. Remember that WIV had been referred to as a type of galloping mostly because the typical response presents a build up of amplitude for higher reduced velocities. But now we know that the response is increasing due to the wake stiffness effect as a function of Reynolds number. We have been arguing that quasi-steady assumptions commonly employed by the classical galloping theory would not fit the WIV phenomenon nor help the understanding of the real flow-structure mechanism. For that reason we have been insisting on a dissociation of WIV from the classical galloping idea.

In the present chapter we have shown that WIV is indeed a wake-dependent type of FIV. Remember that according to the classical galloping theory the oscillations of the body were dependent on the structural stiffness of the system to provide the restoration force. Even more for the wake-flutter phenomenon of interfering cylinder (Chapter 3, page 61), where structural stiffness in 2-dof is required. In our case, however, we showed that a body without any structural stiffness can be excited into FIV. If some stiffness is provided by the flow, the body is able to be excited and sustained into oscillatory motion.

The concept of wake stiffness is a powerful one but it is also requires the existence of an unsteady vortex wake present in the gap. The importance of the unsteady wake is central. Therefore we continue to propose that WIV is not to be understood as a type of classical galloping, but must be interpreted as wake-excited and wake-sustained FIV mechanism.

Chapter 8

Suppression of VIV and WIV with drag reduction

The suppression of vibrations induced by the flow became a real concern for the offshore industry when oil exploration moved towards the so called ultra-deep waters. Nowadays, a single floating platform is able to accommodate more than 40 production risers in complex arrangements together with many other cylindrical structures. As the ocean current changes its direction through the sea depth it becomes practically impossible to prevent flexible structures from falling in the wake of each other. As a result, the high probability of pipes developing WIV increases the risk of damage due to structural fatigue as well as the possibility of clashing between them.

Several suppression solutions have evolved with the offshore industry, some inspired by fundamental aspects of FIV phenomena, some as a consequence of empirical tests. But one lesson was learned: the more we understand the physical flow mechanism the better we can improve our suppression solutions. Now that we know the WIV mechanism combines the vortex shedding of the second body with unsteady interference coming from the upstream wake we have a good possibility to find a solution for this practical engineering problem. The present investigation will start with VIV suppression for a single cylinder and then move on towards WIV suppression of two interfering cylinders. All the time we should keep in mind that

a practical solution that is viable in the field should not increase the drag of the structure. Ideally we want to reduce drag.

This chapter was not intended to be the main focus of the present work, but the development of effective WIV suppressors came naturally as a consequence of the results presented in previous chapters. Therefore this study is just a first attempt to open new possibilities for suppressors. None of them have been optimised or tested outside of laboratory conditions and, although results are rather promising, any real application would require a new round of experiments to optimise and detail the behaviour of the devices.

8.1 Brief review on FIV suppression

It is not difficult to imagine that the idealised solution for suppressing VIV would be to streamline the body and avoid flow separation altogether. Consequently the structure would not be a bluff body anymore. But this is not possible in most of the practical applications due to structural and functional constraints. In the offshore industry, for example, a streamlined riser would be extremely difficult and expensive to produce, store, transport and operate.

Elastic bluff bodies will always be present in engineering design. Therefore we are left looking for other solutions to suppress FIV of bluff bodies. Blevins (1990) suggests three alternatives:

- *Increase $m^*\zeta$.* As we have seen in Chapter 2, if the structural mass and damping of the structure can be increased the response would be reduced. This result could be achieved by increasing viscous friction in the system, employing materials with high internal damping (such as rubber), or installing external dampers. Some of these solutions may not represent a viable option depending on the application. It is easier to achieve high values of $m^*\zeta$ in air rather than in water. Production risers, for example, are already built using complex polymers with high internal damping properties, but still m^* is very low, making $m^*\zeta$ fall in a critical range.

- *Avoid resonance.* If f_0 could be set distant from f_s we would be able to avoid the effect of VIV synchronisation. Blevins (1990) suggests that the reduced velocity would have to be kept below 1.0 for this effect to be achieved. In our results we have seen that severe WIV occurs independently of reduced velocity. Hence this might be a solution for VIV, but probably not for WIV.

- *Add a suppression device.* When the structure cannot be modified according to the suggestions above we are left with the option of installing add-on devices to try to suppress the vibrations. A series of possible solutions for VIV of a single cylinder has been studied by this and other works and will be described later. But the fact that a solution works for suppressing VIV does not mean that it will also work to suppress WIV.

Although add-on VIV suppressors can have a secondary effect of changing the structural damping and natural frequency of the system, they are primarily designed to disrupt or prevent the formation of an organised, two-dimensional vortex wake. That is to say that rather than just correcting structural properties, suppressors aim to act on the fluid-mechanics of the problem, in the origin of the fluid forces.

We know that WIV involves a distinct excitation mechanism. Therefore in the present work we aim to make use of the insight about the WIV mechanism discussed in previous chapters and apply it to the development of an effective suppressor.

8.1.1   VIV suppression of a single cylinder

Basically, the suppression of VIV starts with the disruption of vortex shedding from the body. Zdravkovich (1981) wrote a very comprehensive review of various aerodynamic and hydrodynamic means for suppressing vortex shedding from a static cylinder. Solutions were classified into three categories according to the way they affect the shedding mechanism: (i) Surface protrusions affect separation lines or separated shear layers. They involve helical strakes, fins, surface bumps, among others. (ii) Shrouds affect the entrainment layers around the body. Perforated shrouds and axial slats are two examples. (iii) Near-wake stabilisers affect the later
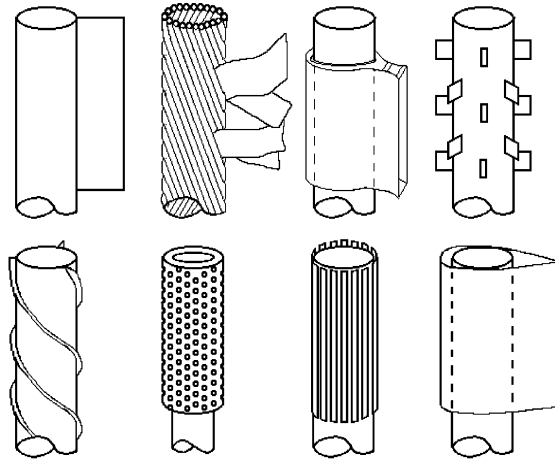
Fig. 8.1: Add-on devices for VIV suppression of cylinders. Top row: splitter plate, ribbons, guiding vane, spoiler plates. Bottom row: helical strakes, perforated shroud, axial slats, streamlined fairing. Reproduced from Blevins (1990).

interaction between shear layers. Splitter plates, guiding vanes and base-bleed are common examples.

A few of the suppressors mentioned above are illustrated in Fig. 8.1. Some may be very effective in inhibiting vortex shedding from a static cylinder, or even reducing the fluctuating forces acting on a structure that vibrates a little. But if high-amplitude vibrations appear the displacement of the cylinder will interfere with the vortex shedding phenomenon (as we have seen to occur during the VIV synchronisation range) and the device might lose its effectiveness completely.

A widely used method for suppressing VIV of long slender bodies of circular cross section is the attachment of helical strakes. Developed originally in the wind engineering field, strakes suffer from two major problems: the first being that they increase drag and the second that, for a given strake height, their effectiveness reduces with decreases in $m^*\zeta$. Whereas a strake height of 10% of cylinder diameter is usually sufficient to suppress VIV in air at least double this amount is often required in water, and this increase in height is accompanied by a corresponding further increase in drag.

For a fixed cylinder it is known that if regular vortex shedding is eliminated, say by the use of a long splitter plate, then drag is reduced. Hence in theory an effective VIV suppression device should be able to reduce drag rather than increase it. This

idea underlies part of the thinking in the present investigation.

A simple harmonic analysis for a linear oscillator model of VIV — developed by Bearman (1984) and presented in Chapter 2 — shows that response is inversely proportional to $m^*\zeta$. Hence the most rigorous way to test the effectiveness of a VIV suppression device is to work at low mass and damping. In the experiments to be described in this work the parameter $m^*\zeta$ was equal to or less than 0.02. Owen *et al.* (2001) described a method for low drag VIV suppression that had shown itself to be effective down to values of $m^*\zeta$ of about 0.5. This is the attachment of large scale bumps to induce three-dimensional separation and eliminate vortex shedding. However, later experiments at lower values of $m^*\zeta$ have shown a return of VIV with amplitudes similar to those of a plain cylinder.

This behaviour has been observed by the present author with even grosser forms of continuous surface three-dimensionalities. The regular vortex shedding has been eliminated from the body when it is fixed but it returns when the cylinder is free to respond under conditions of low mass and damping. From this experience it is concluded that sharp-edged separation from strakes, with its accompanying high drag, is required to maintain three-dimensional separation and suppress VIV. Hence at values of $m^*\zeta$ typical for risers (less than 0.1) it seems that three-dimensional solutions are unlikely to provide the required combination of VIV suppression and low drag.

There are a number of two-dimensional control devices to weaken vortex shedding and reduce drag, with the most well known being the splitter plate. In this chapter we describe the results of experiments to suppress VIV and reduce drag using various configurations of two-dimensional control devices inspired by the splitter plate.

8.1.2 WIV suppression of pair of cylinders

Very few works investigated FIV suppression for bluff bodies with interference. Zdravkovich (1974), which is probably the closest work related to this chapter, only presents a wind tunnel investigation of WIV suppression employing an axial-rod shroud. Despite his level of $m^*\zeta$ being rather high, the shrouds showed to have

some effect in reducing WIV of the second cylinder (the format the data is presented in his paper makes it very difficult to have any quantitative evaluation).

It is interesting to note that the most effective suppression was achieved when both cylinders were fitted with shrouds, and not only the downstream one that was being monitored. This is evidence that our understanding of the excitation mechanism is correct. It is important to disrupt the coherent vortices coming from the upstream cylinder to reduce the interaction with the downstream body. This is exactly what the shrouds are doing.

But it was in another paper that Zdravkovich (1988) brought further insight about VIV suppressors being used in WIV. He wrote: "A wide variety of means for suppressing the vortex-shedding-induced oscillations [VIV] has been developed in the past. These means might not only be ineffective for the interference-induced oscillations [WIV] but even detrimental." To cite an example, Korkischko *et al.* (2007) showed that helical strakes typically effective in reducing VIV on an isolated cylinder are no longer successful if the body is immersed in the wake interference region.

We believe that only with a clear phenomenological understanding of the nature of the excitation will it be possible to start the development of suppressors that effectively reduce WIV. Building up understanding from previous chapters we set out to explore new solutions that not only are successful in suppressing VIV but also act on the vortex-structure interaction that drives WIV.

8.2 Experimental set-up

Experiments with suppressors were performed using the same facilities and models described in Chapter 4. We first started by testing devices in 1-dof, but soon we realised that, due to the nature of the suppression mechanism, experiments in 2-dof would also be necessary to evaluate the dynamic stability of our suppressors. This will become clear during the discussion of the results.

A family of suppression devices was created based on the elementary idea of a splitter plate. Fig. 8.2 present solutions that evolved from a single splitter plate

Single splitter plate

Double splitter plates

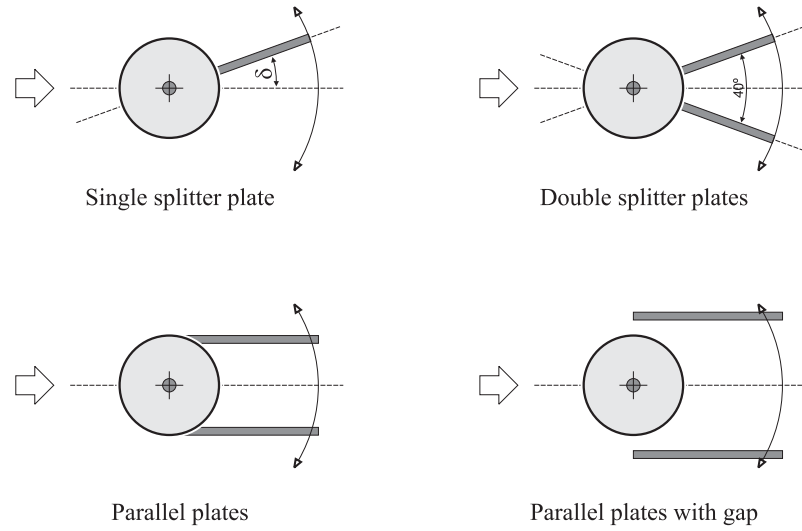Parallel plates

Parallel plates with gap

Fig. 8.2: Sketch of proposed control plates free to rotate about the centre of a circular cylinder: single splitter plate (length varying from $0.25D$ to $2D$), double splitter plates, parallel plates (after Grimminger, 1945), parallel plates with $0.1D$ gap.

to a pair of parallel plates. At first devices were rigidly attached to the cylinder in a way that they could not rotate in relation to the body. However, in practical offshore applications the direction of the current is constantly varying; hence omni-directional devices are required. Therefore we prepared free-to-rotate (f-t-r) devices mounted on bearings at each end of the cylinder and able to pivot around the axis of the body. A small gap was left between the device and the surface of the cylinder to guarantee that no friction would interfere with the system in adjusting itself to the approaching flow.

Table 8.1 presents the structural parameters for all the arrangements of cylinder and suppression device tested. A more detailed description of each device presented in Fig. 8.2 will be given later.

The only flow variable changed during the course of the experiments was the flow velocity U, which, as for full-scale risers, alters both the reduced velocity and the Reynolds number. For each rig, measurements were made using a fixed set of springs and the reduced velocity range covered was from 1.5 to 23 for 1-dof and 1.5 to 13 for 2-dof experiments, where U/Df_{0_y} is defined using the cylinder natural frequency of oscillation in the transverse direction measured in air.

Displacements $\hat{x}$ and $\hat{y}$ were found by measuring the root mean square value of response in each direction and multiplying by $\sqrt{2}$, as explained in Chapter 5.

Table 8.1: Structural properties for suppressors mounted in 1-dof and 2-dof. Symbols as in Fig. 8.3.

	Model	1-dof rig		2-dof rig		
		m^*	$m^*\zeta$	m^*	$m^*\zeta$	f_{0_x}/f_{0_y}
			(10^{-2})		(10^{-2})	
●	Plain cylinder	2.6	1.82	1.6	0.48	1.93
◇	Single splitter plate	2.7	1.89	1.7	0.51	1.89
○	Double splitter plates	2.8	1.96	1.8	0.54	1.88
△	Parallel plates	2.8	1.96	1.8	0.54	1.86
▷	Parallel plates with gap	2.9	2.00	1.9	0.56	1.88

Measurements for the 2-dof pendulum rig represent displacements taken for a location at the mid-length of the model. In addition to response and force measurements, flow visualisation was carried out using laser-illuminated fluorescent dye and hydrogen bubbles. Instantaneous velocity and vorticity fields were obtained with a digital PIV system.

8.3 Results: VIV suppression in 1-dof

Results for the VIV response of a single cylinder in 1-dof have already been discussed in Chapter 5. A preliminary experiment to obtain the VIV response of a cylinder in 2-dof was also performed and will serve as reference for all 2-dof cases. Fig. 8.3 repeats the typical VIV response of a plain cylinder compared with the response measured for the proposed suppressors.

In the present chapter we are interested in evaluating the efficiency of devices not only in suppressing VIV but also in reducing drag. Consequently we will also compare $\overline{C}_x$ for different suppression configurations with mean drag measured for a static cylinder.
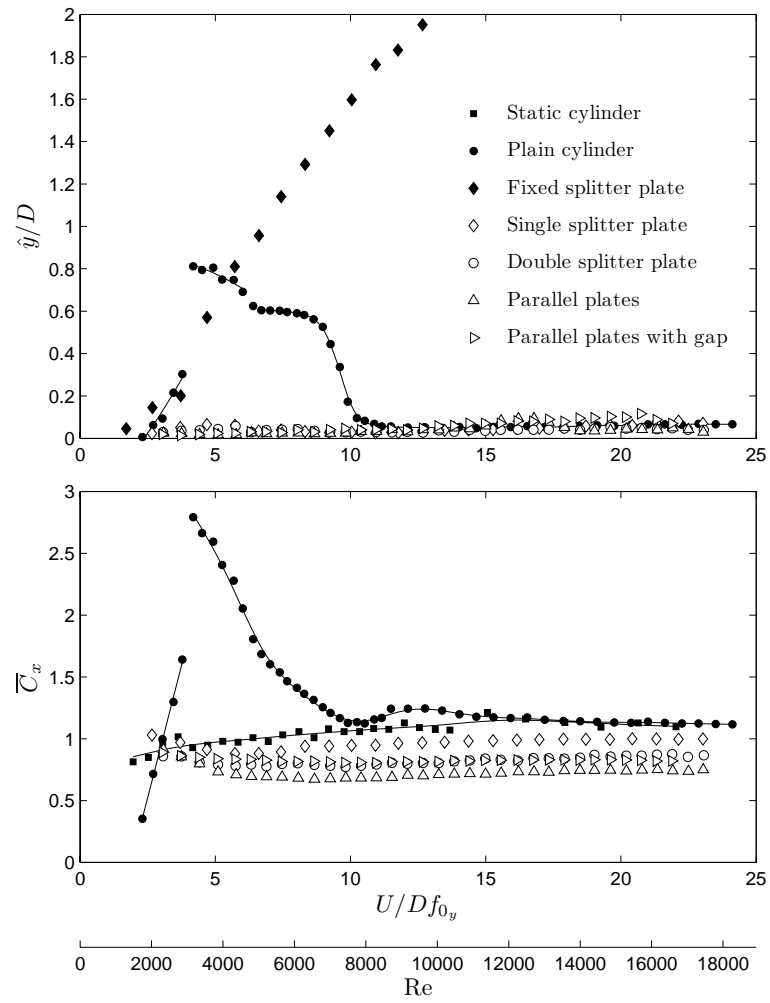
Fig. 8.3: VIV response in 1-dof (top) and mean drag coefficient (bottom) for various suppressors compared with a plain cylinder.

8.3.1 Fixed splitter plate

Splitter plates could be rigidly attached to the rear of the cylinder and tests were carried out with plates of length between $L_{SP}/D = 0.25$ and 2.0. The result in all cases was a very vigorous transverse galloping oscillation that, with increasing reduced velocity, would apparently increase without limit. Fig. 8.3 presents the response for a splitter plate with $L_{SP}/D = 1.0$. In this first experiment the maximum amplitude of transverse oscillation was limited to $2D$ and this was reached at a reduced velocity of about 13. A similar galloping response was also observed for a 2-dof experiment, but this result is not presented here for brevity.

Flow visualisation and PIV measurements were carried out to investigate the interaction between the wake and the fixed splitter plate. Fig. 8.4(a) presents the instantaneous velocity and vorticity fields for $U/Df_{0_y} = 6.0$. The data was acquired when the cylinder is crossing the centreline from left to right, therefore presenting maximum transverse velocity $\dot{y}$. The vorticity contours show that the shear layer separated from the right-hand side of the cylinder apparently reattaches at the tip of the fixed splitter plate. This interaction with the tip and the proximity of the shear layer running along the splitter plate causes a region of lower pressure on the right-hand side of the plate and cylinder.

A transverse force develops in the same direction as the cylinder motion, energy is extracted from the free stream and galloping oscillations are sustained in essentially the same way as for classical galloping of square section cylinders. We also note from Fig. 8.4(a) that the shear layers are free to interact after the splitter plate forming vortices farther downstream. The behaviour described above is illustrated in Fig. 8.5(a) where the resultant velocity approaching the cylinder is the vectorial addition of the free stream velocity U and the cylinder's transverse velocity $\dot{y}$.

8.3.2 Free-to-rotate splitter plate

Since a device to be used in the ocean must have omni-directional effectiveness the next stage was allow the splitter plate to pivot about the centre of the cylinder.

Following the disappointing results with a fixed plate, it was hoped that a
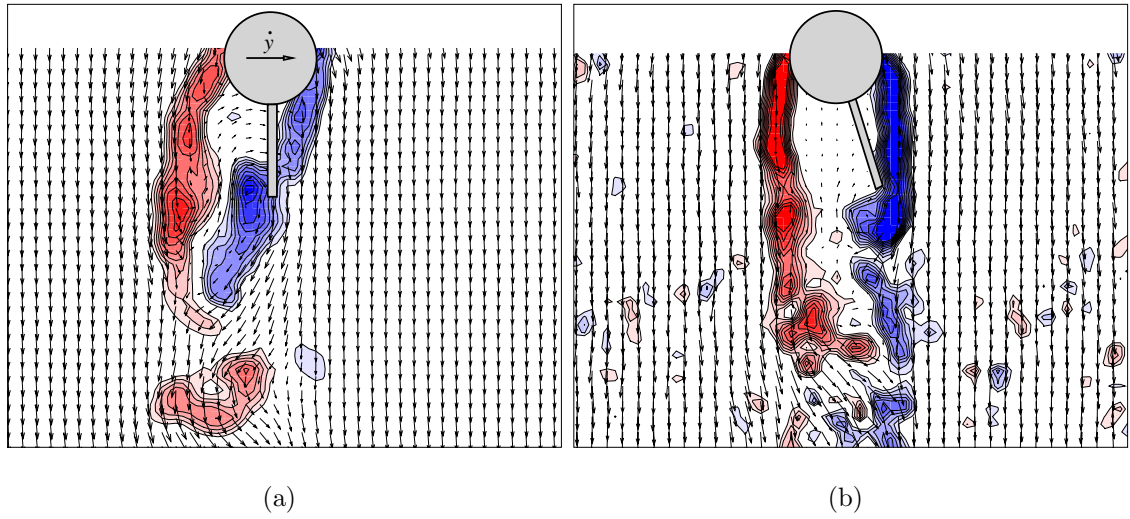
Fig. 8.4: Instantaneous velocity vectors and vorticity contours for fixed and f-t-r splitter plates at $U/Df_{0_y} = 6.0$. (a) Fixed splitter plate under galloping oscillations. (b) Free-to-rotate splitter plate suppressing vibrations.
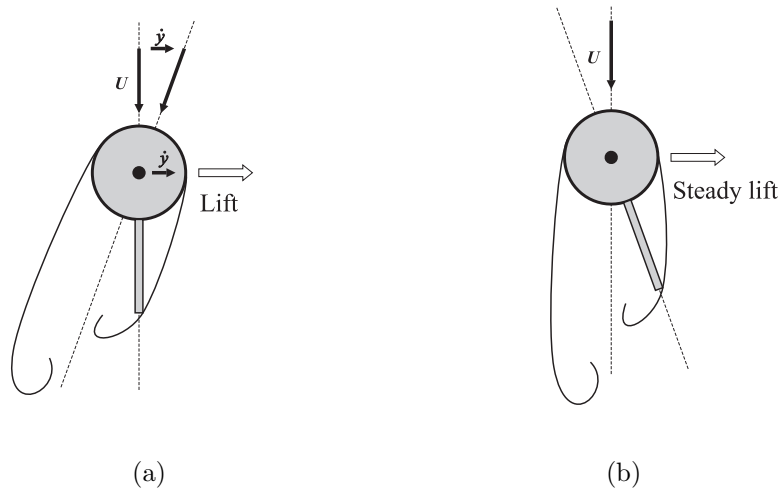

Fig. 8.5: Diagram showing offset position of plate and direction of steady lift force. (a) Fixed splitter plate under galloping oscillations. (b) Free-to-rotate splitter plate suppressing vibrations ($\dot{y} = 0$).
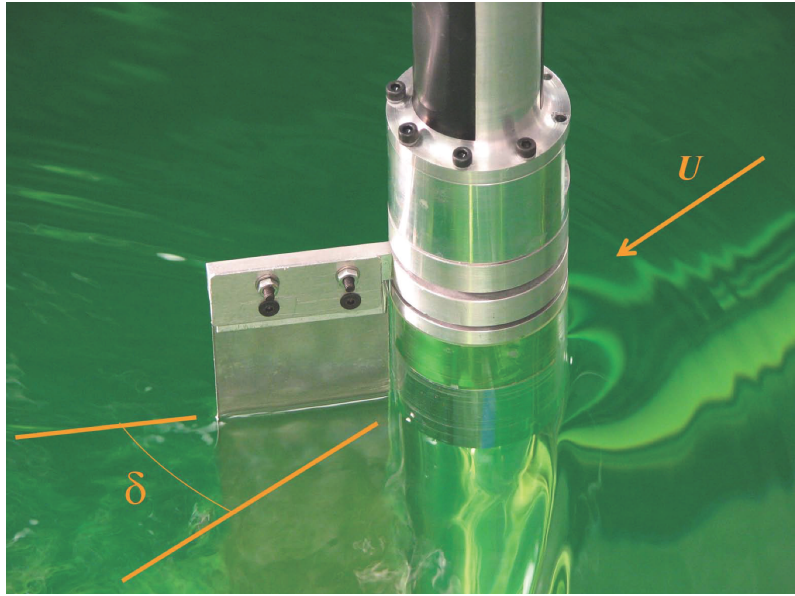
Fig. 8.6: Photograph of the single splitter plate suppressing VIV at $U/Df_0 = 6.0$.

plate free to rotate might provide sufficient hydrodynamic damping to suppress the galloping. However, when a f-t-r splitter plate was used there were found to be two stable positions for the plate at roughly $\delta = \pm 20°$ to the free stream direction and the plate rapidly adopted one or other of these positions when it was released. Fig. 8.6 illustrates this behaviour.

Cimbala & Garg (1991) also observed this bi-stable behaviour for a f-t-r cylinder fitted with a splitter plate. In their experiments the cylinder and the splitter plate were manufactured into one solid body allowed to rotate around the axis of the cylinder. However, the pivoting axis of their system was rigidly mounted on a wind tunnel section not allowing any flow-induced vibration.

Our measurements of transverse response and mean drag coefficients for the $1D$ f-t-r splitter plate are plotted in Fig. 8.3. Results for a plain cylinder, fixed and free, are shown for comparison. A f-t-r splitter plate not only suppressed VIV below $\hat{y}/D = 0.1$ throughout the range of reduced velocity investigated, but also reduced drag below that of a static cylinder.

PIV measurements presented in Fig. 8.4(b) show that on the side to which the plate deflected the separating shear layer from the cylinder appeared to attach to the tip of the plate and this had the effect of stabilising the near wake flow. Vortex

shedding was visible downstream but this did not feed back to cause vibrations.

An unwanted effect was that a steady transverse lift force developed on the cylinder. The splitter plate was free to rotate so the force, caused by differing flow on the two sides of the combination of cylinder and splitter plate, must be acting primarily on the cylinder rather than the plate. As shown in Fig. 8.5(b), the direction of the force was opposite to that which occurs on an aerofoil with a deflected flap, and caused the cylinder to adopt a steady offset position to the side to which the splitter plate deflected. It was this force which was responsible for the strong galloping response with the fixed splitter plate explained earlier. As a cylinder with a fixed splitter plate aligned with the free stream plunges with $\dot{y}$ as in Fig. 8.5(a), say, the instantaneous flow direction is approximately the same as that shown in Fig. 8.5(b).

Results presented so far have been for a f-t-r plate having a length equal to the cylinder diameter. Further tests were carried out with a series of f-t-r splitter plates with various L_{SP} in order to assess the effect of plate length on VIV suppression effectiveness. The results showed that f-t-r splitter plates with lengths between $L_{SP}/D = 0.5$ and 1.5 are all effective in suppressing VIV. Also they all had drag coefficients below the value for a plain fixed circular cylinder. When f-t-r plates outside this range were attached to the cylinder a transverse flow-induced vibration returned. Cimbala & Garg (1991) found stable positions outside this range but this may have been because their system was not allowed to respond to flow-induced excitation. A secondary effect might have been the level of friction in their ball bearings (as will be discussed later in this chapter).

The plates that successfully suppressed VIV adopted slightly different offset angles (δ, defined in Fig. 8.2), depending on plate length. These steady angles are shown plotted in Fig. 8.7 along with results from Cimbala & Garg (1991). It can be seen that the longer the splitter plate the smaller the angle. The dashed line in the figure, given by

$$\delta = \arcsin \frac{D/2}{L_{SP} + D/2},$$ (8.1)

is the angle the plate would adopt if it is assumed that the tip of the plate just intercepts a line leaving the shoulder of the cylinder and trailing back in the flow
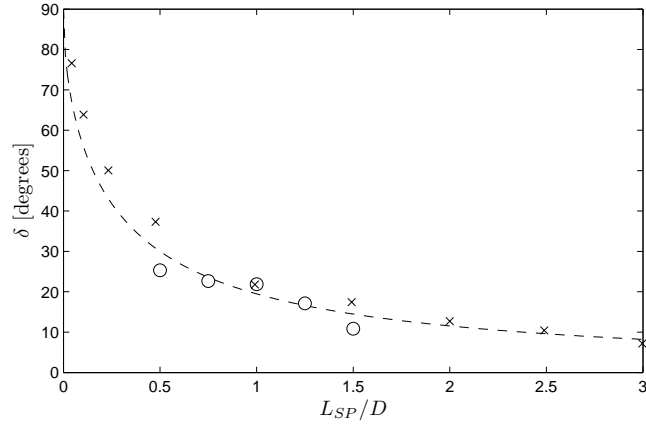
Fig. 8.7: Effect of splitter plate length on its stable offset angle. Key: ○, present work, Re $= 2 \times 10^3 - 1.8 \times 10^4$; ×, Cimbala & Garg (1991), Re $= 5 \times 10^3 - 2 \times 10^4$.
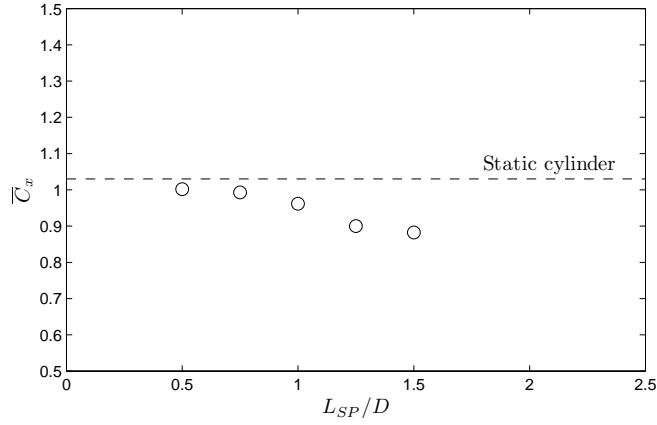
Fig. 8.8: Effect of splitter plate length on mean drag coefficient. $\overline{C}_x$ is averaged for Re $= 2 \times 10^3 - 1.8 \times 10^4$.

direction. The data generally supports the observation that the shear layer from the side of the cylinder to which the splitter plate deflects just reattaches at its tip.

As Fig. 8.8 shows, the length of the plate also has some effect on the mean drag coefficient. Each data point represents an average $\overline{C}_x$ for the whole Re range of the experiments. This result suggests that a successful VIV suppression and drag reduction device using a f-t-r splitter plate can be shorter than one cylinder diameter, but must fall within a defined length range for it to be effective.

8.3.3 Double splitter plates

In order to try to eliminate the steady transverse force found for a f-t-r splitter plate, a pair of plates was introduced. The plates were $1D$ long and set at $\pm20°$ to the free stream direction. The angle between the plates was fixed but the pair of plates was free to pivot about the centre of the cylinder. The configuration is shown as *double splitter plates* in Fig. 8.2.

As shown by the results plotted in Fig. 8.3, this configuration suppressed VIV and reduced drag below that of a plain cylinder. It also eliminated the steady side force found with the single plate. With this arrangement the shear layers from the cylinder stabilised and reattached to the tips of the plates. Downstream of the plates vortex shedding was observed but this did not generate an excitation sufficient to cause any serious VIV. Maximum amplitudes recorded were only around 5% of the cylinder diameter.

8.3.4 Parallel plates

Further variations on the concept of double plates, some inspired by the early work of Grimminger (1945) related to suppressing VIV of submarine periscopes, were also studied. Starting at the $\pm90°$ points, the plates trail back $1D$ from the back of the cylinder and are initially aligned to the flow. Both plates were mounted on ball bearings at the extremity of the cylinder and were always parallel to each other, freely rotating as one body around the centre of the cylinder. In one case there was a negligible gap between the plates and the cylinder (*parallel plates* in Fig. 8.2) and in a second case the gap was set at 10% of the cylinder diameter (*parallel plates with gap*).

In Grimminger's experiments the plates were fixed since the flow direction was known but in our work the plates were free to rotate. It was found that the plates with the very small gap give the better performance. As shown in the plots in Fig. 8.3 of amplitude and drag coefficient against reduced velocity, this configuration of plates provided excellent VIV suppression and the greatest reduction in drag below the plain cylinder value.

8.4   Results: VIV suppression in 2-dof

It has been shown here that various arrangements of two-dimensional control plates are effective in suppressing transverse VIV. However, is this achieved at the expense of larger in-line VIV amplitudes? To answer this question a set of experiments was conducted in the 2-dof rig. Experiments were repeated with various arrangements of plates and the measured $\hat{x}$, $\hat{y}$ and $\overline{C}_x$ are plotted against reduced velocity in Fig. 8.9.

Results for the plain cylinder are also shown and will serve as reference for all other 2-dof curves. Examples of the trajectories of motion are plotted in Fig. 8.11 and will be discussed later. The overall response was found to be in good agreement with results from Jauvtis & Williamson (2004) and Dahl *et al.* (2006).

After confirming that all the devices would successfully suppress VIV in 1-dof oscillations, we mounted the same models in the 2-dof rig. This produced further unexpected findings. Starting with the single splitter plate, we found out that the plate was not able to stabilise in the expected $\pm 20°$ position, but oscillated severely from one side to the other and the cylinder developed high amplitudes, both in-line and transverse. We observed that the splitter plate oscillated so much that it almost reached the $\pm 90°$ positions. This behaviour was also observed for all the other devices.

Figs. 8.9(a) and (c) present the transverse and in-line amplitudes versus reduced velocity and show that all devices led to considerable vibrations of the cylinder, in many cases greater than that for the plain cylinder. As one might expect, almost all drag coefficients presented in Fig. 8.9(e) were increased above the ones for a plain cylinder.

8.4.1   Effects of torsional resistance and rotational inertia

Apart from moving from 1-dof to 2-dof, the only other change in the apparatus was to replace the old bearings in the mounts for the suppression devices by new ones with lower friction. This prompted us to consider additional parameters that might be important in stabilising the devices.

Two additional parameters that may influence the effectiveness of the suppression
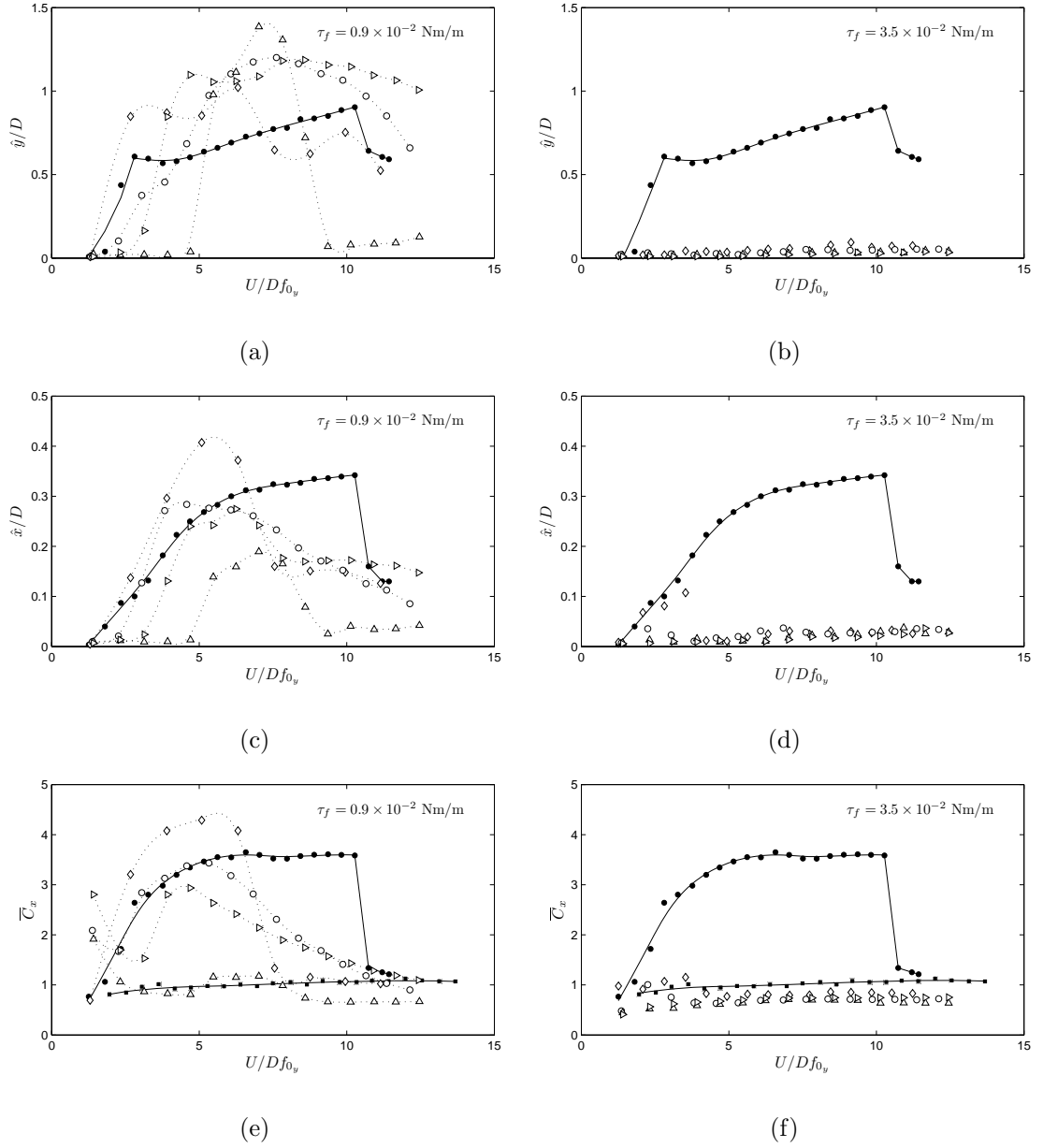
Fig. 8.9: Cross-flow displacement (top), streamwise displacement (middle) and drag coefficient (bottom) versus reduced velocity for devices with 2-dof. Torsional friction below critical value in (a), (c) and (e). Torsional friction above critical value in (b), (d) and (f). For key please refer to Fig. 8.3.
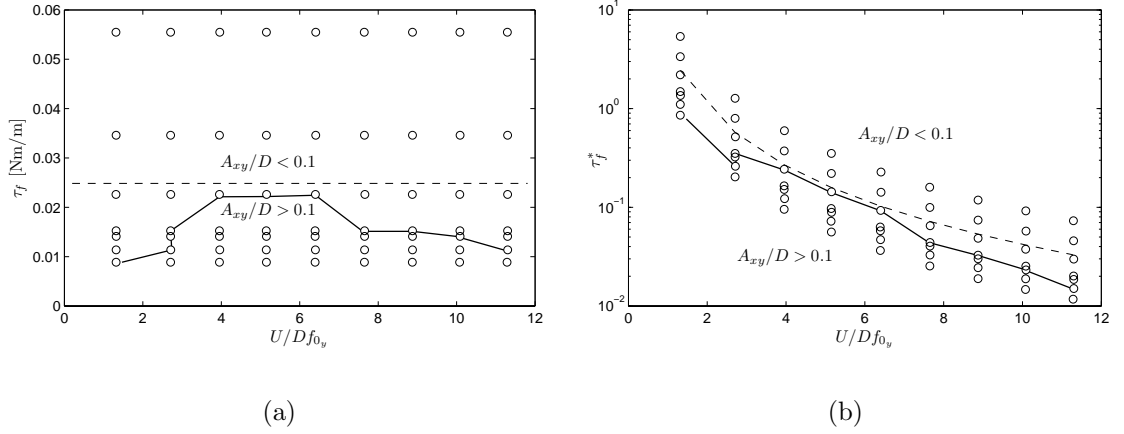
Fig. 8.10: VIV suppression map for a f-t-r splitter plate showing dependence on torsional friction. The solid line represents the contour where $A_{xy}/D = 0.1$. (a) Torsional friction versus reduced velocity. (b) Non-dimensionalised torsional friction parameter versus reduced velocity.

devices are: the rotational inertia of the plates and the torsional resistance resulting from friction in the bearings holding the plates. Experiments with mass added to the splitter plate to increase its rotational inertia produced no obvious change in behaviour. However, we noted that small increases in torsional friction were sufficient to suppress vibration. This finding prompted a study of the effect of torsional friction which we now knew would lead to severe oscillations if it was below some critical value and presumably would result in galloping oscillations if it was too large.

A simple modification was made to the apparatus in order to control the torsional resistance, which was varied in small increments between $\tau_f = 0.9 \times 10^{-2}$ and 5.5×10^{-2} Nm per unit length of the cylinder, with the lowest value being for just the natural friction of the bearings. With a value higher than $\tau_f = 5.5 \times 10^{-2}$Nm/m the splitter plate did not move over the range of reduced velocity tested and galloping returned.

A set of 56 runs varying the reduced velocity was completed for the single splitter plate model of length $1D$ in order to map the amplitude response for different values of τ_f. The displacement amplitude parameter

$$A_{xy} = \sqrt{\hat{x}^2 + \hat{y}^2} \qquad (8.2)$$

was determined for each run and maps of the cases studied are shown in Fig. 8.10(a).
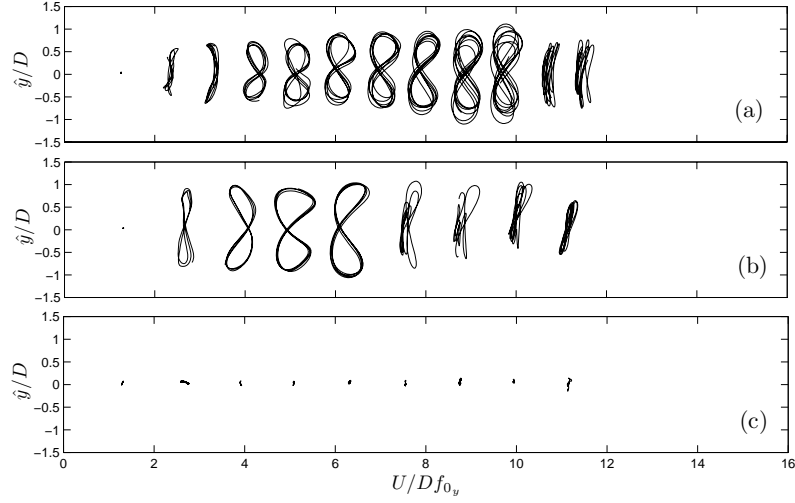
Fig. 8.11: A few cycles of 2-dof trajectories versus reduced velocity: (a) plain cylinder, (b) f-t-r splitter plate with $\tau_f = 0.9 \times 10^{-2}$ below critical and (c) f-t-r splitter plate with $\tau_f = 3.5 \times 10^{-2}$ above critical. $\hat{y}/D$ and $\hat{x}/D$ are plotted to the same scale.

The solid line gives an indication of the effectiveness of suppression. For all points above that contour A_{xy}/D is less than 0.1.

A non-dimensional friction torque parameter, defined by

$$\tau_f^* = \frac{\tau_f}{\rho U^2 D^2}, \tag{8.3}$$

represents the ratio of structural torsional resistance to a hydrodynamic torque. Use of this parameter provides a means of determining the required torsional resistance for full-scale risers. Fig. 8.10(b) presents the same stability map as shown in Fig. 8.10(a) but instead plots the non-dimensional friction torque parameter τ_f^* on the vertical axis. The dashed line is for $\tau_f = 2.5 \times 10^{-2}$Nm/m, illustrating that any value of torsional friction between this line and the upper threshold would be sufficient to suppress VIV with a single splitter plate.

Fig. 8.11 shows examples of trajectories of motion for a single splitter plate with two different torsional friction levels, below and above the critical value, compared with the response of a plain cylinder. In the low-friction case of $\tau_f = 0.9 \times 10^{-2}$Nm/m (b) the splitter plate was unstable and the trajectories show amplitudes higher than those for a plain cylinder (a). However, when the friction level was set to $\tau_f = 3.5 \times 10^{-2}$Nm/m (c) the trajectories are little more than small dots over the whole range of reduced velocity.

192

Table 8.2: Drag reduction for 2-dof VIV suppressors. Symbols as in Fig. 8.3. $\overline{C}_x$ averaged in the range Re $= 2 \times 10^3 - 1.8 \times 10^4$.

	Model	$\overline{C}_x$	Drag reduction
■	Static cylinder	1.03	Reference
◇	Single splitter plate	0.88	14%
○	Double splitter plates	0.70	32%
△	Parallel plates	0.63	38%
▷	Parallel plates with gap	0.69	33%

We next wanted to verify that the other suppressors would also work if the torsional friction was set to a suitable critical value. Because the critical value was unknown for each device, we arbitrarily chose the value $\tau_f = 3.5 \times 10^{-2} \mathrm{Nm/m}$ from the single splitter plate map of Fig. 8.10(a), which is in a region where suppression is effective. All devices were set at this torsional friction level and runs over a range of reduced velocity were performed. Figs. 8.9(b) and (d) show results that should be compared with the low-friction case in the first column. Immediately we notice that the amplitude levels in both directions of motion are very much less than those for the low-friction case. In fact, at this torsional friction level all suppressors were effective in reducing VIV below 5% of cylinder diameter.

Fig. 8.9(f) shows that all devices reduced drag below that of a fixed cylinder for most of the range of reduced velocity. The drag coefficients in Table 8.2 are averaged over the Re range of the experiments and show that parallel plates achieved the highest average drag reduction of 38% when compared with a plain fixed cylinder. Hence for each test case the Reynolds number range is the same and for the freely mounted models the reduced velocity ranges are also the same.

It seems likely that different suppressors might have different stability boundaries for torsional resistance, but there is clearly a range of τ_f within which VIV suppression would be achieved for the devices we studied. A further observation is that the critical torsional friction required to stabilise the splitter plate in 2-dof motion is greater than that required for 1-dof, presumably because in-line vibrations play some role in rotating the device.

Short-tailed fairing
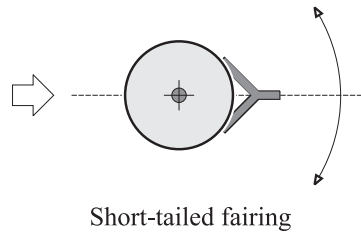
Fig. 8.12: f-t-r short-tailed fairing fitted to a cylinder. Geometry after Pontaza & Chen (2006).
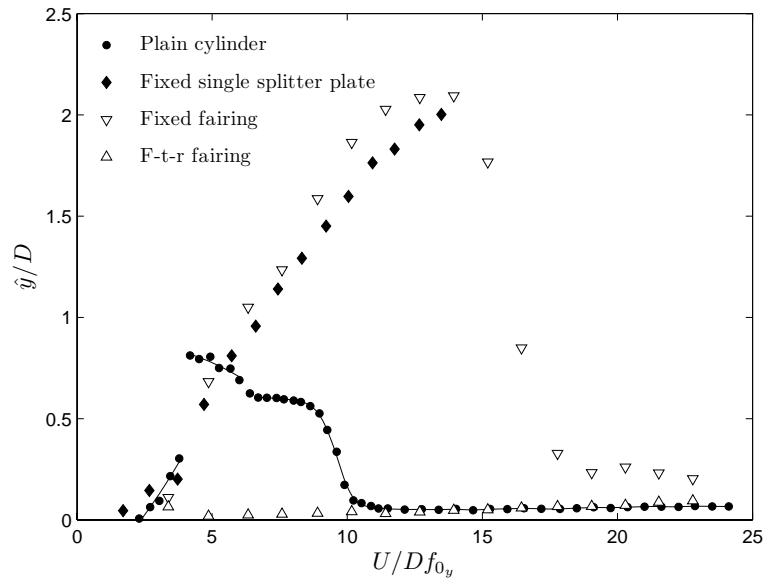
Fig. 8.13: Response of a fixed and f-t-r fairing.

8.4.2 VIV suppression with a short-tailed fairing

One last suppression device tested was the triangular fairing with a flat tail piece presented in Fig. 8.12. This geometry is already employed by the offshore industry following its appearance as a commercial device to reduce VIV (Allen & Henning, 1995). The geometry adopted in this work was based on the proportions found in Pontaza & Chen (2006).

Response in 1-dof

The response of the fairing was first studied in 1-dof motion. In Fig. 8.13 we observe that a cylinder fitted with a fixed fairing responds in a similar way to the fixed splitter plate described earlier, however this time the amplitude reaches values just above $\hat{y}/D = 2.0$ before rapidly falling to lower levels at about a reduced velocity of 14.

Although fairings are being used to suppress VIV in practical offshore applications, our results show that a fixed fairing can cause severe galloping over a considerable range of reduced velocity.

Once the fairing was allowed to rotate about the centre of the cylinder the response was completely different. The fairing tilted to an inclined position in just the same way as the single splitter plate did and the low displacement amplitude levels shown in Fig. 8.13 prove that it successfully suppressed vibrations in 1-dof. Although for certain reduced velocities the drag coefficient appeared to be below that of a fixed cylinder, the mean drag calculated for the whole range showed a slight drag increase of 2%.

Response in 2-dof

The fairing was tested in the 2-dof rig also varying the torsional resistance parameter and was the only suppressor to present a dissimilar behaviour from the others. We indeed noticed that a f-t-r fairing with sufficient torsional resistance would also tilt and find a stable inclined position, just like the single splitter plate. In the low-friction case the fairing did not find a stable position, but caused vibrations comparable to a plain cylinder. However, we noticed that when the torsional friction was increased to $\tau_f = 3.5 \times 10^{-2} \mathrm{Nm/m}$, and the fairing had eventually stabilised in an inclined position, vibration was reduced. Even so, with 2-dof the fairing was not as effective in suppressing VIV as the other longer suppressors.

It appears that for both 1-dof and 2-dof experiments the fairing behaved in a similar manner to a single splitter plate of length $0.5D$. By examining Figs. 8.2 and 8.12 it is clear that the characteristic length of the fairing is half that of other suppressors. Consequently vibrations might be caused because the fairing is not long enough to delay the vortex shedding sufficiently downstream of the body and vortices are somehow feeding back and exciting the cylinder.

After this study we can say that we have a better understanding of the principle behind the way fairings work to reduce VIV. Such a short fairing like this is not able to avoid flow separation, therefore it is not working as a streamlining "fairing" at all. Just like the single splitter plate, the fairing also generates a mean lift force

towards the side to which it is deflected. In practice, long risers are fitted with a series of fairings mounted along the span of the pipe. We believe that some fairings might randomly deflect to one side whereas others find a stable position at the opposite side, in a way that the resultant lift force generated on the entire riser is neutralised. This prediction was not verified in our experiments but we believe on-site observations would help to clarify this point.

8.5 WIV suppression in 1-dof

We are able to investigate the effectiveness of the same devices described above simply by placing a static cylinder upstream. WIV experiments were conducted only in 1-dof, therefore $f_0 \equiv f_{0_y}$. Knowing that the WIV response naturally decreases with increasing x_0, we tested devices at $x_0/D = 4.0$ where we have found, in previous chapters, the most vigorous WIV response. There is no reason to believe that a suppressor would lose efficiency if x_0 is increased beyond 4.0.

But before moving on to investigate the effectiveness of two-dimensional control plates, we wanted to verify the WIV behaviour of the most widespread of the VIV suppressors: helical strakes.

8.5.1 WIV with helical strakes

We performed WIV experiments with the downstream cylinder fitted with helical strakes. The model had a diameter of 68mm, a strake height of $0.1D$ and a helical pitch of $5D$. We are aware that this geometry does not match the propositions currently employed by the offshore industry, but still it provides some insight on the ineffectiveness of strakes in reducing vibrations when there is flow interference from upstream. Separation was kept at $x_0/D = 4.0$ and only the downstream cylinder was fitted with strakes. The upstream cylinder was left plain in order to generate a coherent vortex wake in the gap and excite WIV.

Fig. 8.14 presents the results compared to the reference VIV and WIV curves for plain cylinders. First, we note that this configuration of strakes is able to reduce the VIV amplitude by 44% at the resonance peak. The level of vibration remains
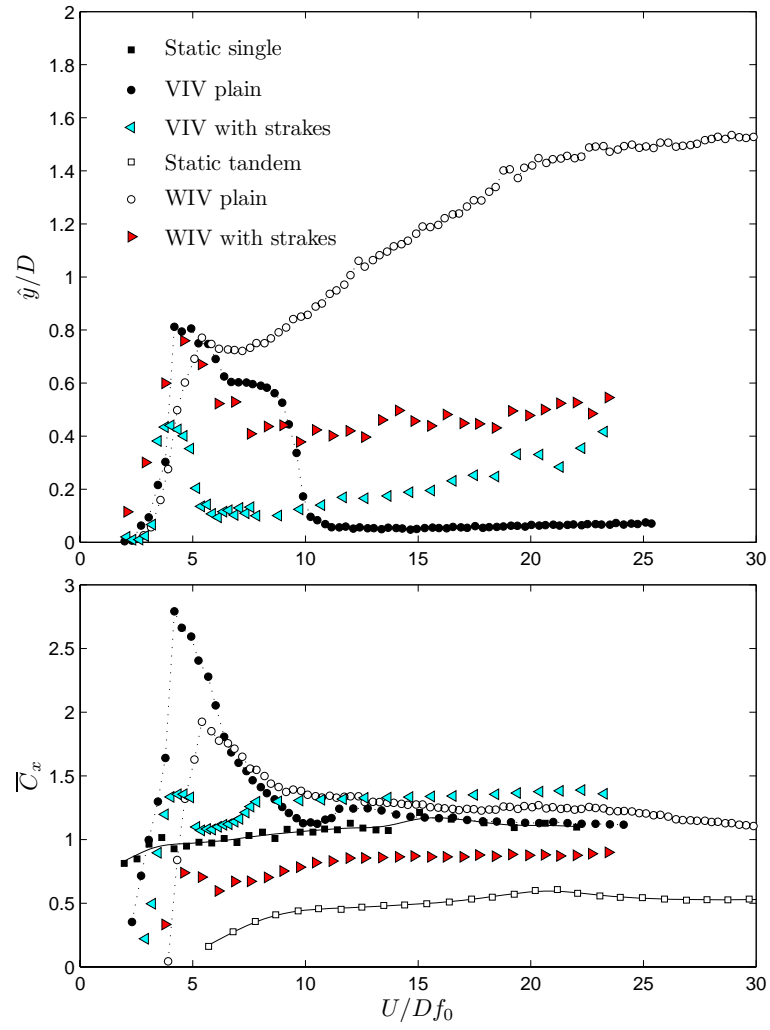
Fig. 8.14: WIV response in 1-dof (top) and mean drag coefficient (bottom) for a cylinder fitted with strakes.

fairly low around $\hat{y}/D = 0.1$ up to reduced velocity 10, after which vibration builds up again reaching amplitudes around 0.4 at $U/Df_0 = 23$. This increasing response appears to be an effect of random fluctuations in lift and drag generated by the disruption of the flow by the strakes. The energy content of force fluctuation increases with flow speed, and so does the random response.

Once a plain cylinder is placed $4D$ upstream the response changes significantly. The amplitude returns to $\hat{y}/D = 0.8$ at the VIV resonance peak, then falls slightly as reduced velocity is increased, but remains at a considerably high level around 0.5 for the rest of the reduced velocity range. As we can see the response does not reach the high values of WIV found for plain cylinders, but still the significant level of response is enough to conclude that the strake has lost efficiency when flow interference is present.

In Fig. 8.14 we can also see the level of drag generated by the device. On average, the cylinder with strakes showed a 26% drag increase when compared to a static single cylinder. In a similar way, the downstream cylinder with strakes presented even higher drag relative to a static cylinder in tandem.

Knowing how the WIV mechanism works, we are able to conclude that the unsteady wake from upstream is still able to interact with the downstream body and enhance the response. An ideal WIV suppressor has to work not only in disrupting the vortex formation from its own cylinder, but also avoiding the vortex-structure interference in the gap. If WIV suppression with drag reduction is to be achieved the helical strake is not the solution to be followed.

8.5.2   Free-to-rotate parallel plates

In the previous section we have shown that two-dimensional control plates are very successful in suppressing VIV of a single cylinder. Therefore we selected the most efficient solution tested above — the parallel plates that produced less drag — to verify its effectiveness in suppressing WIV.

The downstream cylinder, which was mounted on the 1-dof elastic rig, could be fitted with free-to-rotate plates. The upstream cylinder was kept fixed and could
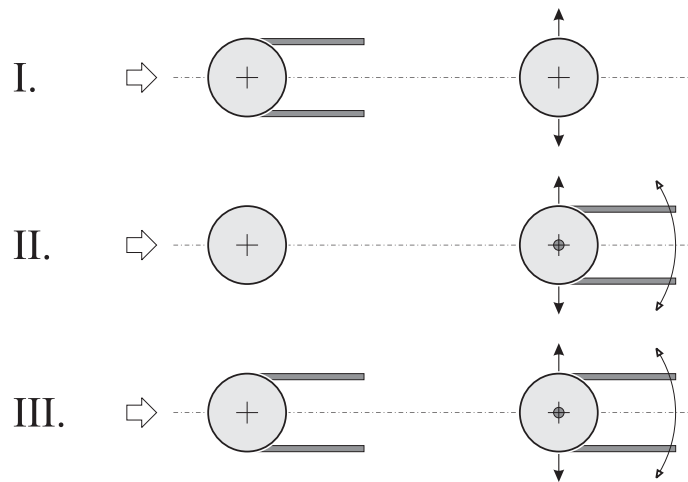
Fig. 8.15: Configurations of cylinders fitted with parallel plates. $x_0/D = 4.0$.

be fitted with an identical pair of fixed parallel plates. This way, three different configurations were tested fitting the devices on one or both cylinders at a time, as shown in Fig. 8.15.

WIV response

We started our investigation by fitting an elastically mounted cylinder with parallel plates but placing a static plain cylinder downstream — almost like configuration I in Fig. 8.15, but with the upstream cylinder being the one free to oscillate. We observed that the presence of the downstream cylinder did not interfere with the response of the upstream cylinder, but the suppressor was still effective and the body did not perform significant vibrations. This was important to validate our hypothesis that an upstream cylinder fitted with f-t-r parallel plates would behave as a static cylinder due to the effectiveness of the suppressor, at least for $x_0/D > 4.0$. This being true, we could replace the upstream cylinder by a fixed cylinder fitted with fixed parallel plates and concentrate our attention at the response of the downstream cylinder.

Results are presented in Fig. 8.16. The first set shows the response for a plain downstream cylinder when the upstream cylinder is fitted with fixed plates (configuration I in Fig. 8.15). We know that WIV is related to the unsteady vortices from the upstream cylinder and we believe the amplitude of vibration is directly
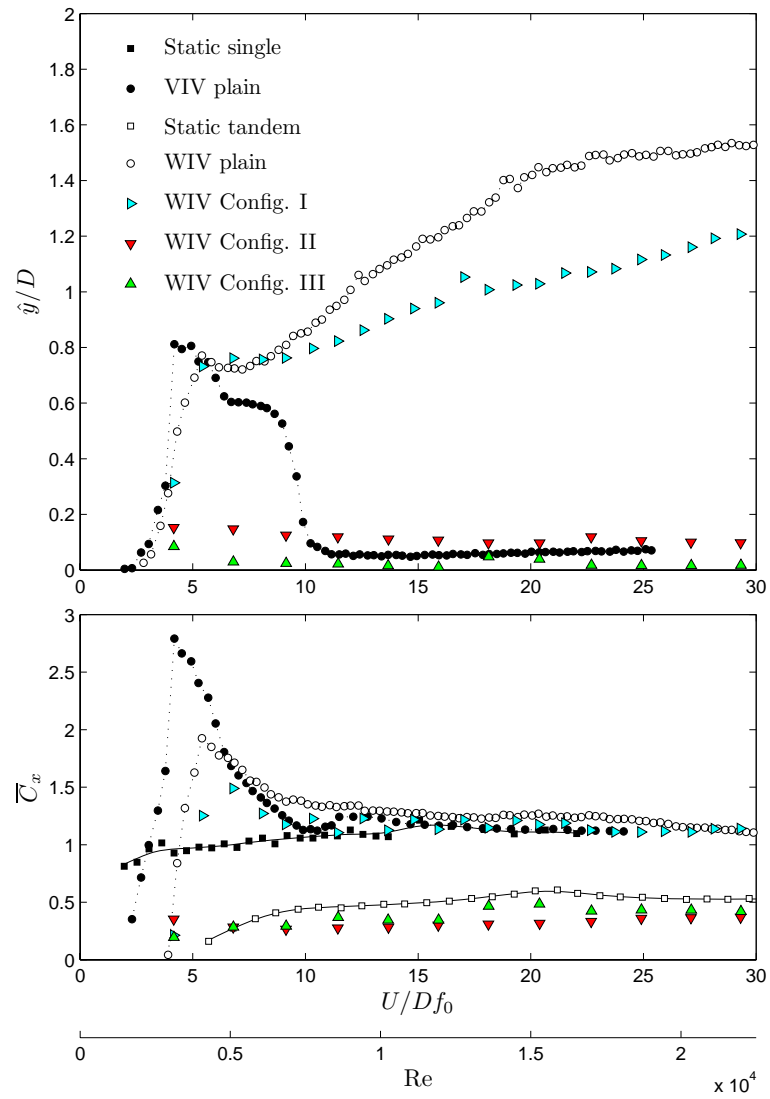
Fig. 8.16: WIV response in 1-dof (top) and mean drag coefficient (bottom) for cylinders fitted with parallel plates. Please refer to Fig. 8.15.

related to the intensity of vortices formed in the wake in the gap. We also know that the parallel plates work by delaying the interaction between the two shear layers, thus delaying the formation of vortices and weakening the wake in the gap. (The fact that the drag on a single cylinder fitted with parallel plates is less than the drag on a plain fixed cylinder proves that the wake being generated is weaker.) Therefore, since the plates do not annihilate the formation of vortices from the first cylinder, but weaken them, the amplitude of vibration of the downstream cylinder is expected to be less than that observed for a pair of plain cylinders under WIV. This is exactly what we see in Fig. 8.16. If the upstream cylinder is the only one fitted with parallel plates (configuration I) the downstream cylinder would still suffer WIV, though with a reduced amplitude level.

Now, in configuration II (Fig. 8.15) the cylinder fitted with f-t-r plates is positioned downstream of a plain static cylinder and Fig. 8.16 presents a remarkable result. The WIV of the downstream cylinder was suppressed to levels around 10% of a diameter, the same level of residual vibration measured for a single cylinder under VIV for reduced velocities after the synchronisation region. This level of vibration is already considered to be rather low and we could say that the parallel plates have successfully suppressed vibration to a desirable point. Based on the results presented in previous chapter, we know that the upstream cylinder in configuration II is shedding vortices as an isolated cylinder. In principle, the wake coming from the upstream cylinder has the same characteristics as the wake found between two plain cylinders in tandem arrangement. Therefore the parallel plates must be acting not only on the vortex shedding mechanism of the downstream cylinder, but also on the vortex-structure interaction this body encounters with the approaching flow. As a result, the vigorous type of WIV is suppressed.

As we have demonstrated in Chapter 7, the mass and damping parameters of the system play an important role and may reduce WIV for certain critical values (Bokaian & Geoola, 1984; Zdravkovich & Medeiros, 1991). We might suggest that the presence of two long plates along the cylinder axis may increase the hydrodynamic added mass and damping in the direction of movement. This change could be responsible for reducing the response but probably not for suppressing the

vibration completely. Therefore we believe the plates are acting directly on the WIV excitation mechanism as we understand it.

Finally, in configuration III we note the response of the downstream cylinder being suppressed to even lower levels. In configuration II we saw that the plates on the second body did a good job to counteract the WIV excitation coming from upstream. Now that the unsteadiness of the wake is also reduced by the presence of parallel plates installed upstream, the response of the second body is further reduced.

From this series of experiments we conclude that it is essential to install parallel plates on the downstream cylinder to suppress WIV; if plates are installed on the upstream cylinder the result is further improved.

The results presented in the present work refer only to a separation of $x_0/D = 4.0$. We already know that the excitation mechanism may change as x_0 is reduced below a critical separation. We also know that the plates require a minimum length to work. If we reduce the gap or enlarge the plates we may fall again in the gap-flow-switching range and a vigorous response may return.

Drag reduction

Considering a pair of fixed cylinders in tandem arrangement, it is known that the mean flow profile that reaches the second cylinder has a deficit in velocity compared to the free stream flow. Hence, the second cylinder of a tandem pair experiences less drag when compared to the first cylinder, which is exposed to the incident free stream U (Fig. 6.1, page 106). However, as the body oscillates in and out of the wake interference region, this shielding effect is reduced and $\overline{C}_x$ is increased.

Fig. 8.16 also presents two reference curves for drag on static cylinders: one measured for a single cylinder and the other for the downstream cylinder of a tandem pair. We clearly see that the level of $\overline{C}_x$ in tandem is already half of that found for a single static cylinder. Therefore, a correct evaluation of drag reduction for WIV suppressors must take $\overline{C}_x = 0.49$ as a reference and not $\overline{C}_x$ around unity.

Both configurations that successfully suppressed WIV (II and III) also reduced drag when compared to a fixed cylinder in tandem arrangement. Table 8.3

Table 8.3: Drag reduction for WIV in 1-dof. Symbols as in Fig. 8.16. $\overline{C}_x$ averaged in the range Re = $2 \times 10^3 - 1.8 \times 10^4$.

Model		$\overline{C}_x$	Drag reduction
□	Static tandem	0.49	Reference
▽	Parallel plates: Config. II	0.33	33%
△	Parallel plates: Config. III	0.38	22%

summarises the data plotted in Fig. 8.16. It is interesting to note that while the upstream wake with weaker vortices found in configuration III helps to reduce the amplitude of response, it does not have as large an effect in reducing drag. It seems that the upstream cylinder fitted with parallel plates experiences a drag reduction as well, generating a wake that reaches the second cylinder with a weaker velocity deficit. This reduction in the velocity deficit must be incurring a drag penalty on the downstream body. While configuration II produced 33% of drag reduction, configuration III was limited to 22%.

8.5.3 Single splitter plate as a WIV suppressor

Now that we know that parallel plates are effective in suppressing VIV and WIV, we might have a brief look into the WIV response of a cylinder fitted with a single splitter plate. As we know, a f-t-r splitter plate requires a stable deflected position in order to suppress VIV. This is achieved at the cost of a steady lift force being generated towards the side the plate has deflected. We saw that if the plate is not able to stabilise, say by having very low torsional resistance, it will wobble from one side to the other as the cylinder oscillates.

Now, we saw that the wake coming from the upstream cylinder is full of coherent vortices that are responsible for the WIV excitation. This may lead to the question: With unsteady pressure fluctuations coming from the upstream wake, is it possible for a f-t-r splitter plate fitted on the downstream cylinder to find a stable position? In order to investigate this possibility, we performed one last experiment replacing the parallel plates in configuration II by a f-t-r splitter plate. The results are presented
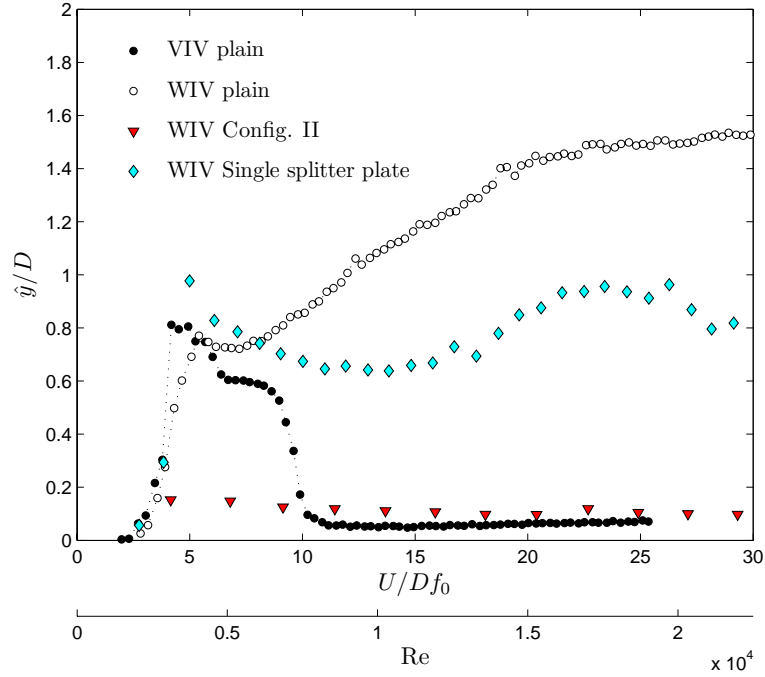
Fig. 8.17: WIV suppression with f-t-r splitter plate and parallel plates.

in Fig. 8.17.

The plate was installed with a torsional friction above the critical value found for VIV. Even though, it was not able to stabilise around $\delta = \pm 20°$ or any other angle, but oscillated vigorously as the cylinder responded with amplitude between 0.6 and 1.0 for the range of reduced velocities. It appeared that the vortex-structure interaction present in the wake was indeed acting on the plate to prevent it from finding a stable angle.

The WIV excitation mechanism becomes even more complex when the splitter plate is pivoting around the cylinder. We already know that, during WIV, the lift force acting on the downstream cylinder has a steady component acting towards the centreline. Imagine a cylinder with a f-t-r splitter plate slightly offset from the centreline of the wake; the lower pressure on the internal face of the cylinder will also act on the plate, deflecting it inwards. We already know that a splitter plate generates a mean lift towards the side it is deflected; hence also pointing towards the centreline. We have the combination of two forces, one originating from the wake stiffness and other generated by the deflected plate, acting in the same inward

204
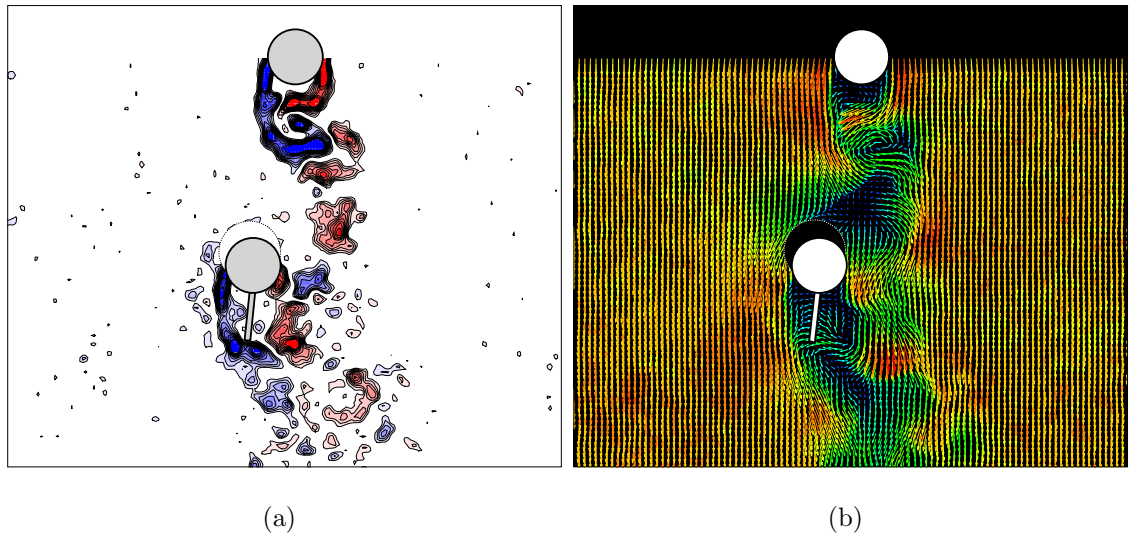
Fig. 8.18: Instantaneous vorticity contours (a) and velocity vectors (b) for a f-t-r splitter plate under WIV at $U/Df_0 = 6.0$.
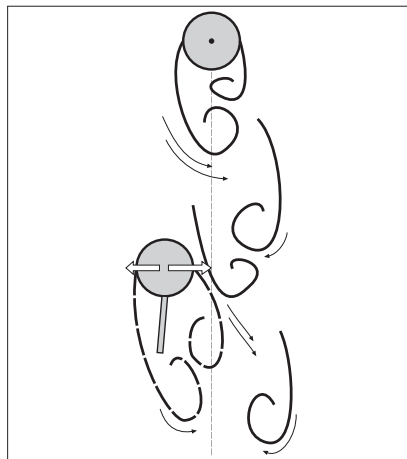
Fig. 8.19: Sketch of competing lift forces generated by wake interaction with a f-t-r splitter plate under WIV.

direction.

Now consider the cylinder represented in Fig. 8.18 (a sketch is presented in Fig. 8.19). At this instant the cylinder is returning from its outmost displacement, still with low cross-flow velocity. The splitter plate shows a small outward deflection angle that will change while the body plunges across the wake. Again we see the competition of lift induced by the wake and generated by the plate, as expressed by the arrows in Fig. 8.19. It is this complex interaction that prevents the plate from stabilising and sustaining the oscillations.

Only a device that does not require an asymmetric stable deflection will be effective in suppressing WIV. The parallel plates are successful because they do not depend in a deflected position to interact with the shear layers nor generate the consequent steady lift. This instability observed for a f-t-r splitter plate must occur for any non-symmetric device, including the short-tailed fairing considered above. In spite of being used by the offshore industry as a VIV suppressor, the fairing may well not work if the riser encounters interference from the wake generated from other bodies. As we see, the result is even worse than the typical VIV vibration, persisting with high levels of response for the rest of the reduced velocity range.

8.6 Conclusion

8.6.1 VIV suppression

Suppression of cross-flow and in-line VIV of a circular cylinder, with resulting drag coefficients less than that for a static plain cylinder, has been achieved using two-dimensional control plates free to rotate around the body.

- Response below $\hat{y}/D = 0.1$ was achieved at a value of the $m^*\zeta < 2 \times 10^{-2}$ for 1-dof and $m^*\zeta < 0.56 \times 10^{-2}$ for 2-dof motion.

- Considerable drag reduction was achieved by all suppressors, yet the best solution was the parallel plates which produced a 38% reduction in drag when compared to a static cylinder.

- A f-t-r splitter plate was also found to suppress VIV but this configuration develops a mean transverse force. This force can be eliminated by using a pair of splitter plates arranged so that the shear layers that spring from the cylinder attach to the tips of the plates.

- Short fairings with a characteristic length of $0.5D$ proved to reduce amplitude levels (at the expense of a mean transverse force) but were not as efficient as other longer suppressors. Rather than reducing drag for the entire range of reduced velocities tested, the fairing increased it for certain velocities.

8.6.2 WIV suppression

Cross-flow WIV suppression with drag reduction was also achieved when f-t-r parallel plates were installed on the downstream cylinder of a pair.

- Response below $\hat{y}/D = 0.1$ was achieved at a value of the $m^*\zeta < 2 \times 10^{-2}$ for 1-dof motion.

- If both cylinders are fitted with suppressors, which must be the case for an offshore installation, the reduction in drag can amount to 22% compared to a static downstream cylinder in tandem arrangement. If only the downstream cylinder is fitted with parallel plates the drag reduction is around 33%.

- A f-t-r- splitter plate was found not to suppress WIV due to intense vortex-structure interference with the upstream wake. We suggest only devices that do not require a non-symmetric stable position will be efficient in WIV. Therefore, short fairings that behave as splitter plates are unlikely to provide WIV suppression.

- It was demonstrated that helical strakes, at least the one configuration tested, lose their suppression efficiency when unsteady excitation is present in the upstream wake.

8.6.3 Concluding remarks

The level of torsional friction plays a fundamentally important role, needing to be high enough to hold the devices in a stable position, while still allowing them to realign if the flow direction changes. Devices with torsional friction below a critical value oscillate themselves as the cylinder vibrates, sometimes increasing the amplitude of cylinder oscillation higher than that for a plain cylinder. All devices with torsional friction above the critical value appeared to suppress VIV and reduce drag for 1-dof and 2-dof motions. However, if the torsional resistance is above a limiting threshold the suppressors may not rotate and an undesired galloping response can be initiated.

The present study proves that suppressors based on parallel plates have great potential to suppress VIV and WIV of offshore structures with considerable drag reduction. Future work should concentrate on optimising the devices in respect of overall length and geometry. Also, a more detailed parametric investigation on the effects of rotational inertia and torsional resistance should be carried out for each specific solution.

Chapter 9

Conclusion

Most of the points presented in this chapter have been dealt with in more detail in the conclusion sections at the end of the respective chapters. Nevertheless, it summarises the main findings and contributions of the present study.

9.1   WIV excitation mechanism

As we have discussed in Chapter 3, so far the wake-displacement mechanism proposed by Zdravkovich (1977) seemed to be the most plausible explanation for the WIV phenomenon, even though he could not conclude how the wake was being 'displaced' to generate the necessary phase lag to sustain the vibrations. In Chapter 6 we have concluded that WIV is indeed a wake-dependent type of FIV. Yet we found that it is the unsteadiness of the wake that plays a role in the WIV process and not simply the displacement of a steady flow field. We could say that Zdravkovich's 'wake-displacement' theory needs to be understood more as a 'vortex-displacement' mechanism.

We argue that the WIV mechanism is sustained by unsteady *vortex-structure interactions* that input energy into the system as the downstream cylinder oscillates across the wake.

- We conclude that WIV is not a resonant phenomenon. While VIV finds its maximum amplitude of vibration at $f_s = f_0$, WIV keeps increasing $\hat{y}$ even

when f_s is much higher than f_0. In the shear flow experiment we removed the upstream shedding frequency of the system, leaving only f_s that is generated by the second cylinder. As a result, the oscillations returned to a typical VIV response meaning that the upstream frequency — or the upstream vortex shedding — was somehow important to sustain the excitation. Nonetheless, for the sake of classification, WIV is essentially a type of vortex-induced mechanism in the sense that it requires the interaction of the structure with vortices, even though these vortices are coming from an upstream wake.

- Energy input from the fluid to the structure will only occur when there is a phase lag greater than $\phi = 0°$ or less than $180°$ between the fluid force and displacement. Coherent vortices impinging on the second cylinder and merging with its own vortices induce fluctuations in lift that are not synchronised with the motion. Strong vortices from the upstream wake induce considerable changes in the lift force; a favourable phase lag is most likely to occur in a disturbed wake that is constantly changing and interacting with the body. Remove the unsteady vortices from the wake and WIV will not be excited.

- The characteristic response of the second cylinder agrees with the theory presented above. Irregular envelopes of displacement and lift indicate that the second cylinder encounters different wake configurations for each cycle. This is not possible in a steady flow, but is observed when an irregular vortex-structure interaction is present. As the second cylinder is moved farther downstream, vortices coming from the upstream wake have more time to diffuse and the induced vortex-structure interaction is weakened. Flow three-dimensionality may also increase with x_0 and contribute to reduce the response.

Now, one may think that if the origin of the WIV mechanism is so strongly dependent on the unsteadiness of the vortex wake coming from the upstream body — or on the phase lag that those vortices generate — it is possible to think about some configuration of the upstream wake that will suppress WIV instead of enhancing it. By this we mean: is there a possibility that the phase lag originated in the upstream

wake has a destructive effect suppressing the excitation of the downstream cylinder altogether?

This fact was not observed in the present work; rather the second cylinder always has presented some oscillatory motion. But this hypothesis finds support from other observations reported in the literature. Previously (Assi, 2005), we have performed experiments with a pair of rigid cylinders when both cylinders were free to respond in the cross-flow direction. At that time, this configuration brought too many variables into the system and did not help our understanding of the phenomenon.

We observed that when both cylinders were free to vibrate for separations larger than the critical, the upstream cylinder would behave as an isolated cylinder under VIV and the downstream cylinder would respond with WIV most of the time. However, sometimes the downstream cylinder would stop vibrating but remain static behind the first cylinder, even though the upstream cylinder was responding with VIV. Sometime this suppression of WIV would last for a few seconds, but at others the downstream cylinder would remain static for several cycles of oscillation of the upstream body.

This observation fits remarkably well with our current understanding. It shows that it is possible for an oscillating upstream cylinder to generate a developed wake that actually suppresses the WIV of the downstream body. All that is necessary is the correct combination of phase lag in the wake that is interacting with the second cylinder. Of course the probability of WIV being suppressed was observed to be much smaller than WIV being excited, but it was shown to be possible. On the other hand, this kind of WIV suppression was never observed (including this present work) if the upstream cylinder is held static. This suppressing wake mode must be generated only by the vortex shedding from an oscillating upstream cylinder.

Huera-Huarte & Bearman (2009) performed experiments with two long and flexible cylinders in tandem. They also observed that for some configurations the upstream cylinder responding in VIV suppressed the WIV response of the downstream one. Although they did not explain how such an interaction was possible, their observations are in remarkable agreement with our theory proposed in the present work.

9.2 Characteristics of the WIV response

In Chapter 7 we have made $f_0 = 0$ to shown that a body without any structural stiffness can be excited into oscillatory motion if enough stiffness is provided by the flow. We have introduced the concept of *wake stiffness*, a fluid dynamic effect that can be associated, to a first approximation, with a linear spring with stiffness proportional to $|\partial \overline{C}_y|$ and Re.

The concept of wake stiffness is a powerful one but it is also requires the existence of an unsteady vortex wake present in the gap. The importance of the unsteady wake is central. Therefore we conclude that WIV is not to be understood as a type of classical galloping, but must be interpreted as wake-excited and wake-sustained FIV mechanism.

- The experiment without springs was crucial in the understanding of the phenomenon and proved that a cylinder mounted without springs is able to develop oscillatory motion. A simple analytical model suggested that the amplitude of response should increase with Reynolds number; this was also verified by experimental data. However, such a simple model that does not account for nonlinear effects in the fluid force is not able to predict the correct level of amplitude.

- We proved that the steady lift towards the centreline not only provides some restoration for a quasi-static system but is, in fact, responsible for the characteristic WIV response of a cylinder that is free to vibrate. The wake stiffness concept does not explain the excitation mechanism but it predicts rather well the characteristic signature of the WIV response both in terms of displacement and frequency. We can say that while unsteady vortex-structure interactions provide the energy input to sustain the vibrations, it is the wake stiffness phenomenon that defines the character of the WIV response.

- A simple linear model was able to predict the frequency of response rather well. It was confirmed that the cylinder without springs does not respond following the vortex shedding frequency f_s. Instead the response matches the frequency

branch f_w associated with wake stiffness, which was well predicted by the model. A cylinder with springs responds with a frequency that combines some effect from f_w and f_0, yet different from both.

- We observed a gradual transition from an initial VIV regime to a dominant WIV regime as flow speed was increased. The boundaries between them were found to be related to the resonances $f_s = f_0$ and $f_w = f_0$. During the transition we find an intermediate condition in which VIV is losing strength and WIV is taking control. Beyond $f_w = f_0$ the wake stiffness effect is dominant over the spring stiffness and reduced velocity becomes irrelevant; k is very relevant in the first regime, but k_w becomes dominant in the second.

- As expected, the x_0 separation between both cylinders was confirmed to have a significant effect on the response. We suggest this effect is related to an increase in vortex diffusion and flow three-dimensionality as the gap is enlarged. The first VIV regime suffered no influence of x_0 and the local resonance peak kept the same level of displacement for all separations. On the other hand, the second WIV regime showed a strong influence of x_0, with the characteristic WIV branch of response gradually disappearing with increasing separation

9.3 Suppression of VIV and WIV with drag reduction

Based on the correct understanding of the WIV mechanism, we conclude that suppressors based on parallel plates have great potential to suppress VIV and WIV of offshore structures with considerable drag reduction.

- Suppression of cross-flow and in-line VIV of a circular cylinder, with resulting drag coefficients less than that for a static plain cylinder, has been achieved using two-dimensional control plates free to rotate around the body. The best solution was the parallel plates which produced a 38% reduction in drag when

compared to a static cylinder. A f-t-r splitter plate was also found to suppress VIV but this configuration develops a mean transverse force.

- Cross-flow WIV suppression with drag reduction was also achieved when f-t-r parallel plates were installed on the downstream cylinder of a pair. If both cylinders are fitted with suppressors, which must be the case for an offshore installation, the reduction in drag can amount 22% compared to a static downstream cylinder in tandem arrangement. It was demonstrated that helical strakes, at least the one configuration tested, lose their suppression efficiency when unsteady excitation is present in the upstream wake.

- A f-t-r splitter plate was found not to suppress WIV due to intense vortex-structure interference with the upstream wake. We suggest only devices that do not require a non-symmetric stable position will be efficient in WIV. Therefore, short fairings that behave as splitter plates are unlikely to provide WIV suppression.

- The level of torsional friction (τ_f) plays a fundamentally important role, needing to be high enough to hold the devices in a stable position, while still allowing them to realign if the flow direction changes. Devices with τ_f below a critical value oscillate themselves as the cylinder vibrates, sometimes increasing the amplitude of cylinder oscillation higher than that for a plain cylinder. On the other hand, if τ_f is above a limiting threshold the suppressors may not rotate and an undesired galloping response can be initiated.

9.4   Further work

We can think of a vast list of further investigations originating from the present study; surely more will appear in the future. But among them, the most significant must be the development of an unsteady model to represent the phenomenon; therefore, we start with this one.

9.4.1 Development of an improved, unsteady model for WIV

We have shown that WIV had been referred to as a type of galloping mostly because the typical response presents a build up of amplitude for higher reduced velocities. But now we know that the response is increasing due to the wake stiffness effect as a function of Reynolds number. We argue that quasi-steady assumptions, commonly employed by the classical galloping theory, would not fit the WIV phenomenon as we now understand it. For that reason we have been insisting on a dissociation of WIV from the classical galloping idea.

No matter how good the wake stiffness approach was in regards to the frequency of oscillation, the displacement response is somewhat more complex and is not fully captured by this first approximation. We believe this is due to the simplicity in modelling the term $\hat{C}_y \sin \phi$. A simple harmonic model as the one we have employed cannot account for nonlinear effects that might be important to the system. It will not be able, for example, to predict the asymptotic effect that is limiting the displacement.

The complex interaction between body and wake causes $|\partial \overline{C}_y|$ and $\hat{C}_y \sin \phi$ to be coupled in such a way that we cannot simply analyse them independently. Since we believe both wake-stiffness and vortex-impulse terms originate in the same fluid mechanic phenomenon, we are not able to uncouple and isolate their effects into linearly independent terms. An improved, nonlinear model is necessary to account for more complex fluid-dynamic phenomena that we have identified to exist but were not considered in our model.

9.4.2 Effect of mass and damping

According to the analysis presented in Chapter 7, the WIV response should be inversely proportional to the product $m^*\zeta$. This is a rather straightforward conclusion that finds support in the analyses of other types of FIV mechanisms as well. Bokaian & Geoola (1984) and Zdravkovich & Medeiros (1991) showed that damping has a significant effect on the WIV response. By varying ζ they were able

to control the overlapping of the VIV and WIV regimes.

We have also preformed preliminary tests with varying m^* and ζ, but they were not presented in this thesis for brevity. We found, as expected, that the amplitude of response is more sensitive to variations in ζ than to variations in m^*. However, further investigation is required to completely understand this dependency.

9.4.3   Retro lock-in

While performing experiments at $x_0/D = 3.0$ we noticed that the lift force on the upstream cylinder had some correlation with the oscillations of the second body. We knew that, at smaller separations, pressure fluctuations resulting from the movement of the downstream cylinder could propagate upstream and interfere with the wake of the first body. But by placing a hot-film probe in the near wake of the upstream static cylinder we were able to verify that the vortex shedding of that body was in fact synchronised by the oscillations of the other. That is, there was a lock-in phenomenon occurring with the shedding of the upstream cylinder (which was static) that was induced by the movement of another body placed $3D$ downstream. We have called this phenomenon 'retro lock-in'.

If the separation is increased, the oscillations of the downstream cylinder will not feedback on the shedding of the upstream body and it will shed vortices as an isolated cylinder. Other than that, if the upstream body is close enough but does not show significant oscillations, the shear layers from the upstream cylinder may reattach and a developed wake will never be formed in the gap. Therefore, retro lock-in is only verified for certain separations that allow some communication between the oscillations of the downstream cylinder and the shedding mechanism of the upstream, while still allowing for a developed wake to be formed. In our experiments, it was only observed for separations between $x_0/D = 2.5$ and 3.0 when the second body had considerable amplitude of oscillation.

9.4.4 Increase the number of degrees of freedom

Now that we have a better understanding of the WIV excitation mechanism, we are ready to increase the number of degrees of freedom and investigate their effect on the response.

The first step would be to allow the downstream cylinder to vibrate in 2-dof while holding the upstream one static. We have performed preliminary WIV experiments employing the 2-dof rig described in the present work, but the discussion of these results is out of the scope of this text. It is already known that a downstream cylinder with 2-dof may respond with the wake-flutter mechanism described in Chapter 3. If the second cylinder is placed, say, at the same $x_0/D = 4.0$ that we have been investigating the response could be an overlapping of VIV, WIV and wake-flutter.

Another possibility would be to allow both cylinders to oscillate, first in 1-dof and later in 2-dof, in order to show that the suppressing effect observed by Assi (2005) is related to these condition. If the cylinders are mounted in 2-dof rigs we would be able to evaluate potential conditions for clashing.

In a third step we would investigate the interaction between two flexible cylinders. In that case we would be closer to the real riser condition, but the great number of variables in the problem would make it almost impossible to understand any physical mechanism other than simply acquiring overall responses.

9.4.5 Optimisation of suppression devices

The present study proved that suppressors based on parallel plates have great potential to reduce drag and suppress VIV and WIV of offshore structures. Future work would concentrate on optimising the devices with respect to overall length and geometry. We already know that an effective splitter plate can be shorter than $1D$, but we also would like to investigate the optimal length for parallel plates as far as suppression and drag reduction are concerned. In addition, a detailed parametric investigation on the effects of rotational inertia and torsional resistance should be carried out for the splitter plate and each of the specific solutions.

And finally, the use of two-dimensional control plates represents only one family

of devices found to suppress VIV and WIV. It is possible that other devices like shrouds and guiding vanes are capable of suppressing WIV as well.

Appendix A

Spectrum plots

This appendix presents a brief explanation about how the power spectral density (PSD) contour plots have been generated in the present work.

We take the example of the lift force measured on the downstream cylinder. If we fix a certain flow speed and acquire the lift signal for a large number of cycles, we will end up with a typical PSD plot of power versus frequency. If we repeat this process for a number of flow speeds, stacking graphs along a reduced velocity axis, we will end up with the three-dimensional plot presented in Fig. A.1(a). If all the frequency peaks had more or less a similar power magnitude, we would be able to identify branches of dominant frequency along the reduced velocity axis. If we look at Fig. A.1(a) from the top, and express the peak height only by colour, we would see the contour plot presented in Fig. A.1(b). Because the peaks at higher reduced velocity have more energy content than the peaks at lower reduced velocities, they overwhelm the colour scale and we are not able to make sense of the frequency branches for lower reduced velocities.

Now, we can repeat the same process but normalising each individual PSD plot by its maximum power value; i.e. instead of plotting power on the vertical axis we plot a normalised power (PSD*) that varies between 0 and 1 for each reduced velocity. This would make all reduced velocities have at least one dominant peak at PSD$^* = 1$ in red, as shown in Fig. A.2(a). Hence we would be able to follow the development of frequency branches along the reduced velocity axis as represented

(a)   (b)

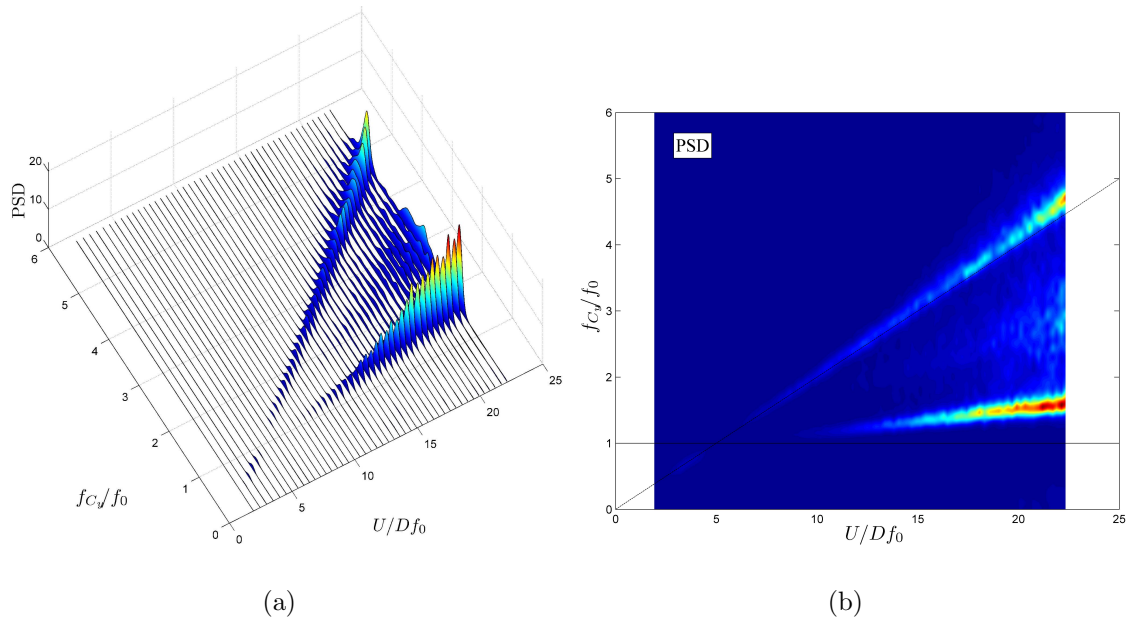Fig. A.1: Examples of PSD plots.

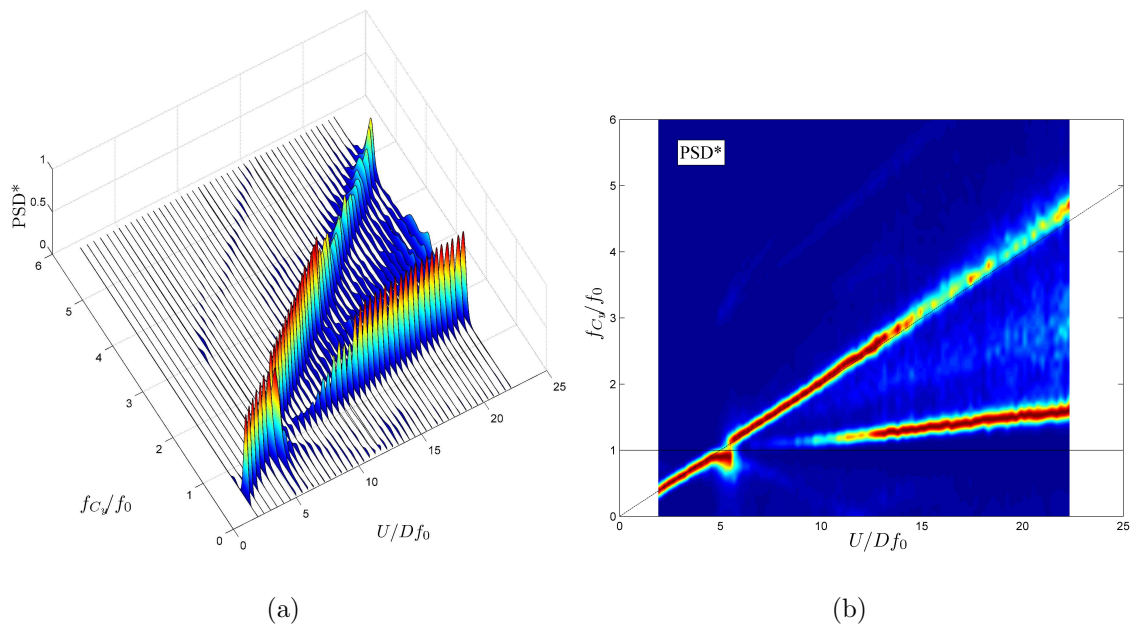(a)   (b)

Fig. A.2: Examples of normalised PSD*. All similar plots in the present work have been generated like this one.

in Fig. A.2(b) without losing information for lower reduced velocities.

All plots presented in the present work have been generated as Fig. A.2(b). However, this normalisation brings one counter effect: we are not able to compare power intensity between one flow speed and another, but only in a vertical line across the reduced velocity axis.

Bibliography

ALAM, M. M., MORIYA, M., TAKAI, K. & SAKAMOTO, H. 2003 Fluctuating fluid forces acting on two circular cylinders in tandem arrangement at a subcritical reynolds number. *J. Wind Eng. Industrial Aerodynamics* **91**, 139–154.

ALLEN, D. W. & HENNING, D. L. 1995 Small fixed teardrop fairings for vortex induced vibration suppression. United States Patent (number 5,410,979).

ASSI, G.R.S. 2005 Experimental study of the flow interference effect around aligned cylinders. Master's thesis, University of São Paulo, São Paulo, Brazil, in Portuguese. Available from www.ndf.poli.usp.br/∼gassi.

ASSI, G.R.S., MENEGHINI, J.R., ARANHA, J.A.P., BEARMAN, P.W. & CASAPRIMA, E. 2006 Experimental investigation of flow-induced vibration interference between two circular cylinders. *J. Fluids Structures* **22**, 819–827.

BEARMAN, P.W. 1984 Vortex shedding from oscillating bluff bodies. *Ann. Rev. Fluid Mech.* **16**, 195–222.

BEARMAN, P.W., GARTSHORE, I.S., MAULL, D.J. & PARKINSON, G.V. 1987 Experiments on flow-induced vibration of a square-section cylinder. *J. Fluids Structures* **1**, 19–34.

BEARMAN, P. W. 1967 On vortex street wakes. *J. Fluid Mech.* **28**, 625–641.

BEST, M.S. & COOK, N.J. 1967 The forces on a circular cylinder in a shear flow. *Tech. Rep.* 103. University of Bristol, Aeronautical Engineering Dept.

BLEVINS, R.D. 1990 *Flow-Induced Vibration*, 2nd edn. Van Nostrand Reinhold.

BOKAIAN, A. & GEOOLA, F. 1984 Wake-induced galloping of two interfering circular cylinders. *J. Fluid Mech.* **146**, 383–415.

BOKAIAN, A. & GEOOLA, F. 1985 Wake displacement as cause of lift force on cylinder pair. *J. Engineering Mechanics* **111**, 92–99.

BRANKOVIC, M. 2004 Vortex-induced vibration attenuation of circular cylinders with low mass and damping. PhD thesis, Imperial College, London, UK.

BRIKA, D. & LANEVILLE, A. 1999 The flow interaction between a stationary cylinder and a downstream flexible cylinder. *J. Fluids Structures* **13**, 579–606.

CARMO, B.S., SHERWIN, S.J., BEARMAN, P.W. & WILLDEN, R.H.J. 2008 Wake transition in the flow around two circular cylinders in staggered arrangements. *J. Fluid Mech.* **597**, 1–29.

CARMO, B. S. 2005 Estudo numérico do escoamento ao redor de cilindros alinhados. Master's thesis, University of São Paulo, São Paulo, Brazil, in portuguese.

CHEN, S.S 1986 A review of flow-induced vibration of two circular cylinders in crossflow. *J. Pressure Vessel Tech.* **108**, 382–393.

CHEN, S.S 1987 A general theory for dynamic instability of tube arrays in crossflow. *J. Fluids Structures* **1**, 35–53.

CIMBALA, J.M. & GARG, S. 1991 Flow in the wake of a freely rotatable cylinder with splitter plate. *AIAA Journal* **29**, 1001–1003.

DAHL, J.M., HOVER, F.S. & TRIANTAFYLLOU, M.S. 2006 Two-degree-of-freedom vortex-induced vibrations using a force assisted apparatus. *J. Fluids Structures* **22**, 807–818.

DRESCHER, H. 1956 Messung der auf querongestromte zylinder ausgeubten seitlich veranderten drucke. *Zeitschrift für Flugwissensschaft* **4**, 17–21.

VAN DYKE, M. 1982 *An album of fluid motion*, 1st edn. Parabolic Press.

GERRARD, J.H. 1966 The mechanics of the formation region of vortices behind bluff bodies. *J. Fluid Mech.* **25**, 401–13.

GOVARDHAN, R. & WILLIAMSON, C.H.K. 2000 Modes of vortex formation and frequency response of a freely vibrating cylinder. *J. Fluid Mech.* **420**, 85–130.

GOVARDHAN, R. & WILLIAMSON, C.H.K. 2002 Resonance forever: existence of a critical mass and an infinite regime of resonance in vortex-induced vibration. *J. Fluid Mech.* **473**, 147–166.

GRANGER, S. & PAIDOUSSIS, M.P. 1996 An improvement to the quasi-steady model with application to cross-flow-induced vibration of tube arrays. *J. Fluid Mech.* **320**, 163–184.

GRIMMINGER, G. 1945 The effect of rigid guide vanes on the vibration and drag of a towed circular cylinder. *Tech. Rep.* 504. David Taylor Model Basin.

HAHN, S.L. 1996 *Hilbert Transforms in Signal Processing*. Artech House.

DEN HARTOG, J.P. 1956 *Mechanical Vibrations*, 4th edn. McGraw Hill.

HORI, E. 1959 Experiments on flow around a pair of parallel circular cylinders. In *Proc. 9th Japan National Congress for Applied Mech., Tokyo, Japan.*, pp. 231–234.

HOVER, F.S. & TRIANTAFYLLOU, M.S. 2001 Galloping response of a cylinder with upstream wake interference. *J. Fluids Structures* **15**, 503–512.

HUERA-HUARTE, F.J. & BEARMAN, P.W. 2009 Wake structures and vortex-induced vibrations of a long flexible cylinder part 1: Dynamic response. *J. Fluids Structures* **25**, 991–1006.

IGARASHI, T. 1981 Characteristics of the flow around two circular cylinders arranged in tandem. *Bulletin of JSME - Japan Soc. Mech. Eng.* **24**, 323–331.

JAUVTIS, N. & WILLIAMSON, C.H.K. 2004 The effect of two degrees of freedom on vortex-induced vibration at low mass and damping. *J. Fluid Mech.* **509**, 23–62.

KHALAK, A. & WILLIAMSON, C.H.K. 1999 Motions, forces and mode transitions in vortex-induced vibrations at low mass-damping. *J. Fluids Structures* **13**, 813–851.

KING, R. & JOHNS, D.J. 1976 Wake interaction experiments with two flexible circular cylinders in flowing water. *J. Sound Vibration* **45**, 259–283.

KORKISCHKO, I., MENEGHINI, J.R., CASAPRIMA, E . & FRANCISS, R. 2007 An experimental investigation of the flow around isolated and tandem straked cylinders. In *BBVIV5 5th Conf. on Bluff Body Wakes and Vortex-Induced Vibrations, Brazil*.

LANEVILLE, A. & BRIKA, D. 1999 The fluid and mechanical coupling between two circular cylinders in tandem arrangement. *J. Fluids Structures* **13**, 967–986.

LIN, J.C., TOWFIGHI, J. & ROCKWELL, D. 1995 Instantaneous structure of the near-wake of a circular cylinder: on the effect of reynolds number. *J. Fluids Structures* **9**, 409–418.

LIN, J.C., YANG, Y. & ROCKWELL, D. 2002 Flow past two cylinders in tandem: instantaneous and average flow structure. *J. Fluids Structures* **16**, 1059–1071.

LJUNGKRONA, L., NORBERG, C. & SUNDEN, B. 1991 Free-stream turbulence and tube spacing effects on surface pressure fluctuations for two tubes in an in-line arrangement. *J. Fluids Structures* **5**, 701–727.

MAEKAWA, T. 1964 Study on wind pressure against acsr double conductor. *Electrical Engineering in Japan* **84**.

MAIR, W.A. & MAULL, D.J. 1971 Aerodynamic behaviour of bodies in the wakes of other bodies. *Phil. Trans. Royal Soc.* **269**.

MORETTI, P.M. 1993 Flow-induced vibrations in arrays of cylinders. *Annu. Rev. Fluid Mech.* **25**, 99–114.

MORSE, T.L. & WILLIAMSON, C.H.K. 2009 Prediction of vortex-induced vibration response by employing controlled motion. *J. Fluid Mech.* **In Press**, In Press.

NAUDASCHER, E. & ROCKWELL, D. 1994 *Flow-Induced Vibrations. An Engineering Guide.*, 1st edn. A.A. Balkema.

NORBERG, C. 1998 Ldv-measurements in the near wake of a circular cylinder. In *Advances in Understanding of Bluff Body wakes and Flow-Induced Vibration* (ed. C.H.K. Williamson & P.W. Bearman), pp. 1–12. ASME.

OWEN, J.C., BEARMAN, P.W. & SZEWCZYK, A.A. 2001 Passive control of viv with drag reduction. *J. Fluids and Structures* **15**, 597–605.

PAIDOUSSIS, M.P., MAVRIPLIS, D. & PRICE, S.J. 1984 A potential-flow theory for the dynamics of cylinder arrays in cross-flow. *J. Fluid Mech.* **146**, 227–252.

PAIDOUSSIS, M.P. & PRICE, S.J. 1988 The mechanisms underlying flow-induced instabilities of cylinder arrays in crossflow. *J. Fluid Mech.* **187**, 45–59.

PARKINSON, G.V. 1971 Wind-induced instability of structures. *Phil. Trans. Royal Soc. London* **269**, 395–413.

PARKINSON, G.V. 1989 Phenomena and modelling of flow-induced vibrations of bluff bodies. *Progress in Aerospace Sciences* **26**, 169–224.

PONTAZA, J.P. & CHEN, H.C. 2006 Numerical simulations of circular cylinders outfitted with vortex-induced vibrations suppressors. In *ISOPE Int. Soc. Offshore and Polar Eng.*.

PRICE, S.J. 1975 Wake-induced flutter of power transmission conductors. *J. Sound Vibration* **38**, 125–147.

PRICE, S.J. 1976 The origin and nature of the lift force on the leeward of two bluff bodies. *Aeronautics Quarterly* **26**, 1154–168.

PRICE, S.J. 1984 An improved mathematical model for the stability of cylinder rows subject to cross-flow. *J. Sound Vibration* **97**, 615–640.

PRICE, S.J. 1995 A review of theoretical models for fluidelastic instability of cylinder arrays in crossflow. *J. Fluids Structures* **9**, 463–518.

ROSHKO, A. 1954 On the drag and shedding frequency of two-dimensional bluff bodies. *Tech. Rep.* TN–3169. NACA.

RUSCHEWEYH, H. P. 1983 Aeroelastic interference effects between slender structures. *J. Wind Eng. and Industrial Aerodynamics* **14**, 129–140.

SARPKAYA, T. 1979 Vortex-induced oscillations, a selective review. *J. Appl. Mech.* **46**, 241–258.

SAVKAR, S.D 1970 Wake-induced oscilaltions in transmission line bundles. In *IEEE Summer Power Meeting and EHV Conference, Los Angeles, USA.*.

SCHAEFER, J.W. & ESKINAZI, S. 1958 An analysis of the vortex street generated in a viscous fluid. *J. Fluid Mech.* **6**, 16.

SCHLICHTING, H. 2000 *Boundary-layer theory*, 8th edn. Springer.

SNAJ 1986 *Directory of ship hydrodynamics research laboratories in japan.*. The Society of Naval Architects of Japan, Towing Tank Committee.

SUMNER, D., PRICE, S.J. & PAIDOUSSIS, M.P. 2000 Flow-pattern identification for two staggered circular cylinders in cross-flow. *J. Fluid Mech.* **411**, 263–303.

WARDLAW, R.L. & WATTS, J.A. 1974 Wind-tunnel and analytical investigations into the aeroelastic behaviour of bundled conductors. IEEE Power Engineering Society Summer Meeting, anahein, California, USA.

WILLIAMSON, C.H.K. & GOVARDHAN, R. 2004 Vortex-induced vibrations. *Annu. Rev. Fluid Mech.* **36**, 413–55.

ZDRAVKOVICH, M.M. 1972 Smoke observations of wakes of tandem cylinders at low reynolds numbers. *The Aeronautical Journal* **76**, 108–114.

ZDRAVKOVICH, M.M. 1974 Flow-induced vibrations of two cylinders in tandem and their suppression. In *Int. Symp. of Flow Induced Structural Vibrations* (ed. E. Naudascher), pp. 631–639.

ZDRAVKOVICH, M.M. 1977 Review of flow interference between two circular cylinders in various arrangements. *J. Fluids Eng.* pp. 618–633.

ZDRAVKOVICH, M.M. 1981 Review and classification of various aerodynamic and hydrodynamic means for suppressing vortex shedding. *J. Wind Eng. Industrial Aerodynamics* **7**, 145–189.

ZDRAVKOVICH, M.M. 1985 Flow induced oscillations of two interfering circular cylinders. *J. Sound Vibration* **101**, 511–521.

ZDRAVKOVICH, M.M. 1988 Review of interference-induced oscillations in flow past two circular cylinders in various arrangements. *J. Wind Eng. Industrial Aerodynamics* **28**, 183–200.

ZDRAVKOVICH, M.M. 1997 *Flow around circular cylinders, Volume 1*, 1st edn. Oxford University Press.

ZDRAVKOVICH, M.M. 2003 *Flow around circular cylinders, Volume 2*, 1st edn. Oxford University Press.

ZDRAVKOVICH, M.M. & MEDEIROS, E.B. 1991 Effect of damping on interference-induced oscillations of two identical circular cylinders. *J. Wind Eng. Industrial Aerodynamics* **38**, 197–211.

ZDRAVKOVICH, M.M. & STANHOPE, D.J. 1972 Flow pattern in the gap between two cylinders in tandem. Internal report FM 5/72. University of Salford.